遺伝子ハンドリング技術を用いた単一細胞内調節タンパク質の機能解析法の開発

(研究課題番号 11559016)

平成 11 年度～平成 12 年度科学研究費補助金

基盤研究(B)(2)研究成果報告書

平成 15 年 3 月

研究代表者　石渡　信一

(早稲田大学・理工学部・教授)

はしがき

この報告書は、平成１１年度（1999年4月）から１２年度（2001年3月）までの２年間で行った文部省（文部科学省）科学研究費基盤研究B（２）展開「遺伝子ハンドリング技術を用いた単一細胞内タンパク質の機能解析法の開発（課題番号11559016）」の研究成果をまとめたものである。これと並行して、平成１０年度（1998年4月）から１４年度（2002年3月）にわたる４年間に、科学研究費基盤研究A（２）「超分子システム内での１分子機能・分子間協調の顕微画像化と解析（課題番号10308030）」を行ったので、その成果報告書も今回あわせて出版した。本成果報告書は、本来研究が終了した一昨年春に発行すべきだったが、本研究課題の成果発表が遅れたことや、引き続く研究課題のスタートなどで遅れてしまった。

本研究は最終目標として、「mRNA（あるいはDNA）を単一細胞レベルである瞬間に操作し、それによって生じた細胞構造や機能の変化を時々刻々顕微観察・解析すると同時に、適宜細胞を破砕してその構成要素（合成されたタンパク質など）を時系列的に分析できるシステムを開発すること」とした。そのために必要な鍵技術を３つ挙げ、それらの技術について原理検討を行うことを具体的な研究目的として掲げた。その３つの技術とは、

１）細胞内への不活性化遺伝子（特にmRNA）の人為的導入とその再活性化制御技術、
２）細胞内タンパク質、遺伝子１分子の顕微観察技術、
３）細胞内の構成要素の瞬時回収技術、である。

本研究課題の遂行には、安田賢二（当時日立基礎研：現、東大大学院総合文化研究科）と岡野和宣（日立中研）の両氏の協力が必要不可欠であった。その間、本格的な遺伝子組換え技術については、2000.4に東條正（1992.3学部卒：東大医科研で博士号取得）を博士研究員として迎えたことで導入することができた。また、本研究には多くの大学院生たちが関与している。とくに本研究課題については、野崎貴之（2001.3修士了）がその中心となった。本研究と並行して行っている一分子機能計測や筋収縮系の研究については、特に川口憲治（1999.3修士了）、藤原郁子（2000.3修士了、2003.3博士取得）、佐々木大輔、鈴木団、上村想太郎（現、D２）、島本勇太（現、M2）らによって行われた。筋生理については、藤田英明（2000.3博士号取得：現、ワシントン州立大）が中心となった。1998.10からは船津高志氏が物理学科教員として赴任したことにより、助手の多田隈尚史氏（1997.3修士了）らとともに、光学顕微鏡技術をはじめ様々な面で協力をえた。さらに、幾つかのグループと共同研究を行った。福田紀男、栗原敏（慈恵医大）、豊島陽子研（東大総合文化研究科）、末次志郎、竹縄忠臣（東大医科研）、河合正隆（アイオワ大）の諸氏との研究は、幸い論文としてまとめることができた。岡崎国立共同研究機構・統合バイオサイエンスセンター（当時、慶応義塾大学・理工学部・物理学科）木下一彦研究室とは、かわらぬ研究交流を続けている。本研究課題ついては、当初の目的を十分に達成したとは言い難いが、今後の研究遂行の上で多くの指針（少なくとも私にとって）を得ることができたと思っている。この機会に、記して皆様に感謝します。

平成15年3月　　研究代表者　石渡信一

研究業績

研究成果の概要

1）**DNA の固定化と選択的回収法（DNA チップの開発）（文献４、６）：**クロム基盤上への DNA 固定化法と、赤外レーザー照射・温度パルス法による選択的な回収法を確立し、その方法の詳細を論文として公表した。これは DNA チップの一つの形態である。

2）**Caged DNA 合成の試み（未発表）：**DNA 塩基のアミノ基を（4,5-dimethoxy-2-nitrobenzyl bromide（DMNBB）で化学修飾し、DNA の複製機能を一旦失活させ、それを紫外線マイクロフラッシュ法によって再活性化するという方針で Caged DNA の合成を試みた。一時は PCR 法によって確認できたと思われたが、再現性に問題があり、DNA 塩基のアミノが化学修飾に対して活性が高くないと結論した。さらに、Caged 遺伝子を調製したという論文が発表されたので、我々は方針を転換し、新手法の開発に力を入れた。

3）**GFP-アクチンの心筋培養細胞内発現（未発表）：**ニワトリの未分化筋芽細胞・マウス筋芽細胞株 C2C12 へ、蛍光性タンパク質 GFP を fusion したアクチンのプラスミドを導入すること、そしてその未分化細胞を筋管へと分化させることを試みた。まず、アクチン分子の N 末端と C 末端にそれぞれ GFP を導入し培養心筋細胞を発現させてところ、細胞は正常に発達し、GFP アクチンが筋収縮系に組み込まれることを示す画像が得られた（共焦点蛍光顕微鏡による観察）。つぎに、アクチン分子を２つの部分に分割し、そこに、前後を入れ替えた GFP を導入した。そうすることによって GFP の構造を不安定化し、アクチン分子に加わる力によって生じる分子歪みに応じて GFP の蛍光性が変化することを期待した。分割する場所を２箇所検討した結果、両方とも、大量発現させると、細胞は正常には発達しないことが分かった（少量の場合には発達するように見えたが、発現量をコントロールすることができず、再現性が乏しかった）。

4）**アクチンフィラメントのストレスセンサー応用（未発表）：**アクチンフィラメントに加わる張力を蛍光画像化し、アクチンフィラメントをストレスセンサーとして利用するための方法を開発しようと、幾つかの試みをした。特殊な GFP-アクチンを発現させたが、単一フィラメントの特性解析には至らなかった。

5）**ケモカインリセプターの１分子画像化（論文準備中）：**細胞表面でケモカインリセプターを１分子蛍光画像化し、ケモカイン結合に伴う走化性と、レセプターの集合性や運動性を顕微鏡解析した。リセプターはリガンド結合に関わらず２量（数量）体を形成することが明らかになった。

キーワード

（1）ケージド遺伝子　（2）温度パルス法　（3）DNA チップ　（4）PCR 法　（5）筋芽細胞　（6）GFP-アクチン　（7）アクチンフィラメント　（8）ストレスセンサー

研　究　組　織

研究代表者

石渡　信一　　（早稲田大学理工学部・教授）

研究分担者

安田　賢二　　（東京大学大学院総合文化研究科・助教授）

岡野　和宣　　（(株) 日立製作所中央研究所・主任研究員）

藤田　英明　　（日本学術振興会・特別研究員）

東條　正　　（早稲田大学理工学総合研究センター・客員研究員）

(研究協力者)

研　究　経　費

平成１１年度	８，８００千円
平成１２年度	４，２００千円
計	１３，０００千円

研 究 発 表

1．学会誌等

1) Kato, H., Nishizaka, T., Iga, T., Kinosita,Jr., K. and Ishiwata, S. (1999). *Proc. Natl. Acad. Sci. USA* **96**, 9602-9606. "Imaging of thermal activation of actomyosin motors."

2) Fujita, H. and Ishiwata, S. (1999). *Biophys. J.* **77**, 1540-1546. "Tropomyosin modulates pH dependence of isometric tension."

3) Fukuda, N., Kajiwara, H., Ishiwata, S. and Kurihara, S. (2000). *Circ. Res.* **86**, e1-e6. "Effects of MgADP on length dependence of tension generation in skinned rat cardiac muscle."

4) Yasuda, K., Okano, K. and Ishiwata, S. (2000). *Biotechniques* **28**, 1006-1011. "Focal extraction of surface-bound DNA from a microchip using photo-thermal denaturation."

5) Kawai, M., Kawaguchi, K., Saito, M. and Ishiwata, S. (2000). *Biophys. J.* **78**, 3112-3119. "Temperature change does not affect force between single actin filaments and HMM from rabbit muscles."

6) Okano, K., Yasuda, K. and Ishiwata, S. (2000). *Sensors & Actuators* B **64**, 88-94. "Position-specific release of DNA from a chip by using photothermal denaturation."

7) Kawaguchi, K. and Ishiwata, S. (2000). *Biochem. Biophys. Res. Comm.* **272**(3), 895-899. "Temperature dependence of force, velocity and processivity of single kinesin molecules."

8) Nishizaka, T., Seo, R., Tadakuma, H., Kinosita,Jr., K. and Ishiwata, S. (2000). *Biophys. J.* **79**(2), 962-974. "Characterization of single actomyosin rigor bonds - Load-dependence of lifetime and mechanical properties-."

9) 石渡信一 (2000). *トライボロジスト* **45**, 119-125. "筋収縮滑り運動機構とトライボロジー"

10) 藤田英明、佐々木大輔、石渡信一 (2000). *バイオサイエンスとインダストリー* **58**, 256-259. "生体分子モーター系における分子シンクロナイゼーションの研究"

11) Kawaguchi, K. and Ishiwata, S. (2001). *Science* **291**, 667-669. "Nucleotide-dependent single- to double-headed binding of kinesin."

12)K. Yasuda. (1999). *Jpn. J. Appl. Phys.* **38**, 3316-3319. "Measurement of microscopic spatial distribution of acoustic radiation force using microspheres and electrostatic force."

13)K. Yasuda. (2000). *Sensors and Actuators B* **64**, 128-135. "Non-destractive,

non-contact handling method for biomaterials in micro-chamber by ultrasound."

2．出版物

1) Ishiwata,S., Tadashige,J., Masui,I., Nishizaka,T. and Kinosita,Jr.,K. (2001). In Molecular Interactions of Actin: Actin Structure and Actin-binding Proteins. (eds. C.G. dos Remedios and D.D. Thomas) Springer Verlag, Heidelberg, pp. 79-94. "Microscopic analysis of polymerization and fragmentation of individual actin filaments."

3．口頭発表

【国内】

1) K. Okano, K. Yasuda and S. Ishiwata "Release of specific DNAS from a DNA chip by using photothermal denaturation" 固体センサ・アクチュエーター国際会議（仙台）1999. 6.
2) 川口憲治、上村想太郎、石渡信一　「キネシンの単頭-双頭結合変換」第３７回日本生物物理学会年会（和光市市民文化センター・埼玉）1999. 10.
3) 鈴木団、藤田英明、石渡信一　「A 帯中における単一アクチンフィラメントの張力発生」第３７回日本生物物理学会年会（和光市市民文化センター・埼玉）1999. 10.
4) 藤田英明、福田賢司、佐々木大輔、石渡信一　「MgADP 収縮におけるトロポニン C、ミオシン調節軽鎖の制御作用」第３７回日本生物物理学会年会（和光市市民文化センター・埼玉）1999. 10.
5) 佐々木大輔、藤田英明、石渡信一　「共焦点蛍光顕微鏡による心筋線維 SPOC の筋節長振動波形解析」 第３７回日本生物物理学会年会（和光市市民文化センター・埼玉）1999. 10.
6) 五嶋淳、加藤宏一、石渡信一　「アクチンフィラメントのリング形成」第３７回日本生物物理学会年会（和光市市民文化センター・埼玉）1999. 10.
7) 藤原郁子、高橋真、多田隈尚史、船津高志、石渡信一　「単一アクチンフィラメントの重合ダイナミクスの顕微解析」第３７回日本生物物理学会年会（和光市市民文化センター・埼玉）1999. 10.
8) 安田賢二、岡野和宣、五嶋淳、野崎貴之、石渡信一　「集束レーザー局所加熱による DNA チップからの DNA 選択回収」第３７回日本生物物理学会年会（和光市市民文化センター・埼玉）1999. 10.
9) 石渡信一　「生体分子モーター系にみる自励振動現象：1 分子から分子集団への機能構築」第７２回日本生化学会大会（パシフィコ横浜）1999. 10.
10) 石渡信一　「生体運動を担う分子モーターの仕組み」物性研短期研究会、1999. 11.
11) 岡野和宣、Li Tao、安田賢二、五嶋淳、野崎貴之、石渡信一　「レーザー熱誘起による DNA マイクロチップからの DNA 回収」分子生物学会（福岡）1999. 12.
12) 藤原郁子、高橋真、多田隈尚史、船津高志、石渡信一　「単一アクチンフィラメントの重合過程の実時間顕微鏡解析」筋収縮・細胞運動研究会（帝京大学・東京）1999. 12.
13) 佐々木大輔、藤田英明、石渡信一　「心筋線維ＳＰＯＣにおける筋節長振動の顕微鏡解析」筋収縮・細胞運動研究会（帝京大学・東京）1999. 12.
14) 藤原郁子、高橋真、多田隈尚史、船津高志、石渡信一　「Mg^{2+}, Ca^{2+}-アクチンの重合ダイナミクスの単一アクチンフィラメント解析」生体運動研究合同班会議　（千里ライフサイエンスセンター・大阪）2000. 1.

15) 藤田英明、福田賢司、佐々木大輔、石渡信一　「MgADP 収縮におけるミオシン調節軽鎖のアロステリック制御」生体運動研究合同班会議（千里ライフサイエンスセンター・大阪）2000. 1.

16) 福田紀男、佐々木大輔、石渡信一、栗原敏　「心筋の長さ－張力関係のメカニズム」日本生理学会、2000. 3.

17) M.Suzuki, H.Fujita and S.Ishiwata "Application of laser optical tweezers to force measurement in the minimum unit of muscle contractile system" 8th International Conference on Laser Application in Life Sciences（早稲田大学・東京）2000. 8.

18) I. Fujiwara, S. Takahashi, H. Tadakuma, T. Funatsu and S. Ishiwata "Real-time analysis of polymerization process of single actin filaments through fluorescence imaging with evanescent field illumination" 8th International Conference on Laser Application in Life Sciences（早稲田大学・東京）2000. 8.

19) 石渡信一　「Single molecular mechano-chemistry of motor proteins studied by laser optical tweezers」8th International Conference on Laser Application in Life Sciences （早稲田大学・東京） (Invited Talk)　2000. 8.

20) D. Sasaki and S. Ishiwata "Molecular synchronization in the myocardial contractile system that bears the rhythm of heartbeat" The 1st international symposium on molecular synchronization for design of new materials system,　2000. 9.

21) 石渡信一　「レールがレールでなくなる時」第 38 回日本生物物理学会（東北大学・仙台）（招待講演）2000. 9.

22) 新原岳雄、大沼清、石渡信一、安田賢二　「サイズ・パターン制御されたニワトリ胚培養心筋ネットワークの研究」　第 38 回日本生物物理学会（東北大学・仙台）2000. 9.

23) 藤原郁子、高橋真、多田隈尚史、船津高志、石渡信一　「重合・脱重合ダイナミクスにおける単一アクチンフィラメントの長さ揺らぎの顕微解析」第 38 回日本生物物理学会（東北大学・仙台）2000. 9.

24) 鈴木団、藤田英明、石渡信一　「最小筋収縮系に見られる単一アクチンフィラメントのステップ状の動きと力発生」第 38 回日本生物物理学会（東北大学・仙台）2000. 9.

25) 佐々木大輔、藤田英明、福田紀男、栗原敏、石渡信一　「心筋 SPOC 振動周期と心拍数との相関」第 38 回日本生物物理学会（東北大学・仙台）2000. 9.

26) 福田紀男、佐々木大輔、石渡信一、栗原敏　「心筋の長さ-張力関係のメカニズム」第 38 回日本生物物理学会（東北大学・仙台）2000. 9.

27) 五島淳、加藤宏一、石渡信一　「アクチンリングの形成メカニズム」第 38 回日本生物物理学会（東北大学・仙台）2000. 9.

28) 上村想太郎、川口憲治、石渡信一　「キネシン・微小管結合様式の 1 分子顕微解析」第 38 回日本生物物理学会（東北大学・仙台）2000. 9.

29) 瀬尾隆造、石渡信一　「キネシン・微小管結合の寿命とその負荷依存性」第 38 回日本

生物物理学会（東北大学・仙台）2000. 9.

30) 藤原郁子、高橋真、多田隈尚史、船津高志、石渡信一　「単一アクチンフィラメント重合・脱重合ダイナミクスの定量的解析」日本生化学会（横浜）2000. 10.

31) 藤原郁子、高橋真、多田隈尚史、船津高志、石渡信一　「エヴァネッセント場照明法を用いた単一アクチンフィラメント重合ダイナミクスの実時間顕微解析」レーザー顕微鏡研究会（東京）2000. 11.

32) S. Ishiwata "Role of actin in force generation" The 11th Takeda Science Foundation Symposium on Bioscience =COE International Conference=（淡路）(Invited Talk) 2000. 11.

33) S. Uemura, K. Kawaguchi and S. Ishiwata "Microscopic analysis of binding mode of single kinesin molecules with microtubule" The 11th Takeda Science Foundation Symposium on Bioscience =COE International Conference=（淡路）2000. 11.

34) M. Suzuki, H. Fujita and S. Ishiwata "Motility assay in the myosin filament lattice" The 11th Takeda Science Foundation Symposium on Bioscience =COE International Conference=（淡路）2000. 11.

35) I. Fujiwara, S. Takahashi, H. Tadakuma, T. Funatsu and S. Ishiwata "Direct observation of polymerization process of single actin filaments" 筋収縮・細胞運動研究会（帝京大学・東京）2000. 12.

36) 佐々木大輔、藤田英明、福田紀男、栗原敏、石渡信一　「心筋収縮系における SPOC 振動周期と心拍数との相関」生体運動研究合同班会議（早稲田大学・東京）2001. 1.

37) 鈴木団、藤田英明、石渡信一　「A 帯中における単一クロスブリッジあたりの発生張力」生体運動研究合同班会議（早稲田大学・東京）2001. 1.

38) 東條正、多田隈尚史、上野太郎、青木大輔、石渡信一、船津高志　「好中球走化性因子受容体の生細胞上での一分子計測」生体運動研究合同班会議（早稲田大学・東京）2001. 1.

39) 石渡信一　「分子モーターの生物理学」第 56 回日本物理学会　シンポジウム（中央大・八王子）2001. 3.

【海外】

1) S. Ishiwata "Regulation mechanism as revealed using a thin filament-reconstituted contractile system" Gordon Research Conference, Colby-Sawyer College (USA) (Invited Talk) 1999. 6.

2) H. Fujita and S. Ishiwata "Modulation of pH-tension relation by tropomyosin in thin filament-reconstituted cardiac muscle fibers" Gordon Research Conference, Colby-Sawyer College (USA) 1999. 6.

3) K. Kawaguchi and S. Ishiwata "Single-molecule analysis of single-headed and double-headed binding of kinesin with a microtuble" Gordon Research Conference,

Colby-Sawyer College (USA) 1999. 6.

9) H. Fujita, S. Ishiwata "Modulation of pH-tension relation by tropomyosin: Investigation using thin filament-reconstituted cardiac muscle fibers" XIII International Biophysics Congress, New Delhi (India) 1999. 9.

4) M. Kawai, K. Kawaguchi, M. Saito and S. Ishiwata "Temperature change does not affect the force measured between single actin filaments and heavy meromyosin molecules prepared from rabbit skeletal muscles" European Muscle Conference (United Kingdom) 1999. 9.

5) S. Ishiwata and K. Kawaguchi "Nucleotide- and loading rate-dependent switching of single- to double-headed binding of kinesin" 44th Annual Meeting of the Biophysical Society, New Orleans (USA) 2000. 2.

6) K. Kawaguchi and S. Ishiwata "Effect of temperature on force generation and velocity of single kinesin molecule" 44th Annual Meeting of the Biophysical Society, New Orleans (USA) 2000. 2.

7) M. Kawai, K. Kawaguchi, M. Saito and S. Ishiwata "Temperature change does not affect the force measured between single actin filaments and heavy meromyosin molecules prepared from rabbit skeletal muscles" 44th Annual Meeting of the Biophysical Society, New Orleans (USA) 2000. 2.

8) N. Fukuda, D. Sasaki, S. Ishiwata and S. Kurihara "Understanding of sarcomere length (SL)-dependent tension generation in skinned cardiac muscle" 44th Annual Meeting of the Biophysical Society, New Orleans (USA) 2000. 2.

9) J. Goshima, H. Kato and S. Ishiwata "Ring formation of actin filaments in an *in vitro* motility assay" 3rd East Asian Biophysics Symposium, 慶州 (Korea) 2000. 5.

10) M. Suzuki, H. Fujita and S. Ishiwata "Microscopic measurements of force generation by single actin filaments in the A-band" 3rd East Asian Biophysics Symposium, 慶州 (Korea) 2000. 5.

11) I. Fujiwara, S. Takahashi, H. Tadakuma, T. Funatsu and S. Ishiwata "Analysis of polymerization - depolymerization dynamics of single actin filaments -Comparison between Mg^{2+}- and Ca^{2+}- actin-" 3rd East Asian Biophysics Symposium, 慶州 (Korea) 2000. 5.

12) K. Okano, G. Chen, K.. Yasuda, S. Ishiwata, "DNA preparation by using a DNA chip" 4th International Symposium on Micro Total Analysis System (Micro-TAS2000), (Netherlands) 2000. 5.

13) S. Ishiwata "Single molecular characterization of protein motors" International Workshop on signaling neuropeptides and conformation of macromolecules (Moscow) (Invited Talk) 2000. 9.

14) S. Ishiwata "Single-molecular mechanics of motor proteins" Aspen Workshop on Single

Molecule Biophysics, Aspen (USA) 2001. 1.

15) I. Fujiwara, S. Takahashi, H. Tadakuma, T. Funatsu and S. Ishiwata "Microscopic analysis of polymerization process of single actin filaments" 45th Annual Meeting of the Biophysical Society, Boston (USA) 2001. 2.

16) M. Suzuki, H. Fujita and S. Ishiwata "Force generation on single actin filaments in the A-band motility assay system" 45th Annual Meeting of the Biophysical Society, Boston (USA) 2001. 2.

17) N. Fukuda, J. O-uchi, H. Kajiwara, S. Ishiwata and S. Kurihara "Effect of Acidosis on length dependence of tension generation in skinned cardiac muscle" 45th Annual Meeting of the Biophysical Society, Boston (USA) 2001. 2.

4．研究成果による工業所有権の出願・取得状況

【国内特許】

1) 特願 2000-356827 「一細胞長期培養顕微観察装置」安田賢二、金子邦彦、四方哲也、井之上一平、若本祐一、森口裕之

2) 特願平 11-157268「ポリヌクレオチド分離方法および装置」安田賢二、岡野 和宣、加藤宏一

3) 特願平 11-871「分析装置および分析方法」安田賢二

【米国特許】

1) United States Patent 6,183,970 "Polynucleotide probe chip and polynucleotide detection method" Okano Kazunori, Kambara Hideki, Uematsu Chihiro, Matsunaga Hiroko, Irie Takashi, Kajiyama Tomoharu, Yasuda Kenji. February 6, 2001.

2) United States Patent 6,093,370 "Polynucleotide separation method and apparatus therefor" Yasuda Kenji, Okano Kazunori. Kato Hirokazu. July 25, 2000.

Proc. Natl. Acad. Sci. USA
Vol. 96, pp. 9602–9606, August 1999
Biophysics

Imaging of thermal activation of actomyosin motors

HIROKAZU KATO*†, TAKAYUKI NISHIZAKA‡, TAKASHI IGA†, KAZUHIKO KINOSITA, JR.‡§, AND SHIN'ICHI ISHIWATA†‡¶‖**

*Central Research Laboratory, Hitachi Ltd., Hatoyama, Saitama 350-0395, Japan; †Department of Physics, School of Science and Engineering, ¶Advanced Research Institute for Science and Engineering, ‖Materials Research Laboratory for Bioscience and Photonics, Waseda University, Tokyo 169-8555, Japan; ‡Core Research for Evolutional Science and Technology (CREST) "Genetic Programming" Team 13, Kawasaki 216-0001, Japan; and §Department of Physics, Faculty of Science and Technology, Keio University, Yokohama 223-8522, Japan

Communicated by Shinya Inoue, Marine Biological Laboratory, Woods Hole, MA, June 14, 1999 (received for review December 8, 1998)

ABSTRACT **We have developed temperature-pulse microscopy in which the temperature of a microscopic sample is raised reversibly in a square-wave fashion with rise and fall times of several ms, and locally in a region of approximately 10 μm in diameter with a temperature gradient up to 2°C/μm. Temperature distribution was imaged pixel by pixel by image processing of the fluorescence intensity of rhodamine phalloidin attached to (single) actin filaments. With short pulses, actomyosin motors could be activated above physiological temperatures (higher than 60°C at the peak) before thermally induced protein damage began to occur. When a sliding actin filament was heated to 40–45°C, the sliding velocity reached 30 μm/s at 25 mM KCl and 50 μm/s at 50 mM KCl, the highest velocities reported for skeletal myosin in usual *in vitro* assay systems. Both the sliding velocity and force increased by an order of magnitude when heated from 18°C to 40–45°C. Temperature-pulse microscopy is expected to be useful for studies of biomolecules and cells requiring temporal and/or spatial thermal modulation.**

Recent advances in optical microscopic techniques have made it possible to image single protein molecules in solution (1, 2) and investigate the dynamic nature of molecular motors (3–8). To introduce an additional dimension to this technology, we have developed temperature-pulse microscopy (TPM), in which a microscopic sample(s) in aqueous solution is heated reversibly.

There have been several reports on the effects of temperature jumps under an optical microscope: for example, on physiological functions of muscle fibers (9–12) and on phase transition phenomena in membranes of phospholipid vesicles and cells (13). To prevent thermal deterioration of biological samples, and to confirm the absence of the deterioration, it is highly desirable to restore the starting temperature as soon as the measurement is finished. In our TPM, temperature is elevated spatially and temporally by illuminating a lump of metal particles by IR laser; a concentric temperature gradient is created around the lump of metal particles. When the laser beam is shut off, the heat is rapidly dissipated into the surrounding medium. Thus, a square-wave temperature pulse with rise and fall times of less than 10 ms is generated. Exposure to high temperature is minimized, and repetitive thermal cycling is easily programmed. The local heating also permits simultaneous observation of the sample behaviors at various temperatures.

In the microscopic temperature-imaging techniques reported so far, the temperature was estimated either from the thermal quenching of fluorescence (14–16) or from the thermal shift of the fluorescence spectrum (13). Here, we applied the former technique. In our TPM, a concentric temperature gradient is formed around the metal aggregate, as assessed from thermal quenching of a fluorescent dye bound to actin filaments with a slope of 1–2°C/μm and extension out to 10–20 μm. The temperature distribution on single actin filaments also could be imaged.

We have applied this TPM technique to the thermal activation of sliding movement and tension development of actomyosin motors in an *in vitro* motility assay. We demonstrate that the motor functions can be thermally activated even at temperatures that are high enough to normally damage the proteins, if the duration of the temperature pulse is short enough.

MATERIALS AND METHODS

TPM. As schematically illustrated in Fig. 1, local heating was achieved by illuminating an aggregate of metal particles in the sample with an IR laser beam (1 W Nd:YLF laser, 1,053–1,000 p: λ = 1.053 μm; Amoco Laser, Naperville, IL; 50–100 mW on the sample plane). In most experiments we used aluminum (0.1 μmϕ; AL-014050, Nilaco, Tokyo), but gold (0.5 μmϕ; AU-174020, Nilaco), silver (0.07 μmϕ; AG-404050, Nilaco), and platinum (1.0 μmϕ; PT-354012, Nilaco) powders served equally well. The metal particles spontaneously formed aggregates in the sample and had irregular shapes. [Heat production by laser irradiation also can be achieved in other ways. For example, we have deposited, by vacuum evaporation, a thin layer of metal on a glass surface in the form of a regular array of μm-sized circles (not shown). This method allowed well-controlled and reproducible heating, whereas the use of amorphous metal aggregates described here is very simple. A magnetic bead also can be used (17).]

The presence of Al aggregates did not affect the *in vitro* motility for at least 2 h. The actin filament temperature was estimated from thermal quenching of the fluorescence of rhodamine phalloidin bound to the filament. The fluorescence images were taken with an image intensifier (KS1381; Video Scope International, Washington, DC) connected to a charge-coupled device camera (CCD-72; Dage MTI, Michigan City, IN) at the video rate of 30 frames/s. The decay lag in this camera system was well within one frame (33 ms). For the measurement of the rise and fall times of the temperature pulse, an image intensifier (ILS-3a; nac, Tokyo) connected to a high-speed camera (HSV-500DM; nac) was used at a rate of 500 frames/s.

The fluorescence image of labeled filaments at *T*°C was divided by that at 18°C (reference temperature) to yield the intensity ratio (*r*) in every pixel (18). *r* was related with *T* in a control experiment in which the temperature of the microscope stage was held at precise temperatures with the use of a thermal insulation chamber, which took about 45 min for

The publication costs of this article were defrayed in part by page charge payment. This article must therefore be hereby marked "*advertisement*" in accordance with 18 U.S.C. §1734 solely to indicate this fact.

PNAS is available online at www.pnas.org.

Abbreviation: TPM, temperature-pulse microscopy.

**To whom reprint requests should be addressed at: Department of Physics, School of Science and Engineering, Waseda University, Tokyo 169-8555, Japan. E-mail: ishiwata@mn.waseda.ac.jp.

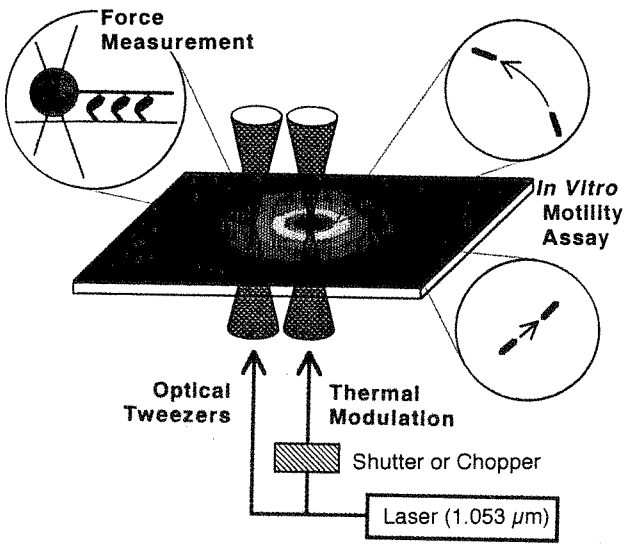

FIG. 1. Schematic illustration of TPM system. Metal aggregates of irregular shape and several to 10 μm in size, lumps of metal particles of 0.1–1.0 μm in diameter, are scattered on a glass coverslip in an *in vitro* motility assay system under an optical microscope. A peripheral, not the central, portion of one of the aggregates is illuminated by focusing an IR laser beam. If the central portion is illuminated, the aggregate is frequently blown off or the surrounding medium gets boiled. The metal aggregate that absorbs the laser light functions as a local heat source, around which a concentric temperature gradient is formed. Sliding movement of actin filaments occurs at temperature-dependent velocities, as illustrated by movement in circles. When tension is measured, the incident laser beam is split into two; one constitutes optical tweezers that hold a polystyrene bead attached at the rear end of an actin filament, and the other illuminates a metal aggregate. For repetitive temperature modulation, a chopper or shutter is used.

stabilization (Nikon). Room temperature was maintained at 18°C ± 1°C. We obtained the empirical equation $r = 1 - \alpha(T - T_0)$, where α and T_0 are, respectively, 0.018°C^{-1} and 18°C, in agreement with a spectroscopic measurement in a cuvette (fluorescence spectrophotometer F-4500, Hitachi, Tokyo). The temperature estimated from the fluorescence intensity averaged over a short (< a few μm) filament fluctuated from frame to frame, with a SD of ± 5°C over the duration of 0.5 s (15 frames). Spectroscopic studies in a cuvette (19) indicated that rhodamine phalloidin tended to detach from actin at high temperatures. We confirmed that the half-time for detachment under the solvent condition examined here was approximately 12 min at 35°C and 3 min at 45°C, which was much longer than the duration of the temperature pulse (<10 s). Photobleaching of rhodamine fluorescence was negligible within the period of time we examined. Thus, the linear relationship between relative fluorescence intensity and temperature, $r(T)$, is attributed solely to reversible thermal quenching of rhodamine.

Proteins. Actin and heavy meromyosin (a fragment of myosin prepared by chymotryptic digestion) were prepared from rabbit white skeletal muscle as described (20). Actin filaments were labeled with rhodamine phalloidin (Molecular Probes) according to Yanagida *et al.* (21).

***In Vitro* Motility Assay.** Details of the *in vitro* motility assay and tension measurement performed under an inverted microscope (TMD300; an oil-immersion objective lens with a phase ring, ×100 numerical aperture = 1.3 or ×60 numerical aperture = 1.4; Nikon) equipped with optical tweezers have been described (7, 8). The assay buffer used was 25 mM KCl/2.0 mM ATP/4.0 mM $MgCl_2$/25 mM imidazole-HCl, pH 7.4/1.0 mM EGTA/10 mM DTT with an oxygen-scavenger enzyme system (22); in one experiment where the highest sliding velocity was recorded, 50 mM KCl was used instead of 25 mM KCl, in which 1% (wt/vol) of methylcellulose was included to suppress the dissociation of actin filaments from the glass surface at high ionic strength. An *in vitro* motility cell was prepared by infusing 30 μg/ml heavy meromyosin in the assay buffer containing 0.5 mg/ml BSA. To measure the tension, a polystyrene bead of 1.0 μm in diameter was attached at the rear end of an actin filament through a barbed end capping protein, gelsolin, covalently attached to the bead (23), and the bead was trapped with optical tweezers (trap stiffness, 0.14 pN/nm). In this case, the laser beam was split into two by a polarizing beam splitter (Sigma Koki, Hidaka, Japan); one beam was used for optical tweezers and the other for heating. Movement of the bead in the trap was detected in a phase-contrast image under a dual-view microscope (18) and analyzed with sub-nm precision.

RESULTS AND DISCUSSION

A steady, concentric temperature gradient was produced within 10 ms around the metal after laser illumination was started, as monitored by the fluorescence intensity of the temperature-sensitive rhodamine phalloidin attached to actin filaments in the sample chamber (Fig. 2 *A–D*). Temperatures on a single actin filament could be imaged (Fig. 2*E*), even during sliding as shown below. A temperature difference as large as 40°C could be created across a high-magnification image, allowing simultaneous evaluation of sample behaviors over a wide range of temperatures. When the laser illumination was terminated, the sample cooled down to the original temperature within 10 ms, presumably because of the presence of a substance of large heat conductivity (glass and water) in contact with the small heat source. For a long actin filament, a temperature gradient around 2°C/μm was demonstrated (Fig. 2*E*).

First, we examined the effects of the temperature gradient on the sliding movement of a long actin filament. When the temperature of the front portion of a sliding filament was higher, the filament was straightened and sliding was smooth. However, when the temperature of the rear portion was higher, buckling occurred at the middle of the filament, the buckled portion being on the glass surface without looping out into the medium. In all likelihood, front motors can pull the whole filament, whereas rear motors cannot efficiently push the front portion because of the flexibility of the filament (20, 25, 26). When the rear part is faster, formation of a superhelix may be expected at the slow/fast junction, because a sliding actin filament has been shown to rotate as a right-handed screw (3, 20, 26). Indeed we observed a superhelix when the front part of an actin filament was completely fixed on a glass surface (20). In the present experiment, the temperature gradient in the running filament could not be maintained for a sufficiently long period to allow the buckled portion to loop out.

Then, we observed reversible acceleration of sliding movement by repetitive application of relatively long temperature pulses (0.5 to several seconds) by using a chopper. As shown in Fig. 3, sliding velocities reversibly reached two steady-state values within 1/30 s: the average velocities were 1.9, 19.3, 2.5, 20.7, and 2.2 μm/s, respectively, at 18°C, 41°C, 19°C, 40°C, and 15°C, which were estimated from the average fluorescence intensity of the sliding filament according to the relation, $r(T)$, described above. (Note that the coverslip temperature was maintained at 18°C ± 1°C.) On average, the sliding velocities at 25 mM KCl, the ionic strength usually used for *in vitro* motility assays (24), were 2.0 ± 0.1 (n = 6), 10 ± 1.5 (n = 6), and 20 ± 1.8 (n = 6) μm/s at 18°C, 30°C, and 40°C, respectively. For comparison, thermostatic regulation of the whole stage resulted in the average sliding velocities, respectively, of 2.0 ± 0.1 (n = 6), 8.0 ± 0.5 (n = 6), 13 ± 0.7 (n = 6), and 22 ± 2.1 (n = 6) μm/s at 18°C, 30°C, 40°C, and 50°C, consistent with previous reports (27–29). In this case, the

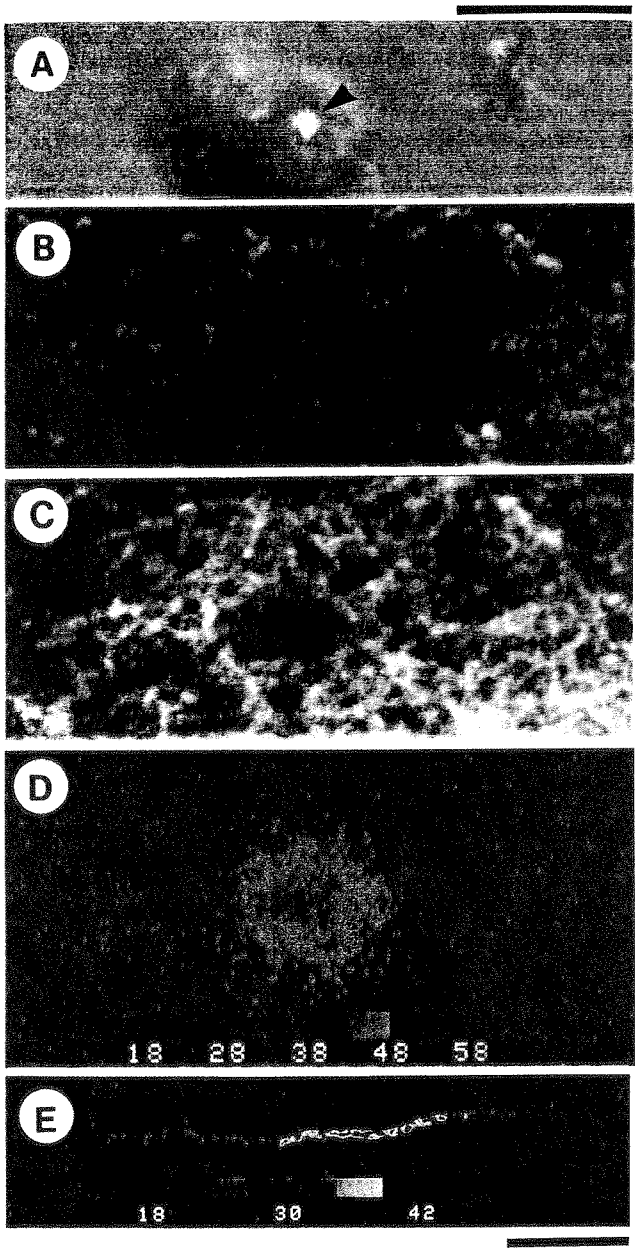

FIG. 2. Imaging of temperature distribution on actin filaments around the metal aggregate. (*A*) Phase-contrast image corresponding to the central part of fluorescence images (*B–D*). A laser beam was focused at a periphery (shown by an arrowhead) of a lump of Al particles of irregular shape. (*B–D*) Fluorescence images of a two-dimensional network of rhodamine phalloidin-labeled actin filaments (12 μg/ml) attached to heavy meromyosin molecules that adhered to the glass surface coated with nitrocellulose (24). Excess actin filaments were washed away, so that filaments were mostly in focus and thus within 1 μm of the glass surface. (*B*) Fluorescence image of the actin network taken in a single video frame coincident with laser illumination for 1/30 s under shutter control. A periphery of a ≈10-μm lump of Al particles observed in *A* was illuminated. Fluorescence under and close to the metal aggregate disappeared because of excessively high temperature. (*C*) A single-frame fluorescence image obtained two video frames after *B*; the image was indistinguishable from that obtained before laser illumination at 18°C ± 1°C, i.e., temperature of the coverslip. (*D*) Two-dimensional temperature distribution constructed from the ratio of the fluorescence intensities of the images *B* and *C*. (*E*) Temperature distribution on a single actin filament; only in this micrograph, the background fluorescence intensity was subtracted. In *D* and *E*, the temperature is scaled in pseudocolor as shown in color bars in °C unit. (Scale bars: upper one for *A–D*, lower one for *E*, 10 μm.)

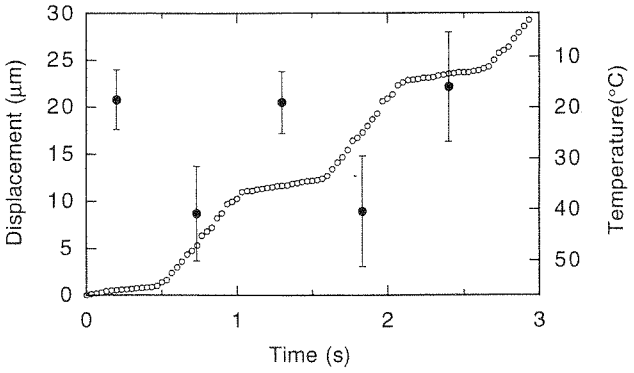

FIG. 3. Time course showing reversible changes in the sliding movement of an actin filament with repetitive temperature pulses. Displacement of the centroid of the fluorescence image of the actin filament (1.0 μm long) is shown by ○ every 1/30 s. A laser pulse of 0.53-s duration was given every 1.07 s. The temperature was estimated from the average intensity of the actin filament in each frame at 30 frames/s. ● and error bars show the average ± SD for 14 consecutive frames (0.47 s). The coverslip temperature was kept at 18°C ± 1°C.

sliding filaments tended to detach from the glass surface at higher temperatures, e.g., within 1 min at 50°C, suggesting gradual deterioration of motor functions. The higher velocities obtained with our TPM at 40°C demonstrate that the motors can be fully activated for a short period of time before thermally induced protein damage begins.

Next, we examined sliding movement of an actin filament during very short temperature pulses by using a shutter (Fig. 1). When illuminated with a laser pulse with a duration of 1/16 s, an abrupt displacement of the actin filament, by as much as 1.6 μm, occurred, corresponding to a sliding velocity of about 26 μm/s (Fig. 4 *A* and *B*). The average temperature during this 1/16-s illumination was estimated to be 45°C and the maximum temperature exceeded 60°C (Fig. 4*C*). On shortening the duration of the temperature pulse, the degree of abrupt displacement correspondingly decreased, i.e., 1 μm (average sliding velocity, 32 μm/s) for 1/32 s, 0.5 μm (32 μm/s) for 1/64 s, and 0.2 μm (26 μm/s) for 1/128-s illumination. The fact that the displacement was proportional to the duration of the temperature pulse implies that steady-state sliding at the high temperature already was achieved at the shortest duration of 1/128 s. In the Huxley scheme (30), the steady-state velocity of unloaded sliding is given by $hg_2/2$, where h is the maximal distance over which a myosin head attached to actin can exert positive tension (power stroke) and g_2 is the rate of unbinding for the head that has undergone a power stroke and is exerting a negative tension. The increase in the sliding velocity by more than an order of magnitude upon heating likely resulted from a corresponding increase in g_2 rather than in h. That is, the rate of unbinding, which is presumably coincident with the ADP release under the present condition where ATP was abundant, increases sharply with temperature. The rate of head binding is likely to also increase with temperature, because otherwise the actin filament would tend to float into the medium, and the tension, proportional to the number of heads attached to the filament, would be greatly reduced whereas our experiment showed the contrary (see below). The high temperature coefficient of the rate of ATP hydrolysis (22), a 5-fold increase from 22°C to 30°C, is consistent with these views. Kitamura *et al.* (31) have reported that the sliding distance per head per ATP can be as long as 30 nm, a value difficult to explain with a conventional power stroke model. Even so, the distance per ATP is not critically dependent on temperature (31), and thus the unbinding rate has to increase with temperature.

The sliding velocities, v, obtained under the long and short temperature pulses were fitted with an Arrhenius equation,

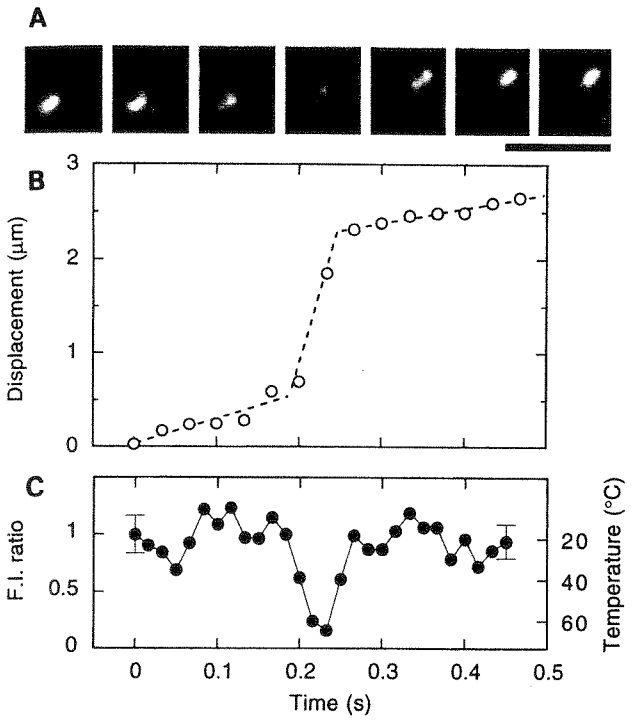

FIG. 4. Time course showing a reversible change in the sliding movement of an actin filament with a single temperature pulse. (*A*) Snapshots of a sliding actin filament (1.1 μm long) at 1/30-s intervals. A laser pulse of 1/16-s duration was given halfway at 0.19 s. (Scale bar, 5 μm.) (*B*) Time course of sliding movement of the actin filament; displacement of the centroid of the fluorescence image of the actin filament is shown by ○. (*C*) The temperature estimated from the average intensity of the filament at 1/60-s intervals. In this particular case, odd and even fields of interlaced images were analyzed separately. The coverslip temperature was kept at 18°C ± 1°C.

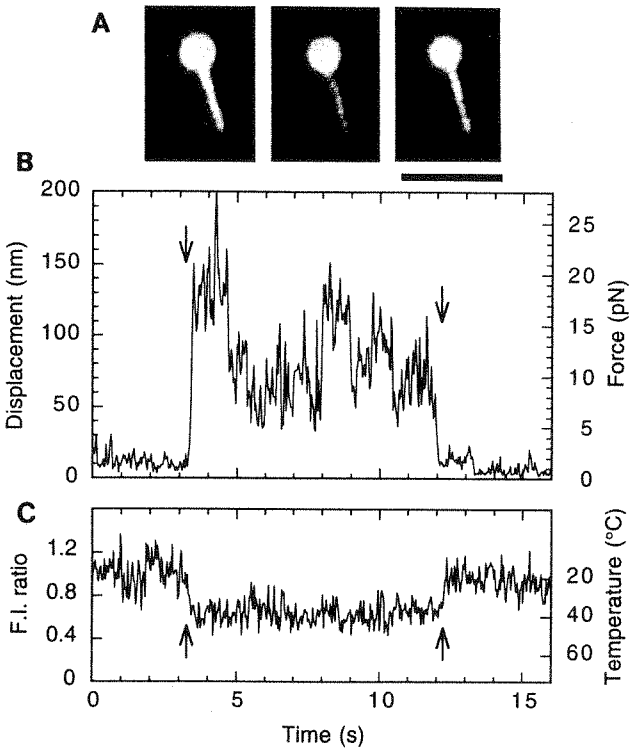

FIG. 5. Tension response of a single actin filament to a temperature pulse. (*A*) Fluorescence image of a bead-tailed actin filament (3.7 μm long) obtained by averaging 15 video frames for 0.5 s before, during, and after the temperature pulse, respectively, from left to right. The bead was coated with rhodamine-labeled BSA (23). The bead brightness is clipped in the central portion. (Scale bar, 5 μm.) (*B*) Time course of tension generation (displacement of the bead); a shutter for laser illumination was opened and closed at the times indicated by the left and right arrows, respectively. (*C*) Temperature was estimated from the fluorescence intensity profile obtained at the middle portion of the actin filament during the laser illumination and was 40°C ± 5°C (estimated by averaging the fluorescence intensity over 0.5 s). Only in this case, the fluorescence intensity gradually decreased with photobleaching because of prolonged laser illumination. The coverslip temperature was kept at 18°C ± 1°C.

$v(T) = v_0 \exp(-E_a/RT)$ where v_0 is a constant and R is the gas constant. The apparent activation energies, E_a, turned out to be 100 kJ/mol between 18°C and 30°C and 50 kJ/mol between 30°C and 45°C. These activation energies agree with those of prior reports (27–29), although the transition between the two temperature regions in the previous studies was at about 20°C rather than 30°C as shown here. The discrepancy could be the result of thermal deterioration that might have occurred at lower temperatures in the previous studies.

Next, to examine the potential of skeletal myosin for high sliding velocity, we used a higher ionic strength (50 mM KCl) (29), resulting in 52 ± 5 μm/s (n = 8) for a 0.5-s period at 46°C ± 7°C (n = 8) (estimated by averaging the fluorescence intensity over 0.5 s for each sample). The sliding velocity obtained here is the highest reported for skeletal myosin in a usual *in vitro* motility assay, although there is a report that the velocity of a large bead coated with myosin (65 μm in diameter) reached 500 μm/s at room temperature in a specially designed motility assay system (32). Faster sliding at higher ionic strength has been observed at lower temperatures (29). High salt may induce faster release of strongly bound heads (g_2 above) and/or the reduction of weakly binding interactions (33) that precede strong binding and that may impede sliding (34). The weakly binding interactions operate mainly at low ionic strengths (33).

We applied TPM to tension generation on single actin filaments. The tension record presented in Fig. 5 shows that an abrupt increase in tension (from 2 pN to 15–20 pN), in other words, sliding movement extending over a longer distance (10 nm to 100–150 nm) from the center of an optical trap, occurred after the temperature jump. A large tension fluctuation was observed around steady-state levels that were maintained for 1–2 s, during each of which the actin filament appeared to slide in one direction. The abrupt changes in the steady tension level, observed several times at 40°C in Fig. 5*B*, may be attributable to slight changes in the sliding direction resulting in a different number of heavy meromyosin molecules that can interact with the actin filament. The tension fluctuation did not correlate with the fluctuation of fluorescence intensity, indicating that the tension fluctuation is not attributable to temperature fluctuation. The average tension increased 5- to 10-fold with the increase in temperature from 18°C to 40°C and paralleled the increase in sliding velocity (Figs. 3 and 4).

In muscle fibers, it was reported that force rose by a factor of 2 to 3 (9, 11, 12, 35) between 5°C and 20°C but only by a factor of ≈1 (9, 12) or ≈1.5 (11) between 20°C and 40°C, much less than the 5- to 10-fold increase in our case. In principle, an increase in tension implies that each myosin head while attached to an actin filament exerts a larger force, and/or that a larger number of heads are attached at any instant. However, the former possibility, an increase in tension per attached head, is unlikely to be the major factor for the 5- to 10-fold increase in tension observed here. The number of attached heads must increase with temperature. Because the increase in the sliding velocity at no external load points to an increase in the rate of unbinding, as discussed above, the rate of head binding to actin has to increase with temperature more than the increase in the unbinding rate. This enormous increase in

binding rate is probably peculiar to the *in vitro* system. On the glass surface, unlike muscle interior, an actin filament tends to float into the medium by Brownian motion. Myosin heads cannot bind to the filament unless the filament happens to be close to the heads. The binding is thus cooperative in that binding of one head greatly facilitates the binding of neighboring heads. A slight increase in the affinity of myosin to actin, enough to account for the fiber data, will be amplified by this cooperativity.

As demonstrated by TPM, motor activity can be reversibly enhanced without denaturation upon raising the temperature above physiological levels (instantaneously, higher than 60°C). We can study the effects of various temperatures (and also the temperature gradient) at the same time for different molecules and different periods of time for the same molecules. The TPM described here can be improved to meet various applications. For example, the heat source of any size and shape can be made by microfabrication techniques. TPM in combination with real-time imaging of temperature on proteins should find broad applications in the studies of the energetics of protein–protein interactions and the response of cellular processes to thermal modulation, not only limited to cell motility but also on various aspects of cellular metabolism and signal transduction within and between cells.

This research was supported by Grants-in-Aid for Scientific Research, for Scientific Research on Priority Areas and for the High-Tech Research Center Project from the Ministry of Education, Science, Sports and Culture of Japan, by Core Research for Evolutional Science and Technology (CREST) of Japan Science and Technology Corporation and by a Waseda University Special Grant-in-Aid.

1. Funatsu, T., Harada, Y., Tokunaga, M., Saito, K. & Yanagida, T. (1995) *Nature (London)* **374,** 555–559.
2. Sase, I., Miyata, H., Corrie, J. E. T., Craik, J. S. & Kinosita, K., Jr. (1995) *Biophys. J.* **69,** 323–328.
3. Sase, I., Miyata, H., Ishiwata, S. & Kinosita, K., Jr. (1997) *Proc. Natl. Acad. Sci. USA* **94,** 5646–5650.
4. Ishijima, A., Kojima, H., Funatsu, T., Tokunaga, M., Higuchi, H., Tanaka, H. & Yanagida, T. (1998) *Cell* **92,** 161–171.
5. Svoboda, K., Schmidt, C. F., Schnapp, B. J. & Block, S. M. (1993) *Nature (London)* **365,** 721–727.
6. Finer, J. T., Simmons, R. M. & Spudich, J. A. (1994) *Nature (London)* **368,** 113–119.
7. Miyata, H., Hakozaki, H., Yoshikawa, H., Suzuki, N., Kinosita, K., Jr., Nishizaka, T. & Ishiwata, S. (1994) *J. Biochem.* **115,** 644–647.
8. Nishizaka, T., Miyata, H., Yoshikawa, H., Ishiwata, S. & Kinosita, K., Jr. (1995) *Nature (London)* **377,** 251–254.
9. Goldman, Y. E., McCray, J. A. & Ranatunga, K. W. (1987) *J. Physiol. (London)* **392,** 71–95.
10. Davis, J. S. & Harrington, W. F. (1987) *Proc. Natl. Acad. Sci. USA* **84,** 975–979.
11. Bershitsky, S. Y. & Tsaturyan, A. K. (1992) *J. Physiol. (London)* **447,** 425–448.
12. Ranatunga, K. W. (1996) *Biophys. J.* **71,** 1905–1913.
13. Liu, Y., Cheng, D. K., Sonek, G. J., Berns, M. W., Chapman, C. F. & Tromberg, B. J. (1995) *Biophys. J.* **68,** 2137–2144.
14. Kolodner, P. & Tyson, J. A. (1982) *Appl. Phys. Lett.* **40,** 782–784.
15. Romano, V., Zweig, A. D., Frenz, M. & Weber, H. P. (1989) *Appl. Phys. B* **49,** 527–533.
16. Zohar, O., Ikeda, M., Shinagawa, H., Inoue, H., Nakamura, H., Elbaum, D., Alkon, D. L. & Yoshioka, T. (1998) *Biophys. J.* **74,** 82–89.
17. Washizu, M., Kurosawa, O., Suzuki, S. & Shimamoto, N. (1996) *SPIE* **2716,** 133–143.
18. Kinosita, K., Jr., Itoh, H., Ishiwata, S., Hirano, K., Nishizaka, T. & Hayakawa, T. (1991) *J. Cell Biol.* **115,** 67–73.
19. De la Cruz, E. M. & Pollard, T. D. (1994) *Biochemistry* **33,** 14387–14392.
20. Nishizaka, T., Yagi, T., Tanaka, Y. & Ishiwata, S. (1993) *Nature (London)* **361,** 269–271.
21. Yanagida, T., Nakase, M., Nishiyama, K. & Oosawa, F. (1984) *Nature (London)* **307,** 58–60.
22. Harada, Y., Sakurada, K., Aoki, T., Thomas, D. D. & Yanagida, T. (1990) *J. Mol. Biol.* **216,** 49–68.
23. Suzuki, N., Miyata, H., Ishiwata, S. & Kinosita, K., Jr. (1996) *Biophys. J.* **70,** 401–408.
24. Kron, S. J., Toyoshima, Y. Y., Uyeda, T. Q. P. & Spudich, J. A. (1991) *Methods Enzymol.* **196,** 399–416.
25. Sellers, J. R. & Kachar, B. (1990) *Science* **249,** 406–408.
26. Tanaka, Y., Ishijima, A. & Ishiwata, S. (1992) *Biochim. Biophys. Acta* **1159,** 94–98.
27. Anson, M. (1992) *J. Mol. Biol.* **224,** 1029–1038.
28. Winkelmann, D. A., Bourdieu, L., Ott, A., Kinose, F. & Libchaber, A. (1995) *Biophys. J.* **68,** 2444–2453.
29. Homsher, E., Wang, F. & Sellers, J. R. (1992) *Am. J. Physiol.* **262,** C714–C723.
30. Huxley, A. F. (1957) *Prog. Biophys. Biophys. Chem.* **7,** 255–318.
31. Kitamura, K., Tokunaga, M., Hikikoshi-Iwane, A. & Yanagida, T. (1999) *Nature (London)* **397,** 129–134.
32. Suda, H. & Ishikawa, A. (1997) *Biochem. Biophys. Res. Commun.* **237,** 427–431.
33. Brenner, B. (1987) *Annu. Rev. Physiol.* **49,** 655–672.
34. Tawada, K. & Sekimoto, K. (1991) *J. Theor. Biol.* **150,** 193–200.
35. Bershitsky, S. Y., Tsaturyan, A. K., Bershitskaya, O. N., Mashanov, G. I., Brown, P., Burns, R. & Ferenczi, M. A. (1997) *Nature (London)* **388,** 186–190.

Tropomyosin Modulates pH Dependence of Isometric Tension

Hideaki Fujita* and Shin'ichi Ishiwata*#§¶

*Department of Physics, School of Science and Engineering, #Advanced Research Institute for Science and Engineering, and §Materials Research Laboratory for Bioscience and Photonics, Waseda University, Tokyo 169-8555, and ¶Core Research for Evolutional Science and Technology, "Genetic Programming" Team 13, Kawasaki 216-0001 Japan

ABSTRACT We investigated the effect of pH on isometric tension in actin filament-reconstituted and thin filament-reconstituted bovine cardiac muscle fibers in the pH range of 6.0–7.4. Thin filament was reconstituted from purified G-actin with either bovine cardiac tropomyosin (Tm) or rabbit skeletal Tm in conjunction with cardiac or skeletal troponin (Tn). Results showed that isometric tension decreased linearly with a decrease in pH. The slope of the pH-tension relation, $\Delta F/\Delta$pH (Δrelative tension/Δunit pH), was 0.28 and 0.44 in control cardiac fibers and skeletal fibers, respectively. In actin filament-reconstituted fibers without regulatory proteins, $\Delta F/\Delta$pH was 0.62, namely larger than that in cardiac or skeletal fibers. When reconstituted with cardiac Tm-Tn complex (nTm), $\Delta F/\Delta$pH recovered to 0.32, close to the value obtained in control cardiac fibers. When reconstituted with skeletal nTm, $\Delta F/\Delta$pH recovered to 0.48, close to the value for control skeletal fibers. To determine whether Tm or Tn is responsible for the inhibitory effects of nTm on the tension decrease caused by reduced pH, thin filament was reconstituted with cardiac Tm and skeletal Tn, or with skeletal Tm and cardiac Tn. When cardiac Tm was used, pH dependence of isometric tension coincided with that of control cardiac fibers. When skeletal Tm was used, the pH dependence coincided with that of control skeletal fibers. Furthermore, closely similar results were obtained in fibers reconstituted with actin and either cardiac or skeletal Tm without Tn. These results demonstrate that Tm but not Tn modulates the pH dependence of active tension.

INTRODUCTION

It is known that intracellular pH decreases when muscle fatigues, and in the onset of ischemia and hypoxia. A decrease in pH causes decreases in active tension, shortening velocity, and Ca^{2+} sensitivity in skinned muscle fibers (Dawson et al., 1978; Edman and Matiazzi, 1981; Donaldson and Hermansen, 1978; Fabiato and Fabiato, 1978; Robertson and Kerrick, 1979; Chase and Kushmerick, 1988; Cooke et al., 1988; Metzger and Moss, 1987). Moreover, ATPase activity increases when pH is reduced (Curtin et al., 1988), resulting in an increase in tension cost (Godt and Kentish, 1989; Potma et al., 1994).

The degree of the effect of reduced pH depends on the muscle type. For example, the rightward shift in the pCa-tension relationship is greater in cardiac than in skeletal muscle (Donaldson and Hermansen, 1978; Metzger et al., 1993). Furthermore, the decrease in maximum isometric tension is greater in skeletal muscle with predominantly fast twitch fibers than in soleus muscle, which has predominantly slow twitch fibers (Metzger and Moss, 1987; Potma et al., 1994). Because different isoforms of myofilament proteins are expressed in these fiber types (Nadal-Ginard and Mahdavi, 1989), this difference in pH dependence among different fiber types may be caused by a difference in their protein isoforms. It is known that different Tn isoforms are involved in the different pH effects on Ca^{2+} sensitivity (Solaro et al., 1986, 1989; Palmer and Kentish, 1994; Kawashima et al., 1995, Parsons et al., 1997). However, it is not known whether different Tm isoforms are involved in the difference in pH dependence on maximum isometric tension. It may be possible to examine this by using muscle fibers prepared from transgenic animals expressing Tm isoforms (Palmiter et al., 1996). In the present study, we investigated this possibility through the use of thin filament-reconstituted cardiac muscle fibers (Fujita et al., 1996; Fujita and Ishiwata, 1998).

The thin filament in skeletal or cardiac muscle fibers can be selectively removed using calf plasma gelsolin, an actin filament-severing protein (Funatsu et al., 1990, 1993; Yasuda et al., 1995). Actin filaments in such thin filament-removed cardiac muscle fibers can be fully reconstituted by adding exogenous actin (Fujita et al., 1996; Fujita and Ishiwata, 1998; Ishiwata et al., 1998). Furthermore, thin filament possessing full Ca^{2+} sensitivity can then be reconstituted by adding regulatory proteins Tm and Tn to the actin filament-reconstituted fibers. We found that, as in control muscle fibers, pH dependence of tension development in actin filament-reconstituted bovine cardiac muscle fibers in the absence of regulatory proteins was nearly linear in the pH range 6.0–7.4, but that the slope was steeper. The original slope was regained by reconstitution with bovine cardiac nTm (Tm and Tn). Furthermore, fibers reconstituted with rabbit skeletal nTm showed a pH dependence resembling that of rabbit skeletal muscle. Similar modulation of pH dependence of isometric tension was also observed in fibers reconstituted with actin and Tm but without Tn. These results demonstrate that $\Delta F/\Delta$pH depends on the type of Tm isoform, such that Tm modifies the pH dependence of isometric tension.

Received for publication 9 February 1999 and in final form 7 June 1999.

Address reprint requests to Dr. Shin'ichi Ishiwata, Department of Physics, School of Science and Engineering, Waseda University, 3-4-1 Okubo, Shinjuku-ku, Tokyo 169-8555, Japan. Tel.: +81-3-5286-3437; Fax: +81-3-3200-2567; E-mail: ishiwata@mn.waseda.ac.jp.

0006-3495/99/09/1540/07 $2.00

MATERIALS AND METHODS

Solutions

The solutions used were as follows: rigor solution, 170 mM KCl, 1.0 mM $MgCl_2$, 1.0 mM EGTA, and 10 mM 3-(*N*-morpholino)propanesulfonic acid (MOPS) (pH 7.0); relaxing solution, 117 mM KCl, 5.0 mM $MgCl_2$, 4.0 mM ATP, 1.0 mM EGTA, 10 mM MOPS (pH 7.0), and 20 mM 2,3-butanedione 2-monoxime (BDM); contracting solution, 117 mM KCl, 4.25 mM $MgCl_2$ (2.2 mM free Mg^{2+}), 2.2 mM ATP (2.0 mM $MgATP^{2-}$), 2.0 mM EGTA, 20 mM MOPS (pH 6.6–7.4) or 2-(*N*-morpholino)ethanesulfonic acid (MES) (pH 6.0–6.4), and 2.0 mM $CaCl_2$. ATP (disodium salt) was purchased from Boehringer Mannheim (Mannheim, Germany); EGTA, MOPS, and MES were from Dojindo Laboratories (Kumamoto, Japan). Tetramethyl rhodamine-5-iodoacetamide (Rh-IA) and fluorescein phalloidin (Fl-Ph) were purchased from Molecular Probes (Eugene, OR). Other chemicals were of reagent grade.

Muscle fibers and proteins

Glycerinated bovine cardiac muscle fibers and rabbit white skeletal muscle fibers were prepared in a solution composed of 50% (v/v) glycerol, 0.5 mM $NaHCO_3$, 5.0 mM EGTA, and 2.0 mM leupeptin. Glycerinated fibers were stored at −20°C and used within 2–8 weeks. Bovine plasma gelsolin was prepared according to the method of Kurokawa et al. (1990). Actin was extracted from acetone powder (Kondo and Ishiwata, 1976) of bovine cardiac muscle according to the method of Spudich and Watt (1971). Purified G-actin was stored at 0°C and used within 1 week. Tm, Tn, and nTm were prepared from bovine cardiac muscle and from rabbit white skeletal muscle according to the method of Ebashi et al. (1968) and purified using DEAE Sephadex A-25 (Pharmacia, Sweden). Tm labeled with Rh-IA (9% labeled) was prepared according to the method of Ishii and Lehrer (1990).

Tension measurement

A thin muscle bundle (~1 mm in length, ≤60 μm in diameter) was carefully stripped from a glycerinated bovine cardiac muscle fiber with a pair of forceps under a stereomicroscope just before experiments. To prepare a suitably thin bundle, dissection was carried out in glycerol solution at about −10°C (Fukuda et al., 1996). Both ends of the bundle were fixed to thin tungsten wires with enamel (commercial nail polish for cosmetic use), one of which was attached to a tension transducer (AE-801; SensoNor a.s, Holten, Norway). The muscle bundle was then immersed in rigor solution containing 1% Triton X-100 for 20 min to remove residual portions of the membrane system. After Triton X-100 was washed out with rigor solution, the bundle was immersed in the relaxing solution. Active tension was measured with a pen recorder (VP-6533A; National, Japan) by immersing the muscle bundle in the contracting solution. Active tension of control cardiac muscle fibers were 60–80 kN/m^2 (cf. Fujita et al., 1996). The maximum activated tension in control and actin filament-reconstituted fibers did not change with the addition of creatine kinase (1.0 mg/ml)/creatine phosphate (10 mM), suggesting that ATP depletion within the muscle bundles did not occur, probably because the diameter of the muscle bundle was small (≤60 μm) and the solution was continuously stirred (Yamaguchi, 1998). The measurement chamber used was a silicon-coated aluminum block (10 cm × 10 cm × 1 cm) with several small wells (7 mm in diameter) filled with ~0.4 ml each of experimental solutions (Horiuti, 1986). The bundle was immersed just below the surface at the deepest part of the solution droplet in the well such that only 1–2 s was required for the transfer of the bundle from one solution to another. Measurements were carried out at 25°C.

Removal and reconstitution of actin filaments

Removal and reconstitution of the actin filament were performed as previously described (Fujita et al., 1996; Fujita and Ishiwata, 1998; Ishiwata et al., 1998). In brief, thin cardiac muscle bundles were immersed in contracting solution containing 20 mM BDM (to suppress tension development during gelsolin treatment, which requires Ca^{2+}) and 0.3 mg/ml gelsolin at 2°C for 80 min to selectively remove thin filament. We confirmed that no active tension developed after gelsolin treatment. The bundles were then immersed in actin-polymerizing solution (80 mM KI, 4.0 mM $MgCl_2$, 4.0 mM ATP, 4.0 mM EGTA, 20 mM BDM, and 20 mM K-phosphate, pH 7.0) containing 1 mg/ml purified G-actin, which was mixed just before use. G-actin in the polymerizing solution was freshly prepared just before use and exchanged every 7 min to avoid nucleation. Actin polymerization was performed for a total of 28 min (7 min × 4). Removal and reconstitution procedures were carried out at 2°C. Relaxation of the actin filament-reconstituted fibers was achieved by immersing the fibers in relaxing solution containing 20 mM BDM. Activation of actin filament-reconstituted fibers was achieved by washing out BDM relaxing solution with contracting solution. There was no Ca^{2+} sensitivity in actin filament-reconstituted fibers.

Reconstitution of thin filaments

To reconstitute the thin filament, actin filament-reconstituted fibers were immersed in relaxing solution containing 3 mg/ml nTm and 20 mM BDM at 2°C for 12 h. To reconstitute fibers with skeletal Tm and cardiac Tn, or with cardiac Tm and skeletal Tn (chimera nTm fibers), the fibers were first immersed in relaxing solution containing 1.5 mg/ml Tm and 20 mM BDM at 2°C for 12 h. The fibers were then immersed in relaxing solution containing 1.5 mg/ml Tn and 20 mM BDM at 2°C for 5 h. These thin filament-reconstituted fibers showed no active tension development in the absence of Ca^{2+}, but did develop tension when Ca^{2+} was added in the absence of BDM. Fibers that developed less than 70% of the tension obtained before reconstitution with regulatory proteins were not used.

To confirm the binding of Tm to the reconstituted actin filaments in the fibers, thin filaments were reconstituted with Rh-IA-labeled Tm instead of unlabeled Tm according to the same procedure as described above. The fibers were then fixed with relaxing solution containing 1% formaldehyde for 30 min and stained with 6.6 μM Fl-Ph in relaxing solution for 5 h at 2°C to visualize actin filaments. They were then mounted on a coverslip and washed with relaxing solution containing 4.5 mg/ml glucose, 0.22 mg/ml glucose oxidase, 0.036 mg/ml catalase, and 10 mM dithiothreitol. Preparations were observed under a laser scanning confocal microscope equipped with a 25-mW Ar laser at 488 nm (Fluoview-IX/AR; Olympus Co., Tokyo). No crossover between fluorescence images of rhodamine (>610 nm; red) and fluorescein (510–540 nm; green) was detectable. As shown in Fig. 1, *A* and *B*, the distribution of Rh-IA was identical to that of Fl-Ph except for the weak fluorescence at the Z line, showing that incorporated Tm was bound to actin filaments except at the Z line. Control cardiac muscle fibers were also incubated with Rh-IA-labeled Tm for 12 h at 2°C in BDM relaxing solution and then stained with Fl-Ph after formaldehyde fixation. As shown in Fig. 1, *C* and *D*, fluorescence of Rh-IA was not detectable, indicating that Tm was not incorporated into the thin filaments in control fibers.

RESULTS

pH dependence of isometric tension in actin filament-reconstituted and thin filament-reconstituted fibers

Fig. 2 shows pen traces of isometric tension measured at various pH values in actin filament-reconstituted fibers. First, glycerinated cardiac muscle fibers were treated with gelsolin (*arrow G* in Fig. 2). Removal of thin filaments was verified by measuring active tension, which was negligible after gelsolin treatment. The muscle bundles were then treated with actin-polymerizing solution (*arrow A* in Fig. 2),

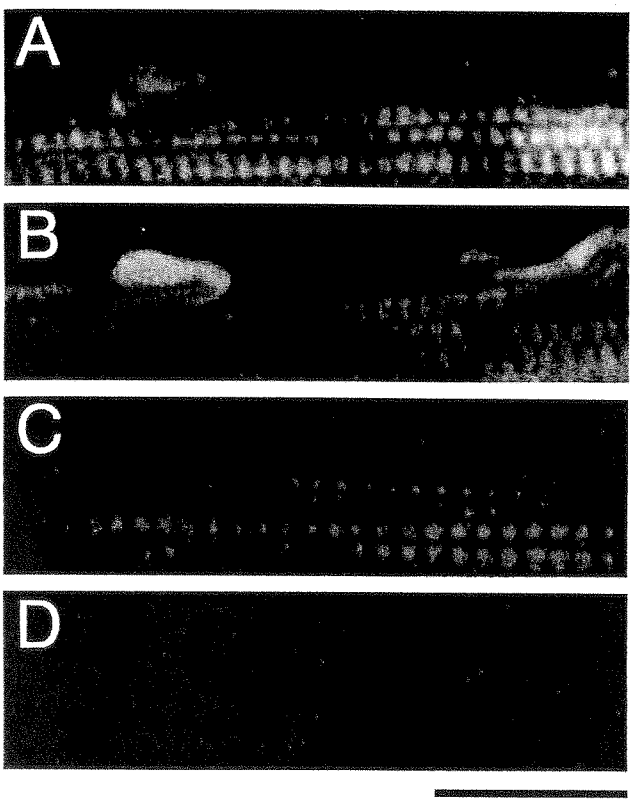

FIGURE 1 Confocal fluorescence micrographs showing the distribution of actin filaments labeled with Fl-Ph (*A, C*) and Tm labeled with Rh-IA (*B, D*) in thin filament-reconstituted (*A, B*) and control (*C, D*) cardiac muscle fibers. Bar, 20 μm.

and the pH dependence of active tension was measured. pH was increased stepwise from 6.0 to 7.0 at a 0.2 interval, and decreased again stepwise to 6.0. Active tension increased in proportion to the increase in pH and decreased in proportion to the decrease in pH. Relative tension was calculated by dividing average tension by that at pH 7.0. The stability and durability of the reconstituted muscle fibers with respect to contractile properties were indistinguishable from those of control fibers (Fig. 2).

The pH dependence of isometric tension in the actin filament- and thin filament-reconstituted fibers is shown in Fig. 3. In control bovine cardiac and rabbit skeletal muscle fibers, the pH-tension relation was nearly linear in the pH range 6.0–7.4. The slope of the pH-tension relation was greater in skeletal than in cardiac muscle fibers, with $\Delta F/\Delta$pH of 0.28 for cardiac (Fig. 3, *empty circles, thick line*) and 0.44 for skeletal muscle fibers (Fig. 3, *empty triangles, thin line*). $\Delta F/\Delta$pH in actin filament-reconstituted fibers without regulatory proteins was 0.62, the greatest value of all combinations tested (Fig. 3, *empty squares, dotted line*). When thin filament was reconstituted with bovine cardiac nTm, $\Delta F/\Delta$pH decreased to 0.32, close to the control value (Fig. 3, *filled circles, thick broken line*). The thin filament-reconstituted fibers did not develop active tension in the absence of Ca^{2+}. These results indicate that the regulatory proteins suppressed the decrease in tension caused by decreasing pH. In fibers reconstituted with rabbit skeletal nTm, $\Delta F/\Delta$pH was 0.48, close to that of the control skeletal fibers (Fig. 3, *filled triangles, thin broken line*).

pH-tension relation in fibers reconstituted with actin and chimera nTm

To determine whether Tm or Tn is responsible for the pH dependence, the pH-tension relation was examined in fibers reconstituted with chimera nTm, i.e., either cardiac Tm (cTm) and skeletal Tn (sTn), or skeletal Tm (sTm) and cardiac Tn (cTn). In fibers reconstituted with cTm + sTn, the relation resembled that in cardiac muscle fibers (Fig. 4, *half-filled circle*), with a $\Delta F/\Delta$pH value of 0.29, whereas in those reconstituted with sTm + cTn it resembled that in skeletal muscle fibers (Fig. 4, *half-filled triangle*), with a $\Delta F/\Delta$pH value of 0.44. These results indicate that the pH-tension relation is modified by Tm but not by Tn.

To confirm that the chimera nTm fibers were constructed successfully, the pCa-tension relation was examined. Fibers reconstituted with sTm + cTn showed a pCa-tension relation indistinguishable from that of control cardiac muscle fibers at pH 7.0 (Fig. 5 *A*) and pH 6.4 (Fig. 5 *B*). At pH 7.0, the Hill coefficient (n_H) for control cardiac and chimera nTm fibers was 1.9 and 2.0, respectively, and the pCa_{50} value, an indicator of Ca^{2+} sensitivity, was 6.05 and 6.1, respectively. The respective values at pH 6.4 were 2.0 and 2.0, and 5.6 and 5.55. A rightward shift in the pCa-tension relation by a decrease in pH was observed in control and chimera fibers to the same degree. The Hill coefficient did not change significantly with a decrease in pH from 7.0 to 6.4.

pH-tension relation in fibers reconstituted with actin and Tm

Next, we examined the pH-tension relation of fibers reconstituted with actin and Tm. Tm-reconstituted fibers generated active tension in a Ca^{2+}-insensitive manner because of the lack of Tn. In cTm-reconstituted fibers, $\Delta F/\Delta$pH was 0.33 (Fig. 6, *empty circle*), similar to that of control cardiac fibers, whereas in sTm-reconstituted fibers it was 0.49 (Fig. 6, *filled circle*), similar to that of control skeletal fibers. $\Delta F/\Delta$pH values for various types of muscle models thus obtained are summarized in Table 1. The difference in the pH-tension relation between different Tm isoforms was statistically significant, whereas there was no statistically significant difference between different Tn isoforms when the same Tm isoform was used.

DISCUSSION

Experiments using thin filament-reconstituted fibers

Actin polymerization was performed for only 28 min (7 min × 4) instead of the 42 min (7 min × 6) used in the

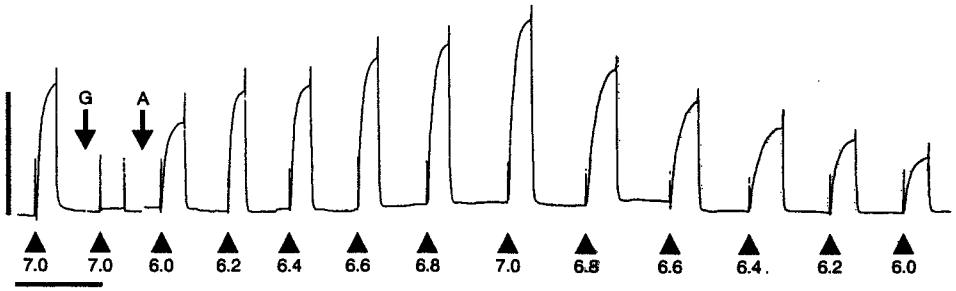

FIGURE 2 Recordings of isometric tension at varying pH in actin filament-reconstituted cardiac muscle fibers. After measurement of control tension, fibers were immersed in contracting solution containing 0.3 mg/ml gelsolin and 20 mM BDM for 80 min at 2°C (*arrow G*). After confirmation that fibers developed no active tension after gelsolin treatment, they were immersed in actin polymerizing solution containing 1 mg/ml G-actin for a total of 28 min (7 min × 4) at 2°C (*arrow A*). Arrowheads indicate solution change. pH values of contracting solutions are indicated below the arrowheads. Spikes are artifacts due to solution change. Active tension at varying pH was measured at 25°C. Relaxation was obtained by immersing the fiber in relaxing solution containing 20 mM BDM at 2°C. Vertical and horizontal bars, 2×10^{-4} N and 2 min, respectively.

original work (Fujita et al., 1996) to minimize fiber damage due to repeated high-tension developments. Consequently, the average tension developed in the actin filament-reconstituted fibers was closely similar to that in the control fibers. The only problem with this actin filament reconstitution method is that it was difficult to control the extent of tension recovery after reconstitution, which varied between preparations (Fujita et al., 1996). Because this variability makes it difficult to quantitatively analyze the difference between active tension of control fibers and actin filament-reconstituted fibers, experiments should have been designed to compare the properties of reconstituted and control fibers, using the same actual fiber. Here, the decrease in active tension with decreasing pH was compared between actin (thin) filament-reconstituted fibers and their controls. These properties were reproducible and reliable, as reported here.

In the present study, we succeeded in constructing chimera nTm fibers composed of either skeletal Tm and cardiac Tn or vice versa. To construct chimera nTm-reconstituted fibers, actin filament-reconstituted fibers were first

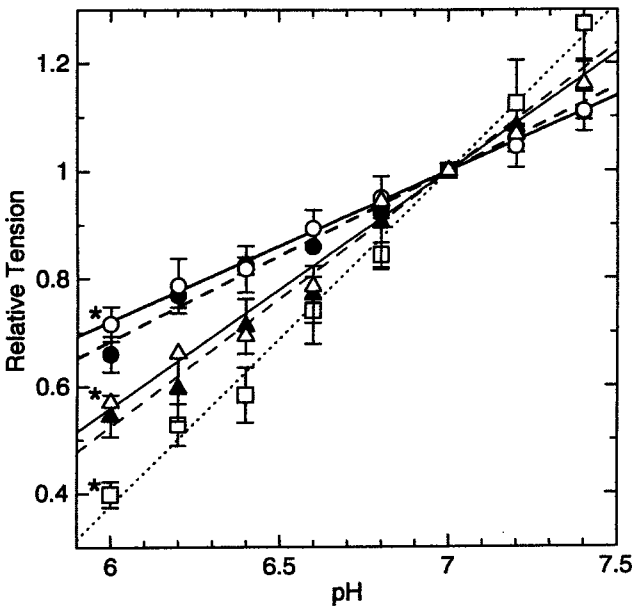

FIGURE 3 Effect of pH on isometric tension in control cardiac muscle fibers (*empty circles, thick line*), control skeletal muscle fibers (*empty triangles, thin line*), actin filament-reconstituted muscle fibers (*empty squares, dotted line*), thin filament-reconstituted fibers with cardiac nTm (*filled circles, thick broken line*), and thin filament-reconstituted fibers with skeletal nTm (*filled triangles, thin broken line*). Relative tension was normalized to that at pH 7.0. Lines are fitted by least-squares fit. Vertical bars show SD calculated from three to five data points. Active tension was measured at 25°C. The difference between any two data points marked with * at pH 6.0 was statistically significant ($p < 0.001$ by Student's *t*-test).

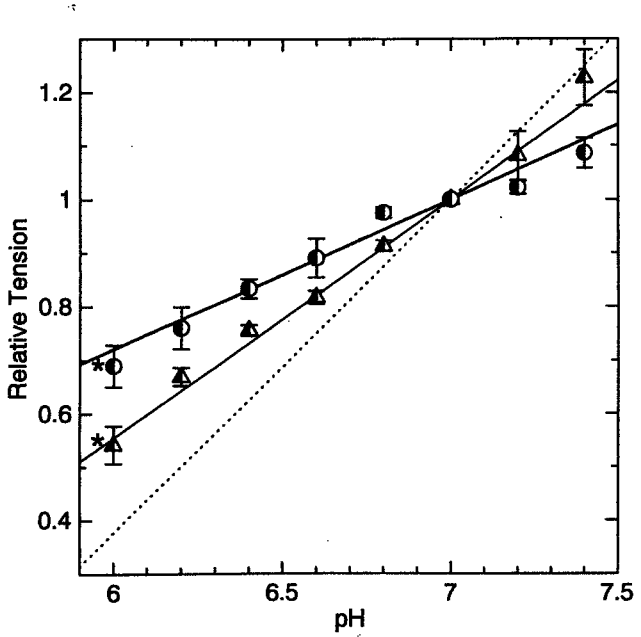

FIGURE 4 Effect of pH on isometric tension in fibers reconstituted with cTm and sTn (*half-filled circles*), and with sTm and cTn (*half-filled triangles*). Thick, thin, and dotted lines show, respectively, the fitted lines for control cardiac, control skeletal, and actin filament-reconstituted fibers obtained in Fig. 3. Relative tension was normalized to that at pH 7.0. Vertical bars show SD calculated from three to five data points. Active tension was measured at 25°C. The difference between two data points marked with * at pH 6.0 was statistically significant ($p < 0.01$ by Student's *t*-test).

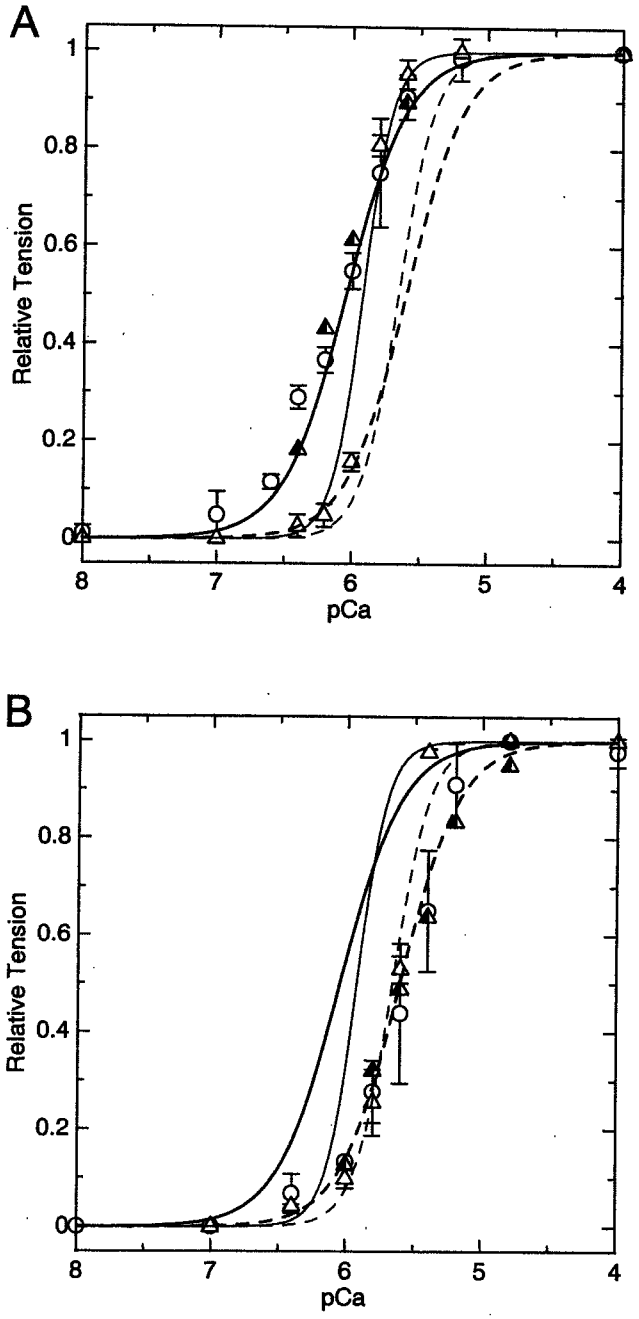

FIGURE 5 pCa-tension relation of control cardiac (*empty circles*), control skeletal (*empty triangles*), and (sTm + cTn)-reconstituted fibers (*half-filled triangles*) at pH 7.0 (*A*) and pH 6.4 (*B*). Thick and thin lines are the curves fitted for control cardiac and skeletal fibers (*solid line*, pH 7.0; *broken line*, pH 6.4), respectively. Relative tension was normalized to that at pCa 4.0. Vertical bars show SD calculated from three to five data points. Active tension was measured at 25°C.

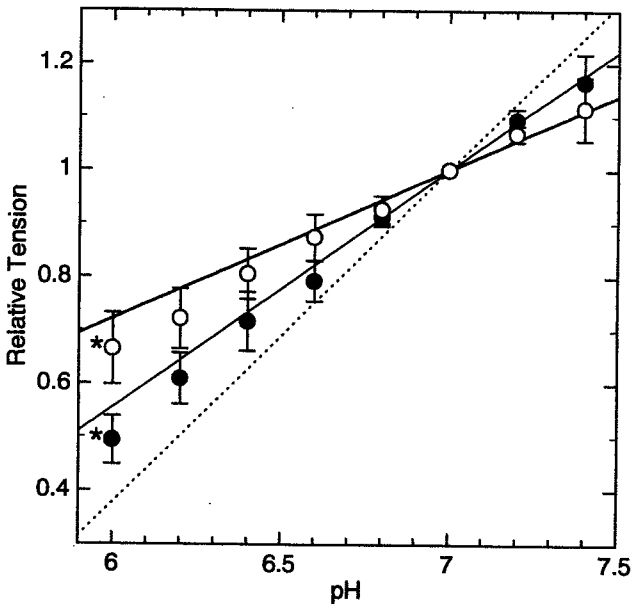

FIGURE 6 Effect of pH on isometric tension in fibers reconstituted with cTm (*empty circles*) and sTm (*filled circles*). Thick, thin, and dotted lines show, respectively, fitted lines for control cardiac, control skeletal, and actin filament-reconstituted fibers obtained in Fig. 3. Relative tension was normalized to that at pH 7.0. Vertical bars show SD calculated from three to five data points. Active tension was measured at 25°C. The difference between two data points marked with * at pH 6.0 was statistically significant ($p < 0.01$ by Student's *t*-test).

reconstituted with Tm and then with Tn so that nonspecific binding of Tn to actin filaments was avoided (Ishiwata and Kondo, 1978). The purity of added proteins was confirmed by sodium dodecyl sulfate-polyacrylamide gel electrophoresis before reconstitution (data not shown), but the quality of reconstitution (e.g., the stoichiometry of actin, Tm, and Tn) in the reconstituted fibers could not be evaluated by sodium dodecyl sulfate-polyacrylamide gel electrophoresis because of the small amount of proteins. To confirm the reconstitution of thin filaments, the pCa-tension relation was therefore examined. On the basis that both the pCa_{50} value and the Hill coefficient in the chimera nTm fibers were determined by the type of Tn (Fig. 5), we conclude that the function of thin filaments was fully recovered.

Maximum decrease in active tension by decreased pH in actin filament-reconstituted fibers

In control cardiac muscle fibers, active tension decreased linearly with a decrease in pH in the range of pH 6.0–7.4 (Fig. 3, *empty circles*), which is consistent with the previous results (Metzger and Moss, 1987; Godt and Kentish, 1989; Solaro et al., 1989). Although a linear decrease in active

TABLE 1 $\Delta F/\Delta pH$ values for various types of muscle model

Control			Thin filament-reconstituted		
			cTn	sTn	no Tn
Cardiac	0.28*	cTm	0.32*	0.29#	0.33§
Skeletal	0.44*	sTm	0.44#	0.48*	0.49§
Actin reconstituted	0.62*				

*Taken from Fig. 3.
#Taken from Fig. 4.
§Taken from Fig. 6.

tension by reduced pH was also observed in actin filament-reconstituted fibers (Fig. 3, *empty squares*), $\Delta F/\Delta pH$ was more than twice that of control cardiac fibers. Because the only difference between control cardiac muscle fibers and actin filament-reconstituted fibers is the presence of regulatory proteins (Fujita et al., 1996), the difference in $\Delta F/\Delta pH$ should be related to regulatory proteins. Given that isometric tension is thought to be proportional to the population of attached cross-bridges, the decrease in active tension with reduced pH may be the result of cross-bridge detachment.

Several factors can be considered in the regulation of the number of attached cross-bridges. Myosin has a positively charged loop (called loop 2) in the upper 50-kDa domain, and actin has four corresponding negatively charged acidic residues located at the N-terminus in subdomain 1. These are assumed to make the initial contact in the actin-myosin interaction (Chaussepied and Van Dijk, 1999). Additionally, there are many histidine residues that have neutral pK values. In theory, a decrease in pH from 7.0 to 6.0 should decrease the proportion of negatively charged carboxyl groups (assume pK 4.7) by ~5% and increase that of positively charged imido groups (assume pK 6.5) by ~70%. The large decrease in active tension by reduced pH in the actin filament-reconstituted fibers may be primarily attributed to the effect of these changes in surface charge on the actin-myosin interaction. Changes in the charge distribution of actin, myosin, or both may also modulate secondary factors that affect the actin-myosin interaction, such as the distance between thick and thin filaments.

Modulation of the pH dependence of active tension by regulatory proteins

Given that the protein composition of skeletal nTm-reconstituted fibers is considered to be the same as that of cardiac muscle fibers with the exception of regulatory proteins, the results shown in Fig. 3 indicate that the differing pH dependency among muscle types is attributable to regulatory protein isoforms. We therefore conclude that the type of regulatory proteins modulates the pH dependence of active tension: the pH dependence of fibers reconstituted with sTm and cTn resembled that of the control skeletal muscle fibers (Fig. 4, *half-filled triangle*), whereas fibers reconstituted with cTm and sTn resembled that of control cardiac muscle fibers (Fig. 4, *half-filled circle*). These findings demonstrate that the pH dependence of active tension is modulated by Tm, and that Tn has no effect on this variable.

When Tm alone (cardiac or skeletal) was added to actin filament-reconstituted fibers, $\Delta F/\Delta pH$ decreased in both cases (Fig. 6). The effect was similar with nTm. These results support the conclusion that Tm alone modulates the pH dependence of active tension. It has been reported that the binding of Tm to actin is stabilized by lowering pH (Tanaka, 1972). The difference among Tm isoforms in modulating the pH dependence of active tension may be due to differences in the stability of Tm isoforms binding to actin filaments.

Three-dimensional modeling of thin filament showed that Tm does not cover the charged group on actin's surface in the presence or absence of Ca^{2+} (Lehman et al., 1995). However, because negative staining was used to visualize Tm, which may alter its location, the possibility remains that Tm is closer to the charged residues in vivo. In addition, the effect of Tm on the pH-tension relation may be attributable to allosteric regulation of charge distribution on actin filaments. That is, the presence of Tm may affect the accessibility of charged groups on actin, even though they are distant from the area covered by Tm.

Mammalian Tm has α and β subunits, which can be arranged as two isomers, $\alpha\alpha$ and $\alpha\beta$ (Eisenberg and Kielley, 1974). The amino acid sequence of these α and β subunits in rabbit skeletal and cardiac muscle is identical (Stone and Smillie, 1977; Lewis and Smillie, 1980). The subunits differ by 39 residues, including two residues, giving a more negative net charge on the β (Mak et al., 1979). Because the α:β ratio depends on muscle type (in general, the ratio of α to β in cardiac muscle is larger than that in skeletal muscle), the modulation of pH dependence of isometric tension in actin filament-reconstituted fibers may also be due to differences in charge distribution on Tm isoforms.

The present study used rabbit fast skeletal Tm and bovine cardiac Tm, both of which are a mixture of α and β Tm. It is not clear whether the difference in pH dependence of active tension between skeletal and cardiac Tm (Figs. 3 and 4) results from a difference in skeletal and cardiac Tm or in rabbit and bovine Tm. However, this ambiguity does not change our major conclusion that Tm modulates the pH dependence of active tension. The molecular basis of Tm's modulation of pH dependence of active tension may be clarified by reconstitution of thin filaments by the use of purified α and β Tm or mutant Tm with different charge distribution. This awaits further investigation.

The smaller decrease in active tension in an acidic environment in cardiac muscle than in skeletal muscle may have developed during the process of evolution. The ability to survive an acidic environment is of particular advantage for cardiac muscle cells, which are often subject to lowered pH induced by cardiac hypoxia and ischemia.

We thank Prof. M. Kawai of the University of Iowa for his critical reading of the manuscript.

This research was partly supported by Grants-in-Aid for Scientific Research, for Scientific Research on Priority Areas, and for the High-Tech Research Center Project from the Ministry of Education, Science, Sports, and Culture of Japan; and by Grants-in-Aid from Japan Science and Technology (CREST). HF is a recipient of a Research Fellowship from the Japan Society for the Promotion of Science for Young Scientists.

REFERENCES

Chase, P. B., and M. J. Kushmerick. 1988. Effects of pH on contraction of rabbit fast and slow skeletal muscle fibers. *Biophys. J.* 53:935–946.

Chaussepied, P., and J. Van Dijk. 1999. Role of charges in actomyosin interactions. *In* Molecular Interactions of Actin. C. G. dos Remedios and D. D. Thomas, editors. Springer-Verlag, Heidelberg, in press.

Cooke, R., K. Franks, G. B. Luciani, and E. Pate. 1988. The inhibition of rabbit skeletal muscle contraction by hydrogen ions and phosphate. *J. Physiol. (Lond.).* 395:77–97.

Curtin, N. A., K. Kometani, and R. C. Woledge. 1988. Effects of intracellular pH on force and heat production in isometric contraction of frog muscle fibres. *J. Physiol. (Lond.).* 396:93–104.

Dawson, M. J., D. G. Gadian, and D. R. Wilkie. 1978. Muscular fatigue investigated by phosphorus nuclear magnetic resonance. *Nature.* 274: 861–866.

Donaldson, S. K., and L. Hermansen. 1978. Differential, direct effects of H^+ on Ca^{2+}-activated force of skinned fibres from the soleus, cardiac and adductor magnus muscle of rabbits. *Pflügers Arch.* 367:55–65.

Ebashi, S., A. Kodama, and F. Ebashi. 1968. Troponin. I. Preparation and physiological function. *J. Biochem. (Tokyo).* 64:465–477.

Edman, K. A., and A. R. Matiazzi. 1981. Effects of fatigue and altered pH on isometric force and velocity of shortening at zero load in frog muscle fibers. *J. Muscle Res. Cell Motil.* 2:321–334.

Eisenberg, E., and W. W. Kielley. 1974. Troponin-tropomyosin complex. *J. Biol. Chem.* 249:4742–4746.

Fabiato, A., and F. Fabiato. 1978. Effects of pH on the myofilaments and the sarcoplasmic reticulum of skinned cells from cardiac and skeletal muscles. *J. Physiol. (Lond.).* 276:233–255.

Fujita, H., and S. Ishiwata. 1998. Spontaneous oscillatory contraction without regulatory proteins in actin filament-reconstituted fibers. *Biophys. J.* 75:1439–1445.

Fujita, H., K. Yasuda, S. Niitsu, T. Funatsu, and S. Ishiwata. 1996. Structural and functional reconstitution of thin filaments in the contractile apparatus of cardiac muscle. *Biophys. J.* 71:2307–2318.

Fukuda, N., H. Fujita, T. Fujita, and S. Ishiwata. 1996. Spontaneous tension oscillation in skinned bovine cardiac muscle. *Pflügers Arch.* 433:1–8.

Funatsu, T., H. Higuchi, and S. Ishiwata. 1990. Elastic filaments in skeletal muscle revealed by selective removal of thin filaments with plasma gelsolin. *J. Cell Biol.* 110:53–62.

Funatsu, T., E. Kono, H. Higuchi, S. Kimura, S. Ishiwata, T. Yoshioka, K. Maruyama, and S. Tsukita. 1993. Elastic filaments in situ in cardiac muscle: deep-etch replica analysis in combination with selective removal of actin and myosin filaments. *J. Cell Biol.* 120:711–724.

Godt, R. E., and J. C. Kentish. 1989. Effects of pH on isometric force, MgATPase, and tension-cost of skinned skeletal muscle fibres of the rabbit and cardiac muscles from rat. *J. Physiol. (Lond.).* 418:68P.

Horiuti, K. 1986. Some properties of the contractile system and sarcoplasmic reticulum of skinned slow fibers from *Xenopus* muscle. *J. Physiol. (Lond.).* 373:1–23.

Ishii, Y., and S. S. Lehrer. 1990. Excimer fluorescence of pyrenyliodoacetamide-labeled tropomyosin: a probe of the state of tropomyosin in reconstituted muscle thin filaments. *Biochemistry.* 29:1160–1166.

Ishiwata, S., T. Funatsu, and H. Fujita. 1998. Contractile properties of thin (actin) filament-reconstituted muscle fibers. *Adv. Exp. Med. Biol.* 453: 319–329.

Ishiwata, S., and H. Kondo. 1978. Studies on the F-actin-tropomyosin-troponin complex. II. Partial reconstitution of thin filaments by F-actin, tropomyosin and the tropomyosin binding component of troponin (TN-T). *Biochim. Biophys. Acta.* 534:341–349.

Kawashima, A., S. Morimoto, A. Suzuki, F. Shiraishi, and I. Ohtsuki. 1995. Troponin isoforms dependent pH dependence of the Ca^{2+}-activated myofibrillar ATPase activity of avian slow and fast skeletal muscles. *Biochem. Biophys. Res. Commun.* 207:585–592.

Kondo, H., and S. Ishiwata. 1976. Uni-directional growth of F-actin. *J. Biochem. (Tokyo).* 79:159–171.

Kurokawa, H., W. Fujii, K. Ohmi, T. Sakurai, and Y. Nonomura. 1990. Simple and rapid purification of brevin. *Biochem. Biophys. Res. Commun.* 168:451–457.

Lehman, W., P. Vibert, P. Uman, and R. Craig. 1995. Steric-blocking by tropomyosin visualized in relaxed vertebrate muscle thin filaments. *J. Mol. Biol.* 251:191–196.

Lewis, W. G., and L. B. Smillie. 1980. The amino acid sequence of rabbit cardiac tropomyosin. *J. Biol. Chem.* 255:6854–6859.

Mak, A. S., L. B. Smillie, and G. R. Stewart. 1979. A comparison of the amino acid sequences of rabbit skeletal muscle α- and β-tropomyosins. *J. Biol. Chem.* 255:3647–3655.

Metzger, J. M., and R. L. Moss. 1987. Greater hydrogen ion-induced depression of tension and velocity in skinned single fibres of rat fast than slow muscles. *J. Physiol. (Lond.).* 393:727–742.

Metzger, J. M., M. S. Parmacek, E. Barr, K. Pasyk, W. Lin, K. L. Cochrane, L. J. Field, and J. M. Leiden. 1993. Skelatal troponin C reduces contractile sensitivity to acidosis in cardiac myocytes from transgenic mice. *Proc. Natl. Acad. Sci. USA.* 90:9036–9040.

Nadal-Ginard, B., and V. Mahdavi. 1989. Molecular basis of cardiac performance. *J. Clin. Invest.* 84:1693–1700.

Palmer, S., and J. C. Kentish. 1994. The role of troponin C in modulating the Ca^{2+} sensitivity of mammalian skinned cardiac and skeletal muscle fibres. *J. Physiol. (Lond.).* 480:45–60.

Palmiter, K. A., Y. Kitada, M. Muthuchamy, D. F. Wieczorek, and R. J. Solaro. 1996. Exchange of β- for α-tropomyosin in hearts of transgenic mice induces changes in thin filament response to Ca^{2+}, strong cross-bridge binding, and protein phosphorylation. *J. Biol. Chem.* 271: 11611–11614.

Parsons, B., D. Szczesna, J. Zhao, G. van Slooten, W. G. L. Kerrick, J. A. Putkey, and J. D. Potter. 1997. The effect of pH on the Ca^{2+} affinity of the Ca^{2+} regulatory sites of skeletal and cardiac troponin C in skinned muscle fibres. *J. Muscle Res. Cell Motil.* 18:599–609.

Potma, E. J., I. A. van Graas, and G. J. M. Stienen. 1994. Effects of pH on myofibrillar ATPase activity in fast and slow skeletal muscle fibers of the rabbit. *Biophys. J.* 67:2404–2410.

Robertson, S. I., and W. G. L. Kerrick. 1979. The effects of pH on Ca^{2+}-activated skinned rabbit skeletal muscle fibres. *Pflügers Arch.* 380:41–45.

Solaro, R. J., S. C. El-Saleh, and J. C. Kentish. 1989. Ca^{2+}, pH and the regulation of cardiac myofilament force and ATPase activity. *Mol. Cell. Biochem.* 89:163–167.

Solaro, R. J., P. Kumar, E. M. Blanchard, and A. F. Martin. 1986. Differential effects of pH on calcium activation of myofilaments of adult and perinatal dog hearts. *Circ. Res.* 58:721–729.

Spudich, J. A., and S. Watt. 1971. The regulation of rabbit skeletal muscle contraction. I. Biochemical studies of the interaction of the tropomyosin-troponin complex with actin and the proteolytic fragments of myosin. *J. Biol. Chem.* 246:4866–4871.

Stone, D., and L. B. Smillie. 1977. The amino acid sequence of rabbit skeletal α-tropomyosin. *J. Biol. Chem.* 253:1137–1148.

Tanaka, H. 1972. The helix content of tropomyosin and the interaction between tropomyosin and F-actin under various conditions. *Biochim. Biophys. Acta.* 278:556–566.

Yamaguchi, M. 1998. Modulating factors of calcium-free contraction at low [MgATP]: a physiological study on the steady states of skinned fibres of frog skeletal muscle. *J. Muscle Res. Cell Motil.* 19:949–960.

Yasuda, K., T. Anazawa, and S. Ishiwata. 1995. Microscopic analysis of the elastic properties of nebulin in skeletal muscle myofibrils. *Biophys. J.* 68:598–608.

UltraRapid Communication

Effects of MgADP on Length Dependence of Tension Generation in Skinned Rat Cardiac Muscle

Norio Fukuda, Hidetoshi Kajiwara, Shin'ichi Ishiwata, Satoshi Kurihara

Abstract—The effect of MgADP on the sarcomere length (SL) dependence of tension generation was investigated using skinned rat ventricular trabeculae. Increasing SL from 1.9 to 2.3 μm decreased the muscle width by ≈11% and shifted the midpoint of the pCa-tension relationship (pCa_{50}) leftward by about 0.2 pCa units. MgADP (0.1, 1, and 5 mmol/L) augmented maximal and submaximal Ca^{2+}-activated tension and concomitantly diminished the SL-dependent shift of pCa_{50} in a concentration-dependent manner. In contrast, pimobendan, a Ca^{2+} sensitizer, which promotes Ca^{2+} binding to troponin C (TnC), exhibited no effect on the SL-dependent shift of pCa_{50}, suggesting that TnC does not participate in the modulation of SL-dependent tension generation by MgADP. At a SL of 1.9 μm, osmotic compression, produced by 5% wt/vol dextran (molecular weight ≈464 000), reduced the muscle width by ≈13% and shifted pCa_{50} leftward to a similar degree as that observed when increasing SL to 2.3 μm. This favors the idea that a decrease in the interfilament lattice spacing is the primary mechanism for SL-dependent tension generation. MgADP (5 mmol/L) markedly attenuated the dextran-induced shift of pCa_{50}, and the degree of attenuation was similar to that observed in a study of varying SL. The actomyosin-ADP complex (AM.ADP) induced by exogenous MgADP has been reported to cooperatively promote myosin attachment to the thin filament. We hereby conclude that the increase in the number of force-generating crossbridges on a decrease in the lattice spacing is masked by the cooperative effect of AM.ADP, resulting in depressed SL-dependent tension generation. The full text of this article is available at http://www.circresaha.org. (***Circ Res.* 2000;86:e1-e6.**)

Key Words: MgADP ■ pimobendan ■ Ca^{2+} sensitivity ■ cardiac muscle ■ sarcomere length

An alteration in ventricular end-diastolic volume results in a marked change in cardiac output.[1,2] This intrinsic ability of the heart to alter cardiac output forms the basis for the Frank-Starling law of the heart. It is well established that twitch tension and Ca^{2+} responsiveness in cardiac muscle preparations are enhanced as muscle length (ie, sarcomere length [SL]) is increased within the normal physiological range (SL from ≈1.8 to ≈2.3 μm).[1-5] Although a number of studies have been conducted to account for the SL dependence of tension generation in living myocardium, its mechanism has not been completely elucidated.[6] However, at the myofilament level, there is an increasing amount of evidence suggesting that the SL dependence is primarily due to a change in the interfilament lattice spacing that accompanies the SL change.[7-9] A possible consequence of the decreased lattice spacing is an increase in the probability of myosin attachment to the thin filament, resulting in an increase in the number of force-generating crossbridges.[7,10,11] Ishiwata and Oosawa[12] proposed a model based on the Ca^{2+}-dependent flexibility of the thin filament, in which they assumed that (1) the muscle volume (ie, the lattice volume) remains constant on a change in SL and that (2) there is a critical distance between the thick and thin filaments for tension generation. This model quantitatively explains both the stretch-induced increase in the steady isometric tension and the slower (or faster) rate of tension development (or decline) at a shorter SL,[13,14] supporting the hypothesis that a change in the lattice spacing plays a pivotal role in determining the SL-dependent Ca^{2+} sensitivity of tension. Alternatively, it was proposed that the length-dependent change in myofilament activation is caused by cardiac troponin C (TnC), which acts as a "length sensor" in the cardiac muscle contractile system.[15,16] However, this idea has attained little experimental evidence from other groups, and it was challenged by McDonald et al,[17] who reported that the expression of skeletal TnC in ventricular myocytes of transgenic mice did not alter the SL dependence of Ca^{2+} sensitivity of tension in skinned myocytes. Thus, it is unlikely that TnC alone acts as a "length sensor" in cardiac muscle.

It is known that the degree of activation of the thin filament is regulated not only by the binding of Ca^{2+} to TnC but also

Received August 26, 1999; accepted November 17, 1999.

From the Department of Physiology (II) (N.F., H.K., S.K.), The Jikei University School of Medicine, Nishishinbashi, Minato-ku, Tokyo, Japan; Department of Physics (S.I.), School of Science and Engineering, Advanced Research Institute for Science and Engineering (S.I.), and Materials Research Laboratory for Bioscience and Photonics (S.I.), Waseda University, Okubo, Shinjuku-ku, Tokyo, Japan.

Previously published in abstract form (*Circulation.* 1998;98[suppl I]:I-258).

Address reprint requests to Dr Shin'ichi Ishiwata, Department of Physics, School of Science and Engineering, Waseda University, 3-4-1 Okubo, Shinjuku-ku, Tokyo 169-8555, Japan. E-mail ishiwata@mn.waseda.ac.jp

***Circulation Research* is available at http://www.circresaha.org**

by the formation of strong-binding crossbridges, such as the rigor[18,19] and crossbridges that bind ADP.[20–22] Fukuda et al[22] reported that the actomyosin-ADP complex (AM.ADP) induced by exogenous MgADP can "turn on" adjacent actin molecules in a cooperative manner so that the actin and myosin interaction becomes possible, just as if Ca^{2+} were bound to TnC. Consequently, upon the addition of MgADP, the pCa-tension relationship for skinned cardiac muscle is shifted to the left, showing greater Ca^{2+} sensitivity of tension.[21–23]

To investigate the influence of the formation of strong-binding crossbridges on SL-dependent tension generation in cardiac muscle, we measured the SL-dependent shift of the pCa-tension relationship in the presence of varying concentrations of MgADP using skinned rat ventricular trabeculae. The formation of strong-binding crossbridges is known to increase the affinity of TnC for Ca^{2+}.[3,5,24] Thus, to clarify whether the effect of MgADP is based on the increased affinity of TnC for Ca^{2+}, we examined the effect of pimobendan, a Ca^{2+} sensitizer, which promotes Ca^{2+} binding to TnC.[25,26] A preliminary report has been published in abstract form.[27]

Materials and Methods

Experimental Procedure

The heart was removed from male Wistar rats (250 to 300 g) anesthetized with sodium pentobarbital (50 mg/kg IP). The rats were supplied by Saitama Experimental Animals Supply (Saitama, Japan), and the present study conforms with the *Guiding Principles for the Care and Use of Animals* approved by the Council of the Physiological Society of Japan. Thin trabecula muscles with the diameter of 100 to 150 μm were dissected from the right ventricle in oxygenated Tyrode solution without Ca^{2+} at 30°C. The preparations were skinned by superfusion with 1% vol/vol Triton X-100 in the relaxing solution (in mmol/L: MgATP 4, MOPS 10, EGTA 10, free Mg^{2+} 1, and ionic strength 180 [pH 7.0]) for 60 minutes at ≈2°C. The ionic strength (IS) was adjusted with KCl. The preparations were then washed with the relaxing solution to remove Triton X-100 and stored at −20°C in the relaxing solution containing 50% vol/vol glycerol and 2 mmol/L leupeptin for 1 week or less.

Both ends of the preparation were tied to thin tungsten wires with a silk thread. One end was attached to a tension transducer (BG-10; Kulite Semiconductor Products, Inc, Leonia, NJ) and the other to a micromanipulator (Narishige, Tokyo, Japan). The SL was adjusted to either 1.9 or 2.3 μm by measuring laser light diffraction in the relaxing solution. Ca^{2+}-activated isometric tension was measured in activating solutions containing 4 mmol/L MgATP, 10 mmol/L MOPS, 1 mmol/L free Mg^{2+}, a varying concentration of free Ca^{2+} (adjusted with Ca/[10 mmol/L EGTA]), 0.1 mmol/L P^1,P^5-di(adenosine-5′)pentaphosphate (AP_5A), 15 mmol/L creatine phosphate (CP), 15 U/mL creatine phosphokinase (CPK), and 180 mmol/L IS [pH 7.0], at the two SLs with/without MgADP or pimobendan (donated by Nippon Boehringer Ingelheim; Kawanishi, Hyogo, Japan).

The control pCa-tension relationship without MgADP or pimobendan was first obtained at a SL of 1.9 μm and then at 2.3 μm. By using the same preparation, the pCa-tension relationships in the presence of MgADP or pimobendan were obtained at the two SLs. Each pCa-tension relationship was obtained by cumulatively raising the Ca^{2+} concentration from the relaxing condition. Because we noted a variation in n_H (and related parameters), depending on the preparation, paired experiments were carried out on the same preparation. Finally, maximal Ca^{2+}-activated tension (at pCa 4.8) was measured at the two SLs in the control condition without MgADP or pimobendan to examine the reproducibility of tension development. We only used the data in which the final tension values were greater than 70% of those measured at the beginning of the experiment.

The muscle width was measured under a microscope (Nikon SMZ645) at a magnification of ×225. The concentrations of chemicals in solutions were estimated by computer calculation.[28] All experiments were carried out at 20±0.2°C.

Data and Statistical Analyses

The pCa-tension relationship was fitted to the Hill equation: $\log[P/(100-P)]=n_H[pCa_{50}-pCa]$, where P is the relative tension expressed as a percentage of the maximum ($+Ca^{2+}$, pCa 4.8), n_H is the Hill coefficient, and pCa_{50} is $-\log[Ca^{2+}]$ at P=50. All data are expressed as mean±SEM. Paired Student's *t* test was used, and statistical significance was verified at $P<0.05$.

Results

Effect of MgADP on the Length Dependence of Ca^{2+} Sensitivity of Tension

Figure 1 shows the effect of MgADP on the SL dependence of Ca^{2+} sensitivity of tension. In the control condition without MgADP or pimobendan, maximal absolute Ca^{2+}-activated tension values were 52.5±4.7 and 77.9±4.1 mg (n=17; $P<0.001$) at SL 1.9 and 2.3 μm, respectively, and pCa_{50} was shifted leftward by about 0.2 pCa units by increasing SL from 1.9 to 2.3 μm. The degree of the SL-dependent shift of pCa_{50} was consistent with the result of a previous study using rat ventricular muscle strips.[29] In the absence of MgADP, the muscle width was reduced from 132±6 to 118±4 μm (n=4; $P<0.001$) on extension of SL during relaxation (ie, ≈11% reduction): The addition of MgADP (up to 5 mmol/L) did not change the muscle width at either SL (131±7 and 117±5 μm [n=4; $P<0.001$] at SL 1.9 and 2.3 μm, respectively, in the presence of 5 mmol/L MgADP).

Consistent with our previous studies using skinned bovine cardiac muscle,[22,23] MgADP shifted the pCa-tension relationship to the left in a concentration-dependent manner (Figure 1). Concomitantly, the SL-dependent shift of the pCa-tension relationship was diminished in a concentration-dependent manner; in the presence of 5 mmol/L MgADP, ΔpCa_{50} was decreased to ≈20% of the control value (Figure 1C, inset).

Change in Hill Coefficient With MgADP

	Figure 1A		Figure 1B		Figure 1C	
SL	Control	0.1 mmol/L	Control	1 mmol/L	Control	5 mmol/L
1.9 μm	5.81±0.28	5.78±0.40	4.77±0.45	4.74±0.32	4.96±0.55	2.43±0.08*
2.3 μm	5.10±0.29	5.03±0.56	4.17±0.14	3.97±0.07	5.31±0.31	2.21±0.10*

Values from left and right columns were obtained from Figures 1A, 1B, and 1C, respectively (mean±SEM [n=4 to 5]). *$P<0.05$ compared with corresponding control (−MgADP) values.

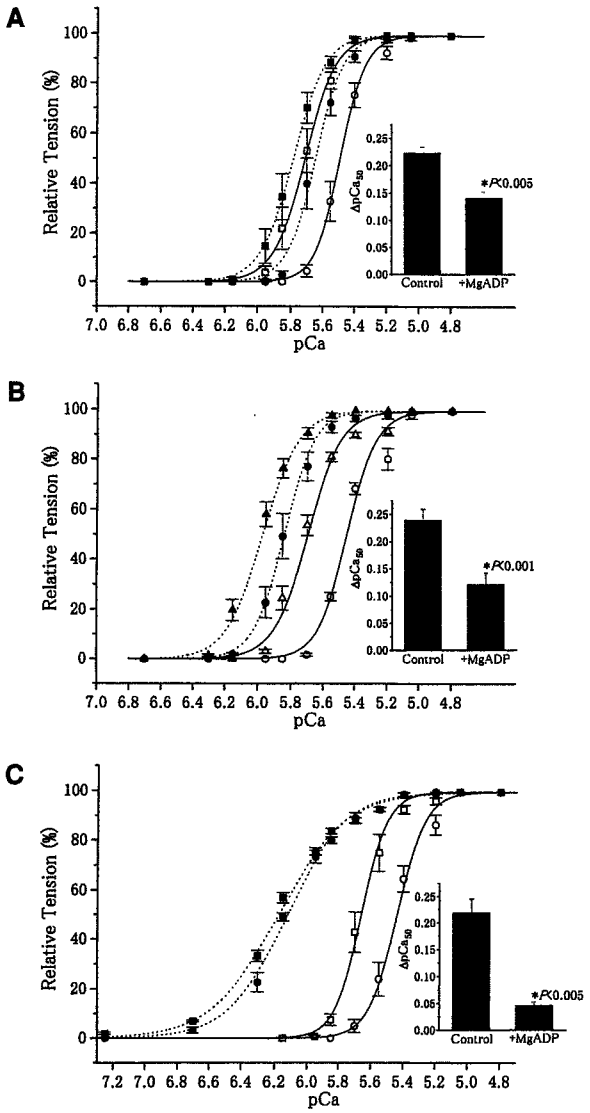

Figure 1. Effects of MgADP on pCa-tension relationships at different SLs. Solvent conditions: 4 mmol/L MgATP, 10 mmol/L MOPS (pH 7.0), 1 mmol/L free Mg^{2+}, varying [Ca^{2+}] (pCa adjusted by Ca/EGTA), 0.1 mmol/L AP_5A, 15 mmol/L CP, 15 U/mL CPK, and IS maintained at 180±1 mmol/L. MgADP was added to the above solution at a concentration of 0.1, 1, or 5 mmol/L. The ATP regenerating system (CP-CPK) was not added for experiments that used MgADP. Panels A, B, and C show the effects of MgADP at concentrations of 0.1, 1, and 5 mmol/L, respectively, on the pCa-tension relationships at SLs of 1.9 μm (circles) and 2.3 μm (squares); note that different muscle preparations were used. Solid lines and open symbols indicate pCa-tension relationships in the absence of MgADP; dotted lines and closed symbols, those in the presence of MgADP. Data obtained for each preparation were fitted to the Hill equation, and the results were simulated by the Hill equation with the mean values of pCa_{50} and n_H. Each inset represents ΔpCa_{50} (ie, difference between the values of pCa_{50} at long and short SLs) in the absence (control) and presence of MgADP. pCa-tension relationships were normalized by the maximum tension at pCa 4.8. Temperature was maintained at 20±0.2°C. Vertical bars indicate SEM of 4 to 5 data points.

The Table summarizes the n_H values of the pCa-tension relationships shown in Figure 1. MgADP at a concentration of 5 mmol/L significantly decreased n_H at both SLs,[23] whereas no significant changes were observed for 0.1 and 1 mmol/L MgADP.

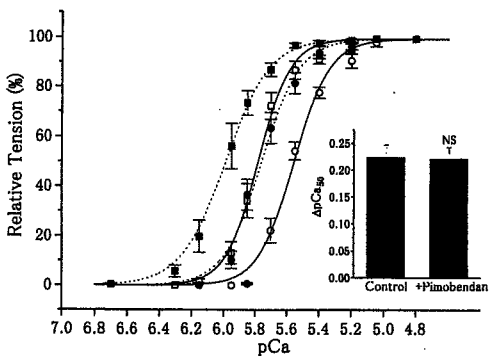

Figure 2. Effects of pimobendan on pCa-tension relationships at different SLs. Conditions are the same as in Figure 1 except that MgADP was absent and 10^{-4} mol/L pimobendan was present as well as CP and CPK. Pimobendan was initially dissolved in DMSO and diluted with the individual solutions. The final concentration of DMSO was 1%, having no effect on tension development. Symbols are the same as in Figure 1 except that dotted lines and closed symbols represent the pCa-tension relationships in the presence of pimobendan at SL 1.9 μm (circles) and at SL 2.3 μm (squares). Inset represents ΔpCa_{50} in the absence (control) and presence of pimobendan. NS indicates not significant compared with control. pCa-tension relationships were normalized with respect to the maximum tension at pCa 4.8. Vertical bars indicate SEM of 4 data points.

Because the ATP regenerating system (CP-CPK) was not used in the presence of MgADP, we estimated the concentration of contaminating MgADP inside the preparation. In the absence of MgADP, the pCa_{50} values obtained with and without CP-CPK were 5.45±0.05 and 5.53±0.05, respectively (n=4; $P<0.001$), at SL 1.9 μm. Thus, we estimated the contaminant MgADP to be ≈0.1 mmol/L under our experimental condition (see Figure 1A). This estimation is within the range of reported values for skinned cardiac and skeletal muscles.[30,31]

Effect of Pimobendan on the Length Dependence of Ca^{2+} Sensitivity of Tension

Pimobendan was reported to shift the pCa-tension relationship to the left with little influence on maximal Ca^{2+}-activated tension in skinned porcine ventricular muscle.[32] In the present study, 10^{-4} mol/L pimobendan substantially shifted the pCa-tension curve to the left at SLs of 1.9 and 2.3 μm, whereas in contrast to MgADP, pimobendan did not diminish the SL-dependent shift of the pCa-tension relationship (Figure 2).

The n_H values in the absence and presence of pimobendan were 4.01±0.27 and 3.93±0.15 (n=4; $P>0.1$), respectively, at SL 1.9 μm and 4.45±0.32 and 3.75±0.12 (n=4; $P>0.1$), respectively, at SL 2.3 μm. Pimobendan did not significantly change n_H at either SL.

Effect of MgADP or Pimobendan on Maximal Tension

Figure 3 summarizes the effect of MgADP or pimobendan on maximal Ca^{2+}-activated tension (pCa 4.8) at SLs of 1.9 and 2.3 μm. It has been reported that MgADP significantly potentiates maximal Ca^{2+}-activated tension in cardiac[22,23,33] and skeletal muscles.[20,33] We also found that MgADP augmented maximal tension in a concentration-dependent manner, and this potentiating effect was significantly less pro-

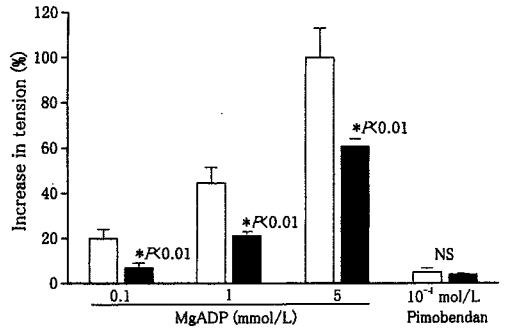

Figure 3. Effects of MgADP or pimobendan on maximal Ca^{2+}-activated tension. Conditions are the same as in Figures 1 and 2 for MgADP and pimobendan, respectively, except that pCa was fixed at 4.8. Open columns show SL 1.9 μm, and filled columns show SL 2.3 μm. NS indicates not significant. The degree of increase in tension was determined with respect to the maximal tension obtained without MgADP or pimobendan at each SL. Vertical bars indicate SEM of 4 to 5 data points for MgADP and 4 data points for pimobendan.

nounced at the longer SL ($P<0.01$). In contrast, pimobendan only minimally increased maximal tension at both SLs, and there was no significant difference in the increases in maximal tension between the two SLs.

Effect of MgADP on Dextran-Induced Shift of the pCa-Tension Relationship

Dextran (5% wt/vol) reduced the width of muscle from 135±5 to 117±4 μm (n=7; $P<0.001$) under the relaxing condition at SL 1.9 μm. The degree of reduction (≈13%) was similar to that observed when increasing SL to 2.3 μm without dextran (≈11%, see above).

In the absence of MgADP, dextran shifted pCa_{50} to the left by 0.19±0.03 pCa units (Figure 4). The degree of the shift of pCa_{50} was comparable, albeit slightly smaller, to what was observed when increasing SL to 2.3 μm (see Figures 1 and 2).

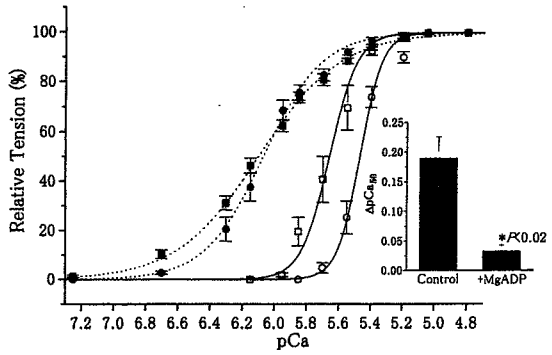

Figure 4. Effect of 5 mmol/L MgADP on pCa-tension relationships in the absence and presence of 5% wt/vol dextran at SL 1.9 μm. Solvent conditions are the same as in Figure 1 except that 5% wt/vol dextran (molecular weight ≈464 000; Sigma) was used to shrink the muscle volume instead of increasing SL to 2.3 μm. Circles indicate in the absence of dextran; squares, in the presence of dextran. Solid lines and open symbols indicate pCa-tension relationships in the absence of MgADP; dotted lines and closed symbols, pCa-tension relationships in the presence of MgADP. Inset represents ΔpCa_{50} (difference between the values of pCa_{50} with and without dextran) in the absence (control) and presence of MgADP. pCa-tension relationships were normalized with respect to the maximal tension at pCa 4.8. Vertical bars indicate SEM of 7 data points.

Maximal tension was also augmented by ≈15% in the presence of dextran as previously reported by other investigators using skinned skeletal[11] and cardiac muscles.[34]

It was found that in the presence of 5 mmol/L MgADP, the dextran-induced increase in apparent Ca^{2+} sensitivity was markedly diminished (Figure 4), and the degree of attenuation was similar to what was obtained in a study of varying SL (see Figure 1C).

The n_H values in the absence and presence of 5 mmol/L MgADP were 6.32±0.61 and 2.52±0.18 (n=7; $P<0.05$), respectively, without dextran and 5.29±0.31 and 1.68±0.06 (n=7; $P<0.05$), respectively, with dextran.

Discussion

We demonstrated that using skinned rat ventricular trabeculae, MgADP increases the Ca^{2+} sensitivity of tension and reduces the magnitude of SL-dependent changes in Ca^{2+} sensitivity. On the other hand, a simple increase in the Ca^{2+} binding affinity of TnC by pimobendan had no effect on the SL-dependent change in the Ca^{2+} sensitivity of tension. We discuss the implications of these results, focusing on the role of strong-binding crossbridges in the regulation of Ca^{2+} sensitivity of tension.

First, an increase in SL results in a decrease in the lateral separation between the thick and thin filaments in living cardiac muscle.[35] Similarly, the interfilament lattice spacing is decreased by increasing SL in skinned (glycerinated) muscle.[36] Although the latter study was conducted using skeletal muscle, it is reasonable to assume that the result can be extended to skinned cardiac muscle. In the present study, we observed that increasing SL from 1.9 to 2.3 μm produced about an 11% reduction in the width of muscle. Thus, it is suggested that there also occurred a corresponding reduction (ie, ≈11%) in the lattice spacing on extension of SL from 1.9 to 2.3 μm.

On the other hand, 5% wt/vol dextran decreased the muscle width by ≈13%. An X-ray diffraction study showed that a reduction in the width of skinned skeletal muscle produced by dextran reflects a proportional change in the lattice spacing.[37] Although an X-ray study has not been conducted with cardiac muscle, the conclusion made, on the basis of skeletal muscle, could be applicable to cardiac muscle.[38] It can thus be said that in the present study, 5% wt/vol dextran decreased the lattice spacing by ≈13%. Given the fact that both an increase in SL and osmotic compression produced a similar reduction in the muscle width and that both increased Ca^{2+} sensitivity of tension to a similar degree (Figures 1, 2, and 4), we consider that the decreased lattice spacing is the primary mechanism for length-dependent tension generation in skinned cardiac muscle.

There was, however, a slight mismatch between the effect of increasing SL and that of osmotic compression on Ca^{2+} sensitivity of tension and maximal Ca^{2+}-activated tension. Increasing SL to 2.3 μm resulted in about an 11% decrease in the muscle width, whereas osmotic compression decreased the width by ≈13%, yet the shift of pCa_{50} and the augmentation of maximal Ca^{2+}-activated tension were somewhat more pronounced by the lengthening. The exact reason(s) for this mismatch is unknown. However, it may be attributable to

some direct effect of dextran on the crossbridge cycle[39] and/or to the shape of the muscle being altered differently by mechanical stretch compared with osmotic compression.[7]

Although Ca^{2+} is a physiological activator of myocardium, it has been known that Ca^{2+} alone does not fully activate the thin filament[40] and that strong-binding crossbridges, such as the rigor complex, can further activate the thin filament.[18] We have reported that the formation of AM.ADP upon the addition of MgADP regulates the number of force-generating crossbridges, synergistically with Ca^{2+} binding to TnC.[20–22] In the present study, we found that MgADP, in addition to its apparent Ca^{2+} sensitizing effect, diminished the SL-dependent shift of the pCa-tension relationship in a concentration-dependent manner (Figure 1). Further, MgADP (5 mmol/L) attenuated the increase in Ca^{2+} sensitivity of tension produced by osmotic compression, to a similar degree observed when SL was increased (Figure 4). As discussed above, SL-dependent tension generation can be largely explained due to a decrease in the lattice spacing, which results in an increase in the number of force-generating crossbridges.[7,10,11] Therefore, it is realized that when force-generating crossbridges predominate inside the muscle through the cooperative effect of AM.ADP, the effect of lattice shrinkage becomes relatively small, leading to depressed SL-dependent tension generation. This interpretation is consistent with the fact that the potentiating effect of MgADP was significantly less pronounced at a longer SL (Figure 3).

Fitzsimons and Moss[9] reported that an application of *N*-ethylmaleimide–modified myosin subfragment 1 to single skinned rat ventricular myocytes diminishes the SL-dependent shift of the pCa-tension relationship. It is thus safe to conclude that when the number of force-generating crossbridges is increased through the cooperative effect of strong-binding crossbridges, the effect of increasing SL (ie, lattice shrinkage) to produce force-generating crossbridges is offset.

In skinned muscle preparations, strong-binding crossbridges promote Ca^{2+} binding to TnC.[24] If TnC acts as a "length sensor" in the cardiac contractile system,[15,16] then it follows that the SL dependence of tension generation would be modulated by a change in the affinity of TnC for Ca^{2+}, and the depressed shift of the pCa-tension relationship seen in the presence of MgADP may have been caused by the increased affinity of TnC for Ca^{2+}. However, pimobendan was found to have no effect on the SL-dependent shift of the pCa-tension relationship (Figure 2). Thus, it is unlikely that the increased affinity of TnC for Ca^{2+} is the major cause of the attenuation of SL-dependent tension generation by MgADP.

McDonald et al[41] hypothesized that the activation state of muscle with a higher cooperativity varies more dramatically as a result of length-induced variations in the number of force-generating crossbridges. However, in the presence of 0.1 or 1 mmol/L MgADP, the SL dependence was significantly diminished (Figures 1A and 1B), whereas n_H was not significantly changed (Table). Thus, it is unlikely that the attenuation of SL-dependent tension generation by MgADP underlies the decreased cooperative activation of the thin filament.

It should be stressed that MgADP as low as 0.1 mmol/L (or ≈0.2 mmol/L when contaminating MgADP is taken into account) augmented maximal and submaximal tension and diminished the SL dependence of tension generation (Figures 1A and 3). Because it has been known that cardiac contractile proteins are more sensitive to MgADP than skeletal muscle proteins,[22,42] it is possible that MgADP at ≈0.1 mmol/L significantly influences cardiac contractile performance, as in the in vitro motility assay system.[43] Recently, Tian et al[44] demonstrated that ≈0.1 mmol/L MgADP significantly increased the left ventricular end-diastolic pressure in intact rat heart. It has been pointed out that in the intracellular milieu of ischemic or hypoxic cardiac muscle, the concentration of ADP increases whereas that of ATP decreases.[45] Reportedly, an increase in the ratio of the concentration of ADP to that of ATP in the vicinity of crossbridges may elicit ischemic contracture.[46] The present results suggest that during ischemia or hypoxia, the accumulation of ADP may impair the Frank-Starling mechanism.

Acknowledgments

This work was supported in part by Grants-in-Aid for Scientific Research, for Scientific Research on Priority Areas, and for High-Tech Research Center Project from the Ministry of Education, Science, Sports and Culture of Japan, by Core Research for Evolutional Science and Technology (CREST) of Japan Science and Technology Corporation, and from the Vehicle Racing Commemorative Foundation. We would like to thank Nippon Boehringer Ingelheim for providing pimobendan, Prof Masataka Kawai of the University of Iowa for critical reading of the manuscript, and Naoko Tomizawa for technical assistance.

References

1. Allen DG, Kentish JC. The cellular basis for length-tension relation in cardiac muscle. *J Mol Cell Cardiol.* 1985;17:821–840.
2. Lakatta EG. Length modulation of muscle performance: Frank-Starling law of the heart. In: Fozzard HA, ed. *The Heart and Cardiovascular System.* New York, NY: Raven Press Publishers; 1991:1325–1352.
3. Allen DG, Kurihara S. The effect of muscle length on intracellular calcium transients in mammalian cardiac muscle. *J Physiol (Lond).* 1982; 327:79–94.
4. Kentish JC, ter Keurs HEDJ, Ricciardi L, Bucx JJJ, Noble MIM. Comparison between the sarcomere length-force relations of intact and skinned trabeculae from right ventricle. Influence of calcium concentrations on these relations. *Circ Res.* 1986;58:755–768.
5. Kurihara S, Komukai K. Tension-dependent changes of the intracellular Ca^{2+} transients in ferret ventricular muscles. *J Physiol (Lond).* 1995;489: 617–625.
6. Fuchs F. Mechanical modulation of the Ca^{2+} regulatory protein complex in cardiac muscle. *News Physiol Sci.* 1995;10:6–12.
7. McDonald KS, Moss RL. Osmotic compression of single cardiac myocytes eliminates the reduction in Ca^{2+} sensitivity of tension at short sarcomere length. *Circ Res.* 1995;77:199–205.
8. Fuchs F, Wang YP. Sarcomere length versus interfilament spacing as determinants of cardiac myofilament Ca^{2+} sensitivity and Ca^{2+} binding. *J Mol Cell Cardiol.* 1996;28:1375–1383.
9. Fitzsimons DP, Moss RL. Strong binding of myosin modulates length-dependent Ca^{2+} activation of rat ventricular myocytes. *Circ Res.* 1998; 83:602–607.
10. April EW, Maughan DW. Active force as a function of filament spacing in crayfish skinned cardiac muscle fibers. *Pflugers Arch.* 1986;407: 456–460.
11. Allen JD, Moss RL. Factors influencing the ascending limb of the sarcomere length-tension relationship in rabbit skinned muscle fibers. *J Physiol (Lond).* 1987;390:119–136.
12. Ishiwata S, Oosawa F. A regulatory mechanism of muscle contraction based on the flexibility change of the thin filaments. *J Mechanochem Cell Motil.* 1974;3:9–17.

13. Endo M. Stretch-induced increase in activation of skinned muscle fibres by calcium. *Nat New Biol.* 1972;237:211–213.
14. Endo M. Length dependence of activation of skinned muscle fibers by calcium. *Cold Spring Harbor Symp Quant Biol.* 1972;37:505–510.
15. Babu A, Sonnenblick E, Gulati J. Molecular basis for the influence of muscle length on myocardial performance. *Science.* 1988;240:74–76.
16. Gulati J, Sonnenblick E, Babu A. The role of troponin C in the length dependence of Ca^{2+}-sensitive force of mammalian skeletal and cardiac muscles. *J Physiol (Lond).* 1990;441:305–324.
17. McDonald KS, Field LJ, Parmacek MS, Soonpaa M, Leiden JM, Moss RL. Length dependence of Ca^{2+} sensitivity of tension in mouse cardiac myocytes expressing skeletal troponin C. *J Physiol (Lond).* 1995;483: 131–139.
18. Bremel RD, Weber A. Cooperation within actin filament in vertebrate skeletal muscle. *Nat New Biol.* 1972;238:97–101.
19. Weber A, Murray JM. Molecular control mechanisms in muscle contraction. *Physiol Rev.* 1973;53:612–673.
20. Shimizu H, Fujita T, Ishiwata S. Regulation of tension development by MgADP and Pi without Ca^{2+}. Role in spontaneous tension oscillation of skeletal muscle. *Biophys J.* 1992;61:1087–1098.
21. Ishiwata S, Yasuda K. Mechano-chemical coupling in spontaneous oscillatory contraction of muscle. *Phase Transitions.* 1993;45:105–136.
22. Fukuda N, Fujita H, Fujita T, Ishiwata S. Regulatory roles of MgADP and calcium in tension development of skinned cardiac muscle. *J Muscle Res Cell Motil.* 1998;19:909–921.
23. Fukuda N, Fujita H, Fujita T, Ishiwata S. Spontaneous tension oscillation in skinned bovine cardiac muscle. *Pflugers Arch.* 1996;433:1–8.
24. Guth K, Potter JD. Effect of rigor and cycling cross-bridges on the structure of troponin C and on the Ca^{2+} affinity of the Ca^{2+}-specific regulatory sites in skinned rabbit psoas fibers. *J Biol Chem.* 1987;262: 13627–13635.
25. Fujino K, Sperelakis N, Solaro RJ. Sensitization of dog and guinea pig heart myofilaments to Ca^{2+} activation and the inotropic effect of pimobendan: comparison with milrinone. *Circ Res.* 1988;63:911–22.
26. Nielsen-Kudsk JE, Aldershvile J. Will calcium sensitizers play a role in the treatment of heart failure? *J Cardiovasc Pharmacol.* 1995;26(suppl 1):S77–S84.
27. Fukuda N, Kajiwara H, Ishiwata S, Kurihara S. Effects of MgADP on sarcomere length (SL)-dependent changes of pCa-tension relation in skinned rat myocardium. *Circulation.* 1998;98(suppl I):I-258. Abstract 1345.
28. Horiuti K. Some properties of the contractile system and sarcoplasmic reticulum of skinned slow fibres from *Xenopus* muscle. *J Physiol (Lond).* 1986;373:1–23.
29. Hibberd MG, Jewell BR. Calcium and length-dependent force production in rat ventricular muscle. *J Physiol (Lond).* 1982;329:527–540.
30. Zhao Y, Kawai M. Inotropic agent EMD-53998 weakens nucleotide and phosphate binding to cross bridges in porcine myocardium. *Am J Physiol.* 1996;271:H1394–H1406.
31. Wang G, Kawai M. Effects of MgATP and MgADP on the cross-bridge kinetics of rabbit soleus slow-twitch muscle fibers. *Biophys J.* 1996;71: 1450–1461.
32. Beier N, Harting J, Jonas R, Klockow M, Lues I, Haeusler G. The novel cardiotonic agent EMD 53998 is a potent "calcium sensitizer." *J Cardiovasc Pharmacol.* 1991;18:17–27.
33. Godt RE, Nosek TM. Changes of intracellular milieu with fatigue or hypoxia depress contraction of skinned rabbit skeletal and cardiac muscle. *J Physiol (Lond).* 1989;412:155–180.
34. Wang YP, Fuchs F. Osmotic compression of skinned cardiac and skeletal muscle bundles: effects on force generation, Ca^{2+} sensitivity and Ca^{2+} binding. *J Mol Cell Cardiol.* 1995;27:1235–1244.
35. Matsubara I, Millman BM. X-ray diffraction patterns from mammalian heart muscle. *J Mol Biol.* 1974;82:527–536.
36. Rome E. Relaxation of glycerinated muscle: low-angle X-ray diffraction studies. *J Mol Biol.* 1972;65:331–345.
37. Kawai M, Wray JS, Zhao Y. The effect of lattice spacing change on cross-bridge kinetics in chemically skinned rabbit psoas muscle fibers, I: proportionality between the lattice spacing and the fiber width. *Biophys J.* 1993;64:187–196.
38. Roos KP, Brady AJ. Osmotic compression and stiffness changes in relaxed skinned cardiac myocytes in PVP-40 and dextran T-500. *Biophys J.* 1990;58:1273–1283.
39. Metzger JM. Effects of phosphate and ADP on shortening velocity during maximal and submaximal calcium activation of the thin filament in skeletal muscle fibers. *Biophys J.* 1996;70:409–417.
40. Swartz DR, Moss RL, Greaser ML. Calcium alone does not fully activate the thin filament for S1 binding to rigor myofibrils. *Biophys J.* 1996;71: 1891–1904.
41. McDonald KS, Wolff MR, Moss RL. Sarcomere length dependence of the rate of tension redevelopment and submaximal tension in rat and rabbit skinned skeletal muscle fibres. *J Physiol (Lond).* 1997;501:607–621.
42. Chase PB, Kushmerick MJ. Effect of physiological ADP concentration on contraction of single skinned fibers from rabbit fast and slow muscles. *Am J Physiol.* 1995;268:C480–C489.
43. Yamashita H, Sata M, Sugiura S, Momomura S, Serizawa T, Iizuka M. ADP inhibits the sliding velocity of fluorescent actin filaments on cardiac and skeletal myosins. *Circ Res.* 1994;74:1027–1033.
44. Tian R, Christe ME, Spindler M, Hopkins JCA, Halow JM, Camacho SA, Ingwall JS. Role of MgADP in the development of diastolic dysfunction in the intact beating rat heart. *J Clin Invest.* 1997;99:745–751.
45. Kammermeier H, Schmidt P, Jungling E. Free energy change of ATP-hydrolysis: a causal factor of early hypoxic failure of the myocardium? *J Mol Cell Cardiol.* 1982;14:267–277.
46. Ventura-Clapier R, Veksler V. Myocardial ischemic contracture. Metabolites affect rigor tension development and stiffness. *Circ Res.* 1994;74: 920–929.

Research Report

Focal Extraction of Surface-Bound DNA from a Microchip Using Photo-Thermal Denaturation

BioTechniques 28:1006-1011 (May 2000)

Kenji Yasuda, Kazunori Okano[1] and Shin'ichi Ishiwata[2]
The University of Tokyo, [1]Hitachi, Ltd. and [2]Waseda University, Tokyo, Japan

ABSTRACT

High-throughput, selective extraction of a particular DNA fragment from a mixture of DNA before PCR amplification is becoming increasingly important in the DNA analysis field. Although the latest microchip technology has enabled real-time DNA expression analysis using hybridization between surface-bound probe DNA and sample DNA, the potential of this technology in purification of a small amount of DNA has not been demonstrated. We report here a method for area-selective release and collection of specific DNA, in which an IR laser beam is focused onto surface-bound sample DNA at the target-spotted area to denature hybridized DNA. First, sample DNA labeled with a fluorescent dye was hybridized to a probe DNA immobilized on a chromium-coated chip. A 1053-nm IR laser beam with an intensity of 10–100 mW was then focused on the target area with a spatial resolution of 10 μm, causing the release of the fluorophore-labeled sample DNA as a result of photo-thermal denaturation. Confirmation of the amount of eluted DNA by PCR amplification after collection indicated that more than 10^{-20} mol DNA/μm² area was eluted from the microchip, representing more than 70% of the chip-bound sample DNA. These results indicate that this method can be applied to the highly sensitive purification of DNA in microchip technology.

INTRODUCTION

Purification and analysis of DNA from a mixture of cell extract are fundamental in molecular and cellular biology and molecular diagnosis. In purification, a DNA library constructed from cloned DNA is usually used. Although the cloning method is widely used and is suitable for the preparation of a large number of DNA, the cultivation step of this method is laborious and time consuming. Recently, molecular biology has moved rapidly towards the study of functional genomics (10) and proteomics. These studies require rapid selection and collection of the target parts of a gene and mRNA from crude samples (3,6). Although the latest chip technology is capable of simple, high-throughput analysis in distinguishing different sequences of DNA by hybridization detection between a chip-bound probe DNA and sample DNA (1,2,8,9), it has not yet been applied to high-throughput purification of DNA, in which a portion of the sample DNA having particular DNA segments is picked up for further analysis.

Here, we propose a new type of DNA purification method using a photo-thermal approach to extract specific DNA bound on a microchip surface. This method is based on the principle that a focused IR beam heats a spotted area on the metal-coated chip surface (4) and that the resulting increase in temperature leads to denaturation of the sample probe DNA. As shown in Figure 1, the method consists of the following four steps: (*i*) sample DNA are loaded onto a chip surface coated with a metal thin layer, on which a group of surface-bound probe DNA are immobilized; (*ii*) sample DNA is hybridized with probe DNA; (*iii*) the chip surface is washed, the hybridized sample DNA are observed and the plate is spot-heated to extract DNA from the spotted area; and (*iv*) the released sample DNA is collected. The advantages of this spot-heating method are that it provides non-contact, spatially distributed denaturation and faster relaxation time in the increase in temperature. It should thus prove highly suitable for extracting target DNA individually from a chip surface on which a crude DNA mixture has been loaded. Steps *i* and *ii* have already been realized in DNA chip technology (1,2,8,9), but steps *iii* and *iv* are not yet tested. Here, we focused on steps *iii* and *iv*, namely the technique for area-specific denaturation and release of surface-bound DNA and subsequent collection of the released DNA.

MATERIALS AND METHODS

Photo-Thermal Denaturation Microscopy System

Figure 2 shows a diagram of the photo-thermal denaturation microscopy system for area-specific extraction of surface-bound DNA. It consists of three different optical units for phase-contrast, fluorescence and 1053-nm IR laser irradiation, respectively (Nd:YLF laser, 1053-100p; Amoco Laser, Naperville, IL, USA; maximum power 100 mW at the focal point when a ×10 objective lens is used). Different probe DNA areas in the matrix are distinguished by phase-contrast microscopy. The amount of surface-bound sample DNA on the microchip was measured by fluorescence microscopy. Phase-contrast and fluorescence images were simultaneously acquired with a dual-view microscopy system (4,5,7): the former through a charge-couple device (CCD) camera and the latter through a CCD camera equipped with an image intensifier. The area of DNA denaturation was brought into focus using the

fluorescence image, and the IR laser beam irradiated the spotted area. The intensity of the IR laser beam can be controlled up to 100 mW at the focal position on the microchip.

Preparation of DNA Chip

Probe DNA was immobilized on a 6-nm-thick chromium-coated glass plate. The chromium surface was modified with an active residue having a glysidoxy group for coupling dsDNA (619 bp, 0.5 pmol, 0.5 µL) onto the surface by the following two reaction steps. First, the glass plate with a chromium surface (45 × 25 × 0.4 mm) was dipped into a solution of 3-glysidoxypropyltrimethoxysilane for 1 h at room temperature (25°C) and dried at 110°C for 30 min. Next, dsDNA was prepared with an amino residue at the 5′-terminus of one strand and sulforhodamine-101 fluorophore at the 5′-terminus of the other strand so as to immobilize the DNA through its amino residue with glysidoxy groups on the chip surface. The dsDNA was a product amplified from a cloned human DNA. The clone has M13 priming sites 5′-CATGACTGGCCGTCGTT-3′ at both ends. It was amplified by PCR with *Taq* DNA polymerase (Amersham Pharmacia Biotech, Little Chalfont, UK) and two primers, 5′-fluorophore-AACGACGGCCAGTCATGCG-3′ and 5′-NH2-AACGACGGCCAGTCATGTG-3′. Thermal cycling for PCR was carried out 35× at 94°C for 30 s, 60°C for 30 s, and 72°C for 60 s. A solution of the product (10 µM dissolved in 0.2 M sodium carbonate buffer, pH 9.5) was dropped onto the activated chip, incubated at 50°C for 45 min and kept at room temperature so that the 5′-terminus of the probe DNA was attached to the chip. The quantity of immobilized DNA was checked by fluorescence microscopy with a confocal scanning fluorescence microscope (LSM-200; Olympus, Tokyo, Japan).

Recovery of DNA Using Photo-Thermal Denaturation

The DNA chip was rinsed and overlaid with 5 µL 20 mM Tris-HCl (pH 7.4) containing 2 mM EDTA (2× TE buffer). A small area on the chip was heated with IR laser (10, 25, 50 and 100 mW on the surface of the chip) using the microscopy system. After IR irradiation, a 4-µL drop of solution from the heated spot was collected into a vessel.

The recovered DNA in the drop was amplified to check quantity. PCR amplification was carried out under the same conditions as described above. The products of this amplification were checked by electrophoresis using a 2% agarose gel followed by staining with 0.5 µg/mL ethidium bromide and analyzed with a fluorescence-image analyzer (FM-Bio® 100; Hitachi Software Engineering, Tokyo, Japan).

Rehybridization of Fluorophore-Labeled DNA with an ssDNA on the Microchip

A 60-nucleotide fluorophore-labeled oligomer ssDNA (60-nucleotide sample DNA) complementary to the 60 nucleotides from the 3′-end of the immobilized strand on the DNA chip was diluted to 2 µM. For rehybridization, the solution was dropped on the chip surface and incubated for 3 min at 60°C. After rehybridization, the chip was rinsed with 2× TE buffer at room temperature and analyzed using the microscopy system.

RESULTS AND DISCUSSION

The purpose of this study was to demonstrate the feasibility of denaturing and extracting sample DNA from a small area by a photo-thermal denaturation procedure. First, we examined the efficiency of denaturation of sample DNA from the chip surface with a conventional heating procedure using a heat block. When the chip was maintained at 95°C for 1 min, all of the sample DNA, which had been hybridized to the surface-bound probe DNA, was released from the chip surface (Figure 3, a and b). As shown in Figure 3b, more

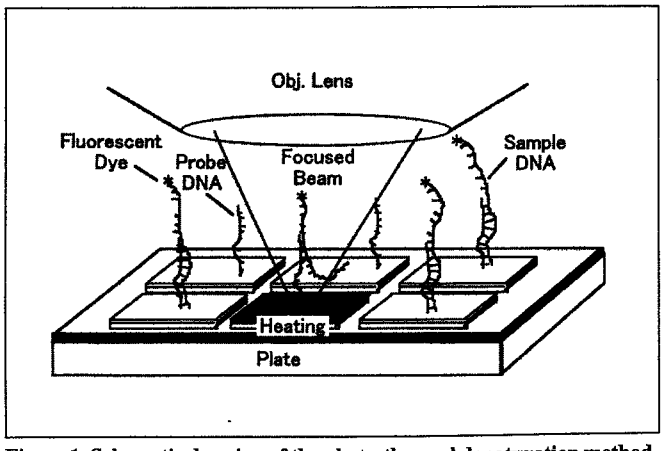

Figure 1. Schematic drawing of the photo-thermal denaturation method. First, the target DNA sample is captured by the immobilized probe DNA on the microchip surface. After the area for spot heating is selected by fluorescence microscopy, the area is heated by irradiation with an IR laser. The sample DNA released into the solution is collected and used for further analysis. The chosen DNA samples attached to the particular area on the chip surface are released by spot heating, which is controlled by the IR focused beam.

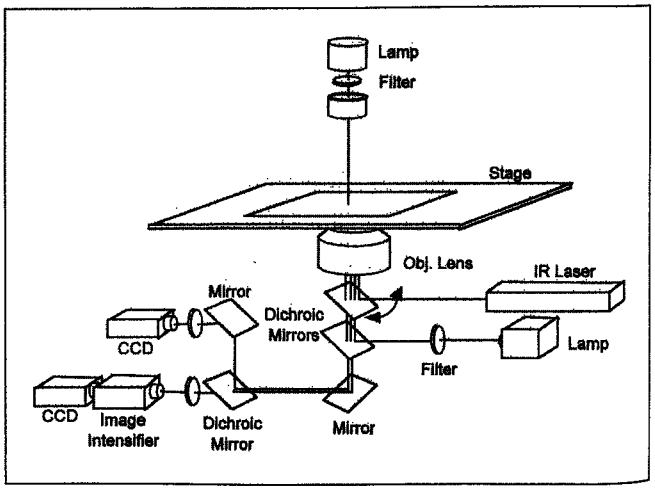

Figure 2. Schematic drawing of the photo-thermal denaturation microscopy system for area-specific extraction of surface-bound DNA. The microscope has three different optical units for phase-contrast, fluorescence and IR laser irradiation (5,7). Dichroic mirrors and band-pass filters direct the beams of the three different wavelengths of light.

than 95% of the fluorescent sample DNA was released from the chip surface. Next, a 2-μM 60-nucleotide sample DNA in 50 mM Tris-HCl (pH 7.5) was loaded onto the chip and successfully rehybridized with the surface-bound probe DNA (Figure 3c). The results indicate the following two facts. First, the integrity of the probe DNA remained intact, with the whole strands undamaged even after denaturation, as indicated by the 60-nucleotide sample DNA successfully attaching to the 3′-end (free end) of probe DNA. Second, the chromium-coated microchip served as a good substrate for the immobilized probe DNA and could release almost 100% of sample DNA, and 70% could be rehybridized on average through the thermal denaturation and renaturation steps. Note that the proportion of irreversibly attached sample DNA on the chromium-coated chip is negligibly small in contrast to the glass surface (Figure 3d). As shown in Figure 3d, the amount of undetached sample DNA on the glass surface was 90% after the denaturation process, in strong contrast to the case with the chromium-coated surface, which was less than 5%. This may

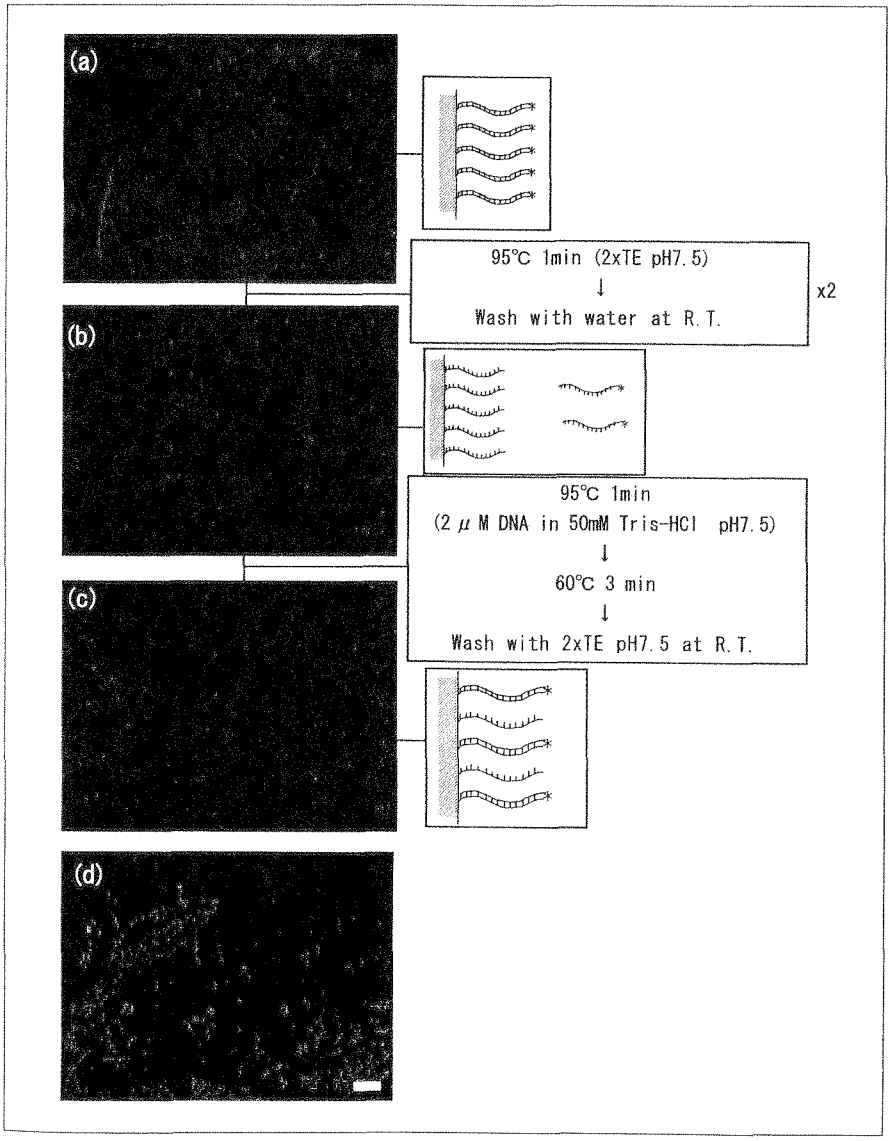

Figure 3. Fluorescence micrographs of the chromium-coated microchip surface and glass surface. (a) Fluorescence image of the chromium-coated microchip with attached fluorescent DNA; (b) the chip after the photo-thermal denaturation process; (c) the chip after rehybridization with the sample; and (d) the glass surface after the denaturation process. Bar, 200 μm.

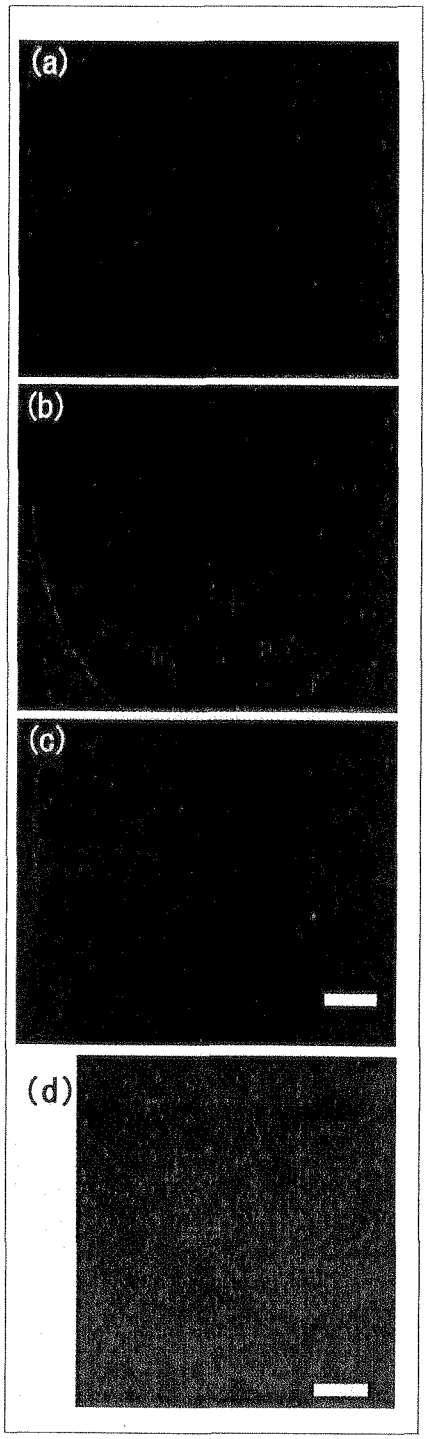

Figure 4. Fluorescence and phase-contrast micrographs of the microchip surface. Fluorescence image of the microchip surface before (a) and after (b) IR laser beam irradiation; (c) the chip after rehybridization with the sample DNA on the IR-irradiated microchip; and (d) phase-contrast micrograph of (c). The numbers traced on the surface of the chromium-coated microchip (100, 50, 25 and 10, respectively) indicate the power of IR laser irradiation for tracing. 100, 50, 25 and 10 mW. The word "HARL" was traced with a 10-mW IR laser beam. Bars, 100 μm.

be due to the charge of chromium (zeta potential) at the boundary of the chip surface, which prevents the nonspecific adsorption of sample DNA directly onto the chip surface.

The chromium-coated microchip has three advantages in the photo-thermal denaturation method. The first is its improvement of the absorbance of the IR laser on the surface of the chip during heating. While absorbance of a glass slide and water is negligibly small at 1053 nm, the 6-nm-thick chromium-coated surface achieved 40% absorption of the IR laser. The second advantage is the high efficiency of silane coupling on the oxydized chromium at the surface of the plate compared with that of the glass surface. In general, silane coupling works far more efficiently on a metal oxide than a glass surface. The third advantage is, as mentioned above, the prevention of nonspecific DNA adsorption.

Before photo-thermal spot heating, the fluorophore-labeled 619-nucleotide ssDNA (standard sample DNA), the complementary pair of whole-length probe DNA was hybridized onto the chromium-coated chip (Figure 4a). Importantly, although the whole area of the microchip was exposed to the standard sample DNA solution, the DNA attached only to the area coated with probe DNA. Next, the 1053-nm focused IR beam irradiated the surface of the chip and scanned it with varying laser power (10–100 mW) (Figure 4b). Bubbles generated by boiling water were sometimes observed at the irradiated area, indicating that the temperature of solution in the focused area exceeds boiling point. Figure 5a shows a magnified image of the area irradiated at 25 mW in Figure 4b. Figure 6a is the trace of fluorescence intensity along the line A-A in Figure 5a. As shown in Figures 5a and 6a, fluorescence intensity decreased in two steps, first to less than 30% in region P with a width of 30 μm and then to less than 5% in region Q with a width of 10 μm.

After photo-thermal extraction, we examined whether the probe DNA is maintained intact after IR irradiation by rehybridizing the 60-nucleotide sample DNA. Figure 4c shows the result of rehybridization between the 60-nucleotide sample DNA and the probe DNA after 10–100 mW IR laser irradiation. As analyzed in the 25-mW case (Figure 5b and Figure 6b), fluorescence intensity in region P recovered to the original level after the rehybridization procedure (width R), but the intensity in region Q did not. Thus, although all nonfluorescent lines traced by the IR beam

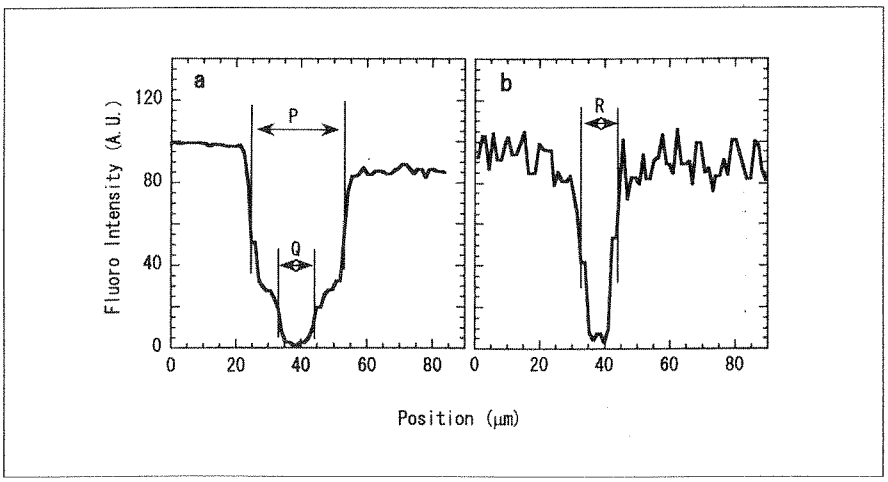

Figure 6. Fluorescence intensities of the IR-irradiated microchip surface. (a) and (b) fluorescence intensity profile along the A-A line in Figure 5, a and b, respectively.

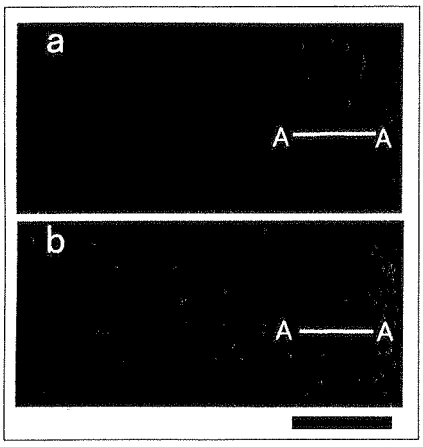

Figure 5. Fluorescence micrographs and intensity profiles of the 25-mW IR-irradiated microchip surface. (a) Fluorescence image of the microchip surface after 25 mW IR laser irradiation (magnified from Figure 4b); and (b) the chip after rehybridization with the sample DNA on the IR-irradiated microchip (magnified from Figure 4c). Bar, 100 μm.

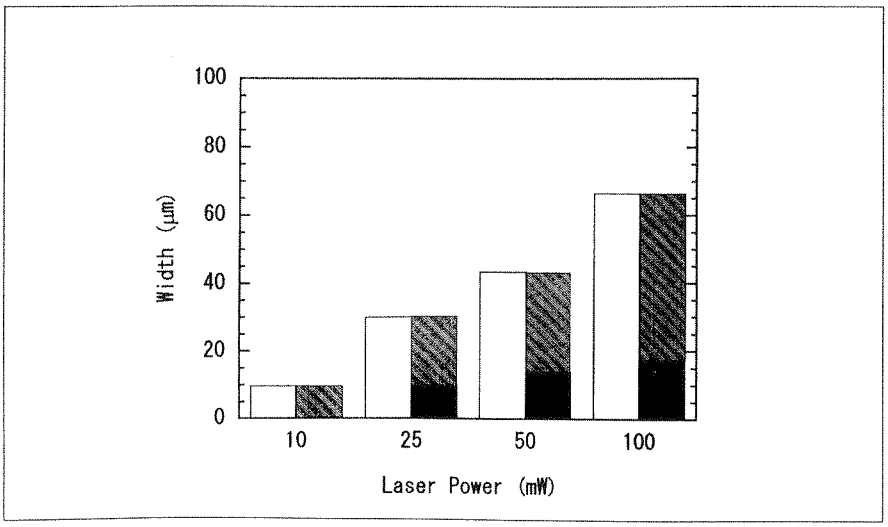

Figure 7. Laser power dependence of DNA denaturation on the microchip surface. Open box, width of the denatured area of the fluorophore-labeled sample DNA after IR irradiation; closed box, width of the damaged area on which no rehybridization occurred after rehybridization; hatched box, width of the rehybridized area after rehybridization.

at greater than 10 mW remained even after the rehybridization process, those traced at 10 mW were completely redecorated with fluorophores (Figure 4c). The width of the traced lines increased as laser power increased (Figure 7). A phase-contrast image (Figure 4d) shows that the chromium film was damaged by IR irradiation stronger than 10 mW. These results demonstrate that the probe DNA remains undamaged after IR irradiation unless the chromium coating has been damaged.

Finally, we measured the amount of sample DNA extracted from the chip after spot-heating a 100 × 10 μm area with a 10-mW IR focused beam. From fluorescence intensity analysis of the beam, more than 70% of the sample DNA was released from the chip surface after irradiation. As shown in Figure 8, the total amount of extract was in the order of 10^{-17} mol, on the basis that the fluorescence intensity of the extracted sample DNA was between that of the 1×10^{-16} mol and 1×10^{-17} mol reference samples after 15 cycles of PCR amplification. This result indicates that this photo-thermal denaturation extracted at least one DNA molecule from a 13 × 13 nm^2 area (10^{-17} mol/1000 μm^2) and further indicates that this method allows the area-specific extraction of a specified sample DNA.

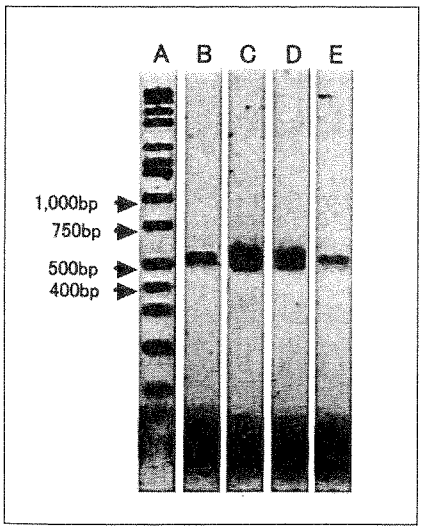

Figure 8. Agarose gel electrophoresis of PCR products amplified from the microchip extract. Five microliters of the DNA products were applied to a 2% agarose gel. Lane A, DNA molecular markers; lane B, sample DNA extracted from 10^3 μm^2 microchip surface; lanes C–E, concentration references, 1×10^{-15}, 10^{-16} and 10^{-17} mol of the same DNA, respectively.

The present study shows the potential of this DNA chip as a DNA purification apparatus. Spatial resolution of the denaturation spot size can be improved by increasing the objective lens magnification. We feel that this photothermal method will greatly enhance separation efficiency of different DNA from crude samples.

ACKNOWLEDGMENTS

We thank Drs. K. Miyauchi, T. Iwayanagi and T. Sakamoto of Hitachi, Ltd. for their support, and Dr. G. Harris for English editing. We also thank Prof. K. Kinosita, Jr. of Keio University and Dr. T. Nishizaka of Core Research for Evolutional Science and Technology (CREST) for their cooperation in consulting on the microscopy system. This research was partly supported by Grants-in-Aid for Scientific Research, for Scientific Research on Priority Areas and for the High-tech Research Center Project from the Ministry of Education, Science, Sports and Culture of Japan [grant no. 11559016 to S.I., no. 11878129 to S.I. and no. 11CE2006 (Komaba Complex Systems Life Science Project) to K.K.] and Grants-in-Aid from the Japan Science and Technology Corporation (CREST).

REFERENCES

1. **Burns, M.A., B.N. Johnson, S.N. Brahmasandra, K. Handique, J.R. Webster, M. Krishnan, T.S. Sammarco, P.M. Man et al.** 1998. An integrated nanoliter DNA analysis device. Science *282*:484-487.
2. **Cheng, J., E.L. Sheldon, L. Wu, A. Uribe, L.O. Gerrue, J. Carrino, M.J. Heller, and J.P. O'Connel.** 1998. Preparation and hybridization analysis of DNA/RNA from *E. coli* on microfabricated bioelectronic chips. Nat. Biotechnol. *16*:541-546.
3. **Kambara, H.** 1998. Recent progress in fluorescent DNA analyzers and methods. Curr. Topics Anal. Chem. *1*:21-36.
4. **Kato, H., T. Nishizaka, T. Iga, K. Kinosita, Jr. and S. Ishiwata.** 1999. Imaging of thermal activation of actomyosin motors. Proc. Natl. Acad. Sci. USA *96*:9602-9606.
5. **Kinosita, K., Jr., H. Itoh, S. Ishiwata, K. Hirano, T. Nishizaka and T. Hayakawa.** 1991. Double-view microscopy with a single camera: real-time imaging of molecular orientations and calcium. J. Cell Biol. *115*:67-73.
6. **Lockhart, D.J., H. Dong, M.C. Byrne, M.T. Follettie, M.V. Gallo, M.S. Chee, M. Mittmann, C. Wang et al.** 1996. Expression monitoring by hybridization to high-density oligonucleotide arrays. Nat. Biotechnol. *14*:1675-1680.
7. **Nishizaka, T., H. Miyata, H. Yoshikawa, S. Ishiwata and K. Kinosita, Jr.** 1995. Unbinding force of a single motor molecule of muscle measured using optical tweezers. Nature *377*:251-254.
8. **O'Donnell, M.J., K. Tang, H. Koster, C.L. Smith and C.R. Cantor.** 1997. High-density, covalent attachment of DNA to silicon wafers for analysis by MALDI-TOF mass spectrometry. Anal. Chem. *69*:2438-2443.
9. **Service, R.F.** 1998. Microchip arrays put DNA on the spot. Science *282*:396-398.
10. **Wang, D.G., J.-B. Fan, C.-J. Siao, A. Berno, P. Young, R. Sapolsky, G. Ghandour, N. Perkins et al.** 1998. Large-scale identification, mapping, and genotyping of single-nucleotide polymorphisms in the human genome. Science *280*:1077-1082.

Received 5 March 1999; accepted 1 December 1999.

Address correspondence to:
Dr. Kenji Yasuda
Department of Life Sciences
Graduate School of Arts and Sciences
The University of Tokyo
3-8-1 Komaba, Meguro
Tokyo 153-8902, Japan
Internet: cyasuda@mail.ecc.u-tokyo.ac.jp

Biophysical Journal Volume 78 June 2000 3112–3119

Temperature Change Does Not Affect Force between Single Actin Filaments and HMM from Rabbit Muscles

M. Kawai,* K. Kawaguchi,† M. Saito,† and S. Ishiwata†

*Department of Anatomy and Cell Biology, College of Medicine, University of Iowa, Iowa City, Iowa 52242 USA and †Department of Physics, School of Science and Engineering, Waseda University, Tokyo, Japan

ABSTRACT The temperature dependence of sliding force, velocity, and unbinding force was studied on actin filaments when they were placed on heavy meromyosin (HMM) attached to a glass surface. A fluorescently labeled actin filament was attached to the gelsolin-coated surface of a 1-μm polystyrene bead. The bead was trapped by optical tweezers, and HMM–actin interaction was performed at 20–35°C to examine whether force is altered by the temperature change. Our experiments demonstrate that sliding force increased moderately with temperature ($Q_{10} = 1.6 \pm 0.2$, ±SEM, $n = 9$), whereas the velocity increased significantly ($Q_{10} = 2.9 \pm 0.4$, $n = 10$). The moderate increase in force is caused by the increased number of available cross-bridges for actin interaction, because the cross-bridge number similarly increased with temperature ($Q_{10} = 1.5 \pm 0.2$, $n = 3$) when measured during rigor induction. We further found that unbinding force measured during the rigor condition did not differ with temperature. These results indicate that the amount of force each cross-bridge generates is fixed, and it does not change with temperature. We found that the above generalization was not modified in the presence of 1 mM MgADP or 8 mM phosphate.

INTRODUCTION

It has been known for some time that myosin cross-bridges generate force by interacting with actin molecules on the thin filament when they are placed in a solution that contains Ca^{2+} and $MgATP^{2-}$. It also has been known that the amount of force generation increases with an increase in the temperature in studies that used mammalian skeletal muscle fibers (Goldman et al., 1987; Zhao and Kawai, 1994; Ranatunga, 1996). To account for this temperature effect, two hypotheses are proposed. One hypothesis assumes that the force per cross-bridge does not change, but the number of force-generating cross-bridges increases with the temperature (Zhao and Kawai, 1994). The other hypothesis assumes that the force per cross-bridge increases with an increase in the temperature, but the number of cross-bridges does not change. In these experiments, force (F) is formulated in the following way:

$$F = \underset{\text{(Fiber)}}{N\sum_i f_i X_i} = \underset{\text{(In vitro motility assay)}}{N f_1 X_1}, \quad (1)$$

where N is the number of active cross-bridges that are involved in cycling. In fiber studies, f_i is the force associated with a cross-bridge at a state i, and X_i is the probability of the cross-bridge at the state i ($0 \le X_i \le 1$). The summation is over the all cross-bridge states (6–7 states were identified in fiber experiments) that are arranged in parallel in half sarcomere. Eq. 1 is modified from Kawai and Zhao (1993) to allow a change in the number of actively cycling cross-bridges (N). In the first hypothesis, X_i changes with temperature, and in the second hypothesis, f_i changes with temperature.

To obtain an insight on which one of the three parameters in Eq. 1 might change with temperature at the molecular level, we designed experiments using an in vitro motility assay, and studied sliding force between heavy meromyosin (HMM) molecules attached to a glass slide and an actin filament attached to a polystyrene bead that was clamped by a laser trap (optical tweezers). In the in vitro motility system, two cross-bridge states have been recognized. One is the attached state ($i = 1$) that generates force ($f_1 > 0$), and the other is the detached state ($i = 2$) that does not generate force ($f_2 = 0$). The fiber form of Eq. 1 can be applied to the in vitro motility system, if we assume that X_1 is the duty ratio (Howard, 1997) and f_1 is the unitary force. In this case, the product f_1X_1 is the average force/cross-bridge. Quite interestingly, our results demonstrate that, although force (F) increases with temperature, this increase is primarily based on the number of cross-bridges (N), but f_1X_1 remains approximately the same as the temperature is changed in the range 20–35°C. A preliminary account of the present work was reported in a recent Biophysical Society meeting (Kawai et al., 1999).

METHODS

Experimental apparatus

The experimental apparatus used here is the same as reported previously (Miyata et al., 1994, 1995; Nishizaka et al., 1995a; Nishizaka, 1996; Ishiwata, 1998). The entire apparatus is mounted on a pneumatic isolation table (Herz Kogyo KK, Tokyo, Japan). The optical system is based on an inverted microscope (TMD-300, Nikon, Tokyo, Japan). The light from an

Received for publication 25 June 1999 and in final form 28 February 2000.

Address reprint requests to Masataka Kawai, Department of Anatomy and Cell Biology, The University of Iowa, Iowa City, IA 52242. Tel.: 319-335-8101; Fax: 319-335-7198; E-mail: masataka-kawai@uiowa.edu.

0006-3495/00/06/3112/08 $2.00

Nd-YLF laser (1053 nm, 1W: Amoco Laser, Naperville, IL) is led through the oil-immersion objective lens (100×, n.a. = 1.3) from down below and traps a polystyrene bead in the flow cell to function as optical tweezers. The trap center of optical tweezers can be moved at a constant rate by controlling a mobile mirror with two DC-servo motors (Optmike-e; Sigma Koki, Hidaka, Japan). The light from a Halogen lamp, filtered at 380–520 nm, illuminates the flow cell, and its image is recorded by the CCD camera. The light from a Hg lamp is filtered at 550 nm and illuminates the flow cell from below. Accompanying fluorescent light (>590 nm) is led into the image intensifier (KS 1381, Video Scope, Washington, DC) before it is recorded by another CCD camera (CCD-72, Dage-MTI, Michigan City, IN). Phase contrast and fluorescence microscope images are combined and monitored on one screen. The combined image is videotaped (Hi8 Video, Sony Corp, Tokyo, Japan) for later analysis.

Flow cell

Both surfaces of a large coverslip (24 × 60 × 0.15 mm) were coated with collodion dissolved in 3-methylbutyl acetate. A small coverslip (20 × 20 × 0.15 mm) was glued to the large coverslip with double-stick tape at two sides. The gap between the two glass surfaces was about 0.1 mm. The total volume of the flow cell was about 25 μl. From one open side, 25 μl of HMM solution (1 μg/ml for rigor, else 60 μg/ml in solution HD) was applied and settled for 1 min to allow the HMM molecules to adsorb on the glass surface. Another 25 μl of HMM solution was applied from the other side. The cell was then washed by 25 μl of an experimental solution (CONT, +P, +ADP, or Rigor; Table 1). After 1 min, 25 μl rhodamine-phalloidin-labeled actin filaments in the same experimental solution were flowed in. Actin filaments were attached to polystyrene beads. The two open sides were then sealed by enamel (nail polish), and the flow cell was placed in the experimental apparatus.

Experimental solutions

Solutions used for the present studies are summarized in Table 1. Before mixing solutions, doubly distilled water was depressurized for 20 min by aspirator to minimize dissolved O_2. ATP was added as $Na_2H_2ATP{\cdot}2H_2O$, Pi as $H_{1.5}Na_{1.5}PO_4$, ADP as $KH_2ADP{\cdot}3H_2O$, EGTA as H_4EGTA, and pH was adjusted to 7.40.

Proteins, actin filaments, and polystyrene beads.

G-actin and HMM were purified from rabbit white skeletal muscles as described (Suzuki et al., 1996). Gelsolin was purified from bovine serum (Kurokawa, 1990). Polystyrene beads (1.0-μm diameter; Suzuki et al., 1996) were washed with carbonate and phosphate buffers, and coated with BSA and gelsolin. Actin was polymerized, rhodamine-conjugated phalloidin was bound, then F-actin was attached to polystyrene beads. Gelsolin binds to F-actin and serves as an anchor at the barbed end.

Temperature study

For experiments at 20 and 25°C, the room temperature was equilibrated to the respective temperatures. For experiments at 30 and 35°C, the inverted microscope, including the stage and the flow cell, was enclosed by a Nikon-plexiglass cover and its inside temperature was controlled. The temperature was measured by a thermister attached to the microscope stage near the flow cell, and regulated within ±1°C of the designated experimental temperature. The temperature in the flow cell was also estimated from thermal quenching of the fluorescence from rhodamine-maleimide conjugated to tubulin subunits of microtubule (Kawaguchi and Ishiwata, manuscript in preparation), a method similar to that reported earlier (Kato et al., 1999). For the purpose of Q_{10} calculation, Q_5 was first obtained and averaged, and then the Q_{10} was calculated as the square of Q_5. Q_5 is defined as the ratio of a parameter, which is measured at two temperatures that are 5°C apart.

RESULTS

Force on cross-bridges at different temperatures

A bead to which an actin filament is attached is placed 5 μm above the HMM-coated glass surface, which is moved to the left to align the filament parallel to the surface (Fig. 1 *A*). Then, the bead is lowered within 1.0 μm from the surface and filament–HMM interaction is performed in the presence of ATP (Fig. 1, *B* and *C*). From the video image (30 frames/sec), the displacement of the bead from the trap center is traced against time (Fig. 2). Sliding force is calculated as Force = k * Displacement, where k is the spring constant of the optical trap (k = 0.29 pN/nm). For detecting small force, the spring constant k was attenuated either to 50 or 30% of the value by inserting an appropriate neutral-density filter on the incident Nd-YLF laser beam. The length of actin filament was determined from the video image. Because the amount of force is proportionate to the length of actin filament (Kishino and Yanagida, 1988), the force value is divided by the length value to obtain force per unit length of the actin filament.

Figure 3 represents force plotted against the temperature for three experimental conditions (control, +Pi, +ADP).

TABLE 1 Solution compositions

	ATP (mM)	Pi (mM)	ADP (mM)	$MgCl_2$ (mM)	EGTA (mM)	KCl (mM)	DTT (mM)	Im-HCl (mM)	BSA (mg/ml)	GOC* (+/−)
AB†	–	–	–	4	1	25	–	25	–	–
HD	–	–	–	4	1	25	2	25	–	–
CONT	1	–	–	4	1	25	10	25	0.5	+
+Pi	1	8	–	4	1	8	10	25	0.5	+
+ADP	1	–	1	4	1	25	10	25	0.5	+
Rigor	–	–	–	3	1	28	10	25	0.5	+

*GOC represents 4.5 mg/ml glucose, 0.216 mg/ml glucose oxidase, and 0.036 mg/ml catalase to remove dissolved O_2 to minimize photo bleaching (Harada et al., 1990). In all solutions, pH was adjusted to 7.40.

†AB, actin buffer; HD, diluting solution for HMM; DTT, Dithiothreitol; Im-HCl, Imidazole-HCl.

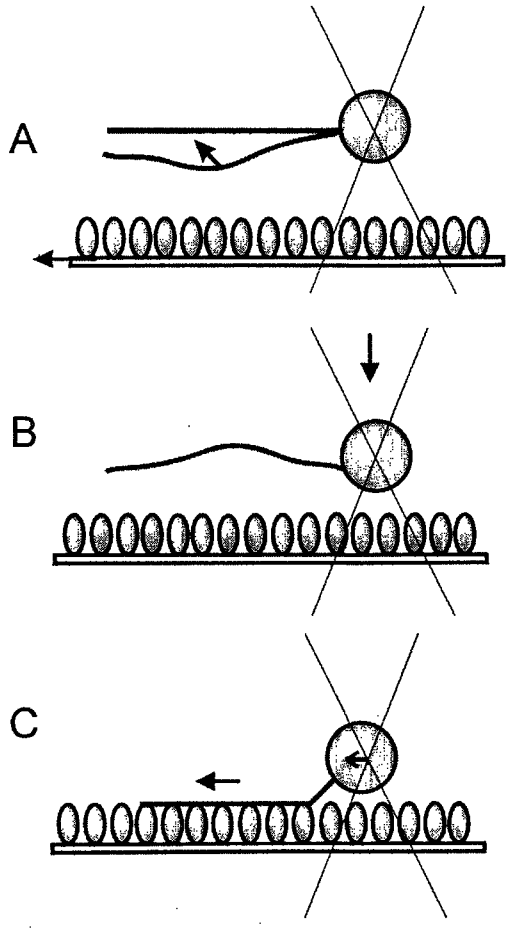

FIGURE 1 The method of measuring force on the single actin filament by optical tweezers. (*A*) An actin filament-attached bead (1 μm in diameter) is placed 5 μm above the HMM-coated glass surface, which is moved to the left (*lower arrow*) to line up the filament in parallel to the glass surface (*upper arrow*). (*B*) The bead is lowered within 1.0 μm from the glass surface (*arrow*). (*C*) The actin filament interacts with HMM to generate leftward force (*larger arrow*). This causes the bead displacement from the trap center indicated by the X mark. The displacement of the bead is measured (*small arrow*) and force is calculated by multiplying the spring constant of the optical tweezers.

Experiments were carried out in the presence of 1 mM ATP (Table 1). For these experiments, 60 μg/ml HMM was used to coat the glass surface. A proportionate relationship between force and the HMM concentration was demonstrated for 0–200 μg/ml HMM (Nishizaka, 1996) under similar experimental conditions. As shown in Fig. 3, a small increase in force was observed as the temperature was increased in the range of 20 to 35°C. This trend was not altered in the presence of 1 mM ADP or 8 mM Pi, except that force was slightly larger in the presence of ADP. From Fig. 3, we calculated Q_{10} for the control condition to be 1.6 ± 0.2 (±SEM, n = 3), Q_{10} in the presence of 8 mM Pi to be 1.8 ± 0.4 (n = 3), and Q_{10} in the presence of 1 mM ADP to be 1.4 ± 0.3 (n = 3). These values were not

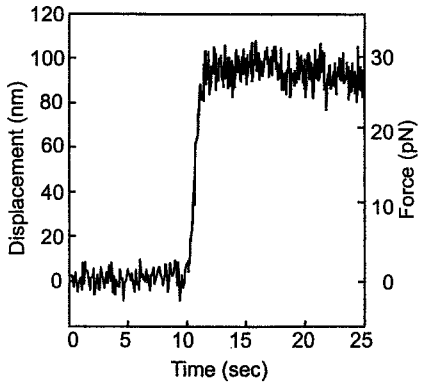

FIGURE 2 The time course to measure force on single actin filament. An actin filament-attached bead is placed within 1.0 μm above the HMM-coated surface, and filament-HMM interaction is performed in the presence of ATP (Fig. 1). The displacement (*left ordinate*) of the bead from the trap center is traced against time at the video rate (30 frames/sec). Sliding force (*right ordinate*) is calculated as Force = k * Displacement, where k is the spring constant of the optical trap (k = 0.29 pN/nm). The length of this particular actin filament was 4.8 μm.

significantly different from the control condition. The averaged Q_{10} for all activating conditions tested was 1.6 ± 0.2 (n = 9).

Cross-bridge number per unit length of the actin filament

Because the total number of cross-bridges (N in Eq. 1) available for interaction with the actin filament may vary

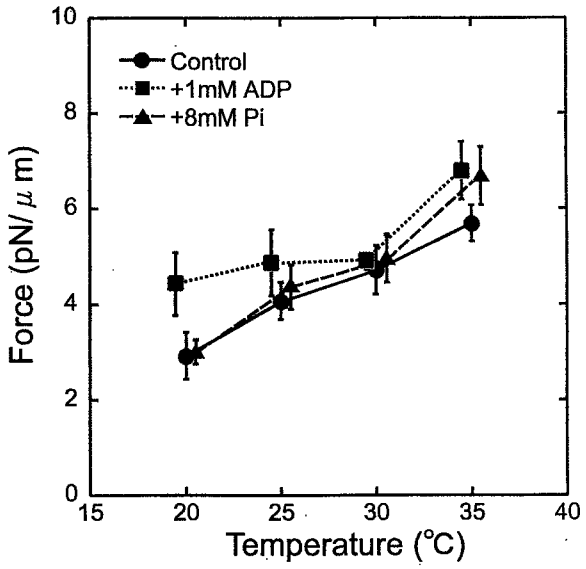

FIGURE 3 Force (pN) per unit length (μm) of actin filament is plotted against the temperature for three experimental conditions (control, +Pi, and +ADP) in the presence of 1 mM ATP. The error bars represent ±SEM. In the control experiment, n = 4, 5, 3, and 5 for 20, 25, 30, and 35°C, respectively. In the presence of Pi or ADP, n = 3 for 20°C, and n = 4 otherwise. Force was measured as shown in Figs. 1 and 2.

depending on the temperature, we counted the cross-bridge number during rigor induction, i.e., in the absence of ATP. For this series of experiments 1 μg/ml HMM was used to coat the glass surface. The method of counting the cross-bridge number and measuring unbinding force in the absence of ATP is depicted in Fig. 4 (see also Fig. 4 of Miyata et al., 1995; Fig. 2a of Nishizaka et al., 1995a; and Fig. 1 of Nishizaka et al., 1995b). The actin filament-attached bead is placed 2–3 μm above the HMM-coated surface, and filament–HMM interaction is performed. This height is necessary to count the cross-bridge number so that the unbound HMM does not rebind to the actin filament. From the video image, the displacement of the bead from the trap center is plotted against time (Fig. 4).

The gap on the trace represents unbinding of a single HMM molecule from the actin filament. The number of gaps is counted and divided by the filament length to obtain the number of cross-bridges per 1 μm of the actin filament. This method determines N in Eq. 1, the number of cross-bridges involved in cycling. A proportionate relationship between the number of cross-bridges and the HMM concentration was demonstrated for 0–15 μg/ml HMM under similar experimental conditions (Nishizaka, 1996, and manuscript in preparation). At a higher concentration, too many cross-bridges are formed, hence, counting the cross-bridge number becomes not possible. The results are plotted in Fig. 5. This figure demonstrates that the number of cross-bridges available for interaction with the actin filament increases with temperature. From Fig. 5, the averaged Q_{10} was calculated to be 1.5 ± 0.2 (n = 3).

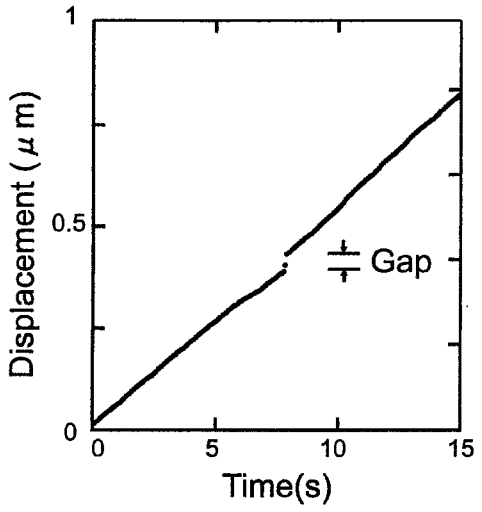

FIGURE 4 The time course to measure the number of cross-bridges and the unbinding force on single HMM molecules in rigor state. An actin filament-attached bead is placed 2–3 μm above the HMM-coated surface, and filament-HMM interaction is performed in the absence of ATP. The displacement of the bead from the trap center is traced against time. The gap on the trace represents unbinding of a single HMM molecule from the actin filament. The number of gaps is counted and divided by the actin filament length to obtain the number of cross-bridges per unit length. The unbinding force is calculated from the gap.

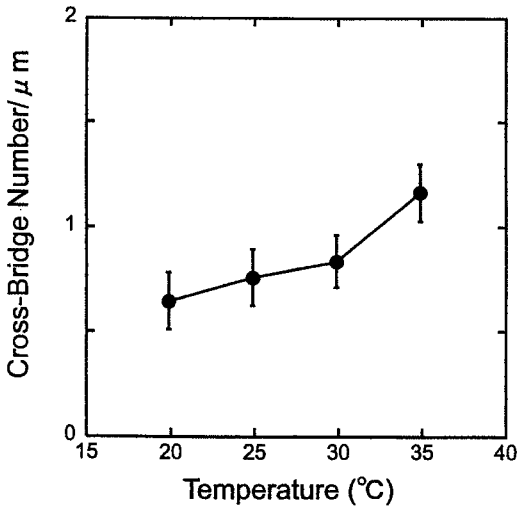

FIGURE 5 The cross-bridge number per unit length (μm) of actin filament in the absence of ATP is plotted against the temperature. The method of counting the cross-bridge number is shown in Fig. 4. The error bars represent ±SEM. n = 3, 4, 4, and 3 for the experiment at 20, 25, 30, and 35°C, respectively.

Corrected force on cross-bridges at different temperatures

Because the number of cross-bridges available for interaction with the actin filament increased with the temperature (Fig. 5), we divided the data of Fig. 3 with the data of Fig. 5, and plotted the results in Fig. 6. The errors in Figs. 3 and 5 were propagated and entered in Fig. 6 in a proper way (see figure legends). Figure 6 represents results from three experimental conditions (control, +1 mM ADP, and +8 mM Pi). Figure 6 demonstrates that the average force per cross-bridge (f_1X_1 in Eq. 1) remained approximately the same as the temperature was changed in the range 20–35°C in three experimental conditions.

Unbinding force

If the force generated by a cross-bridge changes with the temperature, this mechanism implies that a macromolecular change, such as in the shape of the myosin head, occurs when the temperature is elevated. If this is the case, then we expect that "unbinding force" also increases with the temperature. Unbinding force is the force at which a myosin cross-bridge detaches (unbinds) from actin when pulled away by external force, and measured by the "gap" in Fig. 4. The measurement is carried out in the absence of ATP, i.e., when rigor cross-bridges are formed. Unbinding force is plotted against the temperature in Fig. 7. As this figure

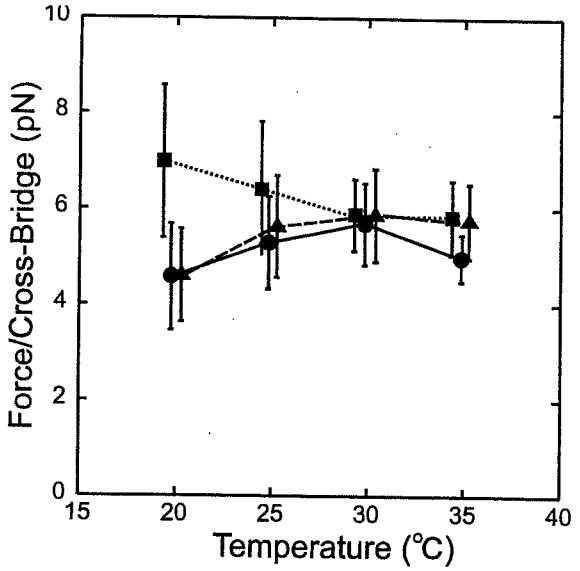

FIGURE 6 Corrected force is plotted against temperature. The data were obtained by dividing the values of force (Fig. 3) with the cross-bridge number (Fig. 5) to compensate for the artifact due to two-dimensional motility assay system, in which the number of HMM molecules within reach to the actin filament changes with the temperature. The same plotting nomenclatures as in Fig. 3 are used. The error bars E_z are calculated by $(E_z/Z)^2 = (E_x/X)^2+(E_y/Y)^2$ where X, Y, Z are the averaged values of Figs. 3, 5, 6, respectively ($Z = X/Y$), and E_x and E_y are SEM of Figs. 3 and 5, respectively.

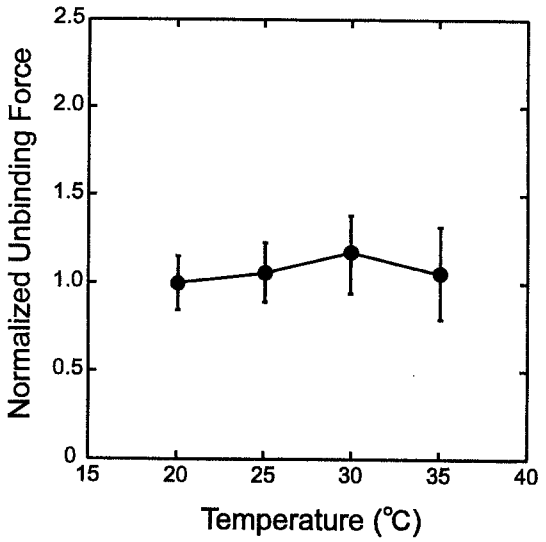

FIGURE 7 Unbinding force in the absence of ATP is plotted against the temperature after normalization at 20°C. The error bars represent ±SEM. n = 14, 17, 12, and 11 for experiments at 20, 25, 30, and 35°C, respectively. For these experiments, 1 μg/ml HMM was used to coat glass surface.

demonstrates, the unbinding force did not change much in the temperature range 20–35°C.

Sliding velocity

Unlike sliding force, the sliding velocity is expected to increase with temperature. To measure the velocity, actin filaments are placed on the HMM-coated surface, and the filaments are allowed to slide over the surface. From the video image (30 frames/sec), the position of the filament is obtained, and the sliding velocity is estimated from the time course in which the translation is linear over 5 μm. The results are plotted in Fig. 8 against the temperature for three experimental conditions (control, +Pi, and +ADP).

The experiments were carried out in the unloaded conditions and in the presence of 1 mM ATP. For this series of experiments, the standard 60 μg/ml HMM was used to coat the glass surface. As shown in Fig. 8, the velocity increased significantly with temperature with the average Q_{10} of 3.0 ± 0.7 (n = 4) in the control condition. The velocity was slightly faster in the presence of 8 mM Pi, and slower in the presence of 1 mM ADP. In this sense, the velocity behaves similar to the apparent rate constant of tension transients. The apparent rate constant $2\pi b$ (the rate constant of delayed tension) is faster in the presence of Pi and slower in the presence of ADP (Kawai and Zhao, 1993). From Fig. 8, Q_{10} in the presence of 8 mM Pi was calculated to be 3.0 ± 1.2 (n = 3), and Q_{10} in the presence of 1 mM ADP was 2.7 ± 0.9 (n = 3). These Q_{10} values were not significantly differ-

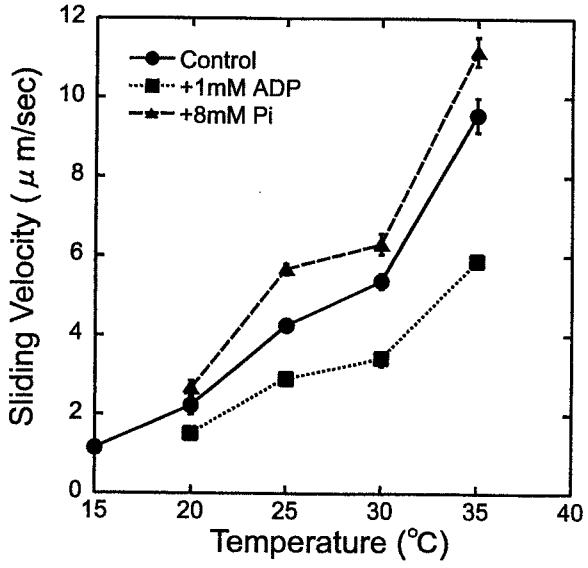

FIGURE 8 Sliding velocity is plotted against the temperature for three experimental conditions (control, +Pi, and +ADP) in the presence of 1 mM ATP. The error bars represent ±SEM. Error bars smaller than the symbol size cannot be seen. In the control experiment, n = 5, 4, 5, and 4 for 20, 25, 30, and 35°C, respectively. In the presence of Pi, n = 4, 3, 4, and 5 for experiments at 20, 25, 30, and 35°C, respectively. In the presence of ADP, n = 4, 5, 4, and 3 for experiments at 20, 25, 30, and 35°C, respectively.

ent from that of the control activating condition. The averaged Q_{10} for all conditions tested was 2.9 ± 0.4 (n = 10).

DISCUSSION

The purpose of the present study was to determine whether the isometric force on a cross-bridge increases with temperature using the in vitro motility assay system. For this purpose, we used synthetic actin filaments attached to polystyrene beads. The actin filaments were visualized by fluorescence as rhodamine-conjugated phalloidin was bound to the filament. HMM was attached to a collodion-coated glass surface. The position of the polystyrene beads were controlled by the laser trap (optical tweezers), and the interaction between HMM molecules and the actin filament was monitored.

We observed an increase in force as the temperature was elevated (Fig. 3; see also Kato et al., 1999). There are two possibilities to account for this increase: the cross-bridge number available for force generation (N in Eq. 1) may increase with temperature, and average force/cross-bridge (f_1X_1 in Eq. 1) may increase with temperature. We determined the cross-bridge number in the absence of ATP (rigor condition), because it is not possible to determine the number in the presence of ATP under the present set up. Interestingly, we found that the cross-bridge number increased with temperature (Fig. 5) just in the same way as force did. This increase may not be a physiological phenomenon, however, because the cross-bridge number is presumably maximized during the rigor induction, hence the number should not change with temperature in a physiological experiment. Therefore, the observed number increase may be specific to the in vitro motility system (Kato et al., 1999). One possibility is that the Brownian motion may release the head portion of HMM that are inadvertently stuck to the glass surface, but it leaves the C-terminus area of HMM attached to the glass surface, so that more HMM molecules become available to interact with the actin filament to generate more force at higher temperatures.

For this reason, we divided isometric force by the cross-bridge number to obtain corrected isometric force (f_1X_1, Fig. 6). We found that the corrected force does not change much with temperature in all three experimental conditions, from which we infer that the average force per cross-bridge does not change much with temperature in the in vitro motility assay system. The corrected force averaged 4.9 pN (range: 4.3–5.5 pN). This is not the unitary force, however, for this force value does not consider a 60× difference in the HMM concentration used in two sets of experiments. To obtain cross-bridge force, the ordinate values of Fig. 6 should be divided by the factor ~60, because the number of cross-bridges available for actomyosin interaction was 60× larger for the experiment of Fig. 3 than for the experiment of Fig. 5. Nishizaka (1996, and manuscript in preparation) demonstrated a proportionate relationship between the cross-bridge number and HMM for up to 15 μg/ml under the rigor condition, but no data are available for concentrations higher than 15 μg/ml. The factor must be >15, but ≤60, because the HMM concentration and the cross-bridge number may be nonlinear in this concentration range. Such nonlinearity is remote, however, because force and the HMM concentration are proportionally related for up to 200 μg/ml HMM under similar experimental conditions (Nishizaka, 1996). Thus, we calculate from our results that the force per cross-bridge (f_1X_1) is somewhere between 0.08 pN and 0.3 pN. The reason why this force value is less than unitary force (f_1) measured between actin and myosin molecules (1–6 pN, Finer et al., 1994; Miyata et al., 1995; Molloy et al., 1995; Ishijima et al., 1996) is because, in our measurement, force is the average over attachment and detachment cycle, whereas the unitary force (f_1) measures force during attachment. It is known that the duty ratio (X_1) is small in the in vitro motility assay system, and it is about 0.1 (Howard, 1997). What is important in this report is our conclusion that the average force per cross-bridge does not change much with temperature.

Although we could not examine the unitary force (f_1) and the duty ratio (X_1) independently, a possibility that both f_1 and X_1 change with temperature in a compensatory manner so that f_1X_1 remains the same is remote, because it is not likely that such compensation takes place at all temperatures we tested, and in all conditions (control, +Pi, and +ADP) we studied (Fig. 6). Furthermore, we measured unbinding force in the absence of ATP and studied the effect of temperature. We found that the unbinding force did not change much with temperature (Fig. 7). From results shown in Figs. 6 and 7, we infer that the HMM molecules do not change their shape much as the temperature is increased. A change in the shape would be necessary if force per cross-bridge or unbinding force were to change with the temperature, because force is presumably a result of the macromolecular architecture of the HMM and actin interrelationship. In this sense, it can be concluded that the result of Fig. 7 (unbinding force does not change with temperature) and the result of Fig. 6 (cross-bridge force does not change with temperature) are consistent.

In experiments using fast-twitch single skeletal muscle fibers, isometric force increases with temperature, and this increase was ascribed to an increase in the number (X_i in Eq. 1) of tension-generating cross-bridges (Zhao and Kawai, 1994), or to an increase in the force (f_i in Eq. 1) supported by an individual cross-bridge (Goldman et al., 1987; Kraft and Brenner, 1997). Both of these mechanisms result in an increase in the average force per cross-bridge (f_iX_i) with temperature. The total number of cross-bridges (N) involved in cycling is assumed not to change with temperature, because maximal activating condition with a saturating Ca^{2+} concentration was used in the fiber experiments. These experiments and mechanisms are primarily based on the temperature range ≤20°C. The effect of temperature is

smaller or absent when temperature is raised over 20°C (Bershitsky and Tsaturyan, 1992; Goldman et al., 1987; Zhao and Kawai, 1994; Ranatunga, 1996). Therefore, our results that the force/cross-bridge does not change much in the temperature range >20°C are consistent with the results on fiber experiments.

Sliding velocity is expected to increase with the temperature. This is because the velocity is limited by one or two steps in the cross-bridge cycle, and their rate constants almost invariably increase with the temperature (Goldman et al., 1987; Zhao and Kawai, 1994). In contrast, tension is determined primarily by the equilibrium constants (Kawai and Zhao, 1993), which may or may not be temperature sensitive. We found that the sliding velocity increased as the temperature was increased from 20 to 35°C (Fig. 8) with Q_{10} = 3.0 under the control-activating condition (Fig. 8). This quotient compares to 1.9 (Anson, 1992), 3.7 (calculated from Fig. 5 *B* of Winkelmann et al., 1995), 5.4 (calculated from Fig. 7 of Homsher et al., 1992), and 2.3–2.8 (calculated from the velocity data at 18°C and 40°C of Kato et al., 1999) under similar experimental conditions. Q_{10} in the presence of Pi (3.0) or ADP (2.7) is similar, but there is no previous work carried out in the presence of Pi or ADP.

It is interesting to point out that the sliding velocity decreases in the presence of ADP, much like in the case of the apparent rate constant. This observation can be explained by the mechanism that MgADP binds to the nucleotide binding site on myosin, and it competitively inhibits the ATP hydrolysis rate and work performance (Kawai and Zhao, 1993). It is also interesting to note that the velocity increases in the presence of Pi, as in the case of the apparent rate constant (Kawai and Zhao, 1993). This result may be consistent with the mechanism that Pi binding accelerates an approach to the steady state, and that the velocity behaves much like the apparent rate constant.

Although it may be difficult to carry out experiments on the actomyosin system because of the complexity of the myosin molecule, studying the temperature effect on the kinesin-microtubule system appears to be easier because kinesin is a smaller and simpler molecule than myosin. By using kinesin and microtubule isolated from bovine and porcine brains, respectively, Kawaguchi and Ishiwata (unpublished work) measured temperature dependence of force using optical tweezers. They found that the unitary force (f_1 in Eq. 1) produced by single kinesin molecules was about 7 pN, and this value did not differ in the temperature range between 20 and 35°C. Although the amino acid sequence of the motor domain of myosin and kinesin bears little homology, the tertiary structure of the motor domain bears a striking similarity in terms of the arrangement of α-helices and β-sheets; hence these two proteins are considered to have evolved from a common ancestor (Kull et al., 1998). It is interesting to know that the force that the two motor proteins generate does not differ at different temperatures, and this particular property was maintained throughout the process of evolution. This fact implies that the temperature insensitivity of the single molecular force is a fundamental property of a motor protein, and supports the idea that force is associated with a particular macromolecular architecture.

The results from single-molecule experiments, however, have to be applied to single-fiber experiments with caution, because there is a large difference in the solution composition in the two experimental systems. In particular, single-fiber experiments were carried out at or near physiological ionic strength (180–200 mM), whereas single-molecule experiments were carried out at a low ionic strength (about 50 mM). Because ionic interactions are weakened by increased ionic strength, single-molecule experiments become increasingly more difficult at higher ionic strength. Because the hydrophobic interaction is not affected by the ionic strength, the relative significance of the hydrophobic interaction is pronounced in single-fiber experiments, whereas the relative significance of the ionic interaction is pronounced in single-molecule experiments. As is well known, an increase in temperature facilitates hydrophobic interaction, because this interaction is endothermic (absorbs heat) and accompanies a large entropy increase (Zhao and Kawai, 1994). Similar temperature effect between a single-fiber system and a single-molecule system, in the temperature range of 20–35°C, suggests to us that the hydrophobic interaction may become saturated in this temperature range.

CONCLUSION

We found that force/cross-bridge does not change with temperature in in vitro assay in the temperature range 20–35°C.

This work was carried out during the tenure of a short-term fellowship to M.K. awarded by Japan Society for Promotion of Science in the summer of 1998. The work was also supported in part by grant IBN 96–03858 from the National Science Foundation and grant-in-aid 99–50437N from the American Heart Association National Center to M.K.; by grants-in-aid for Scientific Research (#10308030), for Scientific Research on Priority Areas (#11167280), for the High-Tech Research Center Project from the Ministry of Education, Science, Sports, and Culture of Japan, and by grants-in-aid for Japan Science and Technology, Core Research for Evolutional Science and Technology to S.I.

REFERENCES

Anson, M. 1992. Temperature dependence and Arrhenius activation energy of F-actin velocity generated in vitro by skeletal myosin. *J. Mol. Biol.* 224:1029–1038.

Bershitsky, S. Y., and A. K. Tsaturyan. 1992. Tension responses to Joul temperature jump in skinned rabbit muscle fibres. *J. Physiol. (Lond.)* 447:425–448.

Finer, J. T., R. M. Simmons, and J. A. Spudich. 1994. Single myosin mechanics: piconewton forces and nanometre steps. *Nature (Lond.)* 368:113–119.

Goldman, Y. E., J. A. McCray, and K. W. Ranatunga. 1987. Transient tension changes initiated by laser temperature jumps in rabbit psoas muscle fibers. *J. Physiol. (Lond.)* 392:71–95.

Harada, Y., K. Sakurada, T. Aoki, D. D. Thomas, and T. Yanagida. 1990. Mechanochemical coupling in actomyosin energy transduction studied by in vitro movement assay. *J. Mol. Biol.* 216:49–68.

Homsher, E., F. Wang, and J. R. Sellers. 1992. Factors affecting movement of F-actin filaments propelled by skeletal muscle heavy meromyosin. *Am. J. Physiol. Cell Physiol.* 262:C714–C723.

Howard, J. 1997. Molecular motors: structural adaptations to cellular functions. *Nature (Lond.)* 389:561–567.

Ishijima, A., H. Kojima, H. Higuchi, Y. Harada, T. Funatsu, and T. Yanagida. 1996. Multiple- and single-molecule analysis of the actomyosin motor by nanometer-piconewton manipulation with a microneedle: unitary steps and force. *Biophys. J.* 70:383–400.

Ishiwata, S. 1998. The use of fluorescent probes. In: *Current Methods in Muscle Physiology*, H. Sugi, editor. Oxford University Press, Oxford, U.K. 199–222.

Kato, H., T. Nishizaka, T. Iga, K. Kinosita, Jr, and S. Ishiwata. 1999. Imaging of thermal activation of actomyosin motors. *Proc. Natl. Acad. Sci. USA.* 96:9602–9606.

Kawai, M., K. Kawaguchi, M. Saito, and S. Ishiwata. 1999. The effect of temperature on sliding force and velocity of actin filaments and HMM. *Biophys. J.* 76:A35.

Kawai, M., and Y. Zhao. 1993. Cross-bridge scheme and force per cross-bridge state in skinned rabbit psoas muscle fibers. *Biophys. J.* 65: 638–651.

Kishino, A., and T. Yanagida. 1988. Force measurements by micromanipulation of a single actin filament by glass needles. *Nature (Lond.)* 334:74–76.

Kraft, T., and B. Brenner. 1997. Force enhancement without changes in cross-bridge turnover kinetics: the effect of EMD 57033. *Biophys. J.* 72:272–282.

Kull, F. J., R. D. Vale, and R. J. Fletterick. 1998. The case for a common ancestor: kinesin and myosin motor proteins and G proteins. *J. Muscle Res. Cell Motil.* 19:877–886.

Kurokawa, H., W. Fujii, K. Ohmi, T. Sakurai, and Y. Nonomura. 1990. Simple and rapid purification of brevin. *Biochem. Biophys. Res. Commun.* 168:451–457.

Miyata, H., H. Hakozaki, H. Yoshikawa, N. Suzuki, K. Kinosita Jr, T. Nishizaka, and S. Ishiwata. 1994. Stepwise motion of an actin filament over small number of heavy meromyosin molecules is revealed in an in vitro motility assay. *J. Biochem.* 115:644–647.

Miyata, H., H. Yoshikawa, H. Hakozaki, N. Suzuki, T. Furuno, A. Ikegami, K. Kinosita, Jr, T. Nishizaka, and S. Ishiwata. 1995. Mechanical measurements of single actomyosin motor force. *Biophys. J.* 68:S286–S290.

Molloy, J. E., J. E. Burns, J. Kendrick-Jones, R. T. Tregear, and D. C. S. White. 1995. Movement and force produced by a single myosin head. *Nature (Lond.)* 378:209–212.

Nishizaka, T. 1996. Microscopic analysis of function and mechanical properties of acto-myosin motor at single molecular level. Doctoral dissertation, Department of Physics, School of Science and Engineering, Waseda University, Tokyo, Japan.

Nishizaka, T., H. Miyata, H. Yoshikawa, S. Ishiwata, and K. Kinosita. Jr. 1995a. Unbinding force of a single motor molecule of muscle measured using optical tweezers. *Nature (Lond.)* 377:251–254.

Nishizaka, T., H. Miyata, H. Yoshikawa, S. Ishiwata, and K. Kinosita, Jr. 1995b. Mechanical properties of a single protein motor of muscle studied by optical tweezers. *Biophys. J.* 68:S75.

Ranatunga, K. W. 1996. Endothermic force generation in fast and slow mammalian (rabbit) muscle fibers. *Biophys. J.* 71:1905–1913.

Suzuki, N., H. Miyata, S. Ishiwata, and K. Kinosita, Jr. 1996. Preparation of bead-tailed actin filaments: estimation of the torque produced by the sliding force in an in vitro motility assay. *Biophys. J.* 70:401–408.

Winkelmann, D. A., L. Bourdieu, A. Ott, F. Kinose, and A. Libchaber. 1995. Flexibility of myosin attachment to surfaces influences F-actin motion. *Biophys. J.* 68:2444–2453.

Zhao, Y., and M. Kawai. 1994. Kinetic and thermodynamic studies of the cross-bridge cycle in rabbit psoas muscle fibers. *Biophys. J.* 67: 1655–1668.

ELSEVIER

Sensors and Actuators B 64 (2000) 88–94

SENSORS AND ACTUATORS B CHEMICAL

www.elsevier.nl/locate/sensorb

Position-specific release of DNA from a chip by using photothermal denaturation

Kazunori Okano [a,*], Kenji Yasuda [b], Shin'ichi Ishiwata [c,d,e,f]

[a] *Bio System Research Department, Central Research Laboratory, Hitachi Ltd., Kokubunji, Tokyo 185-8601, Japan*
[b] *Department of Life Sciences, Graduate School of Arts and Sciences, The University of Tokyo, Tokyo, Japan*
[c] *Department of Physics, School of Science and Engineering, Japan*
[d] *Advanced Research Institute for Science and Engineering, Japan*
[e] *Materials Research Laboratory for Bioscience and Photonics, Waseda University, Japan*
[f] *Core Research for Evolutional Science and Technology (CREST), "Genetic Programming" Team 13, Japan*

Abstract

A photothermal method to recover specific DNA fragments fixed in place on a DNA chip is described. This method uses infrared (IR) laser irradiation to thermally denature and release specific DNA immobilized in a specific area of a chip. A 1053-nm IR laser beam with an intensity of 10–100 mW is focused on the target area at a resolution of 10 μm, and the DNA fragments are released from the chip surface. We have demonstrated that DNA fragments containing different numbers of base pairs (231–799 bp) fixed in place on the DNA chip can be separately recovered. There are enough quantities of recovered DNA fragments that can be amplified by using polymerase chain reaction (PCR). The photothermal method coupled with the DNA chip can therefore be used in highly sensitive purification of DNA and will have many applications in the DNA chip technology.

Keywords: DNA chip; Photothermal denaturation; PCR; Infrared laser

1. Introduction

The purification of DNA fragments from living cells is a fundamental process in molecular biology and molecular diagnosis. We usually prepare a DNA library constructed from cloned DNA [1]. The cloning method is suitable for preparing a large number of DNA fragments, but is very laborious and time-consuming because of its cultivation processes. Nowadays, molecular biology is moving very rapidly towards the stage of functional genomics in which rapid preparation of different parts of genes will be required [2]. If a DNA library is constructed on a chip and any kind of DNA can be individually recovered from the chip, the DNA chip will become a very useful method and will change the way DNA-related experiments are done.

DNA chip technology in molecular biology has made rapid progress over the last 10 years [2–11]. Several approaches have been developed for producing DNA chips of different formats. In 1991, Fodor et al. [3] succeeded in making the microchips by photolithography on a solid surface. A chip containing 65,000 different 20-mer oligonucleotides of defined sequence in an area of 1.6 cm^2 was reported in 1996 [2], and it is now possible to assemble 150,000–300,000 oligonucleotides on one microchip [6]. Presynthesized oligonucleotides can be immobilized on a solid surface [5,7,8] or into a gel element fixed on a glass plate [9,10] by spotting the oligonucleotides. Any DNA produced by chemical syntheses, cloning, and polymerase chain reaction (PCR) can be immobilized on the microchip. The gel-fixed microchip has a high capacity for immobilizing oligonucleotides: 50 fmol of oligonucleotides is immobilized per microchip element of size 40 × 40 μm^2. This is more than 100 times higher than immobiliza-

* Corresponding author. Tel.: +81-423-23-1111; fax: +81-423-27-7833.
E-mail address: okano-k@crl.hitachi.co.jp (K. Okano).

0925-4005/00/$ - see front matter
PII: S0925-4005(99)00489-X

tion capacity of a plane glass surface, and this high capacity increases the hybridization velocity and the dynamic range. DNA microchips have been applied for gene expression analyses [5,11] and detection of single-nucleotide polymorphisms (SNPs) [6]. Matrix-assisted laser desorption/ionization time of flight (MALDI-TOF) mass spectrometry coupled with a DNA chip presents a new strategy for DNA analysis; it can analyze DNA extremely quick [12]. The oligonucleotide chip in reference [13] is very promising because the chip has a structure to control the hybridization by an electrode addressing each element of the chip. The DNA strands in a sample solution can quickly approach the probes immobilized on the chip surface. These DNA chip technologies, however, are mainly used in devices for analyzing a large number of DNA fragments, not for separating and preparing DNA fragments for further applications. A serious problem to be overcome in DNA separation applications is how to individually recover the DNA into aqueous solution from each small area on the microchip surface where DNA fragments are trapped.

Consequently, we developed a DNA preparation method that uses a photothermal approach to recover specific DNA fragments trapped on a chip surface. We found that the recovered DNA can be amplified by PCR and be subsequently characterized by further analysis. It is concluded that the developed method has a high potential for characterizing expressed genes and analyzing the differences between genes by using DNA chip.

2. Principle

The DNA preparation method is based on the fact that the stability of double-stranded DNA is highly dependent on temperature. As most double-stranded DNA fragments are denatured at 90–95°C, DNA hybridized with DNA probes fixed in place on the chip surface can be released by thermal denaturation. The temperature of the chip surface is locally elevated by irradiating a small metal-coated area with an infrared (IR) laser beam as schematically shown in Fig. 1 [14].

The method consists of five processes: (1) hybridizing reaction of sample DNA fragments with probe DNA fixed on the chip surface; (2) washing the chip surface to remove non-specific DNA species; (3) heating a small metal-coated area on the chip by IR laser irradiation to extract specific DNA from the chip surface; (4) collecting the released DNA; and (5) repeating of steps (3) and (4) in order to recover multiple DNA fragments fixed on the chip. This method of photothermal denaturation using an IR laser and a DNA chip rapidly extracts DNA fragments from the chip surface because it does not require any cloning procedure or electrophoretic separation.

3. Experimental

3.1. DNA samples preparation

The DNA samples were prepared by the method previously reported [15] as disclosed below. A half picomole of amplified human genome fragments (8.7 kb, supplied by the Human Genome Center, Institute of Medical Science, University of Tokyo, Japan) was digested with 40 units of *Hsp*92II (Promega, WI, USA). The restriction fragments (400 fmol) were treated with alkaline phosphatase and ligated by 1400 units of T4 DNA ligase (Takara) with 80 pmol of adaptor (5′-pACTGGCCGTCGTTT-3′) supported by 32 pmol of 5′-AAACGACGGCCAGTCATGp-3′. The phosphate residues were introduced into the 5′- and 3′-ends in order to prevent oligomer–oligomer ligation. The products ligated with the adaptor were purified with QIAquick

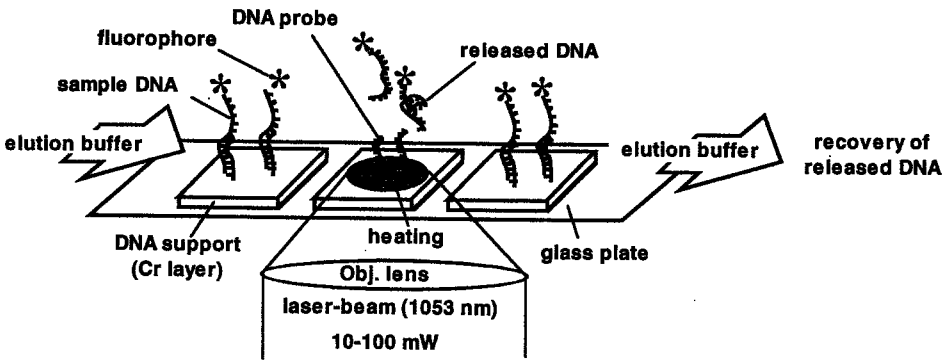

Fig. 1. Schematic illustration of DNA release from a DNA chip by using photothermal denaturation. The DNA hybridized with probe DNA fixed on a solid support can be released by a laser beam (1053 nm, 10–100 mW).

Spin Column (Qiagen, Hilden Germany) to eliminate free oligomers.

By using *Taq* DNA polymerase (0.625 units, Amersham Pharmacia Biotech, Amersham, UK) on a 50-μl scale, the fragments ligated with adaptor (50 amol) were selectively amplified by PCR with primer pairs (10 pmol). The primer pairs (from Sawady Technology, Tokyo, Japan) were 5′-(sulforhodamine-101)-AACGACGGCCAGTCACGNN-3′ and 5′-NH_2-AACGACGGCCAGTCACGNN-3′. Here, N is any one of the four deoxynucleotides for discriminating a complementary DNA fragment by PCR [15]. The thermal cycling reaction was carried out 35 times at 94°C (30 s), 62°C (30 s) and 72°C (60 s). The six products of this amplification were checked by electrophoresis using a 2% agarose gel followed by staining with 0.5 μg/ml ethidium bromide. They were analyzed by a FM-Bio 100 fluorescence image analyzer (Hitachi Software Engineering, Tokyo, Japan). The PCR product lengths were 779 bp (a pair of primers with discrimination sequences NN: AA and TC), 619 bp (NN: CG and TG), 411 bp (NN: GT and TA), 270 bp (NN: CA and TT), 231 bp (NN: CC and TT) and 179 bp (NN: AA and GT).

3.2. Preparation of the DNA chip

DNA was immobilized on a glass chip (45 × 25 × 0.4 mm^3) coated with 6-nm-thick chromium. The chip with the chromium surface was modified with 3-glysidoxypropyltrimethoxysilane to introduce the active residue and to fix double-stranded DNAs (PCR products) on the surface. The PCR products had an amino residue at a 5′-terminus of one strand and sulforhodamine-101 fluorophore at a 5′-terminus of the other strand, so that it was fixed on the chip surface through their amino residue. The chip was sonicated in 1 M KOH aqueous solution, washed with H_2O, and with 50% ethanol to clear the surface. After this pretreatment, the chip was dried for 30 min at 110°C, then dipped in neat 3-glysidoxypropyltrimethoxysilane for 15 min at 25°C followed by treating the same reagent (2%) diluted with 50% ethanol aqueous solution for 30 min. The chip was washed with 50% ethanol and dried at 110°C for 30 min to obtain a glysidoxy-activated chip. A solution of the DNA (10 μM) dissolved in 0.25 M carbonate buffer (pH 9.5) was dropped onto the glysidoxy-activated chip by a pin array coupled with Biomek 2000 Laboratory Automation Workstation (Beckman). Pipette was also used to make DNA chip; in that case, 0.2 μl of PCR products was dropped on the glysidoxy-activated chip. The chips are incubated at 50°C for 10 min in moisture atmosphere then kept at room temperature for 15 min. The remained active residues were blocked with Lys (0.1 M) dissolved in 0.25 M carbonate buffer (pH 9.5). The prepared DNA chips were stored in 20 mM of Tris–HCl (pH 7.5) containing 2 mM ethylenediaminetetraacetic acid (EDTA). The fixed DNA was easily detected by fluorescence imaging under a confocal scanning microscope (LSM-200, Olympus, Tokyo, Japan).

3.3. Recovery of DNA by photothermal denaturation

The DNA chip was overlaid with 25 μl of 20 mM Tris–HCl (pH 7.4) containing 2 mM EDTA. The laser (1053 nm, 10–100 mW on the surface of the DNA chip) was focused on the surface of the chip and about 20 μl drop of solution from the laser-irradiated area was collected in a vessel. A part of recovered DNA (3 μl) was amplified by PCR to check the DNA. The PCR was carried out using a primer (GTAAAACGACGGCCAGT). The amplified products were analyzed by electrophoresis using 2% agarose gel followed by staining with 0.5 μg/ml ethidium bromide. The electropherograms were visualized by a fluorescence image analyzer (FM-Bio 100, Hitachi Software Engineering, Tokyo, Japan).

4. Results and discussion

We made a DNA-arrayed chip as shown in Fig. 2. Each of the six different PCR products was immobilized along separate rows of a 6 × 6 grid. The photo shows a part of the DNA chip. The fluorescence from one spot clearly disappeared through IR laser irradiation, whereas the fluorescence from the untreated spots could be detected. This result indicates that the DNA from a small area was specifically released.

We then experimentally clarified the characteristics on how DNAs were released from the chip. As shown in the fluorescence image of Fig. 3, the fluorophore-labeled DNA (619 bp was immobilized at the fluorescent area on the chip) was removed from the irradiated region and the neighboring area. Bubbles were sometimes observed in the irradiated area, indicating that the solution temperature in the focused region could rise above the boiling point of water. The high temperature enabled the release of a DNA strand hybridized on its complementary strand fixed on the chip surface. It was possible to release the hybridized DNA from a 43-μm-wide denaturation area by 50 mW. However, the chip surface was partially damaged by the IR irradiation at this condition. The chromium came off the glass plate (the darkest area at the center on line a–a′ in Fig. 3), which could be easily observed by a phase-contrast microscope. Therefore, we optimized the laser power to release and recover the hybridized DNA from the chip surface. The fluorescence intensity at the small area of the laser-irradiated surface was measured in order to estimate the relative amount of denatured DNA. The hybridized DNA was released by the laser power ranging from 10 to 100 mW, as shown in Fig. 4 line A. More than 80% of the

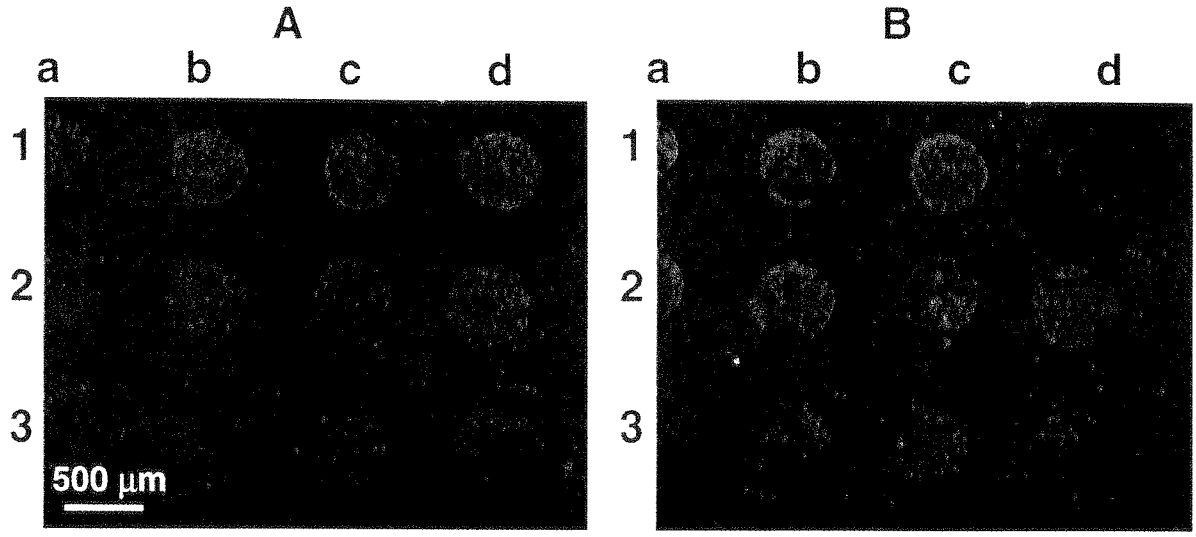

Fig. 2. Parts of fluorescence photographs of a DNA chip. The DNAs of 411, 270, and 231 bp were arrayed at lines 1–3 of each of column from a to d. Photograph A is the DNA chip before IR irradiation and photograph B is the same chip after IR irradiation at 10 mW. The IR laser-irradiated area was 1d.

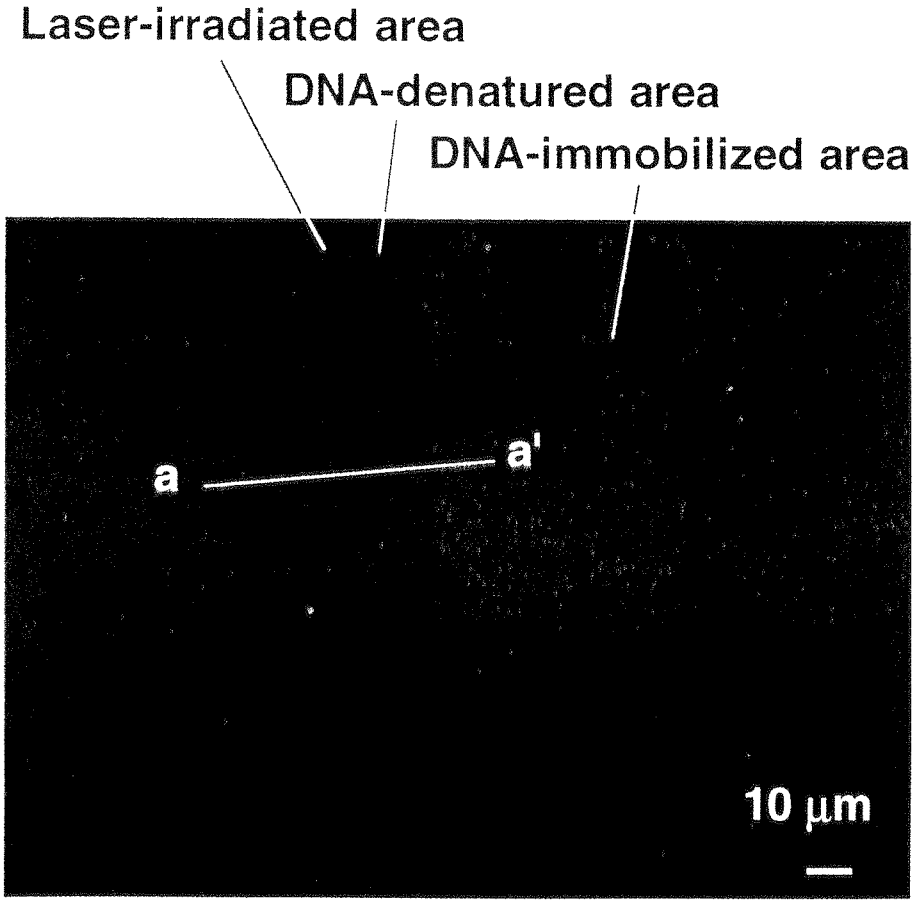

Fig. 3. Laser denaturation of a hybrid complex of sample DNA and probe DNA on chromium solid support (fluorescence image after laser irradiation). The fluorophore-labeled sample DNA disappeared from the small area on the solid support after laser irradiation. Intensity profiles at the a–a′ line under various laser powers are depicted in Fig. 4.

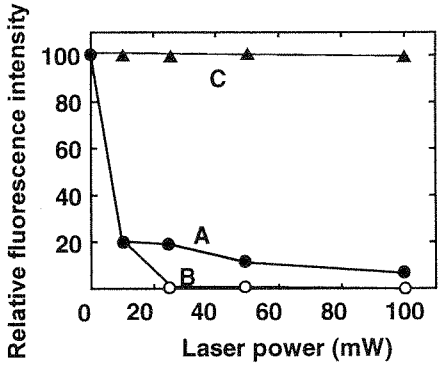

Fig. 4. Relative amounts of denatured DNA at different laser powers. The fluorescence intensity in the DNA-releasing area was measured from a fluorescence image as a relative amount of denatured DNA. The closed circles ● (line A) and open circles ○ (line B) show the fluorescence intensity in the DNA-denatured area and the chip-damaged area, respectively. The chip-damaged area, which was identified by phase-contrast microscopy, is the darkest area and the DNA-denatured area is the neighboring darkest area in Fig. 3. The same chip was treated with a fluorophore-labeled oligomer in order to rehybridize with the probe DNA on the chip surface, and the relative fluorescence intensity (▲, line C) was measured. The chip surface was not damaged at a laser power of 10 mW.

DNA was denatured and released from the chip surface by laser irradiation. It was possible to release the hybridized DNA by 10 mW light without damaging the chromium surface. However, the chip surface was partially damaged by the IR laser irradiation at a power of 25 mW or higher (line B). To prove that the DNA probe (or released DNA) was not damaged in the neighboring area of chromium-damaged area, we dropped a solution of fluorophore-labeled single-stranded DNA (60 base length) onto the surface. As shown by line C in Fig. 4, the previously denatured area was completely rehybridized with the fluorophore-labeled single-stranded oligomer DNA (60 base length), which hybridizes with a sequence near the 3′ end of the immobilized DNA strand. This shows that the DNA probe immobilized on the chip surface was not damaged after IR laser irradiation, because the 60 base length DNA could only hybridize to an intact DNA immobilized on the chip surface.

The recovered DNAs released from five different spots on one chip surface by a 10-mW laser were amplified by PCR. As shown in Fig. 5, one main product was detected in every electrophoresis of recovered DNA (lanes 9–13). The lengths of the products recovered from the DNA chip were about 800, 600, 420, 270, and 230 bp, respectively. They were the same as the intact immobilized DNA (lanes 2–6). Thus, the electropherograms show that the recovered DNA having different numbers of base pairs can be used as a template of PCR amplification. If the released DNA were damaged by the IR laser, the amplified products would not be obtained.

Some extra bands appeared in the electropherograms of recovered DNA. The immobilized DNA were prepared by the PCR using 5′-AACGACGGCCAGTCACGNN-3′ from a mixture of DNA fragments depicted in lane 7. All the fragments have the common sequence of AACGACGGCCAGT at both their 3′-termini. The PCR products in lanes 9–13 were amplified by using a common sequence primer. Since both the immobilized DNA and contaminants can be amplified with a common primer, there were some extra products in the electropherograms.

5. Conclusions

We have experimentally studied the characteristics of photothermal release of DNAs from a DNA chip. The DNA chip technology will allow separation of many different DNA fragments in one step. The procedure developed in the present study for releasing specific DNA fragments from the DNA chip has great potential in the

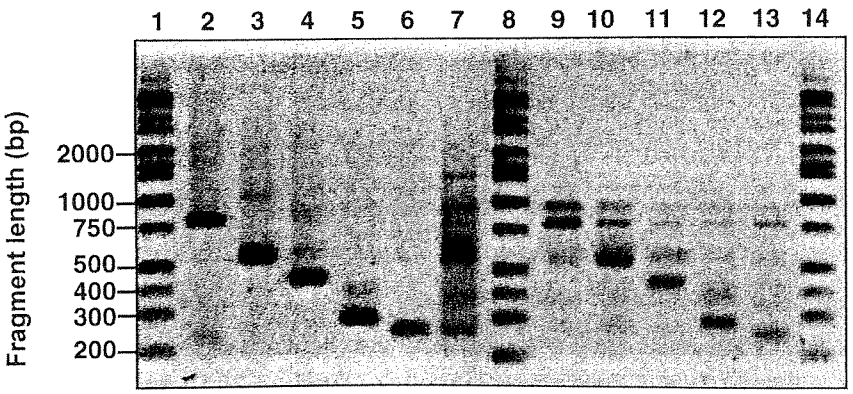

Fig. 5. Electropherograms of PCR products. The templates are DNA fragments recovered from the IR laser-irradiated chip (lanes 9–13), intact immobilized PCR products prepared from a mixture of DNA fragments (lanes 2–6), the mixture of DNA fragments (lane 7), and a marker (lanes 1, 8, and 14).

field of DNA preparation and purification. In general, hybridization reactions occur between not only complementary strands but also strands having similar sequences. The hybridization reaction is carried out at uni-condition because each probe element on the chip is too small to independently control the hybridization condition, e.g., annealing temperature and salt concentration. This is a drawback of the DNA chip because non-specific hybridization of similar DNA sequences with DNA probes on the chip frequently occurs. However, we consider that it will be a merit to analyze rapidly many kinds of DNA fragments because the chip elements can group the fragments according to the similarity of their sequences. Our photothermal method makes it possible to further analyze once the trapped DNA fragments on the chip elements. The DNA chip, coupled with photothermal denaturation, will work at searching DNA fragments of similar sequences (e.g., making a wholesale detection of DNA super family) to the best of its ability.

Molecular biology is rapidly approaching the stage of functional genomics. The screening of total gene expression profiles and the analysis of genome differentiation of species have become major research fields. A preparation method that enables separation of DNAs based on differences in expressed messages or in genomics will become more important. Our photothermal releasing procedure coupled with the DNA chip will have great potential in this field.

Acknowledgements

The authors thank Professor Sakaki for kindly supplying the human genome DNA. This research was partially supported by Grants-in-Aid for Scientific Research, for Scientific Research on Priority Areas and for the High-Tech Research Center Project from the Ministry of Education, Science, Sports and Culture of Japan.

References

[1] P.L. Deininger, Random subcloning of sonicated DNA: application to shotgun DNA sequence analysis, Anal. Biochem. 129 (1983) 216–223.

[2] D.J. Lockhart, H. Dong, M.C. Byrne, M.T. Follettie, M.V. Gallo, M.S. Chee, M. Mittmann, C. Wang, M. Kobayashi, H. Horton, E.L. Brown, Expression monitoring by hybridization to high-density oligonucleotide arrays, Nat. Biotechnol. 14 (1996) 1675–1680.

[3] S.P.A. Fodor, J.L. Read, M.C. Pirrung, L. Stryer, A.T. Lu, D. Solas, Light-directed, spatially addressable parallel chemical synthesis, Science 251 (1991) 767–773.

[4] A.C. Pease, D. Solas, E.J. Sullivan, M.T. Cronin, C.P. Holmes, S.P. Fodor, Light-generated oligonucleotide arrays for rapid DNA sequence analysis, Proc. Natl. Acad. Sci. U.S.A. 91 (1994) 5022–5026.

[5] M. Schena, D. Shalon, R.W. Davis, P.O. Brown, Quantitative monitoring of gene expression patterns with a complementary DNA microarray, Science 270 (1995) 467–470.

[6] D.G. Wang, J.-B. Fan, C.-J. Siao, A. Berno, P. Young, R. Sapolsky, G. Ghandour, N. Perkins, E. Winchester, J. Spencer, L. Kruglyak, L. Stein, L. Hsie, T. Topaloglou, E. Hubbell, E. Robinson, M. Mittmann, M.S. Morris, N. Shen, D. Kilburn, J. Rioux, C. Nusbaum, S. Rozen, T.J. Hudson, R. Lipshutz, M. Chee, E.S. Lander, Large-scale identification, mapping, and genotyping of single-nucleotide polymorphisms in the human genome, Science 280 (1998) 1077–1082.

[7] J.B. Lamture, K.L. Beattie, B.E. Burke, M.D. Eggers, D.J. Ehrlich, R. Fowler, M.A. Hollis, B.B. Kosicki, R.K. Reich, S.R. Smith et al., Direct detection of nucleic acid hybridization on the surface of a charge-coupled device, Nucleic Acids Res. 22 (1994) 2121–2125.

[8] M. Schena, D. Shalon, H. Heller, A. Chai, P.O. Brown, R.W. Davis, Parallel human genome analysis: microarray-based expression monitoring of 1000 genes, Proc. Natl. Acad. Sci. U.S.A. 93 (1996) 10614–10619.

[9] K.R. Khrapko, Yu.P. Lysov, A.A. Khorlyn, V.V. Shick, V.L. Florentiev, A.D. Mirzabekov, An oligonucleotide hybridization approach to DNA sequencing, FEBS Lett. 256 (1989) 118–122.

[10] G. Yershov, V. Barsky, A. Belgovskiy, E. Kirillov, E. Kreindlin, I. Ivanov, S. Parinov, D. Guschin, A. Drobishev, S. Dubiley, A. Mirzabekov, DNA analysis and diagnostics on oligonucleotide microchips, Proc. Natl. Acad. Sci. U.S.A. 93 (1996) 4913–4918.

[11] M.J. Marton, J.L. DeRisi, H.A. Bennett, V.R. Iyer, M.R. Meyer, C.J. Roberts, R. Stoughton, J. Burchard, D. Slade, H. Dai, D.E. Bassett Jr., L.H. Hartwell, P.O. Brown, S.H. Friend, Drug target validation and identification of secondary drug target effects using DNA microarrays, Nat. Med. 4 (1998) 1293–1301.

[12] M.J. O'Donnell, K. Tang, H. Koster, C.L. Smith, C.R. Cantor, High-density, covalent attachment of DNA to silicon wafers for analysis by MALDI-TOF mass spectrometry, Anal. Chem. 69 (1997) 2438–2443.

[13] J. Cheng, E.L. Sheldon, L. Wu, A. Uribe, L.O. Gerrue, J. Carrino, M.J. Heller, J.P. O'Connell, Preparation and hybridization analysis of DNA/RNA from *E. coli* on microfabricated bioelectronic chips, Nat. Biotechnol. 16 (1998) 541–546.

[14] H. Kato, T. Nishizaka, T. Iga, K. Kinosita Jr., S. Ishiwata, Imaging of thermal activation of actomyosin motors, Proc. Natl. Acad. Sci. U.S.A. 96 (1999) 9602–9606.

[15] K. Okano, C. Uematsu, H. Matsunaga, H. Kambara, Characteristics of selective polymerase chain reaction (PCR) using two-base anchored primers and improvement of its specificity, Electrophoresis 19 (1998) 3071–3078.

Biographies

K. Okano is working for Central Research Laboratory, Hitachi as a Senior Research Scientist in research on methodology for analyzing DNA, i.e., DNA fingerprinting, sequencing, and DNA assay. He investigated characteristics of PCR and developed a method to eliminate the false-positive amplification reaction. Furthermore, he demonstrated that any unknown sequenced DNA fragment digested with a restriction enzyme can be grouped in 136 windows by using improved PCR with a library as small as 16 primers.

K. Yasuda is an Associate Professor at the University of Tokyo. He has been studying several fields such as the muscle contractile mechanism, basic and applications of acoustic radiation force, and biochip technologies. In the study, he proposed the non-contact handling method of biomaterials in the microchamber for the high-throughput, contamination-free analysis using acoustic radiation force.

S. Ishiwata is a Professor at Waseda University. He has been studying the mechanism of protein motors on a single molecular level, the molecular synchronization observed in motor assemblies, and the mechanism of formation of the organized structures in muscle. His groups used optical tweezers to successfully measure the mechanical properties of a single actomyosin complex. They demonstrated auto-oscillatory properties of actomyosin motors and reconstitution of thin actin filaments in the contractile apparatus of cardiac muscle.

Biochemical and Biophysical Research Communications 272, 895–899 (2000)
doi:10.1006/bbrc.2000.2856, available online at http://www.idealibrary.com on IDEAL®

Temperature Dependence of Force, Velocity, and Processivity of Single Kinesin Molecules

Kenji Kawaguchi* and Shin'ichi Ishiwata*,†,‡,§,[1]

*Department of Physics, School of Science and Engineering, †Advanced Research Institute for Science and Engineering, and ‡Materials Research Laboratory for Bioscience and Photonics, Waseda University, 3-4-1 Okubo, Shinjuku-ku, Tokyo 169-8555, Japan; and §Core Research for Evolutional Science and Technology, "Genetic Programming" Team 13, Kawasaki 216-0001 Japan

Received May 15, 2000

Using the bead assay in optical microscopy equipped with optical tweezers, we have examined the effect of temperature on the gliding velocity, force, and processivity of single kinesin molecules interacting with a microtubule between 15 and 35°C. The gliding velocity increased with the Arrhenius activation energy of 50 kJ/mol, consistent with the temperature dependence of the microtubule-dependent ATPase activity. Also, the average run length, i.e., a measure of processivity of kinesin, increased on increasing temperature. On the other hand, the generated force was independent of temperature, 7.34 ± 0.33 pN (average ± S.D., n = 70). The gliding velocities decreased almost linearly with an increase in force irrespective of temperature, implying that the efficiency of mechanochemical energy conversion is maintained constant in this temperature range. Thus, we suggest that the force generation is attributable to the temperature-insensitive nucleotide-binding state(s) and/or conformational change(s) of kinesin-microtubule complex, whereas the gliding velocity is determined by the ATPase rate.

Key Words: **kinesin; microtubule; motor proteins; processivity; temperature effect; single molecule analysis; force generation; gliding velocity; Arrhenius activation energy.**

In nerve cells, organelles such as mitochondria and synaptic vesicles travel distances as long as several micrometers at a rate of 2–4 μm/s at physiological temperature (1–3). This movement has been classified as fast axonal transport and appears to be similar to the vesicular movement observed in other cells. Kinesin is a homodimer motor protein that bears such intracellular movements along a microtubule in an anterograde manner as a fast axonal transporter and requires the energy of ATP hydrolysis (4). An important property of kinesin is that it is a processive motor: an individual molecule can move continuously for long distances along the surface of the microtubule. Kinesin moves along the microtubule with 8 nm steps and generates force of 5–8 pN at 25°C (5–9).

In general, chemical reaction proceeds faster at higher temperatures. It has been known that the gliding velocity of microtubule interacting with kinesin molecules increases with an increase in temperature (10, 11). However, this property has not yet been examined by single molecular experiments. Because kinesin functions as a single molecule, single molecular experiments are indispensable. Here, to investigate the temperature effect on single kinesin molecules, we examined single-molecular bead assay under an optical microscope. A single native kinesin molecule purified from bovine brain was attached to a polystyrene bead, and the bead was trapped by optical tweezers and then brought onto a microtubule which was attached to a coverslip (7, 9). As expected from the Arrhenius law on temperature dependence of chemical reactions, the gliding velocity of single kinesin molecules measured by the displacement of the bead increased steadily up to 35°C, and the corresponding Arrhenius plot was linear. The distance over which kinesin molecules continue moving along a microtubule without detachment (run length) was longer at higher temperatures, which is reasonable as a property of kinesin that is an intracellular transporter. Also, we investigated the effect of temperature on the force generation. Interestingly, the force generated by a single kinesin molecule did not change when the temperature was increased from 15 to 35°C. This result suggests that the force generation of kinesin might be programmed to perform the same efficiency irrespective of

[1] To whom correspondence and reprints requests should be addressed at Department of Physics, School of Science and Engineering, Waseda University, 3-4-1 Okubo, Shinjuku-ku, Tokyo 169-8555, Japan. Fax: +81-3-3200-2567. E-mail: ishiwata@mn.waseda.ac.jp.

0006-291X/00 $35.00

temperatures. A preliminary report of this investigation was presented previously (12).

MATERIALS AND METHODS

Proteins. Kinesin was prepared from bovine brain according to the method of Kojima *et al.* (13). Tubulin was purified from porcine brain and labeled with tetramethylrhodamine succinimidyl ester (C-1171, Molecular Probes, Eugene, OR) according to Hyman (14). Microtubules were stabilized with 40 μM taxol.

Bead assay. Kinesin-coated beads were prepared according to Kojima *et al.* (13) with slight modifications. We used fluorescent latex beads (1.0 μm in diameter, carboxylate-modified latex; yellow-green, F-8823; Molecular Probes). The number of kinesin molecules attached to the bead that can interact with a microtubule was estimated by statistical methods (15). All the experiments were performed with beads on which the average number of kinesin molecules was one.

Flow chamber for beads assay. The fluorescent microtubules were introduced into a flow chamber and incubated for 2 min to allow binding of the microtubule to the glass surface of the chamber. The chamber was washed with an assay buffer containing 2 mM $MgCl_2$, 80 mM PIPES (piperazine-1,4-bis(2-ethanesulfonic acid), pH 6.8), 1 mM EGTA and 0.7 mg/ml filtered casein (0.73-19, Nacalai Tesque, Kyoto) to remove unattached microtubules and left for 2 min to coat the glass surface with casein. The chamber was then filled with an assay solution containing the kinesin-coated beads and an oxygen scavenging enzyme system (16) [approximately 0.1 pM kinesin-coated beads, 2 mM $MgCl_2$, 80 mM PIPES (pH 6.8), 1 mM EGTA, 0.7 mg/ml filtered casein, 1 mM ATP (127531, Boehringer Mannheim, Mannheim, Germany), 10 μM taxol (T-1912, Sigma, St. Louis, MO), 10 mM dithiothreitol (DTT), 4.5 mg/ml glucose, 0.22 mg/ml glucose oxidase (G-2133, Sigma), 0.036 mg/ml catalase (C-10, Sigma)], and sealed with enamel. Other chemicals were of reagent grade.

Microscope. A microscopy system used for measuring the interaction of kinesin and microtubule was previously described by Nishizaka *et al.* (17). An inverted microscope (TMD-300; an oil-immersion objective lens with a phase ring, ×100 NA = 1.3; Nikon, Tokyo) was equipped with optical tweezers with 1W Nd: YLF laser (1053-1000p: λ = 1.053 μm; Amoco Laser, IL). The centroid of the phase-contrast image of polystyrene beads was calculated with a frame memory computer (DIPS-C2000; Hamamatsu Photonics, Hamamatsu, Japan) and a fluorescence image of a microtubule was simultaneously acquired with a modified dual-view fluorescence microscope system (18, 19). Stiffness of the optical trap was estimated to be 0.087 pN/nm by the method of Nishizaka *et al.* (17).

Temperature control. For experiments at 15, 20, and 25°C, the room temperature was equilibrated by an air conditioner to each temperature. For experiments at 30 and 35°C, the stage of the inverted microscope that contained the flow cell was covered by a thermal insulation chamber (Nikon, Tokyo) and the temperature of the cell was controlled. The temperature was measured by a thermistor on the microscope stage near the flow chamber and regulated within ±1°C of the designated experimental temperature. We confirmed that the local temperature around the bead trapped by the laser beam did not increase by measuring thermally quenched fluorescence intensity of tetramethyl-rhodamine which was attached to a microtubule (12, 20). The single-molecular bead assay was done after keeping the flow cell for 1 min at each temperature.

Gliding velocity of single kinesin-coated bead. A bead, to which a single kinesin molecule was attached, was manipulated with optical tweezers onto a microtubule adsorbed to a coverslip. After the attachment of the bead to the microtubule was confirmed in the assay solution, the laser beam for optical tweezers was shut off. Then the movement of the bead occurred towards the plus end of a microtubule. From the video image (30 frames/s), the time course of displacement of the bead was obtained. Because the displacement was nearly linear with time, the average gliding velocity could be determined from the slope of the displacement vs. time relationship.

Force generated by single kinesin. A bead, to which a single kinesin molecule was attached, was manipulated onto a microtubule in the assay solution by using optical tweezers. When the bead was placed in contact with a microtubule, the bead was displaced from the trap center, gradually decreasing its displacement velocity until it reached a plateau. The bead stayed at the plateau level for some period of time and then returned to the trap center. On some occasions, however, the bead returned to the trap center before reaching the plateau. These data were not used for the data analyses. From the video image, the displacement of the bead from the trap center was traced against time. Force was calculated from (stiffness of optical trap) × (displacement).

Measurement of the force-velocity curves. To determine the relation between velocity and force, 7 raw data showing the time course of the bead displacement were averaged at each temperature (cf. Fig. 2c). The gliding velocities at various forces were determined from the slope of the average time course of bead displacement in the range of 1-2, 2-3, 3-4, 4-5, 5-6 and 6-7 pN. The velocities at zero force were obtained without applying an external load by an optical trap. To determine the velocity of kinesin molecules under an external load, the velocity of the bead must be corrected by multiplying the factor, 1 + (stiffness of optical tweezers)/(stiffness of kinesin-microtubule complex) (13). But, the stiffness of the kinesin-microtubule complex has been estimated to be larger than approximately 0.4 pN/nm (21), being several times larger than that of optical tweezers, 0.087 pN/nm, so that the correction was not done. Thus, the velocities we estimated may have been a little underestimated except those at no load.

RESULTS AND DISCUSSION

Temperature Effect on Gliding Velocity

First, we examined the effect of temperature on the gliding velocity of the bead without external load (Fig. 1a). The result was similar to the previous results obtained by microtubule gliding assay (10, 11). The Arrhenius plot was linear in this temperature range as shown in Fig. 1b. The activation energy was estimated as 50 kJ/mol from the slope of the Arrhenius plot, consistent with the temperature dependence of the microtubule-dependent ATPase activity (11). The Arrhenius activation energy thus obtained is comparable to that determined in the actomyosin in vitro motility assay (21–24). At temperatures higher than 40°C, however, we could not measure the gliding velocities of beads in the present experimental setup because the beads tended to detach during incubation for 1 min which was required for stabilizing the temperature of the cell in the thermal insulation chamber.

Recently, Böhm *et al.* (10) reported that the Arrhenius plot of microtubule gliding velocity revealed a break at 27°C, resulting in the activation energies of 65 kJ/mol for <27°C and 9 kJ/mol for >27°C. They concluded that the break in the Arrhenius plot results from conformational changes of kinesin and/or microtubule (25). On the contrary, there seemed to be no break at around 27°C in our data (Fig. 1). Besides, a preliminary result (12) of the microtubule gliding as-

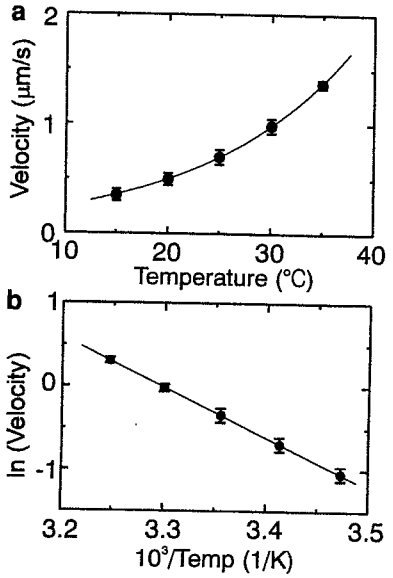

FIG. 1. Temperature dependence of gliding velocity of a single kinesin molecule attached to a bead. (a) Gliding velocity vs temperature. (b) Arrhenius plot of a. The error bars represent ± S.D. for 7 measurements. The velocities of the bead (average ± S.D.) were, 0.35 ± 0.04, 0.50 ± 0.05, 0.71 ± 0.07, 0.99 ± 0.07 and 1.36 ± 0.04 μm/s, respectively, at 15, 20, 25, 30, and 35°C. Solvent conditions, an assay buffer containing 2 mM $MgCl_2$, 80 mM PIPES (pH 6.8), 1 mM EGTA, 0.7 mg/ml filtered casein, 10 mM DTT, 1 mM ATP and an oxygen scavenging enzyme system.

say examined between 35 and 50°C by temperature pulse microscopy (TPM) technique (21) showed that there are no breaks between 15 and 50°C with a unique activation energy of about 50 kJ/mol. As the previous experiments (10) were not a single molecular assay but a multi-molecular one, there is a possibility that kinesin molecules may be thermally damaged due to long incubation at high temperatures might have prevented smooth movement of microtubule. Actually, we confirmed that we could not obtain reliable data when the incubation time of the flow cell was longer than 10 min at 30°C, and even for 1 min at 40°C, because of a gradual deterioration of motility of kinesin.

Temperature Effect on Processivity

From the same data as used for measuring the gliding velocity, we could estimate the run length (= the number of steps times the step size), a measure of processivity, over which kinesin molecules continued moving on a microtubule without detachment. Although the number of data was not large enough to confirm the exponential distribution of the run length (6, 8), we could find that the average run length monotonously increased from approximately 0.7 to 1.5 μm on increasing temperature from 15 to 35°C. This implies that a probability of detachment at every step of kinesin becomes smaller on increasing temperature, suggesting that the hydrophobic interaction is important to stabilize the attached state of kinesin. It is to be noted, however, that the average duration of continuous running decreased with increasing temperature, i.e., approximately 2 s at 15°C and 1 s at 35°C. In any case, such a temperature dependence of run length is important for the physiological function of kinesin as an intracellular transporter that needs to carry an organella for long distances at body temperature.

Temperature Effect on Force Generation

Next, external load was applied to a bead by trapping the bead with optical tweezers. Figures 2a and b, respectively, show examples of raw data for the bead moving away from the trap center at 20 and 35°C. Figure 2c shows the average displacement of the kinesin-coated bead at 20 and 35°C. Seven traces of the

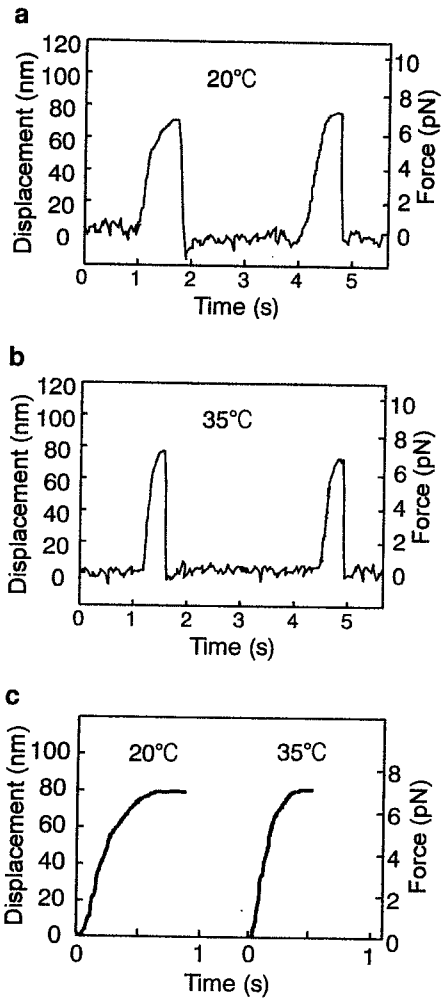

FIG. 2. Time course of force generation of a single kinesin molecule attached to a bead. (a and b) Examples of raw data for the bead moving away from the trap center at 20 (a) and 35 (b) °C. (c) Average (n = 7) of the above data at 20 and 35°C. Force calculated from the bead displacement is shown on the right ordinate. Solvent conditions are the same as in Fig. 1.

displacement of a bead, in which the bead stayed at a plateau level for a period longer than 0.1 s, were superimposed and averaged at each temperature. The gliding velocity gradually decreased with the increase in the external load. The clear difference at these two temperatures was the velocity of the rising phase. Also, we found that the duration between the beginning of tension generation and its end was shorter at higher temperatures. The duration obtained by averaging 7 data (see Figs. 2a and b) was 1.03 ± 0.25 (average ± S.D.), 0.82 ± 0.18, 0.73 ± 0.12, 0.69 ± 0.21 and 0.58 ± 0.18 s, respectively, at 15, 20, 25, 30 and 35°C. Thus, the lifetime of the attached state became shorter by imposing external load.

As summarized in Fig. 3, the steady forces at the plateau level were independent of temperature between 15 and 35°C, i.e., 7.34 ± 0.33 pN (average ± S.D., n = 70). Based on the above results, we suggest that the force generation in kinesin molecules is attributable to the temperature-insensitive nucleotide-binding state(s) and/or conformational change(s) of kinesin-microtubule complex, whereas the gliding velocity is coupled with the temperature-sensitive ATPase rate. It was recently reported that the maximum force generated by acto-myosin (heavy meromyosin) complex is independent of temperature in the same temperature range as examined here (26), although their data were not obtained by single molecular experiments. Thus, it is suggested that the temperature-insensitive force generation and the temperature-sensitive gliding velocity may be common to molecular motors.

Temperature Effect on Force-Velocity Relation

The force-velocity curves for single kinesin molecules at several temperatures shown in Fig. 4 were obtained from the slope of the averaged time course of the bead displacement (force development) as shown in Fig. 2c

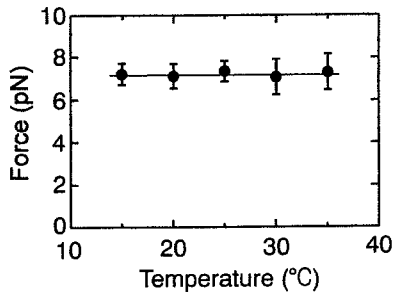

FIG. 3. Temperature dependence of maximum force generated on a single kinesin molecule attached to a bead. The maximum forces (average ± S.D.; data, of which duration at a plateau level was shorter than 0.1 s, were also included for this calculation) were 7.38 ± 0.45 (n = 12), 7.21 ± 0.57 (n = 16), 7.50 ± 0.47 (n = 25), 7.16 ± 0.83 (n = 10) and 7.43 ± 0.83 (n = 7) pN, respectively, at 15, 20, 25, 30, and 35°C. Solvent conditions are the same as in Fig. 1.

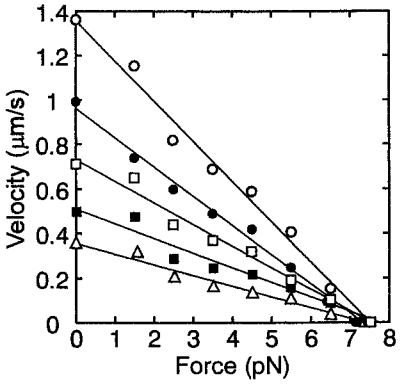

FIG. 4. Temperature dependence of force-velocity relation. From bottom to top, open triangles, 15°C; closed squares, 20°C; open squares, 25°C; closed circles, 30°C; open circles, 35°C. Velocities at various forces were estimated from the average slope of the bead displacement shown in Fig. 2c in the range of 1-2, 2-3, 3-4, 4-5, 5-6 and 6-7 pN. The velocities at zero load on the ordinate were obtained from Fig. 1 and the maximum forces on the abscissa were from Fig. 3. Solvent conditions are shown in Fig. 1.

in the range of 1-2, 2-3, 3-4, 4-5, 5-6 and 6-7 pN. The data on the ordinate and the abscissa of Fig. 4 were, respectively, obtained from Figs. 1a and 3. As seen in Fig. 4, the force-velocity curve was nearly linear in the whole temperature range we examined from zero to the maximum force. Such a linear relationship between force and velocity has previously been reported around room temperature (13, 15, 27).

The maximum work (= force × working distance) that a motor can perform is bounded by the free energy decrease associated with the hydrolysis of one ATP molecule, ~25 kT or ~100 × 10^{-21} J. In the case of kinesin of which step size is 8 nm, the force must be ≤12 pN. Our data showed that a single kinesin molecule is able to generate a force of 7 pN irrespective of temperature (Fig. 3). Thus, provided that each step is associated with the hydrolysis of just one ATP molecule, the efficiency of energy conversion is estimated to be less than 60% because the maximum work performed is 7 pN × 8 nm = 56 × 10^{-21} J. Besides, because both gliding velocity and ATPase activity changed in parallel with the increase in temperature (at least without external load), the efficiency of mechano-chemical energy conversion, which is proportional to (external load = force) × (gliding velocity)/(ATPase activity), seems to be independent of temperature. Motor molecules may be programmed so as to perform the biological movement at a fixed efficiency at any temperatures.

ACKNOWLEDGMENTS

We thank Dr. K. Kinosita, Jr., of Keio University for his critical reading of the manuscript. This research was partly supported by Grants-in-Aid for Scientific Research, for Scientific Research on Priority Areas and for the High-Tech Research Center Project from the

Ministry of Education, Science, Sports, and Culture of Japan, and by Grants-in-Aid from Japan Science and Technology Corporation (CREST). This was also supported by a grant from the Mitsubishi Foundation.

REFERENCES

1. Brady, S. T. (1985). A novel brain ATPase with properties expected for the fast axonal transport motor. *Nature* **317,** 73–75.
2. Grafstein, B., and Forman, D. S. (1980). Intercellular transport in neurons. *Physiol. Rev.* **60,** 1167–1283.
3. Lasec, R. J., Garner, J. A., and Brady, S. T. (1984). Axonal transport of the cytoplasmic matrix. *J. Cell Biol.* **101,** 2181–2193.
4. Howard, J., Hudspeth, A. J., and Vale, R. D. (1989). Movement of microtubules by single kinesin molecules. *Nature* **342,** 154–158.
5. Howard, J. (1996). The movement of kinesin along microtubules. *Annu. Rev. Physiol.* **58,** 703–729.
6. Block, S. M., Goldstein, L. S. B., and Schnapp, B. J. (1990). Bead movement by single kinesin molecules studied with optical tweezers. *Nature* **348,** 348–352.
7. Svoboda, K., Schmidt, C. F., Schnapp, B. J., and Block, S. M. (1993). Direct observation of kinesin stepping by optical trapping interferometry. *Nature* **365,** 721–727.
8. Vale, R. D., Funatsu, T., Pierce, D. W., Romberg, L., Harada, Y., and Yanagida, T. (1996). Direct observation of single kinesin molecules moving along microtubules. *Nature* **380,** 451–453.
9. Higuchi, H., Muto, E., Inoue, Y., and Yanagida, T. (1997). Kinetics of force generation by single kinesin molecules activated by laser photolysis of caged ATP. *Proc. Natl. Acad. Sci. USA* **94,** 4395–4400.
10. Böhm, K. J., Stracke, R., Baum, M., Zieren, M., and Unger, E. (2000). Effect of temperature on kinesin-driven microtubule gliding and kinesin ATPase activity. *FEBS Lett.* **466,** 59–62.
11. Mazumdar, M., and Cross, R. A. (1998). Engineering a lever into the kinesin neck. *J. Biol. Chem.* **273,** 29352–29359.
12. Kawaguchi, K., and Ishiwata, S. (2000). Effect of temperature on force generation and velocity of single kinesin molecule. *Biophys. J.* **78,** 122A (Abstract).
13. Kojima, H., Muto, E., Higuchi, H., and Yanagida, T. (1997). Mechanics of single kinesin molecules measured by optical trapping nanometry. *Biophys. J.* **73,** 2012–2022.
14. Hyman, A. A. (1991). Preparation of marked microtubules for the assay of the polarity of microtubule-based motors by fluorescence. *J. Cell Sci. Suppl.* **14,** 125–127.
15. Svoboda, K., and Block, S. M. (1994). Force and velocity measured for single kinesin molecules. *Cell* **77,** 773–784.
16. Harada, Y., Sakurada, K., Aoki, T., Thomas, D. D., and Yanagida, T. (1990). Mechanochemical coupling in actomyosin energy transduction studied by in vitro movement assay. *J. Mol. Biol.* **216,** 49–68.
17. Nishizaka, T., Miyata, H., Yoshikawa, H., Ishiwata, S., and Kinosita, Jr., K. (1995). Unbinding force of a single motor molecule of muscle measured using optical tweezers. *Nature* **377,** 251–254.
18. Miyata, H., Hakozaki, H., Yoshikawa, H., Suzuki, N., Kinosita, Jr., K., Nishizaka, T., and Ishiwata, S. (1994). Stepwise motion of an actin filament over a small number of heavy meromyosin molecules is revealed in an *in vitro* motility assay. *J. Biochem.* **115,** 644–647.
19. Kinosita, Jr., K., Ito, H., Ishiwata, S., Hirano, K., Nishizaka, T., and Hayakawa, T. (1991). Dual-view microscopy with a single camera: Real-time imaging of molecular orientations and calcium. *J. Cell Biol.* **115,** 67–73.
20. Kato, H., Nishizaka, T., Iga, T., Kinosita, Jr., K., and Ishiwata, S. (1999). Imaging of thermal activation of actomyosin motors. *Proc. Natl. Acad. Sci. USA* **96,** 9602–9606.
21. Ishiwata, S., and Kawaguchi, K. (2000). Nucleotide- and loading rate-dependent switching of single- to double-headed binding of kinesin. *Biophys. J.* **78,** 278A (Abstract).
22. Anson, M. (1992). Temperature dependence and arrhenius activation energy of F-actin velocity generated in vitro by skeletal myosin. *J. Mol. Biol.* **224,** 1029–1038.
23. Homsher, E., Wang, F., and Sellers, J. R. (1992). Factors affecting movement of F-actin filaments propelled by skeletal muscle heavy meromyosin. *Am. J. Physiol.* **262,** C714–C723.
24. Winkelmann, D. A., Bourdieu, L., Ott, A., Kinose, F., and Libchaber, A. (1995). Flexibility of myosin attachment to surfaces influences F-actin motion. *Biophys. J.* **68,** 2444–2453.
25. De Cuevas, M., Tao, T., and Goldstein, L. S. B. (1992). Evidence that the stalk of *Drosophila* kinesin heavy chain is an α-helical coiled coil. *J. Cell Biol.* **116,** 957–965.
26. Kawai, M., Kawaguchi, K., Saito, M., and Ishiwata, S. (2000). Temperature change does not affect force between single actin filaments and HMM from rabbit muscles. *Biophys. J.* **78,** in press.
27. Mayhöfer, E., and Howard, J. (1995). The force generated by a single kinesin molecule against an elastic load. *Proc. Natl. Acad. Sci. USA* **92,** 574–578.

Characterization of Single Actomyosin Rigor Bonds: Load Dependence of Lifetime and Mechanical Properties

Takayuki Nishizaka,*† Ryuzo Seo,* Hisashi Tadakuma,* Kazuhiko Kinosita, Jr.,†‡ and Shin'ichi Ishiwata*†§¶

*Department of Physics, School of Science and Engineering, Waseda University, Tokyo169-8555; †Core Research for Evolutional Science and Technology, Genetic Programming Team 13, Kanagawa 216-0001; ‡Department of Physics, Faculty of Science and Technology, Keio University, Yokohama 223-8522; §Advanced Research Institute for Science and Engineering, Waseda University, Tokyo; and ¶Materials Research Laboratory for Bioscience and Photonics, Waseda University, Tokyo, Japan

ABSTRACT Load dependence of the lifetime of the rigor bonds formed between a single myosin molecule (either heavy meromyosin, HMM, or myosin subfragment-1, S1) and actin filament was examined in the absence of nucleotide by pulling the barbed end of the actin filament with optical tweezers. For S1, the relationship between the lifetime (τ) and the externally imposed load (F) at absolute temperature T could be expressed as $\tau(F) = \tau(0)\cdot\exp(-F\cdot d/k_BT)$ with $\tau(0)$ of 67 s and an apparent interaction distance d of 2.4 nm (k_B is the Boltzmann constant). The relationship for HMM was expressed by the sum of two exponentials, with two sets of $\tau(0)$ and d being, respectively, 62 s and 2.7 nm, and 950 s and 1.4 nm. The fast component of HMM coincides with $\tau(F)$ for S1, suggesting that the fast component corresponds to single-headed binding and the slow component to double-headed binding. These large interaction distances, which may be a common characteristic of motor proteins, are attributed to the geometry for applying an external load. The pulling experiment has also allowed direct estimation of the number of myosin molecules interacting with an actin filament. Actin filaments tethered to a single HMM molecule underwent extensive rotational Brownian motion, indicating a low torsional stiffness for HMM. From these results, we discuss the characteristics of interaction between actin and myosin, with the focus on the manner of binding of myosin.

INTRODUCTION

Recent developments in microscopic techniques have opened up opportunities of studying "single-molecule physiology," which enables us to elucidate protein-protein interactions and their various biological functions under living circumstances in aqueous media. For molecular motors, their individual behaviors have been successfully studied at the single molecule level. Nanometer steps and piconewton forces generated by single molecular motors have been measured under an optical microscope (Svoboda et al., 1993; Finer et al., 1994; Ishijima et al., 1994, 1998; Miyata et al., 1994, 1995; Molloy et al., 1995; Mehta et al., 1999). Single-fluorophore imaging (Funatsu et al., 1995; Sase et al., 1995a) has revealed individual ATP turnovers by myosin and rotational movement between actin and myosin (Sase et al., 1997), suggesting a hopping character for myosin (Kinosita et al., 1998). The mechanisms of motor operation, however, are still unclear. During one cycle of ATP hydrolysis, molecular motors are considered to form different conformations with different affinities for their substrate filaments and to alternate binding and unbinding. Here we focus on the characteristics of unbinding between myosin and actin.

In general, binding and unbinding interactions of proteins are essential for many biological functions, e.g., adhesion between cells, migration of cells on substratum (Nishizaka et al., 2000), recognition between ligands and receptors, processive movement of molecular motors, and so on. Several techniques have been developed to measure forces of protein bonds in the range from the subpiconewton level to a nanonewton. Glass microneedles were first applied to measure the sliding force generated between a microtubule and dynein motors (Kamimura and Takahashi, 1981) and then successfully used to measure the sliding force and the tensile strength of single actin filaments (Kishino and Yanagida, 1988; Tsuda et al., 1996). Individual ligand-receptor binding has been extensively characterized by atomic force microscopy (Nakajima et al., 1997; Fritz et al., 1998). The interaction between avidin and biotin has been examined in detail, and its molecular dynamics has been simulated (Florin et al., 1994; Moy et al., 1994; Grubmuller et al., 1996; Izrailev et al., 1997; Merkel et al., 1999). In the present study we used optical tweezers to characterize single actomyosin rigor bonds.

Optical tweezers, formed by focusing a laser beam, capture a particle of micrometer size without direct contact (Ashkin et al., 1986, 1990). In our previous studies (Nishizaka et al., 1995b), we measured the force required to unbind a rigor bond formed between an actin filament and a single heavy meromyosin (HMM) molecule in the absence of ATP using optical tweezers under a dual-view (fluorescence and phase-contrast) microscope (Kinosita et al., 1991; Sase et al., 1995b; Arai et al., 1999). The average unbinding force was ~9 pN, which is 2–5 times larger than the sliding force (Finer et al., 1994; Ishijima et al., 1994; Miyata et al., 1995) and an order of magnitude smaller than other intermolecular forces (Florin et al., 1994; Tsuda et al., 1996; Fritz et al., 1998). Unbinding under a constant force was a

Received for publication 28 February 2000 and in final form 26 April 2000.

Address reprint requests to Dr. Shin'ichi Ishiwata, Department of Physics, School of Science and Engineering, Waseda University, 3-4-1 Okubo, Shinjuku-ku, Tokyo 169-8555, Japan. Tel.: 81-3-5286-3437; Fax: 81-3-3200-2567; E-mail: ishiwata@mn.waseda.ac.jp.

0006-3495/00/08/962/13 $2.00

stochastic process, and an increase in the load by 10 pN decreased the lifetime of the rigor bond by a factor of 10^2 to 10^3. Interestingly, two types of HMM molecules were found, one with a large (long) and the other with a small (short) unbinding force (lifetime), suggesting "molecular individualism."

In this study, we measured the lifetime of single actomyosin (either HMM or subfragment-1 of myosin (S1)) rigor bonds under various external loads and could formulate the relationship between the lifetime and the load. The stochastic properties of the rigor bonds have been demonstrated. We developed a microscopic way to count the number of myosin molecules attached to the glass surface. Based on the number density of myosin molecules interacting with an actin filament thus measured, we estimated the minimum number of myosin molecules needed to slide actin filaments continuously. Furthermore, the torsional stiffness of single myosin molecules was estimated by observing the rotational Brownian motion of a short actin filament attached to myosin. Throughout the present study, we tried to characterize the interaction with actin of double-headed HMM molecules compared with that of single-headed S1 molecules.

MATERIALS AND METHODS

Dual-view imaging microscopy and optical tweezers system

Fig. 1 shows a schematic diagram of a dual-view (phase-contrast and fluorescence) video microscope imaging system (Kinosita et al., 1991; Nishizaka et al., 1995a,b; Sase et al., 1995b; Arai et al., 1999) equipped with optical tweezers. The inverted microscope (TMD-300; Nikon Co., Tokyo) with a 100× objective with a phase-contrast plate (NA 1.3, fluor 100 Ph; Nikon) was used on an optical bench (HG-LM; Herz Co., Kanagawa, Japan). The optical system included dichroic mirrors (DM 550, DM infrared, Sigma Koki Co., Saitama, Japan; DM 530, Asahi Spectra Co., Tokyo), filters (F 380–520, F 550, F 590; Asahi Spectra), and mirrors. The beam from the sample, which consisted of two components, the phase-contrast image of the bead (wavelength 380–520 nm, the *once-broken* line in Fig. 1) and the fluorescence image of actin filaments (excitation 550 nm and emission > 590 nm; the *dashed line* in Fig. 1), was separated by a beam separator (DM > 530 nm). Colorless filters (HA-30; Hoya Co., Tokyo, and Asahi Spectra) were placed behind the Hg lamp and before the image intensifier to cut off the infrared light. The field stop was positioned between the microscope and the beam separator, and lenses (DLB-50–150PM; Sigma Koki) were positioned before each camera to focus images clearly. The bead image, acquired with a CCD camera (CCD-72; Dage-MTI, Michigan City, IN), was stored in a digital frame memory (DIPS-C2000; Hamamatsu Photonics K. K., Hamamatsu, Japan). The position of the bead was determined by calculating the centroid of its intensity profile with a spatial resolution of nanometer scale (Fig. 2; Miyata et al., 1994; Nishizaka et al., 1995b). The data were analyzed with a personal computer (Apple Japan, Tokyo).

The sample stage of the microscope was replaced with the custom-made stage, on which the position of the objective along the z direction could be controlled by using a piezoelectric microscope positioner (P-720.00; Physik Instrumente GmbH and Co., Waldbronn, Germany) with a power supply (BWS 1202.5; Takasago, Tokyo). Because the drift between the commercial sample stage and the objective is mainly caused by deformation of the gear(s) sustaining a nose piece, the nose piece was removed and the objective was fixed directly to the sample stage to suppress the drift during measurements. Large displacement of the stage (as much as >40 nm) was achieved with the use of high-resolution actuators (HPA-10; Sigma Koki), their controller (Mark-8; Sigma Koki), and a personal computer (Apple Japan, Tokyo) with GPIB (NI488.2; National Instruments Co., Austin, TX). The small displacement (nanometer scale) was adjusted with a piezoelectric substage (p-770.10; Physik Instrumente GmbH and Co.) with a function generator (1915; NF Electronic Instruments, Yokohama, Japan) and an amplifier (BWS 120–2.5; Takasago). The temperature of the microscopic system was stabilized by allowing it to sit for 4–6 h before the measurements.

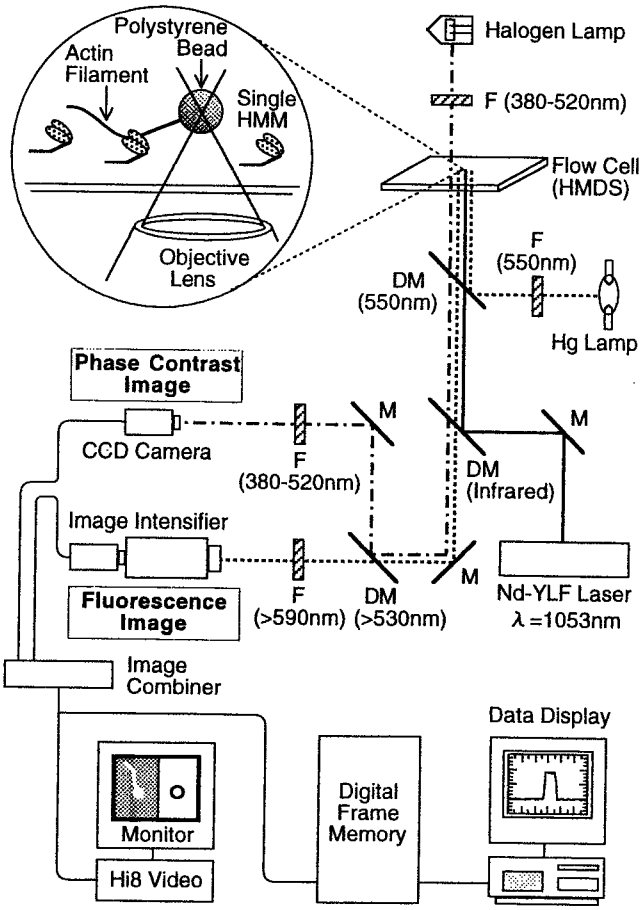

FIGURE 1 Schematic diagram of optical tweezers and dual-view imaging video microscope system. The once-broken lines and the dashed lines represent phase-contrast and fluorescence imaging optical paths, respectively, and the solid lines represent the optical tweezers optical path. The microscope system includes dichroic mirrors (DM) (the wavelength in parentheses shows the wavelength of the reflected light, and the wavelength with the > sign shows the range of wavelength passing through DM), filters (F) (the wavelength in parentheses shows the wavelength of light passing through F), and mirrors (M).

The spatial resolution of the system and the performance of the sample stage were examined by the method shown in Fig. 2. Fig. 2 *A* gives an example showing the position fluctuation of a bead trapped by optical tweezers with a stiffness of 0.27 pN/nm. The standard deviation (SD) of the displacement of the bead trapped for 1 min was 0.84 nm for the x direction and 0.93 nm for the y direction (n = 5). Here these values are considered to be the spatial resolution of our system, with 1/30 s time resolution. In

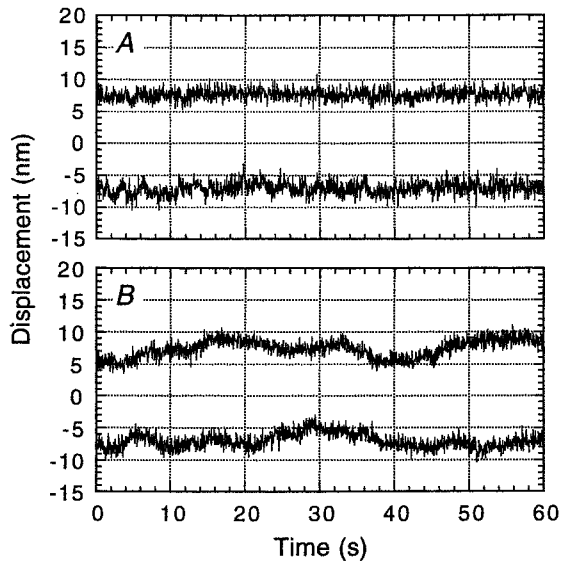

FIGURE 2 Performance of the image analysis system and the sample stage. (*A*) Time course of the displacement of the bead that was trapped in the medium by optical tweezers with a stiffness of 0.27 pN/nm. The displacement reflects both the stability of the trap center and the spatial resolution of our analysis system. (*B*) Displacement of the bead that was fixed to the glass surface. The glass surface was covered with nitrocellulose over the bead, so that the bead was fixed between the nitrocellulose membrane and the glass surface. Thus the displacement of the bead reflects the movement of the sample stage. Upper and lower traces in each figure respectively represent the displacements along the x and y axes.

contrast, to check the drift of the stage, we measured the displacement of the bead fixed to a glass surface by covering it with nitrocellulose (Fig. 2 *B*). The SD of the displacement of the bead for 1 min was 2.1 nm for the x direction and 2.0 nm for the y direction ($n = 10$). They were larger than the spatial resolution of our system, indicating the drift of the microscopic stage or the vibration of the system.

The actin filaments labeled with a fluorescent probe were visualized using another CCD camera equipped with an image intensifier (KS1381; Video Scope International, Washington, D.C.). To observe a phase-contrast image of beads simultaneously, the focus of the phase-contrast image plane was displaced ~0.5 μm (the radius of the bead) higher than the focus of the fluorescence image plane by moving the lenses in front of the camera. Two images were electronically combined (MV24-c; For. A Co., Tokyo) on the same screen to compare the behavior of the actin filament against the displacement of the bead at the same time.

The 1 W Nd:YLF laser (1053–1000p: $\lambda = 1.053$ μm; Amoco Laser Co., Naperville, IL) was coupled with an optical fiber, and the laser was not placed on the optical bench, to avoid a vibration. The position of the optical fiber could be moved along three directions (x, y, and z) and tilted in two directions (xy plane). The laser beam was set parallel with the objective (YTL-25-20PY1; Sigma Koki) and then focused with a custom-made optical apparatus (Nikon and Sigma Koki). The laser beam was led into the microscope from the right-hand side to the position just below the dichroic mirror for fluorescence excitation, which was originally designed to set an analyzer of a DIC microscope. The linear polarization of the laser light was changed to a circular polarization with a quarter wave plate. The laser light could be split into two beams with a set of beam splitters (PBN-20-16040; Sigma Koki) if needed. The trap stiffness we used, 0.1–0.3 pN/nm, was calibrated as described before (Nishizaka et al., 1995b).

In vitro assay system and preparation of bead-tailed F-actin

Actin and myosin were prepared from rabbit skeletal white muscle according to a standard procedure (Kondo and Ishiwata, 1976). HMM prepared by chymotryptic digestion, and s1 by papin digestion of myosin was stored in liquid N_2 (Nishizaka et al., 1993). A bead-tailed actin filament was prepared as previously reported (Suzuki et al., 1996). Bovine plasma gelsolin (Kurokawa et al., 1990) was cross-linked to the carboxylated polystyrene bead (1-μm diameter; Polysciences, Warrington, PA) with 1-ethyl-3-(3-dimethyl-aminopropyl)-carbodiimide (Nacalai Tesque Co., Kyoto), such that the barbed end (B-end) of an actin filament, which corresponds to the rear end when the filament slides, was attached to the bead. The average number of actin filaments attached to the bead was controlled by cross-linking an appropriate amount of bovine serum albumin (BSA) to the bead (BSA/gelsolin = 20:1 w/w). BSA labeled with rhodamine X maleimide (Molecular Probes, Eugene, OR) was also attached to the bead surface to visualize the bead as a fluorescence image (cold BSA/labeled BSA = 19:1). The bead was washed with F-buffer (0.1 M KCl, 2 mM $MgCl_2$, 2 mM 3-(*N*-morpholino)propanesulfonic acid (pH 7.0), 1.5 mM NaN_3, 1 mM dithiothreitol (DTT)) and mixed with 0.2 mg/ml actin filament labeled with rhodamine phalloidin (Molecular Probes) (Yanagida et al., 1984). Before infusion to the flow cell, bead-tailed actin filaments were diluted in F-buffer containing 1 mg/ml BSA to avoid adsorption of the bead to the glass surface. The in vitro assay system was prepared according to the report by Toyoshima et al. (1987), with slight modifications (Nishizaka et al., 1995b). The coverslip, cleaned in a sonicator with neutral detergent, was silanized with hexamethyl disilazane (Nacalai Tesque) (Nishizaka et al., 1995b). HMM and S1 were diluted in an assay buffer (AB) (25 mM KCl, 4 mM $MgCl_2$, 25 mM imidazole-HCl (pH 7.4), 1 mM EGTA, 1 mM DTT) and infused with the flow cell from one side and then from the other side after 60 s. The cell was washed with AB-buffer containing 0.5 mg/ml BSA, 10 mM DTT, 0.22 mg/ml glucose oxidase, 0.036 mg/ml catalase, and 4.5 mg/ml glucose. The bead-tailed actin filament, which was a mixture of 20 nM actin and 0.05% (w/v) bead, was infused. After washing with 3 volumes of AB-buffer containing 0.5 mg/ml BSA and the oxygen scavenger system, the edges of the flow cell were sealed with grease (Toray Dow Corning Silicone, Tokyo). All experiments were done at 30–32°C, except the S1 measurement at 27–32°C.

RESULTS

Direct counting of the number of HMM molecules

First we developed a method for directly counting the number of HMM molecules interacting with actin filaments. Our previous studies showed that the location of each HMM molecule attaching to a glass surface could be determined (Nishizaka et al., 1995a,b). When an actin filament was pulled and taut, HMM molecules could be recognized as a nodal point of the fluctuation of actin filament. By imposing the external load, we broke the nodal point and loosened the filament again (figure 1 *A* of Nishizaka et al., 1995a). Although this technique was useful for determining the location of HMM molecules, it was restricted to a very low density of HMM molecules, because the loosened part of the actin filament immediately attached to adjacent HMM molecules when the distance between adjacent molecules was less than ~1 μm. To solve this difficulty, the bead was manipulated not in the direction parallel to the glass surface but perpendicular to the surface (Figs. 3 and 4). This tech-

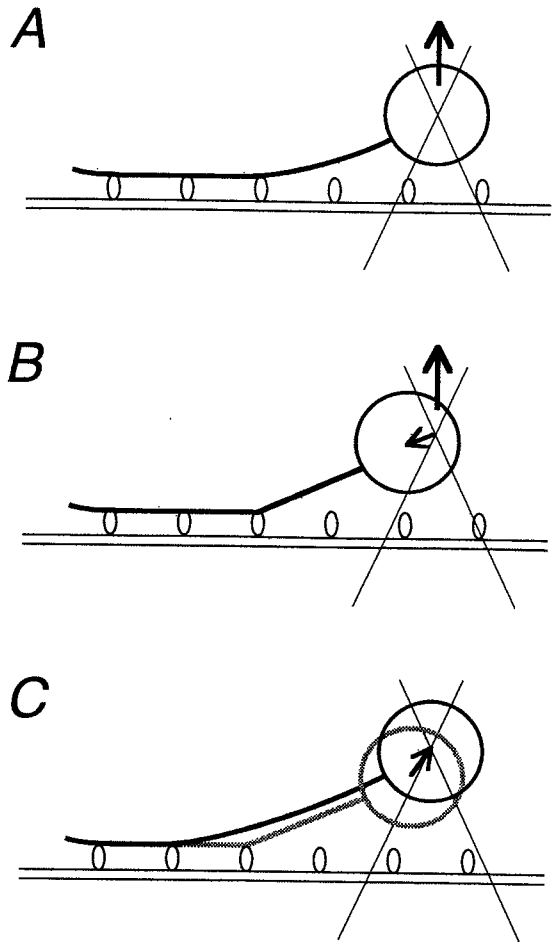

FIGURE 3 Schematic illustration of the technique used to count the number of motor molecules attached to the glass surface. The bead-tailed actin filament bound to HMM molecules was manipulated in the upward (z) direction at a constant rate (*A*). The filament was pulled taut from the HMM molecule (*B*), so that the bead was displaced from the trap center in the direction of the HMM. The bead returned to the trap center when the cross-bridge was broken, and subsequently the actin filament was loosened (*C*).

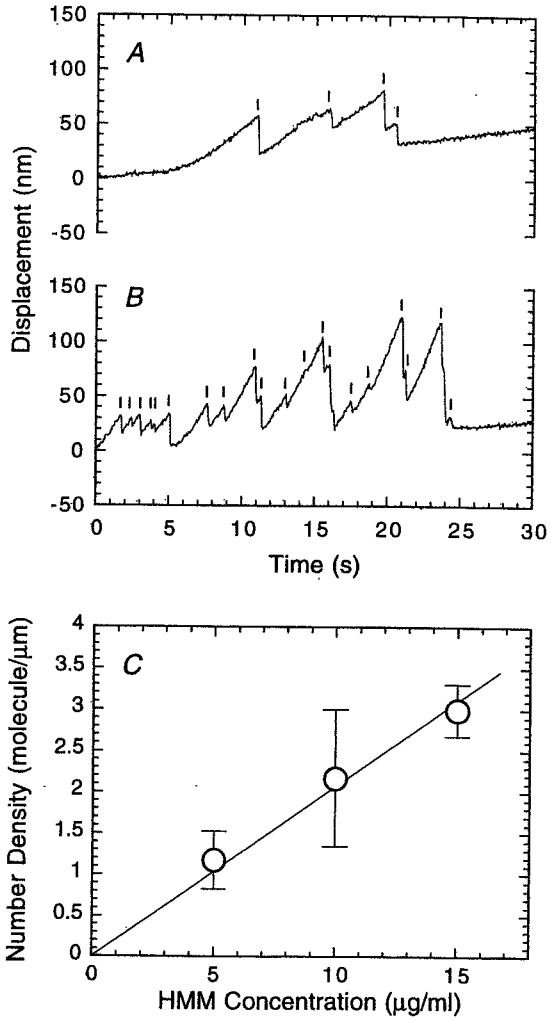

FIGURE 4 (*A* and *B*) Examples of the time course of the bead displacement projected onto the *xy* plane of the glass surface. The objective was moved in the upward (z) direction at a constant rate, 100 nm/s. The glass surface was precoated with 5 and 15 μg/ml HMM in *A* and *B*, respectively. The small bar indicates the moment at which the cross-bridge was broken (cf. Fig. 3 *C*). (*C*) The relation between the concentration of HMM infused into the flow cell and the number density of HMM. Bars indicate the standard deviation (n = 4–5). The slope of a linear approximation is 0.21 molecules/((μg/ml)·μm actin filament).

nique could be used to avoid overcounting the number of molecules.

Fig. 4, *A* and *B*, shows examples of the time course of the bead movement projected onto the *xy* plane with this technique. The trapped bead was manipulated in the upper *z* direction at a constant rate of 100 nm/s by moving the objective with a piezoelectric positioner (Fig. 3 *A*). After the part of the actin filament closest to the bead became taut, the bead began to deviate from the trap center (*sawtooth pattern* in Fig. 4, *A* and *B*; cf. Fig. 3 *B*). Then, after a while, the bead returned to the trap center accompanying the unbinding of the rigor bond. Thus each peak in Fig. 4, *A* and *B*, indicated by a small bar corresponds to the moment at which the cross-bridge was broken (Fig. 3 *C*). Finally, the filament was completely detached from the glass surface (at 21 s in Fig. 4 *A* and 24 s in Fig. 4 *B*). In 0–5 s and 21–30 s in Fig. 4 *A*, the trapped bead was displaced to the *x* direction at a rate of ~2 nm/s, which was accompanied by the upward motion of the objective. This movement is attributable to a slight misalignment between the laser beam and the optical center axis of the objective.

We applied the above method to the HMM solution in the range of 5–15 μg/ml (Fig. 4); at higher HMM concentrations, actin filaments were severed at a nodal point by pulling. The maximum trapping force of our system was estimated to be ~60 pN, indicating that an actin filament can be broken by applying a force less than 60 pN when the

filament is bent at an acute angle (cf. Arai et al., 1999). As shown in Fig. 4 *C*, the average number of HMM molecules that attached to a unit length of an actin filament was proportional to the concentration of infused HMM, and its slope was 0.21 molecules/((μg/ml)·μm actin filament).

We also examined the minimum concentration of HMM needed to achieve smooth sliding movement of actin filaments in the presence of 1 mM ATP. On the glass surface coated with HMM lower than 20 μg/ml, actin filaments could not slide and became detached from the glass surface. At 30 μg/ml HMM, actin filaments ~10 μm in length slid continuously at a speed of 9.3 ± 0.7 μm/s (n = 5), whereas short actin filaments slid intermittently and sometimes became detached. Under these conditions (1 mM ATP and 30 μg/ml HMM), the minimum length of actin filaments that slid continuously for 10 s was 1.4 μm.

Swiveling motion of actin filaments tethered to HMM

On a glass surface that was coated with a low concentration of HMM in the absence of ATP, short actin filaments (1–2 μm long) showed swiveling Brownian motion around a single point over a range of more than 360° (Nishizaka et al., 1995a,b). An example of this swiveling motion is shown in Fig. 7. This observation is analogous to the case of a microtubule tethered by a single kinesin molecule (Hunt and Howard, 1993). By analyzing the swiveling motion of actin filaments, we estimated the torsional stiffness of the flexible part, which is probably located in a HMM molecule.

The direction of a rotating actin filament was estimated from the centroid of its fluorescence image. We chose those actin filaments tethered to the glass surface by a single point that was slightly deviated from the center of the filament. When the filament swiveled around the tether point, the centroid of its fluorescence image also swiveled, showing the direction of the filament (Noji et al., 1997; Yasuda et al., 1998). Before the centroid calculation, noise in the video images was reduced by recording by averaging over 4 consecutive video frames. Actin filaments 1–3 μm long were selected for calculation to avoid the effect of their bending motion in calculation.

Fig. 5 *A* is an example showing the time course of the rotation of the short actin filament. The direction of the filament fluctuated with time. This fluctuation was assumed to be caused by thermal energy, and the torsional stiffness could be estimated as follows: the direction was divided every 1-rad partition, and the probability that the filament existed in each direction of 1 rad width, $P(\theta)$ (θ = torsion angle), was calculated. The energy $E(\theta)$ was thus obtained by the equation $E(\theta) = -k_B T \cdot \ln(P(\theta))$ as shown in Fig. 5 *B*, where k_B is the Boltzmann constant and T is the absolute temperature. The approximation of $E(\theta)$ to a spring shape function, $E(\theta) = \frac{1}{2} k \theta^2$ (k is the spring constant), is shown as a thin line in Fig. 5 *B*. The value of k was estimated to be

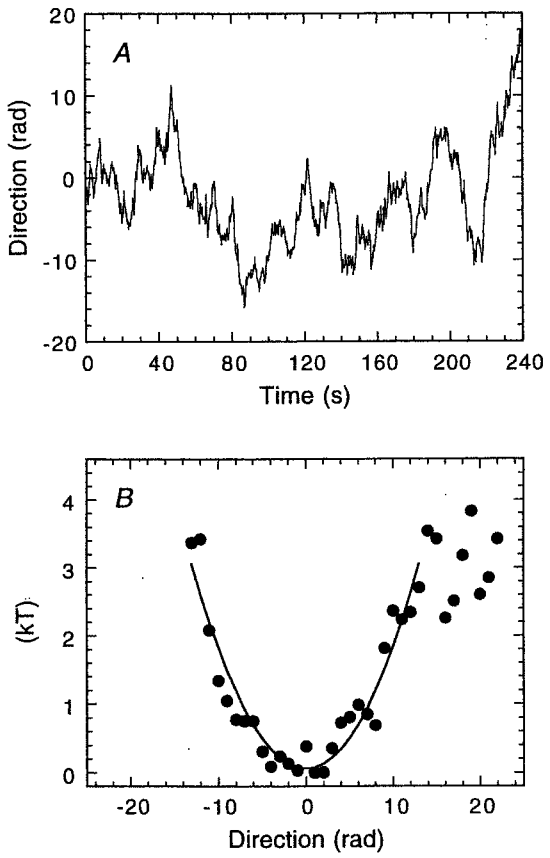

FIGURE 5 (*A*) An example showing the time course of swiveling of a short actin filament tethered to the glass surface through a single HMM molecule (see the short actin filament in Fig. 7, indicated by an *arrow*). (*B*) The energy profile showing the torsional stiffness of the single HMM molecule estimated from *A*. The thin line is an approximation with a spring shape function ($E(\theta) = 1/2 \cdot k\theta^2$, where $E(\theta)$ is energy, k is the spring constant, and θ is the torsion angle), in which the spring constant is 0.074×10^{-21} N · m/rad in the range of ±12 rad.

$2.3 \pm 1.9 \times 10^{-22}$ (± SD, n = 5) N·m/rad. Actin filaments rotated 6.4 times at maximum and 3.8 times on average.

Lifetime of single rigor bonds

In our previous studies (Nishizaka et al., 1995a,b), the unbinding force was measured by moving the trap center with a movable mirror. In the present study, the optical stage was displaced by using a piezoelectric substage, while the trap center was fixed. The advantage of this method is that the imposed load can be precisely determined at any moment. Fig. 6 illustrates how to examine the load dependence of the lifetime of single rigor bonds formed between a single actin filament and a single myosin (HMM or S1) molecule that attached to the glass surface. First the bead attached to the B-end of an actin filament is trapped by optical tweezers (Fig. 6 *A*). When the optical stage is displaced stepwise so as to make the actin filament taut, the

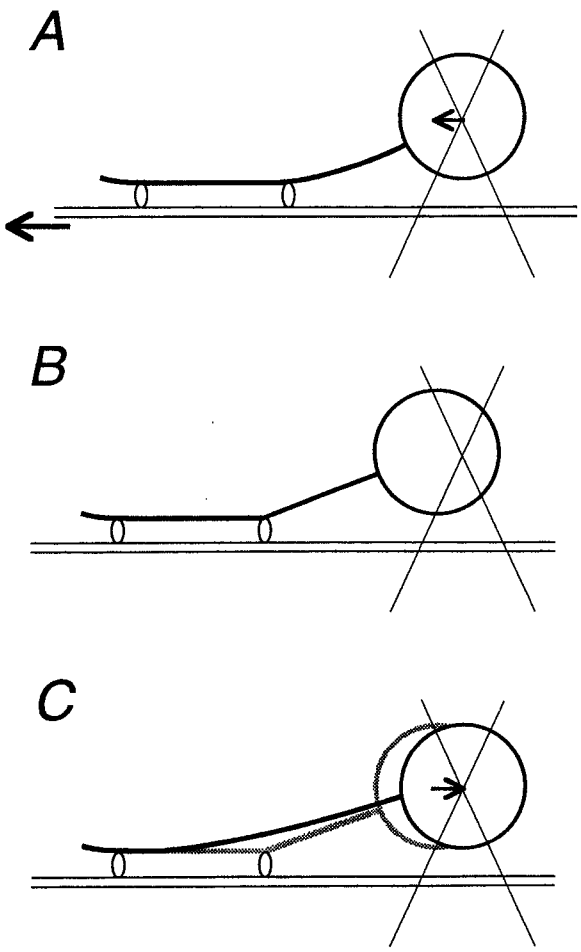

FIGURE 6 Schematic illustration of the procedure to measure the lifetime of the rigor bond between a single actin filament and a single HMM (or S1) molecule. (*A*) The bead-tailed actin filament bound to a motor protein is trapped by optical tweezers, and then the piezoelectric substage is displaced stepwise. (*B*) The filament is pulled taut from the motor protein, and the bead is displaced from the trap center, so that a sudden constant load is imposed on the rigor bond. (*C*) Finally, the bead returns to the trap center accompanying the breakage of the rigor bond, and the filament is loosened again. The time that elapsed between *B* and *C* corresponds to the lifetime of rigor bond.

bead is subsequently displaced from the trap center (Fig. 6, *A* and *B*). Thus a constant load is imposed stepwise on the rigor bond within a video frame, 1/30 s. After a while, the rigor bond is broken, and the bead is returned to the trap center (Fig. 6 *C*). The actin filament is loosened and shows bending Brownian motion again between the bead and the adjacent myosin molecule.

Fig. 7 is a series of fluorescence micrographs showing how to impose an external load on single rigor bonds. An actin filament was first trapped with optical tweezers (Fig. 7 *A*) and tautened by stepwise displacement to the left by the piezoelectric substage (Fig. 7 *B*) because the bead had located to the right of the HMM molecule. In this example, there were two HMM molecules that tethered the actin filament to the glass surface as identified as a nodal point (*arrowheads*), and the actin filament was pulled taut from the first HMM molecule. After a while, the bond was broken (Fig. 7 *C*), such that the lifetime of the rigor bond under a constant load could be directly measured. The actin filament was immediately loosened and showed bending Brownian motion again. When the stage was moved further, the filament was pulled taut from the next HMM molecule (Fig. 7 *D*). The stage was displaced stepwise again, and the second rigor bond was subsequently broken. Thus the actin filament was completely dissociated from the glass surface and the fluorescence image became out of focus (Fig. 7 *E*). Note that in Fig. 7, there is a short actin filament swiveling around a single point (indicated by a *small arrow*), at which a single HMM molecule is considered to be attached. The data in Fig. 5 were obtained from such a fluorescence image.

Fig. 8 *A* is an example of a record showing the time course of the displacement of the bead after stepwise imposition of an external load. When the stage was displaced stepwise (at 1.3 s, as shown by an *arrow*), the actin filament became taut (cf. Fig. 7, *B* and *D*), and the bead was displaced from the trap center. In this example, the external load imposed on the rigor bond was estimated to be 10.6 pN (we could not determine the external load beforehand, because the degree of loosening of an actin filament before applying the load could not be controlled), and the rigor bond was broken 0.43 s after the load was imposed. This observation showed that the lifetime of the actin-HMM rigor bond at no load, ~1000 s, was decreased to 0.43 s by imposing a load of 10.6 pN.

In the case of acto-S1 rigor bonds, spontaneous unbinding occurred, on the average, in ~100 s (Tadakuma et al., manuscript in preparation). Because of this short lifetime, measurement of the load dependence of the lifetime was technically difficult. To solve this problem, we prepared a flow cell coated with a higher density of S1 as compared with HMM, and actin filament was pulled at an acute angle to avoid the possibility of stretching two rigor bonds simultaneously.

Fig. 8 *B* is a summary showing the relationship between the imposed load and the lifetime. While the lifetime of HMM rigor bonds was distributed over a wide range of imposed loads, that of S1 rigor bonds was limited to a narrower range. In the case where a bond was broken within 66 ms (two video frames), we could not precisely determine the imposed load, so that these data (~5% of measurements) were omitted from Fig. 8 *B*. In the case of S1, there were four exceptional cases in which rigor bonds did not break for 60 s over 20 pN. We judge that they are attributable to the aggregation of S1, and thus they are not included in Fig. 8 *B*.

To elucidate the load dependence of the lifetime, we divided loads on the abscissa of Fig. 8 *B* into 3-pN partitions and replotted the time course of the unbinding occurrence of HMM and S1 rigor bonds in each partition, as shown in Fig. 9. The error bars indicate $N^{1/2}$, corresponding to the stan-

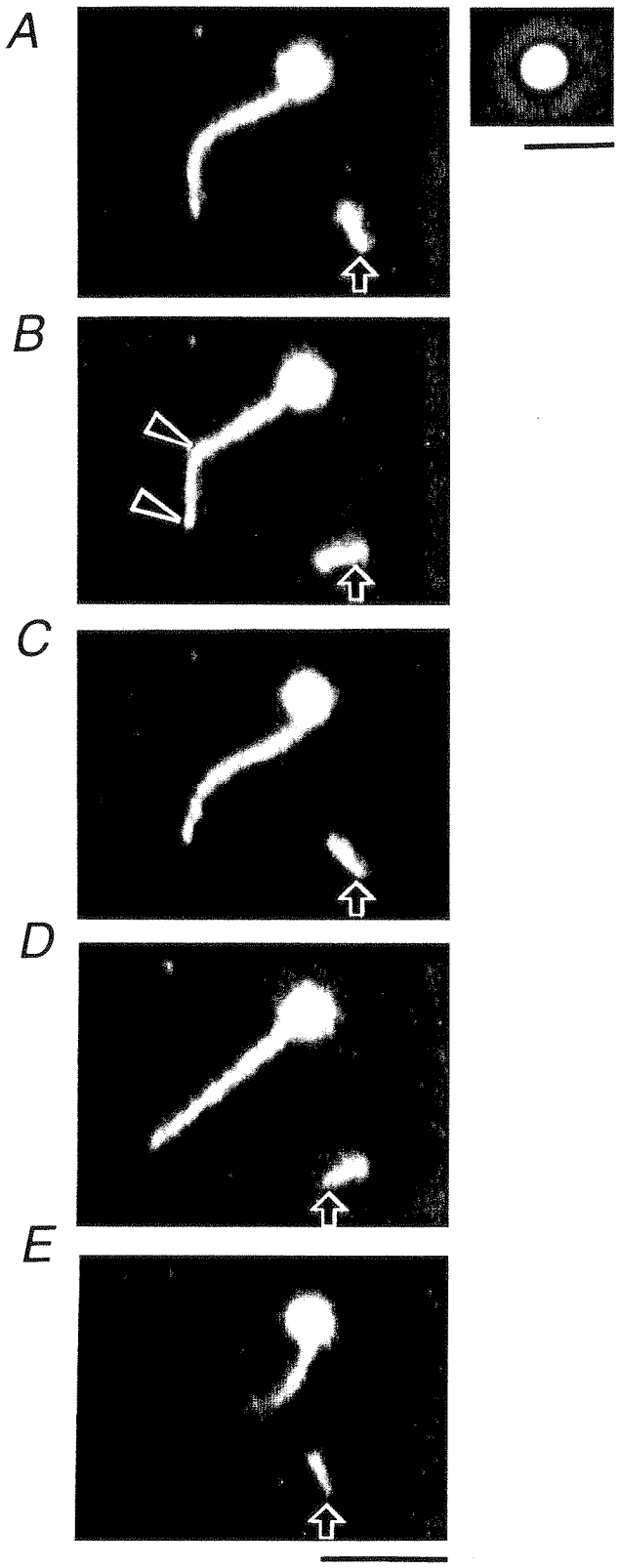

FIGURE 7 A series of fluorescence micrographs showing how to measure the lifetime of single rigor bond(s). (*A*) The bead attached to the B-end of an actin filament was trapped by optical tweezers. (*B*) The flow cell was moved (within 1/30 s) ~200 nm stepwise, using a piezoelectric substage, so that the actin filament was pulled taut from an HMM molecule (*arrowheads*). (*C*) After a while, the rigor bond was broken and the lifetime of the single rigor bond was measured. (*D*) The substage was moved further leftward and displaced stepwise again, such that the filament became nearly straight. (*E*) The filament was detached completely from the glass surface and showed Brownian motion. Note that a short actin filament, tethered to the glass surface through probably only one HMM molecule (indicated by an *arrow*), swiveled in each micrograph. Scale bar, 5 μm. (*upper right*) Phase-contrast image of the bead of *A–E*. Scale bar, 2 μm. The two images were simultaneously observed using the optics of Fig. 1.

dard deviation for events that stochastically occur N times. For S1, and for 9.0–12.0 pN and 12.0- pN of HMM, plots were approximated with the equation of a single exponential decay, $N(t) = N(0)\cdot\exp(-t/\tau)$, where τ is a lifetime of the rigor bond. Deviations of τ were estimated from fitted curves with maximum and minimum τ so as not to deviate from error bars by more than one data point in Fig. 9, and then they were expressed as error bars in Fig. 10. For 0.0–3.0, 3.0–6.0, and 6.0–9.0 pN of HMM, the data were approximated with the sum of two exponential decays, i.e., $N(t) = N_f(0)\cdot\exp(-t/\tau_f) + N_s(0)\cdot\exp(-t/\tau_s)$, where τ_f and τ_s are, respectively, a fast and a slow component of the lifetime, and $N_f(0) + N_s(0) = N_0$ is the total number of data at each region. After an optimum set of τ_f, τ_s, and $N_f(0)$ values was determined, deviations in τ_f and τ_s were independently estimated from fitted curves with maximum and minimum values so as not to deviate from the error bars of all data points. These maximum and minimum values of τ_f and τ_s were expressed as error bars in Fig. 10. The lifetimes thus obtained are summarized in Table 1.

Fig. 10 is a semilogarithmic plot of the data summarized in Table 1. As for the slow component of HMM, the relation between the lifetime, $\tau(F)$, and the imposed load, F, was closely approximated by the equation $\tau(F) = \tau(0)\cdot\exp(-F\cdot d/kT)$ (*thick solid line*). The relations for S1 and for the fast component of HMM were also approximated by this equation, as shown by a dashed line and a thin solid line, respectively. Note that the relation for S1 coincided with that for the fast component of HMM. From these approximation lines, d and $\tau(0)$ were estimated as summarized in Table 2.

DISCUSSION

Minimum number of HMM molecules needed to slide actin filaments continuously

The estimation of the number of myosin molecules interacting with an actin filament is essential for describing the sliding movement of an actin filament in an in vitro motility assay. Unlike myosin V (Mehta et al., 1999) or kinesin (Howard et al., 1989; Vale et al., 1996), the skeletal myosin (myosin II) molecule is not a processive motor, such that multiple motors are required for smooth and continuous

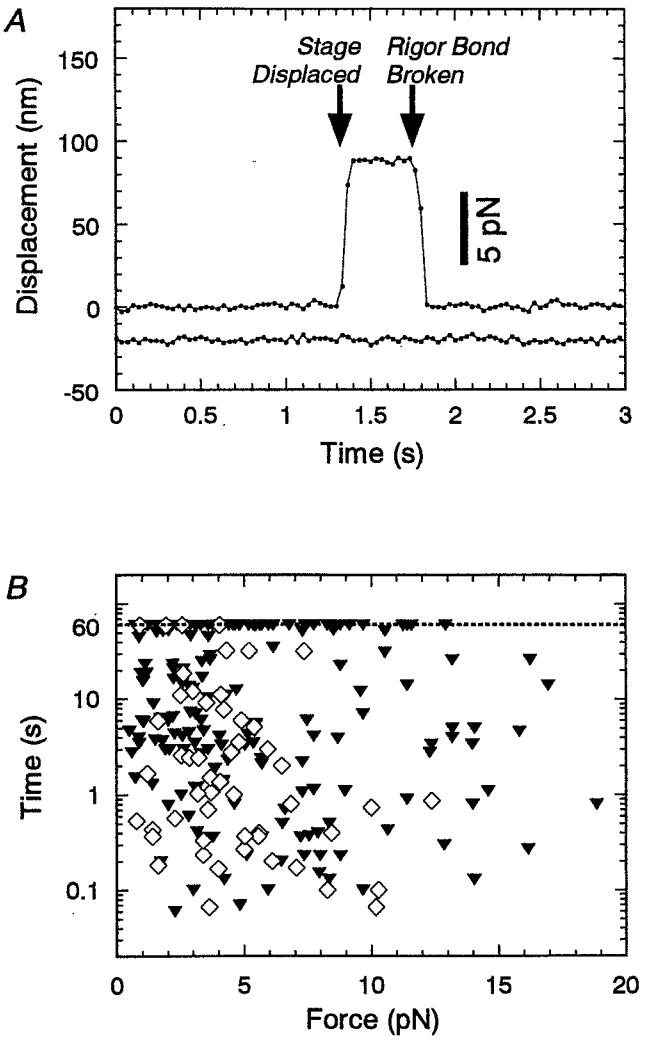

FIGURE 8 Load dependence of the lifetime of single rigor bonds. (*A*) An example of the time course of the displacement of the bead (cf. Figs. 6 and 7). Upper and lower plots show, respectively, the displacement of the bead along and perpendicular to the actin filament. Each dot was plotted every 1/30 s. The stage was displaced stepwise at 1.3 s so as to impose a constant external load, and then the bond was broken after 0.43 s in this example. (*B*) Relationship between the imposed load and the lifetime of rigor bonds of HMM (▼) and S1 (◇). For the rigor bonds not broken within 60 s, the lifetimes are plotted on the dashed line indicating 60 s.

sliding of actin filaments without dissociation. Although we could not directly count the number of HMM molecules during the sliding movement, the number required for smooth sliding of an actin filament could be estimated from our results (Fig. 4). The lowest concentration of HMM required for continuous sliding motion of actin filaments was 30 μg/ml in our method, so that the minimum line density of HMM molecules is estimated to be 30 (μg/ml) × 0.21 (molecules/μm/(μg/ml)) = 6.3 (molecules/μm actin filament). Furthermore, the minimum length of the filament showing the sliding movement was ~1.4 μm under the same conditions. Thus we obtain the minimum number of molecules required for smooth sliding without dissociation, 6.3 (molecules/μm) × 1.4 (μm) = 8.8 (molecules).

We can assume that one ATP hydrolysis of the actomyosin system takes (10–100) ms, as in an in vitro motile system (Harada et al., 1990) and in solution (cf. Goldman, 1987). On the other hand, the probability that at least one myosin head binds to an actin filament is given by $P = 1 - \{(N - n)/N\}^N$, where N is the total number of myosin heads that can interact with the filament and n is the average number of heads that bind to the filament at one time. Therefore, $(1 - P) \times$ (10–100) ms is the dissociation period during which no myosin heads interact with the filament. The diffusion coefficient perpendicular to the filament axis for a 1.4-μm actin filament is calculated to be 1.4×10^{-8} cm^2/s from the equations $D = k_BT/\Gamma_\perp$ and $\Gamma_\perp = 4\pi\eta L/(\ln(L/2r) + \gamma_\perp)$, where $L = 1.4$ μm, $r = 5$ nm, $\eta = 0.010$ g/cm·s, $\gamma_\perp = 0.89$ (Hunt et al., 1994) and $T = 300$ K. Thus the time required for actin filaments 1.4 μm long to diffuse as far as δx, ~17 nm (the size of myosin heads) to 34 nm (its doubled size), within which the filaments can maintain a sliding motion, is calculated to be 0.1–0.4 ms according to the equation $\delta x = (2Dt)^{1/2}$. To make $(1 - P) \times$ (10–100) ms shorter than 0.1–0.4 ms, P should be larger than 0.96–0.999. Together, n should be larger than 3.0–5.8 under $N = 17.6$ (= 8.8 × 2) heads to keep P as 0.96–0.999 ($1 - \{(N - n)/N\}^N = 1 - \{(17.6-3.0)/17.6\}^{17.6} > 0.96$, $1 - \{(17.6-5.8)/17.6\}^{17.6} > 0.999$), suggesting that at least (3.0–5.8)/17.6 ≅ 17–30% of myosin heads always bind to the filament during sliding motion. If all n heads are in a state of producing the active force, the value 17–30% corresponds to the "duty ratio," which is the proportion of the period in which a single head produces the force in one ATPase cycle. However, because some head is only capable of holding the filament without producing active force (Goldman, 1987; Ishiwata and Yasuda, 1993), 17–30% could be an overestimation of the duty ratio.

Torsional stiffness of a single HMM molecule

By analysis of the rotational Brownian motion of a short actin filament tethered to a single HMM molecule, the torsional stiffness has been estimated to be $(2.3 \pm 1.9) \times 10^{-22}$ N·m/rad. The flexible part responsible for this small stiffness must be located at the joint between the S1 and S2 regions, and/or within the S2 region of the HMM molecule (Kinosita et al., 1984; Ishiwata et al., 1987, 1988). Note that this stiffness is so small that the thermal fluctuation energy, k_BT (4.1×10^{-21} N·m), can twist myosin 2.8 times ($(4.1 \times 10^{-21})/(2.3 \times 10^{-22})/2\pi = 2.8$). This small stiffness can explain the following mechanical properties of myosin previously reported: myosin can interact with an actin filament under various orientations (Toyoshima et al., 1989; Molloy et al., 1995), although it modifies the motor functions, such as the sliding velocity and force (Yamada et al., 1990; Sellers and Kachar, 1990; Ishijima et al., 1996). The unbinding

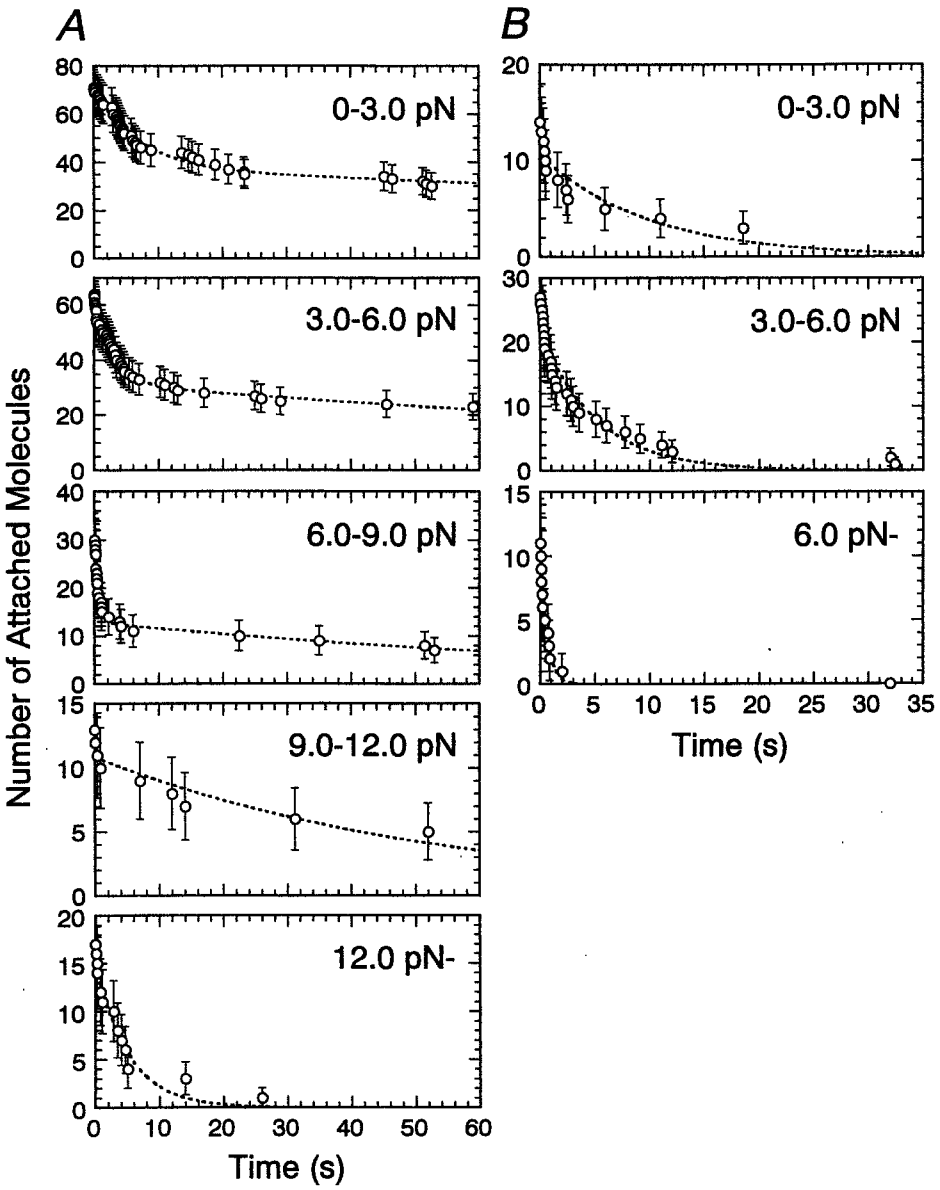

FIGURE 9 Time course of the decrease in the number of attached molecules, N, under various imposed loads, replotted from the data of Fig. 8 *B*. Error bars show standard deviation, which is simply determined as the square of the number of measurements at each point ($\pm N^{1/2}$). (*A*) HMM. Dashed lines indicate the approximation by $N(t) = N(0)\cdot\exp(-t/\tau)$ or $N(t) = N_f(0)\cdot\exp(-t/\tau_f) + N_s(0)\cdot\exp(-t/\tau_s)$ (for details see Results). (*B*) S1. Dashed lines indicate the approximation by $N(t) = N(0)\cdot\exp(-t/\tau)$.

force of rigor bonds is independent of the direction of external load, at least within ±90° (Nishizaka et al., 1995b). Because of the small stiffness, the geometrical relationship of the actin-myosin binding interface is probably maintained.

As for kinesin, the stiffness was estimated to be 1.2×10^{-22} N·m/rad by observing the rotational Brownian motion of an attached microtubule (Hunt and Howard, 1993), which is comparable to that of HMM. Thus such a small torsional stiffness may be common to motor proteins. Surprisingly, kinesin could be twisted more than 30 times by manipulation with optical tweezers without breaking the bond between kinesin and a microtubule (Kuo et al., 1995). This result may not be explainable by twisting of a head-rod junction; thus we alternatively assume that detachment and reattachment occur on one head while the other head binds to a filament. The twisting distortion in the attached head will be released during unbinding, and then the head can bind again without large distortion. If the two heads repeat this process alternately, the filament can rotate in one direction without limitation. We favor this model as an explanation of how protein can rotate more than 30 times without dissociation. If this process also occurred in our actin-HMM complex, the estimated value is an underestimation as a torsional stiffness of single HMM molecules.

Load dependence of lifetime of rigor bonds and binding manner of HMM

In our previous study, we repeatedly measured the load dependence of the lifetime of rigor bonds on the same

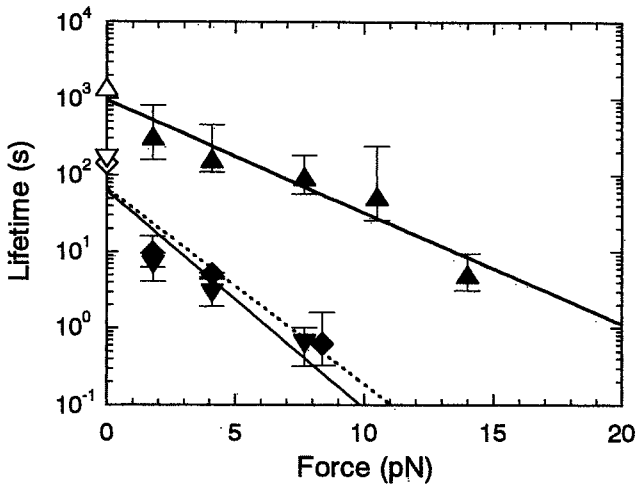

FIGURE 10 Relation between imposed load and lifetime of HMM and S1 rigor bonds. Triangles and inverted triangles show the slow and fast components of HMM, respectively. Squares show the lifetime of S1. Filled symbols were determined from Fig. 9, and open symbols are experimental data obtained without load (Tadakuma et al., manuscript in preparation). Fitted lines show the approximation by the equation $\tau(F) = \tau(0)\cdot\exp(-F\cdot d/k_BT)$. The thick and thin solid lines show the approximation of slow and fast components of HMM, respectively. The dashed line shows the approximation for S1.

acto-HMM rigor complexes (figure 4 in Nishizaka et al., 1995b). In the present study, we improved the mechanical stability of the microscopy apparatus to realize more accurate measurements, especially for longer times. As a result, the spatial resolution became less than 1 nm, and the drifting movement of the stage was restricted to within ~2 nm for 1 min. Such an improvement was essential for quantitatively investigating the relationship between the lifetime and the load.

TABLE 1 Lifetimes of HMM and S1 rigor bonds estimated from the approximation with exponential decay shown in Fig. 9

Load (pN)	Ratio, fast/total	Lifetime (s) τ_f	Lifetime (s) τ_s
A. HMM			
No load	(0.41)	(170)	(1400)
0–3	0.47	6.9	320
3–6	0.51	2.9	160
6–9	0.57	0.64	97
9–12	—	—	53
12+	—	—	5.1
	Lifetime (s)		
B. S1			
No load	(150)		
0–3	9.9		
3–6	5.2		
6–9	0.63		

The data were approximated by the equation of single exponential decay, $N(t) = N(0)\cdot\exp(-t/\tau)$, or the sum of two exponential decays, $N_f(0)\cdot\exp(-t/\tau_f) + N_s(0)\cdot\exp(-t/\tau_s)$. Ratio, $N_f(0)/(N_f(0) + N_s(0))$, means the proportion of cross-bridges having the fast component. Both ratio and lifetimes without load shown in parentheses were determined by the microscopic observation of spontaneous detachment from a glass surface of swiveling short actin filaments (Tadakuma et al., manuscript in preparation).

TABLE 2 Interaction distance, d, and lifetime without external load, $\tau(0)$, for, respectively, single rigor bonds of HMM and S1, estimated from the slope and the extrapolation of the solid and dashed lines in Fig. 10

	d	$\tau(0)$
HMM (fast)	2.7	62
HMM (slow)	1.4	950
S1	2.4	67

We found that the time course of the decrease in the number of attached S1 molecules under an external load nearly followed a single exponential decay (Fig. 9 *B*). In contrast, the decay for HMM was not expressed by a single exponential, except for a large applied force (Fig. 9 *A*), but could be approximated by the sum of two exponentials with different lifetimes. As shown in Table 1, *A* and *B*, the fast component of the lifetime of HMM nearly coincided with the lifetime of S1. One plausible explanation for this result is that HMM molecules that attached to the glass surface are classified into two groups: one having the slow component of lifetimes in which double-headed binding occurs, and another having the fast component in which only single-headed binding is possible, probably because of the adsorption of either head to the glass surface. This explanation will be examined in the future by using single-headed myosin (Harada et al., 1987) or single-headed HMM. The ratio between single-headed and double-headed molecules in our HMM assay is estimated to be nearly 1:1 (Table 1 *A*). We previously suggested the presence of "molecular individualism" in each HMM, based on the fact that each HMM molecule showed the individual load dependence of the lifetime (Nishizaka et al., 1995b). The difference in the number of active heads may be the main reason for this "individuality."

The lifetime, τ, is generally related to the activation energy for unbinding, $\Delta G^{\ddagger}$, through $\tau \propto \exp(\Delta G^{\ddagger}/k_BT)$. This could be extended to a fundamental property of the binding between a ligand and a receptor under an external load, i.e., $\tau(F) = \tau_0\cdot\exp((\Delta G^{\ddagger} - F\cdot d)/k_BT) = \tau(0)\cdot\exp(-F\cdot d/k_BT)$, where $\tau(F)$ is the lifetime under the load F and d is defined as the distance of an intermolecular interaction beyond which the intermolecular bond is ruptured (Bell, 1978; Erickson, 1994). The value of d is generally assumed to be less than a nanometer. Note that even though there is no load, the intermolecular bonds in an aqueous solution break with a lifetime of $\tau(0)$ in a stochastic manner under thermal equilibrium. This aspect is essential for understanding the unbinding force of the bond between proteins. The unbinding force between proteins was previously estimated to be

larger than 100 pN (Kishino and Yanagida, 1988; Florin et al., 1994; Tsuda et al., 1996; Fritz et al., 1998); however, it has been predicted that these values depend on the rate of the increase in the applied load. The unbinding force could be smaller when the external load is applied slowly, e.g., at a rate comparable to the dissociation rate constant. This was confirmed for actin-HMM rigor complex (cf. Fig. 4 in Nishizaka et al., (1995b)) and for avidin-biotin complex: the unbinding force increases from several piconewtons to hundreds of piconewtons as the velocity is increased by 10^6 (Merkel et al., 1999). In the case of P-selectin, the unbinding force was confirmed to increase logarithmically with the increase in the pulling velocities of ligand against receptor (figure 5 in Fritz et al., 1998). Thus the difference in the pulling velocity is considered to be the main reason why the average unbinding force of actin-HMM rigor complex obtained by AFM (Nakajima et al., 1997), ~14 pN, was larger than that obtained with optical tweezers (Nishizaka et al., 1995b), ~9 pN.

The exponential dependence of lifetime on the external load, which was predicted before (Bell, 1978; Erickson, 1994), fits well with our results as shown in Fig. 10. From the slope of the straight lines in Fig. 10, we obtained the values of d: 1.4 nm for the slow component of HMM, 2.7 nm for the fast component of HMM, and 2.4 nm for S1 (Table 2). The value of d for slow HMM components, which corresponds to the double-headed binding, was nearly one-half of those of d for fast HMM components, corresponding to the single-headed binding, and for S1. This difference by a factor of 2 suggests that the external load (F) is evenly shared on each attached head of HMM, such that the external load imposed on each head effectively becomes a half. This suggests that d for the interaction between single-head myosin and actin is ~2.5 nm.

It is expected that the large d value is attributable to the geometry of application of an external load. In fact, regarding the interaction between actin monomers in a filamentous actin, the tensile strength depends on the direction of the applied load to the molecular interface. Tsuda et al. (1996) reported that 600 pN was required for the breakage of the actin filament by straight pull, whereas Arai et al. (1999) reported that the actin filament broke when they applied 1 pN after tying a knot in it. In both measurements, the process of unbinding was observed at a video rate, so that the duration required for breakage was similar. Thus the apparent value of d for the latter may be an order of magnitude larger than that for the former.

In our system, the load was always imposed toward the long axis of an actin filament. The value of d could be decreased when the external load is applied in the direction parallel to the coordinate axis of the interaction potential, which may usually be the direction perpendicular to the intermolecular interface. The proposed structure of myosin head is longitudinally thin, and the actin-binding site is not located at the tip of the head but relatively at the side of the catalytic domain of the head, such that myosin heads bind to an actin filament at an acute angle (Rayment et al., 1993a,b). As a result, the myosin is being pulled from an angle, which would tend to tilt it out of the interface rather than pulling it out perpendicularly. The applied load could induce the distortion of the myosin head around the binding interface, then the activation energy for unbinding is efficiently decreased by a small load, as shown in Fig. 10, which results in the large value of d. In contrast, in the case of avidin-biotin unbinding force measurement by AFM (Florin et al., 1994; Moy et al., 1994), a symmetrical avidin molecule was sandwiched between an AFM cantilever and an agarose bead that was biotinylated (the 50-μm-diameter agarose bead versus the 6-nm-diameter avidin). It is expected that the load was imposed nearly perpendicularly to the interface of the avidin-biotin bond (Grubmuller et al., 1996; Evans and Ritchie, 1997; Izrailev et al., 1997), so that the small value of d was obtained.

X-ray crystallography showed that the myosin head consists of two domains, i.e., a catalytic domain that contains ATP- and actin-binding sites, and a neck domain. One possible hypothesis for how myosin heads generate force is that the neck domain tilts against the catalytic domain like a lever arm and induces a power stroke accompanied by the release of P_i (Rayment et al., 1993a,b; Corrie et al., 1999; Taylor et al., 1999). This structural dynamic is thought to be coupled with the change in the binding affinity between the myosin head and actin (Goldman and Brenner, 1987), although this hypothesis seems to have difficulty explaining the results showing their uncoupling (Ishijima et al., 1998) and multiple unitary displacements of single myosin head per ATP hydrolysis (Kitamura et al., 1999). In general, it is believed that the post-power stroke state has higher binding affinity for actin, and the pre-power stroke state has relatively lower affinity. In our experiments, the actin filament was always pulled in the direction of the reversal of the power stroke of myosin because the bead was attached to the B-end of an actin filament. In other words, we imposed the load so as to change the state of myosin from a post-power stroke state to a pre-power stroke state. If the structure of the myosin head changes from a high-affinity form to a low-affinity form with the application of an external load, the unbinding that occurs very efficiently with an imposed load can also be explained by this mechanism. In this relation, the following experiment is interesting: measurement of the lifetime by pushing the myosin head, which is in the pre-power stroke state with ATP analogs, toward the post-power stroke state along the direction of the power stroke. In this case, the lifetime may become longer because of the transition from the low-affinity state to the high-affinity state.

Finally, we would like to point out that the geometry for applying an external load in our system is similar to that in muscle fibers. The gradual change in the binding affinity, which is assumed in the Huxley and Simmons model (Hux-

ley and Simmons, 1971), may accompany the change in the number of intermolecular bonds at the actomyosin interface. Thus a large value of d may be a feature common to motor proteins.

We thank Drs. Naoya Suzuki, Hidetake Miyata, Ichiro Sase, and Ryohei Yasuda of Keio University and Mr. Madoka Suzuki of Waseda University for their technical support and advice. This research was partly supported by grants-in-aid for Scientific Research, for Scientific Research for Priority Areas, and for the High-Tech Research Center Project to SI from the Ministry of Education, Science, Sports and Culture of Japan, and by grants-in-aid from the Japan Science and Technology Corporation. TN was a Research Fellow of the Japan Society for the Promotion of Science.

REFERENCES

Arai, Y., R. Yasuda, K. Akashi, Y. Harada, H. Miyata, K. Kinosita, Jr., and H. Itoh. 1999. Tying a molecular knot with optical tweezers. *Nature.* 399:446–448.

Ashkin, A., J. M. Dziedzic, J. E. Bjorkholm, and S. Chu. 1986. Observation of a single-beam gradient force optical trap for dielectric particles. *Optics Lett.* 11:288–290.

Ashkin, A., K. Schütze, J. M. Dziedzic, U. Euteneuer, and M. Schliwa. 1990. Force generation of organelle transport measured in vivo by an infrared laser trap. *Nature.* 348:346–348.

Bell, G. I. 1978. Models for the specific adhesion of cells to cells. *Science.* 200:618–627.

Corrie, J. E., B. D. Brandmeier, R. E. Ferguson, D. R. Trentham, J. Kendrick-Jones, S. C. Hopkins, U. A. van der Heide, Y. E. Goldman, C. Sabido-David, R. E. Dale, S. Criddle, and M. Irving. 1999. Dynamic measurement of myosin light-chain-domain tilt and twist in muscle contraction. *Nature.* 400:425–430.

Erickson, H. P. 1994. Reversible unfolding of fibronectin type III and immunoglobulin domains provides the structural basis for stretch and elasticity of titin and fibronectin. *Proc. Natl. Acad. Sci. USA.* 91: 10114–10118.

Evans, E., and K. Ritchie. 1997. Dynamic strength of molecular adhesion bonds. *Biophys. J.* 72:1541–1555.

Finer, J. T., R. M. Simmons, and J. A. Spudich. 1994. Single myosin molecule mechanics: piconewton forces and nanometre steps. *Nature.* 368:113–119.

Florin, E. L., V. T. Moy, and H. E. Gaub. 1994. Adhesion forces between individual ligand-receptor pairs. *Science.* 264:415–417.

Fritz, J., A. G. Katopodis, F. Kolbinger, and D. Anselmetti. 1998. Force-mediated kinetics of single P-selectin/ligand complexes observed by atomic force microscopy. *Proc. Natl. Acad. Sci. USA.* 95:12283–12288.

Funatsu, T., Y. Harada, M. Tokunaga, K. Saito, and T. Yanagida. 1995. Imaging of single fluorescent molecules and individual ATP turnovers by single myosin molecules in aqueous solution. *Nature.* 374:555–559.

Goldman, Y. E. 1987. Kinetics of the actomyosin ATPase in muscle fibers. *Annu. Rev. Physiol.* 49:637–654.

Goldman, Y. E., and B. Brenner. 1987. Special topic: molecular mechanism of muscle contraction. General introduction. *Annu. Rev. Physiol.* 49:629–636.

Grubmuller, H., B. Heymann, and P. Tavan. 1996. Ligand binding: molecular mechanics calculation of the streptavidin-biotin rupture force. *Science.* 271:997–999.

Harada, Y., A. Noguchi, A. Kishino, and T. Yanagida. 1987. Sliding movement of single actin filaments on one-headed myosin filaments. *Nature.* 326:805–808.

Harada, Y., K. Sakurada, T. Aoki, D. D. Thomas, and T. Yanagida. 1990. Mechanochemical coupling in actomyosin energy transduction studied by in vitro movement assay. *J. Mol. Biol.* 216:49–68.

Howard, J., A. J. Hudspeth, and R. D. Vale. 1989. Movement of microtubules by single kinesin molecules. *Nature.* 342:154–158.

Hunt, A. J., F. Gittes, and J. Howard. 1994. The force exerted by a single kinesin molecule against a viscous load. *Biophys. J.* 67:766–781.

Hunt, A. J., and J. Howard. 1993. Kinesin swivels to permit microtubule movement in any direction. *Proc. Natl. Acad. Sci. USA.* 90: 11653–11657.

Huxley, A. F., and R. M. Simmons. 1971. Proposed mechanism of force generation in striated muscle. *Nature.* 233:533–538.

Ishijima, A., Y. Harada, H. Kojima, T. Funatsu, H. Higuchi, and T. Yanagida. 1994. Single-molecule analysis of the actomyosin motor using nano-manipulation. *Biochem. Biophys. Res. Commun.* 199: 1057–1063.

Ishijima, A., H. Kojima, T. Funatsu, M. Tokunaga, H. Higuchi, H. Tanaka, and T. Yanagida. 1998. Simultaneous observation of individual ATPase and mechanical events by a single myosin molecule during interaction with actin. *Cell.* 92:161–171.

Ishijima, A., H. Kojima, H. Higuchi, Y. Harada, T. Funatsu, and T. Yanagida. 1996. Multiple- and single-molecule analysis of the actomyosin motor by nanometer-piconewton manipulation with a microneedle: unitary steps and forces. *Biophys. J.* 70:383–400.

Ishiwata, S., K. Kinosita, Jr., H. Yoshimura, and A. Ikegami. 1987. Rotational motions of myosin heads in myofibril studied by phosphorescence anisotropy decay measurements. *J. Biol. Chem.* 262: 8314–8317.

Ishiwata, S., K. Kinosita, Jr., H. Yoshimura, and A. Ikegami. 1988. Optical anisotropy decay studies of the dynamic structure of myosin filaments. *Adv. Exp. Med. Biol.* 226:267–276.

Ishiwata, S., and K. Yasuda. 1993. Mechano-chemical coupling in spontaneous oscillatory contraction of muscle. *Phase Transitions.* 45: 105–136.

Izrailev, S., S. Stepaniants, M. Balsera, Y. Oono, and K. Schulten. 1997. Molecular dynamics study of unbinding of the avidin-biotin complex. *Biophys. J.* 72:1568–1581.

Kamimura, S., and K. Takahashi. 1981. Direct measurement of the force of microtubule sliding in flagella. *Nature.* 293:566–568.

Kinosita, K., Jr., S. Ishiwata, H. Yoshimura, H. Asai, and A. Ikegami. 1984. Submicrosecond and microsecond rotational motions of myosin head in solution and in myosin synthetic filaments as revealed by time-resolved optical anisotropy decay measurements. *Biochemistry.* 23:5963–5975.

Kinosita, K., Jr., H. Itoh, S. Ishiwata, K. Hirano, T. Nishizaka, and T. Hayakawa. 1991. Dual-view microscopy with a single camera: real-time imaging of molecular orientations and calcium. *J. Cell Biol.* 115:67–73.

Kinosita, K., Jr., R. Yasuda, H. Noji, S. Ishiwata, and M. Yoshida. 1998. F_1-ATPase: a rotary motor made of a single molecule. *Cell.* 93:21–24.

Kishino, A., and T. Yanagida. 1988. Force measurements by micromanipulation of a single actin filament by glass needles. *Nature.* 334:74–76.

Kitamura, K., M. Tokunaga, A. H. Iwane, and T. Yanagida. 1999. A single myosin head moves along an actin filament with regular steps of 5.3 nanometres. *Nature.* 397:129–134.

Kondo, H., and S. Ishiwata. 1976. Uni-directional growth of F-actin. *J. Biochem.* 79:159–171.

Kuo, S. C., K. Ramanathan, and B. Sorg. 1995. Single kinesin molecules stressed with optical tweezers. *Biophys. J.* 68:74s.

Kurokawa, H., W. Fujii, K. Ohmi, T. Sakurai, and Y. Nonomura. 1990. Simple and rapid purification of brevin. *Biochem. Biophys. Res. Commun.* 168:451–457.

Marston, S. B. 1982. The rates of formation and dissociation of actin-myosin complexes. Effects of solvent, temperature, nucleotide binding and head-head interactions. *Biochem. J.* 203:453–460.

Mehta, A. D., R. S. Rock, M. Rief, J. A. Spudich, M. S. Mooseker, and R. E. Cheney. 1999. Myosin-V is a processive actin-based motor. *Nature.* 400:590–593.

Merkel, R., P. Nassoy, A. Leung, K. Ritchie, and E. Evans. 1999. Energy landscapes of receptor-ligand bonds explored with dynamic force spectroscopy. *Nature.* 397:50–53.

Miyata, H., H. Hakozaki, H. Yoshikawa, N. Suzuki, K. Kinosita Jr, T. Nishizaka, and S. Ishiwata. 1994. Stepwise motion of an actin filament

over a small number of heavy meromyosin molecules is revealed in an in vitro motility assay. *J. Biochem.* 115:644–647.

Miyata, H., H. Yoshikawa, H. Hakozaki, N. Suzuki, T. Furuno, A. Ikegami, K. Kinosita, Jr., T. Nishizaka, and S. Ishiwata. 1995. Mechanical measurements of single actomyosin motor force. *Biophys. J.* 68:286s–290s.

Molloy, J. E., J. E. Burns, J. Kendrick-Jones, R. T. Tregear, and D. C. White. 1995. Movement and force produced by a single myosin head. *Nature.* 378:209–212.

Moy, V. T., E. L. Florin, and H. E. Gaub. 1994. Intermolecular forces and energies between ligands and receptors. *Science.* 266:257–259.

Nakajima, H., Y. Kunioka, K. Nakano, K. Shimizu, M. Seto, and T. Ando. 1997. Scanning force microscopy of the interaction events between a single molecule of heavy meromyosin and actin. *Biochem. Biophys. Res. Commun.* 234:178–182.

Nishizaka, T., H. Miyata, H. Yoshikawa, S. Ishiwata, and K. Kinosita, Jr. 1995a. Mechanical properties of single protein motor of muscle studied by optical tweezers. *Biophys. J.* 68:75s.

Nishizaka, T., H. Miyata, H. Yoshikawa, S. Ishiwata, and K. Kinosita, Jr. 1995b. Unbinding force of a single motor molecule of muscle measured using optical tweezers. *Nature.* 377:251–254.

Nishizaka, T., Q. Shi, and M. P. Sheetz. 2000. Position dependent linkages of fibronectin-integrin-cytoskeleton. *Proc. Natl. Acad. Sci. USA.* 97: 692–697.

Nishizaka, T., T. Yagi, Y. Tanaka, and S. Ishiwata. 1993. Right-handed rotation of an actin filament in an in vitro motile system. *Nature.* 361:269–271.

Noji, H., R. Yasuda, M. Yoshida, and K. Kinosita, Jr. 1997. Direct observation of the rotation of F_1-ATPase. *Nature.* 386:299–302.

Rayment, I., H. M. Holden, M. Whittaker, C. B. Yohn, M. Lorenz, K. C. Holmes, and R. A. Milligan. 1993a. Structure of the actin-myosin complex and its implications for muscle contraction. *Science.* 261: 58–65.

Rayment, I., W. R. Rypniewski, K. Schmidt-Base, R. Smith, D. R. Tomchick, M. M. Benning, D. A. Winkelmann, G. Wesenberg, and H. M. Holden. 1993b. Three-dimensional structure of myosin subfragment-1: a molecular motor. *Science.* 261:50–58.

Sase, I., H. Miyata, J. E. Corrie, J. S. Craik, and K. Kinosita, Jr. 1995a. Real time imaging of single fluorophores on moving actin with an epifluorescence microscope. *Biophys. J.* 69:323–328.

Sase, I., H. Miyata, S. Ishiwata, and K. Kinosita, Jr. 1997. Axial rotation of sliding actin filaments revealed by single- fluorophore imaging. *Proc. Natl. Acad. Sci. USA.* 94:5646–5650.

Sase, I., T. Okinaga, M. Hoshi, G. W. Feigenson, and K. Kinosita, Jr. 1995b. Regulatory mechanisms of the acrosome reaction revealed by multiview microscopy of single starfish sperm. *J. Cell Biol.* 131: 963–973.

Sellers, J. R., and B. Kachar. 1990. Polarity and velocity of sliding filaments: control of direction by actin and of speed by myosin. *Science.* 249:406–408.

Suzuki, N., H. Miyata, S. Ishiwata, and K. Kinosita, Jr. 1996. Preparation of bead-tailed actin filaments: estimation of the torque produced by the sliding force in an in vitro motility assay. *Biophys. J.* 70:401–408.

Svoboda, K., C. F. Schmidt, B. J. Schnapp, and S. M. Block. 1993. Direct observation of kinesin stepping by optical trapping interferometry. *Nature.* 365:721–727.

Taylor, K. A., H. Schmitz, M. C. Reedy, Y. E. Goldman, C. Franzini-Armstrong, H. Sasaki, R. T. Tregear, K. Poole, C. Lucaveche, R. J. Edwards, L. F. Chen, H. Winkler, and M. K. Reedy. 1999. Tomographic 3D reconstruction of quick-frozen, Ca^{2+}-activated contracting insect flight muscle. *Cell.* 99:421–431.

Toyoshima, Y. Y., S. J. Kron, E. M. McNally, K. R. Niebling, C. Toyoshima, and J. A. Spudich. 1987. Myosin subfragment-1 is sufficient to move actin filaments in vitro. *Nature.* 328:536–539.

Toyoshima, Y. Y., C. Toyoshima, and J. A. Spudich. 1989. Bidirectional movement of actin filaments along tracks of myosin heads. *Nature.* 341:154–156.

Tsuda, Y., H. Yasutake, A. Ishijima, and T. Yanagida. 1996. Torsional rigidity of single actin filaments and actin-actin bond breaking force under torsion measured directly by in vitro micromanipulation. *Proc. Natl. Acad. Sci. USA.* 93:12937–12942.

Vale, R. D., T. Funatsu, D. W. Pierce, L. Romberg, Y. Harada, and T. Yanagida. 1996. Direct observation of single kinesin molecules moving along microtubules. *Nature.* 380:451–453.

Yamada, A., N. Ishii, and K. Takahashi. 1990. Direction and speed of actin filaments moving along thick filaments isolated from molluscan smooth muscle. *J. Biochem.* 108:341–343.

Yanagida, T., M. Nakase, K. Nishiyama, and F. Oosawa. 1984. Direct observation of motion of single F-actin filaments in the presence of myosin. *Nature.* 307:58–60.

Yasuda, R., H. Noji, K. Kinosita, Jr., and M. Yoshida. 1998. F_1-ATPase is a highly efficient molecular motor that rotates with discrete 120° steps. *Cell.* 93:1117–1124.

解 説　特集・生体の運動機構とバイオトライボロジー

筋収縮滑り運動機構とトライボロジー

石　渡　信　一
早稲田大学 理工学部物理学科
(〒169-8555　東京都新宿区大久保3丁目4-1)

原稿受付　1999年10月12日
"トライボロジスト" 第45巻 第2号 (2000) 119～125

1. はじめに

われわれの体の中で，筋肉ほど身近な生体組織(臓器)は他にない．何しろ手で触ることができる．しかも指圧をして思いきり押したり，ゴリゴリと揉みほぐしたりすることさえできる．そんなことをしても筋肉としての収縮機能は損なわれないし，むしろ硬さがほぐれて気分がよくなりさえする．思えば不思議な臓器である．手指の先でその硬さや状態を感知することができるこの臓器が，分子モータと呼ばれる数十ナノメートル (nm) の大きさのタンパク質が無数に集まったタンパク質集合体であることを思うと，さらにその不思議さは倍加する (サイコロ程度の大きさの筋肉片には，1兆の，そのまた1兆倍個，つまりアボガドロ数個もの分子モータが詰まっている！)．

筋肉，特に骨格筋は非常に細長い細胞で，長軸方向に張力を発生して収縮する (図1の階層構造参照)．われわれの手足を動かす骨格筋の場合，単位断面積 (1 cm²) あたりに発生する最大収縮力は数kg重，数十ニュートン (N) となる．この事実と，筋肉の微細構造から求めたミオシン分子モータの数密度から，分子モータ1個が発生する平均の力を数ピコニュートン (pN) と見積もることができる．最近の1分子顕微鏡計測でもほぼ同じ値が得られている[1,2]．

筋収縮は2種類の筋フィラメント，すなわちミオシン分子の繊維状重合体である太いフィラメントと，アクチン分子の繊維状重合体である細いフィラメントが，互いに"滑り合う"ことによって生じる (滑り運動機構)．この"滑り運動機構"は，1954年に2人のハックスレー (A. F. HUXLEY と H. E. HUXLEY) とその共同研究者達によってNature誌上に並んで発表された．

ところでトライボロジストがもし筋収縮運動の

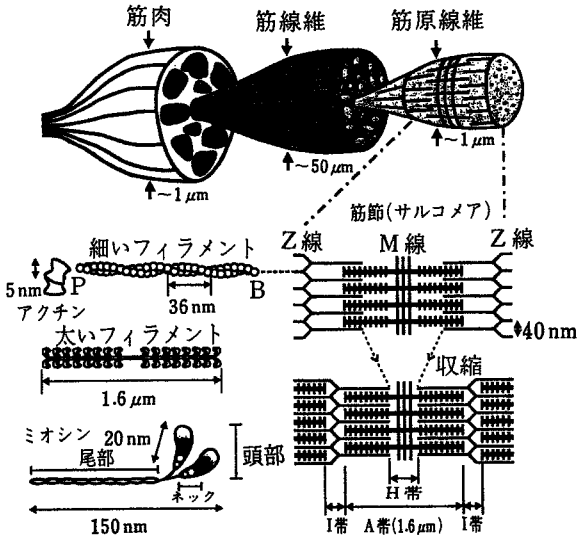

図1　筋線維，筋原線維から単一アクトミオシン分子モータに至る横紋筋収縮系の階層構造 (このような階層性は，横紋筋である骨格筋，心筋に共通のものである．横紋構造をもつ筋収縮系の最小構造単位は，筋節 (サルコメア) と呼ばれる．筋節は，ミオシン分子の繊維状重合体である太いフィラメントと，アクチン分子がらせん状に重合した細いフィラメントが，スメクチック液晶のように整然と配列した格子構造からなっている．ミオシン分子は，アクチンとの結合部位とATP結合部位を含む"頭部"と"尾部"，そして頭部と尾部をつなぐ"首部 (ネック)"からなる)　〔出典：文献1)〕

Sliding Mechanism of Muscle Contraction and Tribology

By Shin'ichi ISHIWATA, Department of Physics, School of Science and Engineering, Waseda University (4-1, Okubo 3-chōme, Shinjuku-ku, Tokyo 169-8555, *E-mail*: ishiwata@mn.waseda.ac.jp)

Key Words: *sliding mechanism, molecular friction, muscle contraction, actomyosin interaction, cross-bridge cycle, tribology, SPOC*

仕組みに関心を寄せるとすれば，その理由の第一は“滑り運動”と呼ばれていることにあるのではないか，と推測する．タンパク質繊維が互いに滑り合うという．そうであるならば，そこには摩擦があるはずだ．しかし，筋収縮機構の研究において“分子摩擦”という概念が登場し，滑り運動機構における生理的な意義が認められるようになったのはごく最近のことである（本号特集掲載：太和田らの解説参照）．

“滑り運動”と名づけられた理由は，筋収縮研究の歴史にある．“滑り運動機構”が実験的な証拠を得た当時，筋収縮は筋タンパク質分子が折りたたまれることによって生じる，とする説が強かった．それに対して，筋収縮は2種類の筋フィラメントがその長さを変えることなく（タンパク質の折りたたみではなく），互いに位置をずらすことによって生じる，という意味で“滑る”と表現したのである．“滑り運動機構”が広く受け入れられるようになるまでには紆余曲折があったが，現在ではこの機構自体に意義を申し立てる研究者はいない．滑り運動機構が認められるようになって以来，この分野では，滑り運動をもたらす“分子機構”の研究に重心が移った．そして50年近い研究の歴史を積み重ね，やっと一つの解答が得られようとしている[1,2]．

（1）アクチンとミオシン頭部の立体構造が，それぞれ1990年と1993年にX線結晶構造解析によって解明されたこと，（2）1分子解析・操作のための顕微鏡法が開発され，モータ1分子の素機能，素過程が解明されつつあること，そして（3）遺伝子解析により，ミオシン分子モータファミリーには15種類もの多くの分子モータが存在し，その運動特性に想像以上の多様性が見出されつつあることなどから，滑り運動機構が文字通り分子レベルで明らかにされつつある．この数年間に，いくつもの驚くべき発見があり，見事な実験が行なわれた．たとえば，この原稿を書いている最中にも，これまで知られていたすべてのミオシン分子モータとは逆向き（P端の向き）に滑り運動をするミオシン分子モータ（myosin VI型；筋収縮系のミオシンはmyosin II型）が発見されたとの報告が，Nature誌上に掲載された[3]．

この小論では，筆者の注目する“滑り運動”機構に関する最近の知見を述べ，さらに筆者の研究室で得られた研究成果を紹介することを通して，筋収縮滑り運動の分子機構の一側面について述べることにしよう．

2. クロスブリッジサイクルと滑り運動機構

まず，アクトミオシン分子モータによるATP（アデノシン3リン酸）加水分解反応のスキームと，各反応ステップにおけるミオシン分子モータ（頭部とネック領域）の構造を模式的に示したのが図2である[4,5]．この図はクロスブリッジサイクルとも呼ばれる．クロスブリッジとは，図1に見られるように，細いフィラメントと太いフィラメントを“架橋”するミオシン頭部を指す．クロスブリッジサイクルの詳細は，ATP加水分解反応と力発生の素過程を結びつけようとする試みの中から，繰り返し繰り返し実験的に検証されてきたものである．特に力発生の分子機構としてミオシン分子の“首振り運動”（クロスブリッジが角度を変える運動）を捉える目的で，スピンラベルや蛍光ラベルをミオシン頭部の先端部あるいはネック領域に導入し，ラベルの向きが“滑り運動”あるいは力発生に伴って変化するか否かが調べられた．

このようなアプローチの一つの集大成が，最近米英の共同研究チームによって報告された[5]．このグループは，分子構造から予測されたミオシンネックの角度変化（Lever-arm-model）を検証することに精力を注いだ．ミオシンネックの角度が変化することを示すためには，適当な部位に選択的に蛍光ラベルを導入したい．ところがこれまでの研究では，導入したラベルがタンパク質に対してブラウン運動する自由度があったために，ラベルの向きはタンパク質の向きを正確には反映していなかった．そこで彼らはタンパク質表面の2箇所に結合する2架橋性蛍光色素を合成した．そして，ネック領域に結合しているミオシン軽鎖LC2（図1のミオシン頭部に記した二つの丸印のうちの下の丸印）の適当な2箇所をシステイン残基で置換し，この色素をラベルした．もちろん，

このラベルを導入することによって分子モータとしての機能が損なわれないことを確認した．こうして，再構成された筋線維が力を発生する際に，蛍光色素の向きがどのように変化するかを時間分解計測した．得られた結果を解釈したものが図2の模式図にまとめられている．注目すべき点は，力発生のステップにおいて，ネック領域の向きが，アクチンフィラメントの長軸に対して鈍角から直角へ，そして鋭角へと変化することを示したことである．このことは，Lever-arm-modelを支持する．

ミオシン頭部の分子変形は，結晶構造解析やX線溶液散乱，それに電子顕微鏡解析などによっても捉えられている[1]．しかも，上記のミオシンVI型の場合には，ネックが逆側に折れ曲がっている電子顕微鏡像が得られている[3]．ところで，力発生との時間的な関係が明らかになっているのは，上で紹介した筋線維を用いた蛍光（あるいはスピン）ラベル法による研究のみである．しかし筋線維を用いる実験には，得られる蛍光色素の配向度が多数分子の平均値であるためか，期待値に比べて角度変化が小さいという弱点がある．今後期待されるのは，蛍光顕微鏡による1分子解析であろう．1分子レベルで，力発生のタイミングと分子の向きとの関係が明らかになれば，何が原因で，何が副産物であるかがよりいっそう明確になるだろう．

以上の成果をまとめたモデル（図2）によれば，一つのクロスブリッジサイクルは，(1)解離したミオシン頭部（M）内でのATP分子のADP（アデノシン2リン酸）と無機リン酸（Pi）への加水分解（MADPPi）と，その後のミオシン頭部のアクチン（A）への結合（AMADPPi複合体；結合が弱いために，ネック領域が揺らいでいる），(2)PiやADPの解離に伴うミオシン・アクチン強結合の形成と，ミオシンネック領域の変形による数pNの力発生，そして10 nmの滑り運動（AMADPからAMへの転移），(3)ATP分子の再結合によるミオシン頭部のアクチンフィラメントからの解離（ミオシン頭部のブラウン運動；A+MATP），そしてこの過程が再び(1)に戻る，というものである．1回の化学サイクル

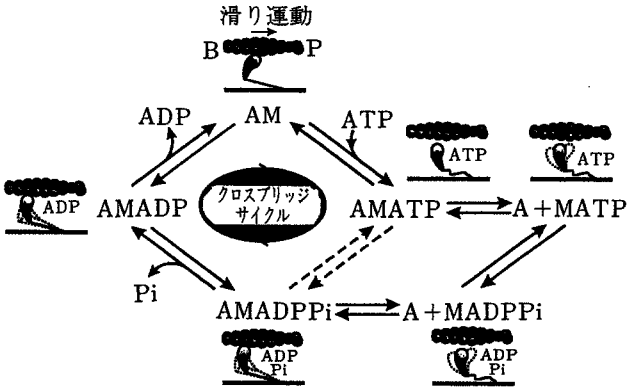

図2　アクトミオシン分子モータのATPaseサイクルと分子間結合様式の模式図（クロスブリッジサイクル）（ミオシンネックに結合しているLC2と呼ばれるミオシン軽鎖に蛍光色素をラベルし，その向きを時分割計測することによって，各状態におけるアクチンフィラメントに対するミオシンネックの傾きが求められる[4,5]）

（ATP加水分解）に伴って1回の力学過程（力発生と滑り運動）が生じる．

ところがこのような研究成果がある一方で，化学サイクルと力学過程とが必ずしも1：1に対応していないことを示す実験結果も存在する[2,6]．まず，ATPがミオシンから遊離するタイミングと，力発生のタイミングとを1分子解析した結果，力発生はATP（ADP）が解離した後に生じることがあるという[6]．これは，図2で示したものと相矛盾する．また，図2で示されたような機構であるならば，1個のATPが加水分解することによる“滑り運動の大きさ”は高々ミオシン頭部の大きさ，あるいはネックの長さ程度のはずである．ところが，1個のATPが加水分解される間にミオシン頭部の大きさの何倍も滑り運動することを示唆する実験結果が報告されている[2]．しかもその滑り運動の間には，アクチン分子の大きさ（約5 nm）に等しいステップを何歩もつづけて踏むという[7]．力学素過程は何か，が問われている．

また，遺伝子組換え技術を用いてミオシンネックの長さを数倍に変えたところ，滑り速度がネックの長さに比例して数倍になった，という実験結果が存在する（これは図2のモデルを支持する[1]）．その一方で，ネックの長さに応じてATP分解速度が上昇する，それが滑り速度が上昇した理由であるとする報告もある（図2のモデルを否

定するものではないが，残念ながらこの手の実験が図2のモデルの決定的証拠にならないことを示唆している)．未だにこのようなどんでん返しの実験結果が報告されている状態である．図2のモデルだけでは，滑り運動分子機構の全貌を説明しきれないのかもしれない．アイデアの飛躍と，決定的実験が求められる所以である．

ところでミオシン分子は，ATPが結合するとアクチンから直ちに解離する．したがってミオシン分子モータは1分子だけでは長距離に渡ってアクチンフィラメントの上を“滑る”ことができない．それに対して，キネシンと呼ばれる分子モータは微小管から容易に解離せず，解離しないままに何回もATP加水分解サイクルをまわる．この性質により，キネシン分子は微小管上を，単頭-双頭結合を交互に繰り返しつつ“歩く”．1分子で機能し，神経細胞の末端に向かって1分子で小胞を運ぶことができる．ミオシン分子はアクチンフィラメント上で“ジャンプする”[8]．しかし，三段跳びのように右・左と交互に単頭結合を繰り返すのか，途中でケンケンのように同じ頭部で結合するのか，などのジャンプの仕方はまったくわかっていない．ただ，単頭ミオシンに比べて双頭ミオシンの方が滑り速度が大きいので，二つの頭部間に何らかの協同性が働いている可能性はある．いずれにしても，筋フィラメントを滑らかに動かすためにはミオシン分子は多数個で機能せざるをえない．このことは筋肉に限らず，II型のミオシン分子モータが働いているすべての細胞運動系に共通する性質である．

3．1分子モータの機能解析

ここで，必ずしも“滑り運動分子機構”に直結するものではないが，1分子レベルでの機能解析を目指すわれわれの研究を紹介しよう[9~12]．われわれは，アクチン・ミオシン間の結合（破断）力や結合寿命を光学顕微鏡下で1分子計測している．その計測法の模式図[9,10]と計測結果の一部[12]を図3に示す．アクチンフィラメントのB端（滑り運動の後ろ端）に結合したプラスチックビーズをレーザ光ピンセットで捕捉する．次に光ピンセットの捕捉中心をB端方向に一定速度で移動することによって，一定の上昇速度で負荷を加える．こうして得られたアクチン・ミオシン硬直結合の破断力分布は，二つのピークからなっていた．負荷上昇速度が小さいときには〔図3(a)〕，それぞれのピークの平均破断力は，約7 pNと15 pNであった．負荷上昇速度が大きくなると〔図3(b)〕，それぞれ約9 pNと18 pNとなり，しかもピークの大きさの比が変化した．このように，負荷の上昇速度が大きいほど，破断力分布は破断力の大きい側に移動した．一般に負荷を加えるとタンパク質間結合の寿命は短くなるが，負荷の上昇速度が大きいほど結合寿命の間に加わる負荷が大きくなる．その結果破断力は大きくなることが，単純なタンパク質間結合について原子間力顕微鏡(AFM)を用いて示されている[13]．この性質は，アクチン・ミオシン硬直結合の場合にもみられたことになる．

ところが，ミオシン分子は2個の頭部をもち，それぞれアクチン分子とほぼ等価に結合しうるという特徴をもつ．この特徴が，破断力ヒストグラムに現われている．まず二つのピークは，それぞれミオシン単頭と双頭の結合破断に対応している．しかも，この二つのピークの大きさの比が負荷上昇速度に依存するということは，ミオシン分子の硬直結合が，単頭結合と双頭結合との間を行き来する平衡関係にあることを示唆する．無負荷の条件下ではこの平衡は双頭結合側に大きく片寄っている．ところが，負荷が加わっている間に双頭結合から単頭結合への変換が生じ，したがって単頭破断の頻度が増すものと推測される．

図2に示したクロスブリッジサイクルの中では，数mMのATPが存在するために硬直結合(AM)の寿命は非常に短い．しかし，硬直結合に関する上記の性質は，クロスブリッジサイクル中の他の分子種にも共通するものであろう．つまり，結合破断の負荷依存性とその速度論は，多数のミオシン分子が集団として一斉に滑り運動する際に重要な意味をもつであろう．

そもそもタンパク質間結合は，熱平衡状態では結合と解離の間を行き来している．そこで分子間結合定数Kは，結合の速度定数k_+と解離定数k_-の比k_+/k_-で与えられ，k_-の逆数がタンパク質

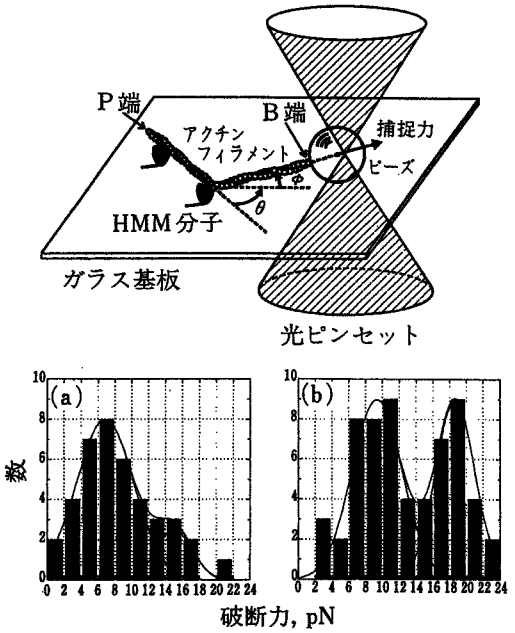

図3　アクチン・ミオシン分子間結合力（破断力）の1分子計測法〔上図：分子間結合力を計測するための模式図[9~11]．アクチンフィラメントのB端（滑り運動の後ろ端）を，B端キャップタンパク質であるゲルゾリンを介して直径1 μmのプラスチックビーズに固定し，ビーズをレーザ光ピンセットによって捕捉・操作する．一方ミオシン分子（実験では，双頭構造を保ち尾部を欠損したミオシンII型の酵素活性断片HMM分子を使用）は，長さ1 μmのアクチンフィラメントあたり約1個の線密度で，ガラス表面にまばらに吸着させてある。レーザ光を集束した光ピンセットによって一方のビーズを捕捉し，ガラス基板あるいは光ピンセットの捕捉中心を，ガラス基板に平行に，一方向に一定速度で動かすことにより，分子間結合に一定速度で負荷を加え続ける．また，変性ミオシンを表面に吸着したビーズを調製し，それをP端側に結合することによって，アクチンフィラメントのP端方向に負荷を加えることもできる．同じミオシン分子について何度でも，様々な角度θで結合･破断を繰り返すことができる．角度ϕは，アクチンフィラメントとガラス基板のなす角度で，10度程度である．ある大きさの負荷で分子間結合が破断すると，ビーズは再び光ピンセットの捕捉中心の位置にもどる．破断する際のビーズの位置（重心）と捕捉中心との距離を求めることによって，破断力を見積もることができる．下図：ATP非存在下で形成されるアクチン･ミオシン（HMM）硬直結合の破断力のヒストグラム[12]．負荷はB端の方向に加えられた．平均約7 pNのピークと，その倍の大きさのピークからなる．（a）と（b）の違いは，負荷上昇速度だけである（a）：5 pN/s，（b）：36 pN/s〕

間結合の平均寿命に相当する．たとえば無負荷のアクチン・ミオシン硬直結合の場合には約1 000秒である．アクチン・ミオシン硬直結合の寿命とその負荷依存性を，顕微鏡下で1分子解析した結果，結合寿命τと負荷Fとの間に

$$\tau=\tau_0\exp(-Fd/k_BT)$$

の関係が成り立つことがわかった[9,11]．ここでτ_0は無負荷時の結合寿命（双頭構造をもつHMM分子の場合には約1 000秒，1個の頭部に相当するS1分子の場合には約100秒），dはタンパク質分子間の相互作用距離，k_Bはボルツマン定数，Tは絶対温度である．

ここで，硬直結合のdの値は約3 nmと見積もられた．この値は分子間結合ポテンシャルの有効距離にしては1桁大きい．dを求める1分子計測は，アビジン-ビオチンなどの単純なタンパク質について主にAFMを用いて研究されているが，1桁小さな値が報告されている．そこでわれわれは，dが大きいことはモータ分子の特徴ではないかと想像する．ミオシン・アクチン間結合部位には多くの分子間力が関与している．そのすべてが一度に外れるのであれば，相互作用距離は1桁小さくなるであろう．しかしミオシン・アクチン間結合の場合には片側から徐々に外れるので，見掛け上dの値が大きくなるのではないか．逆にいえば，破断が徐々に生じるような方向に負荷が加えられたのだ，ということもできる．ところで負荷と滑り力とは，方向が同じで向きが逆，という関係にある．そうであるならば，滑り力発生時のミオシン分子のアクチンへの結合は，分子間結合の数を徐々に増すように，破断の過程と逆の過程をたどるのではないか．化学エネルギー源であるATPが存在しない場合でも，ミオシン・アクチン結合それ自体にこのような性質が備わっている．ATPは分子モータに備わったこの性質を制御するという役割を担っているのかもしれない[9]．このような分子間結合と分子間解離の性質こそ，分子モータの運動性に直結するものではないか，とわれわれは期待している．

4．分子モータ集団の運動特性

図1にみるように，筋収縮系の最小単位である(半)筋節では，多くのミオシン分子が直列，並列に連結して働いている．もしミオシンがキネシン

のような“歩く”分子モータであったなら，多くのモータは互いに運動を妨げあい，がちがちに動かなくなるのではなかろうか．つまり，動くタイミングがよほど揃っていない限り，あるモータがフィラメントの上を進もうとすると，別のモータはまだ力発生の状態に移行していなかったり，あるいは力を出し終わった状態で結合しているだろう．このような状態にある分子モータは“分子摩擦”の原因となる．その結果，多数のモータはまったく無駄な内部仕事をすることになり，ATP の加水分解エネルギーはひたすら熱発生に費やされることになるだろう．骨格筋ミオシン (II 型) の場合には，ATP 加水分解の 1 サイクルに占める，力発生状態にある分子種 (図 2 の AMADP 複合体など) の寿命の割合は，10 %程度と小さいことが知られている．一方，単に結合しているだけの弱結合状態 (図 2 で，AMADPPi 複合体など) も存在するが，いずれにしても多数個の分子モータが働くには都合が良い，“走るモータ”という特徴を備えている．

筋収縮滑り運動機構においては，多数分子が並列に相互作用することによる分子摩擦が存在する．では分子摩擦の筋生理における意味は何か．第一に，分子摩擦に伴う熱発生は，温血動物にとって体温の維持に役立っている．収縮特性に関しては，力を発生している状態にある分子モータと，単に結合しているだけで滑り運動の抵抗となっている分子モータが共存し，(収縮力) — (摩擦力) によって (最大の滑り運動速度) が決まる．さらに，分子摩擦の原因となるであろうミオシン・アクチン結合状態 (たとえば AM 結合や AMADP 結合) が，アクチンフィラメントを通じて分子モータ機能の協同性，協調性を生み出しているという証拠がある．分子間協同性・協調性は，自励振動 (SPOC) 現象などの多分子筋収縮系に特徴的な現象において，特に重要な役割を担っていることが期待される[1,14]．今後は，単一分子モータの素機能・素過程の解明とともに，多分子モータ系固有の高次機能の解明が待たれる．

5. おわりに

トライボロジーの視点から生体運動の分子メカニズムにアプローチしようとすると，ミオシン・アクチン結合部位における原子 (団) レベルでのタンパク質間結合の動的特性 (上で述べたような結合寿命の負荷依存性や，さらに一歩進んで，アミノ酸残基間の分子間結合ポテンシャルの特性など) を取り込む必要があるだろう．そのうえで，多分子運動系の運動特性・運動機構をトライボロジーの視点から捉え，生体運動の分子機構にとって新たな視点が与えられることを期待したい．

文 献

1) 石渡信一編：生体分子モーターの仕組み，シリーズ・ニューバイオフィジックス 4，共立出版 (1997) pp. 214.
2) 柳田敏雄・石渡信一編：ナノピコスペースのイメージング—生物分子モーターのメカニズムを見る—，シリーズ・生物物理から見た生命像 3，吉岡書店 (1997) pp. 164.
3) A. L. WELLS et al.: Myosin VI Is an Actin-based Motor that Moves Backwards, Nature, **401** (1999) 505.
4) Y. E. GOLDMAN: Wag the Tail: Structural Dynamics of Actomyosin, Cell, **93** (1998) 1.
5) J. E. T. CORRIE, B. D. BRANDMEIER, R. E. FERGUSON, D. R. TRENTHAM, J. KENDRICK-JONES, S. C. HOPKINS, U. A. van der HEIDE, Y. E. GOLDMAN, C. SABIDO-DAVID, R. E. DALE, S. CRIDDLE & M. IRVING: Dynamic Measurement of Myosin Light-chain-domain Tilt and Twist in Muscle Contraction, Nature, **400** (1999) 425.
6) A. ISHIJIMA, H. KOJIMA, T. FUNATSU, M. TOKUNAGA, H. HIGUCHI, H. TANAKA & T. YANAGIDA: Simultaneous Observation of Individual ATPase and Mechanical Events by a Single Myosin Molecule during Interaction with Actin, Cell, **92** (1998) 161.
7) K. KITAMURA, M. TOKUNAGA, A. HIKIKOSHI-IWANE & T. YANAGIDA: A Single Myosin Head Moves along an Actin Filament with Regular Steps of~5.3 nm, Nature, **397** (1999) 129.
8) K. KINOSITA Jr., R. YASUDA, H. NOJI, S. ISHIWATA & M. YOSHIDA: F 1-ATPase: A Rotary Motor Made of a Single Molecule, Cell, **93** (1998) 21.
9) T. NISHIZAKA, H. YOSHIKAWA, H. MIYATA, S. ISHIWATA & K. KINOSITA Jr.: Unbinding Force of a Single Motor Molecule of Muscle Measured Using Optical Tweezers, Nature, **377** (1995) 251.
10) 西坂崇之・石渡信一：分子モーターの力学・機能特性を見る，生物物理，**36** (1996) 15.
11) 西坂崇之：アクトミオシン分子モーターの機能と力学特性の一分子顕微解析，早稲田大学理工学部博士論文 (1996) pp. 160.
12) 熊木雄一：アクトミオシン硬直結合の 1 分子顕微解析，早稲田大学理工学部修士論文 (1999).
13) R. MERKEL, P. NASSOY, A. LEUNG, K. RITCHIE & E. EVANS: Energy Landscapes of Receptor-ligand Explored with Dynamic Force Spectroscopy, Nature,

397 (1999) 50.
14) 石渡信一：生体系材料の分子シンクロナイゼーション，ポリファイル，**34** (1997) 25.

著者プロフィール

石渡　信一

1945年生まれ．東京大学理学部物理学科卒業．名古屋大学理学系大学院修了．理学博士．現在，早稲田大学理工学部物理学科教授．専門は，生物物理学．生体分子モーターの1分子・多分子機能解析，筋収縮系の構造と機能の再構築，自励振動(SPOC)現象のメカニズム解析，1分子から分子集合体，そして細胞とその集団の機能構築を目指す．日本生物物理学会，日本物理学会などに所属．

解　説

生体分子モーター系における分子シンクロナイゼーションの研究

Investigation of molecular synchronization in the assembly of molecular motors

超分子システム内における分子シンクロナイゼーション現象として、筋肉が短縮と伸張を繰り返す自励振動現象に着目し、人工的に細いフィラメントを再構築した生体分子モーター系を用いてその分子機構に迫る。

藤田英明
早稲田大学理工学部　佐々木大輔
石渡信一

はじめに

筋収縮は、アクチン分子が重合したアクチンフィラメントに制御タンパク質が結合した細いフィラメントと、主にミオシン分子が重合した太いフィラメントとの相互滑り運動によって起きる。筋肉は一般的に、生理的条件下で収縮か弛緩かの2状態をとる。即ち、筋小胞体からμM以上のCa^{2+}が放出されると制御タンパク質にCa^{2+}が結合し、細いフィラメントはOFF状態からON状態へと遷移する。ところが、除膜した心筋や骨格筋遅筋では、収縮・弛緩の中間濃度(μM程度)のCa^{2+}存在下で、自発的振動状態をとることが知られていた。筆者らは約10年前、Ca^{2+}非存在下であるにもかかわらず、ATPとADPに無機リン酸(Pi)が共存すると振動状態になることを、骨格筋速筋の筋(原)線維、および心筋筋線維で見いだし、この現象をSPontaneous Oscillatory Contraction (SPOC)と名付けた。SPOC現象の化学的性質と力学的性質についてはこの10年間で随分研究されたが、SPOC現象の分子メカニズムについてはいまだに明らかになっていない。そこで、細いフィラメントを人工的に再構成した心筋収縮系を用いてSPOC現象における制御タンパク質の役割を検討した。

1．筋収縮・制御のメカニズム

筋肉の収縮は、太いフィラメントと細いフィラメントが長さを変えずに、相互に滑り合うことによって生じる[1),2)](図1)。筋肉が力を発生するのはミオシン分子とアクチンフィラメントの相互作用によるものであるが、ミオシン分子が力を発生する分子的機構はいまだに解明されていない。ミオシンはATPを加水分解

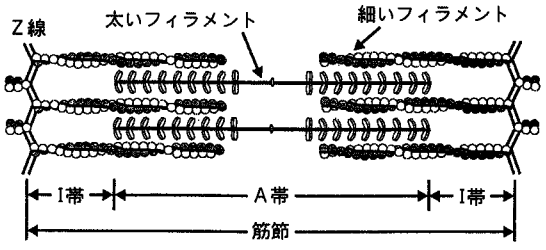

図1　横紋筋収縮系の模式図

筆者紹介：ふじた・ひであき(FUJITA, Hideaki)　早稲田大学理工学部(School of Science and Engineering, Waseda University)助手　1999年早稲田大学大学院理工学研究科博士課程修了　理学博士　専門：生物物理学　連絡先：〒169-8555 東京都新宿区大久保3-4-1　E-mail　fujitah@mn.waseda.ac.jp(勤務先)
ささき・だいすけ(SASAKI, Daisuke)　早稲田大学大学院理工学研究科(Graduate School of Science and Engineering, Waseda University)修士1年　専門：生物物理　連絡先：同　上　E-mail　6991 0513@mn.waseda.ac.jp(在学先)
いしわた・しんいち(ISHIWATA, Shin'ichi)　早稲田大学理工学部(School of Science and Engineering, Waseda University)物理学科教授　1974年名古屋大学大学院理学研究科博士課程単位取得満期退学　理学博士　専門：生物物理学　連絡先：同　上　E-mail　ishiwata@mn.waseda.ac.jp(勤務先)
キーワード：生体分子モーター、分子シンクロナイゼーション、心筋、SPOC、アクチンフィラメント再構成筋

するときに発生する化学エネルギーを仕事に変える分子モーターである。ミオシン単独でのATPase速度は遅いが、アクチンフィラメントと相互作用すると100倍程度加速される。また、力発生はPi放出とそれに続く段階で行われると考えられている。

筋収縮は細胞内Ca^{2+}濃度によって制御される[3]。神経からの信号が筋細胞膜からT管膜を通して内部膜系の筋小胞体に達すると、Ca^{2+}が筋小胞体から放出される。このCa^{2+}が制御タンパク質上のCa^{2+}結合部位に結合すると抑制が外れ、アクチンとミオシンが相互作用して筋肉は収縮する。遊離のCa^{2+}濃度がμM程度で最大張力の50％程度の張力を発生し、10μM程度で飽和に達する。

筋肉の活性化はCa^{2+}だけでなく、アクチンフィラメントに強く結合した(強結合状態)ミオシン頭部によっても生じることが知られている。BremelとWeberは1972年[4]、ATP濃度を下げることにより生成した硬直結合のクロスブリッジがアロステリック(遠隔作用的)に細いフィラメントをON状態にし、そこにほかのミオシン頭部が相互作用できるという制御機構を提唱した。また、硬直結合のクロスブリッジはCa^{2+}感受性を高めることがBrandtらによって示された[5]。一方、ADPが筋肉を活性化し、骨格筋[6,7]と心筋[8]においてCa^{2+}で活性化したときとほぼ同レベルの張力を発生することが分かった。このADPによる活性化もADPを結合した強結合クロスブリッジによるものと考えることができる[7,8]。

2．自励振動現象

通常の筋収縮系はCa^{2+}濃度によって収縮と弛緩の2状態をとるが、昆虫の飛翔筋などでは骨格や組織の弾性を巧みに利用しながら、筋肉自体は常にON状態のまま高速振動を繰り返す。一方、心臓の筋肉も振動を繰り返すが、これは神経系や特殊な細胞の指令によって周期的にCa^{2+}濃度を上げ下げして収縮と弛緩を繰り返させているものである。

弛緩状態(+ATP、$-Ca^{2+}$)にある筋収縮系(細胞膜がない収縮装置だけからなるモデル筋系)にADPを加えていくと張力が発生する(ADP収縮)。SPOC現象はこのADP収縮中の筋収縮系にPiを加えたときに生じる[9]。SPOCの溶液条件は弛緩と収縮の中間条件であり、筋収縮系の第三の状態と考えることができる。SPOC中の筋原線維を観察すると各筋節が遅い収縮と素早い伸長を繰り返し、鋸歯状の波形で振動していることが分かる(図2)。この振動の周期は数秒から20秒程度で、振幅は筋節長の15％程度にも及ぶ。また、ある筋節の振動が隣の筋節へとつぎつぎに伝搬する様子も観察される。さらに、加わる負荷を一定に保つと、筋節長振動が同調する[10]。一方、SPOC中の心筋線維の発生張力は、数秒～20秒程度の周期で振動した。この振動現象は新鮮な溶液が供給されていれば15分以上も安定に続くことからも、この現象が第三の生理状態であることが示唆される。

生理的環境ではATPの加水分解で生じたADPは、ATP再生系によって即座にATPに変換されるため、通常の状態でADP濃度がSPOC条件に達する事は考えにくい。しかし、心筋におけるSPOC条件は骨格筋と比較して低ADP濃度で起きることが分かっており、疲労時や虚血時にSPOC条件を満たす可能性がある。よって、振動そのものが生理的機能である心筋において、SPOCが生理的意味を持つ可能性は大

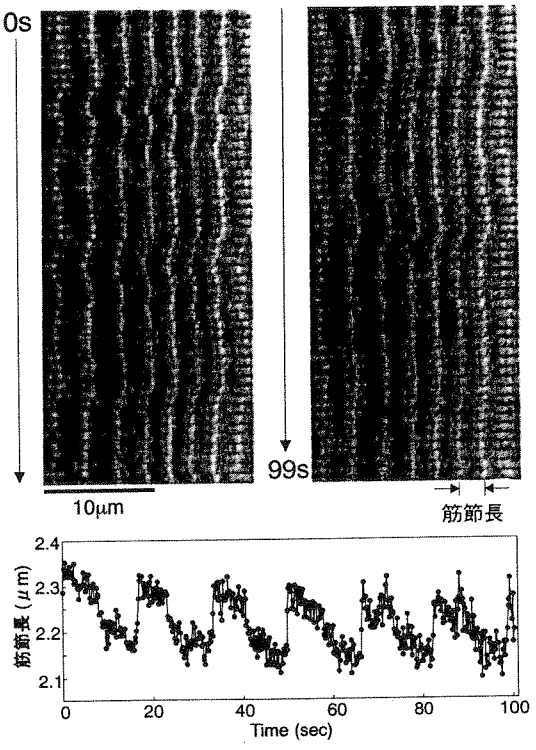

図2　SPOC条件下での心筋筋原線維のレーザー共焦点蛍光顕微鏡像と筋節長変化
上：SPOC中の心筋筋原線維の1秒おきの蛍光連続写真。細いフィラメントを蛍光色素で染色してある。
下：上図矢印部分の筋節長の時間変化を測定した。

きい。SPOCの分子メカニズムはいまだに十分には理解されていないが、コンピューターシミュレーションなどの結果から、AMADPPiのミオシン頭部とAMADPの頭部が、それぞれある一定以上の割合で存在していることが必要だと推測される。

また、JülicherとProst[11]は、多数の分子モーターが弾性要素でつながっているときに、たとえ制御系を考慮に入れなくてもSPOCのような振動が起きることを理論的に示した。光ピンセット法などを用いて分子モーター1個の特性が明らかになりつつある今、ミオシン分子モーターとアクチンフィラメントとの集合体が示すSPOC現象は、分子シンクロナイゼーション(分子間相互作用の協調性)を研究する系として非常に興味深いものである。

3．細いフィラメントの選択的解体と再構築

横紋筋の整った液晶構造がいかにして構築・維持されているのかについては不明な部分も多い。最近、筆者らは骨格筋と心筋において、細いフィラメントの選択的解体・再構築を行い、この問題の分子メカニズムを明らかにした[12),13)]。解体・再構築手法は、筋肉を構成する特定のタンパク質の機能を調べる手段としても有用である。

まず、除膜筋にアクチンフィラメント切断タンパク質であるゲルゾリンを作用させると、細いフィラメントを選択的に除去することができる。細いフィラメントの除去により、筋線維束は張力発生能を失う。この細いフィラメント除去筋に外部から精製したアクチンモノマーを重合条件下で加えることにより、アクチンフィラメントが再構築された。このとき自発的な核形成をできるだけ抑えるために、アクチン重合溶液は7分おきに新しいものと交換し、0℃に保つようにした。このことによって、Z線に残ったアクチンフィラメントの断片を重合核として働かせることができた。このアクチンフィラメント再構成筋は、制御タンパク質が存在しないため、Ca^{2+}濃度に依存せずに張力を発生した。したがって、弛緩はアクトミオシン相互作用の阻害剤である2,3-butanedione 2-monoxime (BDM)を用いて行った。アクチンフィラメント再構成後の張力は、骨格筋では元の張力の30％程度であったが、心筋では135％にも達した。心筋再構成筋における張力増強効果は、アクチンフィラメントの平均長が伸びたためと考えられる。アクチンフィラメントの解体と再構築は、細いフィラメントを蛍光色素で染色し、レーザー走査型共焦点顕微鏡で観察することによって確認された。また、再構成された細いフィラメントの長さ分布と筋フィラメントの格子内での位置を、電子顕微鏡を用いて確認することができた。さらに、制御タンパク質を含む弛緩溶液にアクチンフィラメント再構成筋を12時間浸すことにより、最大発生張力に影響を与えずにCa^{2+}感受性を回復させることに成功した。

以上の結果から、適切な場所に重合核や鋳型構造体があれば、タンパク質の自己集合能によって筋肉のような高次生体構造が構造的にも機能的にも再構築されることが示された。細いフィラメント再構成心筋収縮系は、遺伝的に改変したアクチンや制御系の高次機能の解明に役立つものと考えられる。さらに、蛍光ラベルやスピンラベルしたタンパク質で細いフィラメントを再構成すれば、収縮－弛緩時のタンパク質の構造変化を捕らえることもできるだろう。

4．制御系なしでのSPOC現象

SPOC現象の化学的・力学的性質や発生張力については明らかになってきたが、SPOCの分子メカニズムについてはいまだに不明な点が多い。そこで、細いフィラメント再構成手法を用いてSPOCにおける制御タンパク質の役割を明らかにしようと試みた[14),15)]。

SPOC現象は弛緩状態にある収縮系がADPで活性化されたときに生じることから、まずアクチンフィラメント再構成筋におけるADPの作用を調べた。アクチンフィラメント再構成筋では制御タンパク質が存在しないために、ATPが存在しさえすればCa^{2+}濃度に依存せずに張力を発生した。そこにADPを加えても張力の上昇は見られず、張力の減少だけが観察された。また、ADP、Pi共存下でもSPOCは見られなかった。しかも、Piを添加しても張力の減少が見られなかった。そこで、さらにBDMの阻害作用を調べてみた。アクチンフィラメント再構成筋でも、BDM添加によって張力が減少したが、コントロール筋線維束よりも減少の程度は小さかった。しかし驚くべきことに、Pi存在下でアクチンフィラメント再構成筋にBDMを加えると、10～20 mMの範囲で張力振動が観察された。振動の周期と振幅は、コントロールの筋線維束(BDMなし)での標準SPOC条件のときとほとんど変わらなかった。SPOCの特徴の一つである筋節長振動を筋線維束中で観察するため、アクチンフィラメントを蛍

光色素で染色し、リアルタイム共焦点顕微鏡で蛍光観察した。10 mM BDM存在下でのSPOC中の筋節集団の大きな動きの周期は約20秒であり、これは張力振動の周期と一致した。一方、筋節長の振動の周期は約3秒程度と短く、筋原線維の標準SPOC状態の筋節長振動の周期と一致した。この結果は、制御系が存在しなくても溶液条件さえ満たせばSPOCが起きることを示している。また、Piが存在しないときはBDM添加によって張力を抑制しても、SPOCは見られなかった。このことは、SPOCにとってPiが必須因子であることを示している。

制御タンパク質が存在しなくても、条件さえ整えばSPOC現象は生じる。このことは、SPOCがアクトミオシン分子モーターに内在する現象であることを示している。一方、分子モーターの一種であるダイニン分子も微小管上で高速微小振動することが知られている[16]。自励振動現象は生体分子モーター系にとって一般的な現象である可能性がある。また分子モーター系に限らず、生体機能の多くの場面で自励振動現象が見られる。振動のメカニズムを分子レベルで、しかも分子集合体が示す分子シンクロナイゼーション(協調)という見方で捕らえることは、生体分子機械の高次機能とその仕組みを理解する上で重要なことである。

○参考文献

1) Huxley, A. F. and Niedergerke, R.: *Nature* (*Lond.*), 173, 971～973 (1954)
2) Huxley, H. E. and Hanson, J.: 同上, 173, 973～976 (1954)
3) Ebashi, S. and Endo, M.: *Prog. Biophys. Mol. Biol.*, 18, 123～183 (1968)
4) Bremel, R. D. and Weber, A.: *Nature* (*New Biol.*), 238, 97～101 (1972)
5) Brandt, P. W., Reuben, J. P. and Grundfest, H.: *J. Gen. Physiol.*, 59, 305～317 (1972)
6) Hoar, P. E., Mahoney, C. W. and Kerrick W. G. L.: *Pflügers Arch.*, 410, 30～36 (1987)
7) Shimizu, H., Fujita, T. and Ishiwata, S.: *Biophys. J.*, 61, 1087～1098 (1992)
8) Fukuda, N., Fujita, H., Fujita, T. and Ishiwata, S.: *Pflügers Arch.*, 433, 1～8 (1996)
9) Okamura, N. and Ishiwata, S.: *J. Muscle Res. Cell Motil.*, 9, 111～119 (1988)
10) Yasuda, K., Shindo, Y. and Ishiwata, S.: *Biophys. J.*, 70, 1823～1829 (1996)
11) Jülicher, F. and Prost, H.: *Phys. Rev. Lett.*, 78, 4510～4513 (1997)
12) Funatsu, T., Anazawa, T. and Ishiwata, S.: *J. Muscle Res. Cell Motil.*, 15, 158～171 (1994)
13) Fujita, H., Yasuda, K., Niitsu, S., Funatsu, T. and Ishiwata, S.: *Biophys. J.*, 71, 2307～2318 (1996)
14) Fujita, H. and Ishiwata, S.: 同上, 75, 1439～1445 (1998)
15) Fujita, H. and Ishiwata, S.: 同上, 77, 1540～1546 (1999)
16) Kamimura, S. and Kamiya, R.: *Nature* (*Lond.*) 340, 476～478 (1989)

Nucleotide-Dependent Single- to Double-Headed Binding of Kinesin

Kenji Kawaguchi[1] and Shin'ichi Ishiwata[1,2,3,4]*

The motility of kinesin motors is explained by a "hand-over-hand" model in which two heads of kinesin alternately repeat single-headed and double-headed binding with a microtubule. To investigate the binding mode of kinesin at the key nucleotide states during adenosine 5′-triphosphate (ATP) hydrolysis, we measured the mechanical properties of a single kinesin-microtubule complex by applying an external load with optical tweezers. Both the unbinding force and the elastic modulus in solutions containing AMP-PNP (an ATP analog) were twice the value of those in nucleotide-free solution or in the presence of both AMP-PNP and adenosine 5′-diphosphate. Thus, kinesin binds through two heads in the former and one head in the latter two states, which supports a major prediction of the hand-over-hand model.

Kinesin is a molecular motor that transports membrane-bound vesicles and organelles toward the plus end of a microtubule in various cells including neurons (*1*, *2*). Kinesin takes hundreds of 8-nm steps (the size of tubulin heterodimers composed of α and β subunits) (*3*–*5*) before detachment, so that the run length reaches longer than 1 μm (*3*, *6*). Each step is associated with one cycle of ATP hydrolysis (*7*, *8*). Structural and biophysical evidence shows that stepping of kinesin is triggered by conformational changes in the ATP-bound head (*9*).

A "hand-over-hand" model has been proposed to explain the processive movement of kinesin (Fig. 1) (*5*, *9*–*16*). To substantiate the hand-over-hand model, it is essential to determine the binding mode—either single- or double-headed binding—at each nucleotide state, and the kinetic step at which the transi-

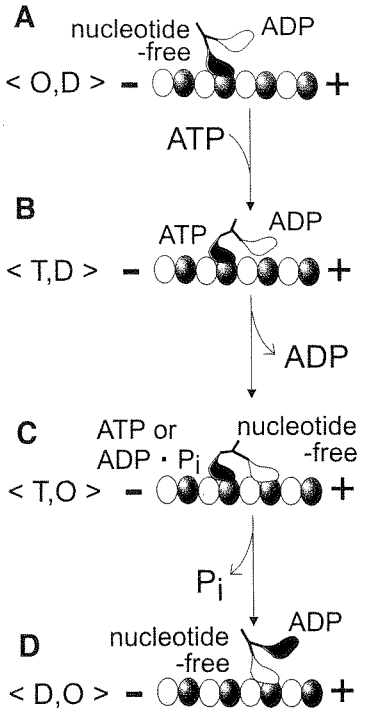

Fig. 1. A simplified version of the hand-over-hand model on the mechanism of kinesin motility proposed to date (*5*, *9*–*16*). O: nucleotide-free; D, T, and P_i: ADP, ATP, and inorganic phosphate, respectively.

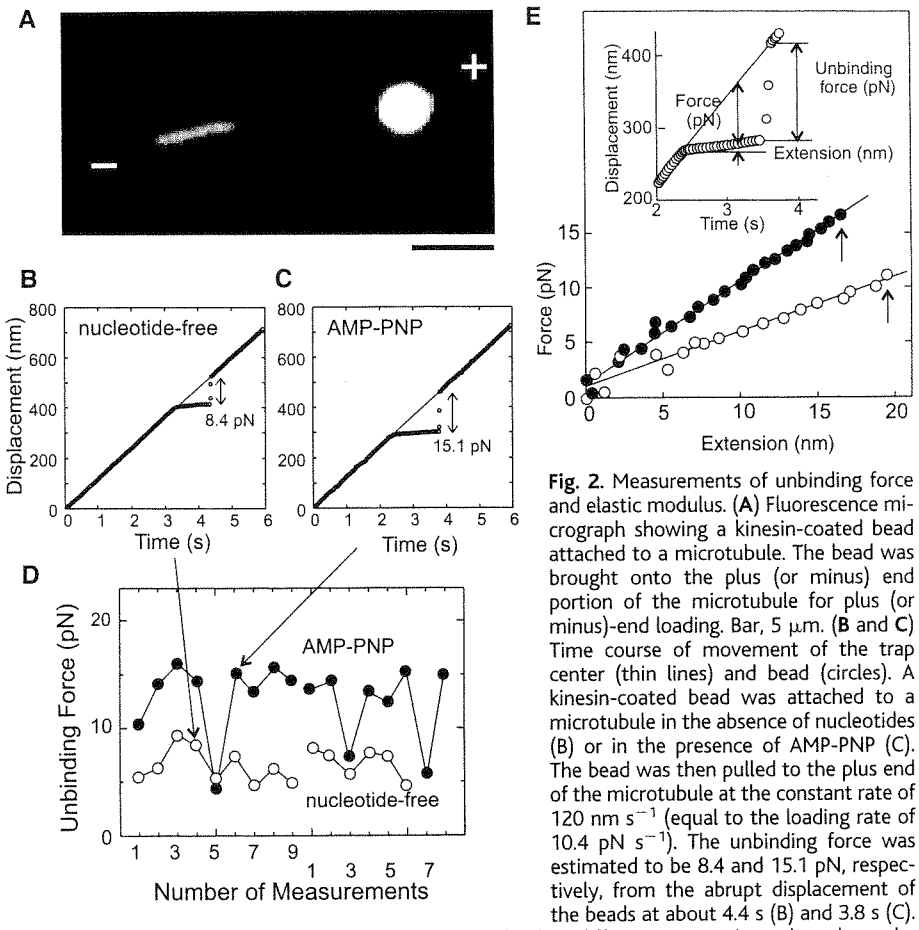

Fig. 2. Measurements of unbinding force and elastic modulus. (**A**) Fluorescence micrograph showing a kinesin-coated bead attached to a microtubule. The bead was brought onto the plus (or minus) end portion of the microtubule for plus (or minus)-end loading. Bar, 5 μm. (**B** and **C**) Time course of movement of the trap center (thin lines) and bead (circles). A kinesin-coated bead was attached to a microtubule in the absence of nucleotides (B) or in the presence of AMP-PNP (C). The bead was then pulled to the plus end of the microtubule at the constant rate of 120 nm s^{-1} (equal to the loading rate of 10.4 pN s^{-1}). The unbinding force was estimated to be 8.4 and 15.1 pN, respectively, from the abrupt displacement of the beads at about 4.4 s (B) and 3.8 s (C). (**D**) Sequential data of unbinding force measurements for four different preparations; data shown by arrows were taken from (B) and (C). Conditions: (B) and (○) in (D), nucleotide-free; (C) and (●) in (D), + AMP-PNP. (**E**) Examples of the force-extension relation (○, nucleotide-free; ●, + AMP-PNP). The relation was obtained from the time course of bead displacement as shown in the inset. To be strict, the force means the force component parallel to the glass surface, and the extension means the displacement of the bead in parallel to the glass surface (*27*). Arrows show the position of unbinding.

tion between the two binding modes occurs (*5*, *9*–*16*). Results of image analysis by cryo-electron microscopy on the dimeric kinesin-microtubule complex have been inconclusive; either single-headed (*13*, *14*) or double-headed (*15*, *16*) binding has been found to predominate both in the absence of nucleotides and in the presence of AMP-PNP. In solution the binding stoichiometry of the kinesin head and the tubulin heterodimer in a microtubule has a molar ratio of 2:1 in both the nucleotide-free state (*17*–*19*) and in the presence of AMP-PNP (*17*), implying a single-headed binding. In these studies, the microtubule was fully decorated by kinesin so that the conformation of kinesin may have been constrained (*16*). The intramolecular interhead distance of kinesin in the crystal structure is about 5 nm (*20*), considerably shorter than the size of the tubulin heterodimer. The kinetics of detachment in solution also suggests the single-headed binding not only in the nucleotide-free condition but also in the coexistence of AMP-PNP and adenosine 5′-diphosphate (ADP) (*21*). Overall, the evidence for the model remains indirect.

To obtain direct evidence for the binding mode at each nucleotide state, we measured the mechanical properties of single kinesin molecules attached to a microtubule in three different solvent conditions (*22*): in the absence of added nucleotides, in the presence of 0.5 mM AMP-PNP and 1 mM ADP, and in the presence of 1 mM AMP-PNP. The first condition corresponds to the ⟨O, O⟩ or ⟨O, D⟩ states (Fig. 1). Although apyrase was added, some proportion of heads may still have bound ADP because the kinesin was purified in the presence of ADP and the detachment rate of ADP is slow (*18*, *19*). The second condition mimics the ⟨T, D⟩ state. Under this condition, only one of the two heads is expected to bind AMP-PNP, while the other head is in the ADP state (*21*). The third condition is considered to represent the ⟨T, O⟩ state (*23*), because the binding ratio of AMP-PNP to kinesin molecules is reported to be 1:1 under the present condition (*23*).

An external load was imposed on a single kinesin-microtubule bead complex (Fig. 2A) (*24*, *25*) as it was moved toward the plus (or minus) end of a microtubule with optical tweezers (*26*, *27*). We repeated unbinding force measurements at nearly the same position on the same microtubule several times for the same bead, presumably for the same kinesin molecule (Fig. 2, B to D). Upon loading toward the plus end, unbinding force in the absence of nucleotides was about 7 pN (Fig. 2D), whereas that in the presence of AMP-PNP could apparently be classified into two components at about 14 pN (major) and 7 pN (minor), the latter corresponding to that in the absence of nucleotides. Using the same data, we obtained the force-extension relation on the kinesin-microtubule complex (Fig. 2E). This relation was almost linear, so that the elastic modulus could be estimated simply from the slope. The elastic modulus could also be classified into two components (compare Figs. 2E and 3, D to F). On the minus-end loading, the unbinding force for both components increased by 45% irrespective of the nucleotide states, keeping the elastic modulus unchanged. This shows that the binding is unstable

[1]Department of Physics, School of Science and Engineering; [2]Advanced Research Institute for Science and Engineering; [3]Materials Research Laboratory for Bioscience and Photonics, Waseda University, 3-4-1 Okubo, Shinjuku-ku, Tokyo 169-8555, Japan. [4]Core Research for Evolutional Science and Technology (CREST), "Genetic Programming" Team 13, Nogawa 907, Miyamae-ku, Kawasaki 216-0001, Japan.

*To whom correspondence should be addressed. E-mail: ishiwata@mn.waseda.ac.jp

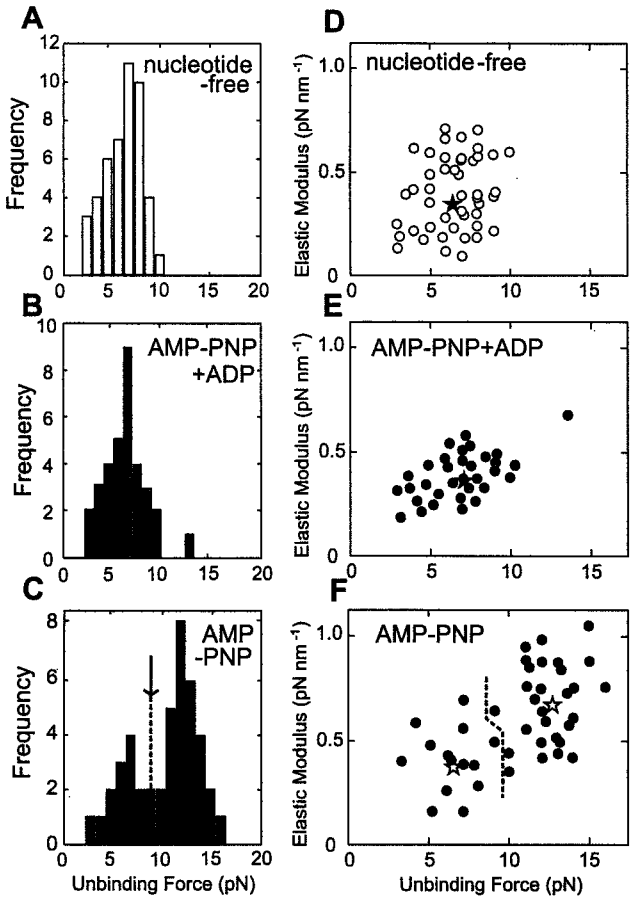

Fig. 3. Distribution of unbinding force (**A** to **C**) and relation between elastic modulus and unbinding force (**D** to **F**) at different nucleotide-binding states. The external load was applied toward the plus end. (A and D) Nucleotide-free (n = 46); (B and E) AMP-PNP + ADP (n = 33); (C and F) + AMP-PNP (n = 43). Unbinding force (pN) ± SD: 6.7 ± 1.8 (A), 7.2 ± 2.0 (B), and 6.6 ± 1.7 (n = 14), 12.8 ± 1.6 (n = 29) (C). Elastic modulus (pN nm^{-1}) ± SD: 0.35 ± 0.14 (D), 0.37 ± 0.16 (E), and 0.39 ± 0.17 (n = 14), 0.67 ± 0.21 (n = 29) (F). Loading rate (pN s^{-1}): 3.5 (A and D), 6.0 (B and E), and 4.3 (C and F). A single Gaussian distribution could simulate unbinding force distribution in (A) and (B). In contrast, the unbinding force distribution in (C) was simulated by the sum of two Gaussian distributions, with S- and L-components defined as the smaller and larger unbinding force, respectively. The boundary between the S- and L-components was determined by the junction of two Gaussian distributions [shown by an arrow (C)]; the boundary in (F) was determined according to that in (C). The average values for S- and L-components are shown by asterisks in (D) to (F).

for the plus-end loading compared with the minus-end loading.

The small (~7 pN; S-) and large (~14 pN; L-) components of unbinding force, respectively, correspond to those of the elastic modulus (Fig. 3). The finding that the unbinding force and the elastic modulus for the L-component were twice those for the S-component strongly suggests that the S- and L-components are attributable to the single- and double-headed binding of kinesin, respectively. Thus, each kinesin head contributes equally to the elastic modulus, such that each head equally shares the external load.

This interpretation shows that the binding mode in the ⟨O, D⟩ state (Fig. 1A) is single-headed. Assuming that AMP-PNP is an ATP analog, single-headed binding is also predominant in the ⟨T, D⟩ state (Fig. 1B). It is highly probable that the attached head binds AMP-PNP (ATP) (*9*), whereas the detached head binds ADP (*9*, *21*), because the attachment of the ADP-bound head was reported to be weak (*17*). In the ⟨T, O⟩ state (Fig. 1C), in contrast, double-headed binding is predominant. Here we find that, based on the bimodal distributions of unbinding force and elastic modulus at one loading rate (Figs. 2D and 3, C and F), both single- and double-headed binding exist. Additionally, we find that the proportion of the S-component decreased as the loading rate increased from 2 to 18 pN s^{-1} and, finally, disappeared at the highest loading rate we examined (18 pN s^{-1}), irrespective of the loading direction. This implies that double-headed binding predominates in the absence of external load. The finding that the unbinding force for the plus-end loading was smaller than that for the minus-end loading suggests that, in the "bridge" structure of double-headed binding (see Fig. 1C), the rear head is relatively unstable so that it tends to be detached. Such an asymmetry for the loading direction regarding the stability of the attached state is favorable for kinesin motors stepping forward.

References and Notes

1. R. D. Vale, in *Guidebook to the Cytoskeletal and Motor Proteins*, T. E. Kreis, R. D. Vale, Eds. (Oxford Univ. Press, Oxford, ed. 2, 1999), pp. 398–402.
2. N. Hirokawa, *Science* **279**, 519 (1998).
3. S. M. Block *et al.*, *Nature* **348**, 348 (1990).
4. K. Svoboda *et al.*, *Nature* **365**, 721 (1993).
5. J. Howard, *Annu. Rev. Physiol.* **58**, 703 (1996).
6. K. Kawaguchi, S. Ishiwata, *Biochem. Biophys. Res. Commun.* **272**, 895 (2000).
7. W. Hua *et al.*, *Nature* **388**, 390 (1997).
8. M. J. Schnitzer, S. M. Block, *Nature* **388**, 386 (1997).
9. S. Rice *et al.*, *Nature* **402**, 778 (1999).
10. R. D. Vale, R. A. Milligan, *Science* **288**, 88 (2000).
11. E. Mandelkow, K. A. Johnson, *Trends Biochem. Sci.* **23**, 429 (1998).
12. D. D. Hackney, *Proc. Natl. Acad. Sci. U.S.A.* **91**, 6865 (1994).
13. K. Hirose *et al.*, *Mol. Biol. Cell* **10**, 2063 (1999).
14. I. Arnal, R. H. Wade, *Structure* **6**, 33 (1998).
15. M. Thormählen *et al.*, *J. Mol. Biol.* **275**, 795 (1998).
16. A. Hoenger *et al.*, *J. Mol. Biol.* **297**, 1087 (2000).
17. A. Lockhart, I. M. Crevel, R. A. Cross, *J. Mol. Biol.* **249**, 763 (1995).
18. Y. Z. Ma, E. W. Taylor, *J. Biol. Chem.* **272**, 724 (1997).
19. S. P. Gilbert, M. L. Moyer, K. A. Johnson, *Biochemistry* **37**, 792 (1998).
20. F. Kozielski *et al.*, *Cell* **91**, 985 (1997).
21. Y. Vugmeyster, E. Berliner, J. Gelles, *Biochemistry* **37**, 747 (1998).
22. Kinesin and tubulin were prepared from bovine (*25*) and porcine (*28*) brains, respectively. Polarity-marked microtubules labeled with tetramethylrhodamine succinimidyl ester (Molecular Probes, Eugene, OR) were prepared according to Hyman (*28*) except that tubulin was not treated with *N*-ethylmaleimide (NEM) (Fig. 2A). Kinesin-coated beads and the flow cell were prepared as described (*6*, *25*). The final solvent condition was ~0.1 pM kinesin-coated beads, 2 mM $MgCl_2$, 80 mM Pipes (pH 6.8), 1 mM EGTA, 0.7 mg ml^{-1} filtered casein, 1 U ml^{-1} apyrase (nucleotide-free condition), 0.5 mM AMP-PNP with 1.0 mM ADP (AMP-PNP + ADP condition) (*21*) or 1 mM AMP-PNP (+ AMP-PNP condition), 10 μM taxol, 10 mM dithiothreitol, and an oxygen-scavenging enzyme system (*6*). All experiments were performed at 25° ± 1°C.
23. B. J. Schnapp *et al.*, *Proc. Natl. Acad. Sci. U.S.A.* **87**, 10053 (1990).
24. K. Svoboda, S. M. Block, *Cell* **77**, 773 (1994).
25. H. Kojima *et al.*, *Biophys. J.* **73**, 2012 (1997).
26. T. Nishizaka *et al.*, *Nature* **377**, 251 (1995).
27. A microscopy system equipped with optical tweezers was as previously described (*26*); the stiffness of the optical trap was estimated to be 0.087 pN nm^{-1}. The bead in the medium was first trapped by optical tweezers and placed in contact with a microtubule for 20 to 30 s, a period considered sufficient to realize the binding equilibrium between kinesin molecule and a microtubule. The trap center was then moved at a constant rate to the plus (or minus) end of the microtubule (Fig. 2A) until the unbinding event occurred. With a single-molecule attachment between the bead and the microtubule, it is possible for the bead to move some distance relative to the microtubule without deviating from the trap center. This is mainly because of the rotational movement of the bead in the trap. This rotational movement is not registered on the position detector. As observed in Fig. 2, B and C, for the first part of the movement of the bead, the kinesin may be attached to the microtubule but does not show in the displacement until the bead-kinesin-microtubule link pulls tight. On the basis of the size and geometry of the kinesin-tethered bead (*24*) (radius of bead, 0.5 μm; length of kinesin, 60 nm), we can estimate that the largest displacement required before the external load is imposed for the unbinding event is ~600 nm. In fact, this displacement was as large as 300 ± 140 nm (n = 122). Also, the actual extension of kinesin is estimated to be 8.3 ± 1 nm (Fig. 2E), which is approximated by 18 nm × cos(θ), where θ (1.1 ± 0.1 rad) is the angle between the kinesin tether and the glass surface. In our bead assay, the external force responsible for the extension of the kinesin-microtubule complex should also be multiplied by cos(θ). Thus, the elastic modulus is kept unchanged.
28. A. A. Hyman, *J. Cell Sci.* **s14**, 125 (1991).

29. We thank K. Kinosita Jr. and T. Nishizaka for continuous collaboration. We are grateful to Y. Y. Toyoshima and T. Yagi for suggestions on the preparation of kinesin and tubulin, and to H. Higuchi for the protocol for kinesin bead assay. We also thank J. Howard, K. Hirose, and W. Rozycki for critical reading of the manuscript. This research was partly supported by Grants-in-Aid for Scientific Research, for Scientific Research on Priority Areas, and for the High-Tech Research Center Project from the Ministry of Education, Science, Sports, and Culture of Japan; by Grants-in-Aid from CREST; and by the Mitsubishi Foundation.

28 September 2000; accepted 18 December 2000

Microscopic Analysis of Polymerization and Fragmentation of Individual Actin Filaments

Shin'ichi Ishiwata[1,2,3,4], Junko Tadashige[1], Ichiro Masui[1], Takayuki Nishizaka[4], and Kazuhiko Kinosita, Jr[4,5]

Introduction

The dynamics of polymerization (and annealing of fragments) and depolymerization (and fragmentation) of actin filaments (F-actin) is a key process in diverse cellular functions, including cell motility. Up to the present, there have been many spectroscopic studies in solution, which have clarified time-dependent but averaged properties, as well as electron microscopic and other studies; but a single filament analysis, which is effective in clarifying not only time-dependent but also nonaveraged properties, has not yet been reported. Thus, direct observation of the polymerization-depolymerization dynamics of individual actin filaments is worthy of investigation.

The polymerization process consists of nucleation and growth phase, and at a steady state, annealing and fragmentation of polymerized filaments occur. The essential elements of these processes have been experimentally clarified and theoretically formulated (Oosawa and Kasai 1962; Oosawa and Asakura 1975). Actin filaments, like microtubules, have a structural polarity, such that the polymerization and depolymerization rates at the two ends of the filaments are different (Oosawa and Asakura 1975; Woodrum et al. 1975; Kondo and Ishiwata 1976; Hayashi and Ip 1976; Pollard and Cooper 1986). The end of the filaments at which the polymerization rate is larger is defined as the barbed (B-) end and the other is called the pointed (P-) end.

After the steady state of polymerization is attained, a treadmill process is expected to occur (Wegner 1976). The B-end of the filament is where filament assembly occurs, while depolymerization occurs at the P-end, such that the length of the filament is maintained nearly constant. The treadmill process has been experimentally demonstrated in solution (cf Wegner 1976; Korn et al. 1987). After actin monomers (G-actin) with ATP are polymerized, the bound

[1] Department of Physics, School of Science and Engineering
[2] Advanced Research Institute for Science and Engineering
[3] Materials Research Laboratory for Bioscience and Photonics, Waseda University, Tokyo 169-8555, Japan
[4] Core Research for Evolutional Science and Technology (CREST) Genetic Programming Team 13, Japan
[5] Department of Physics, Faculty of Science and Technology, Keio University, Yokohama 223-8522, Japan

Results and Problems in Cell Differentiation, Vol. 32
C. dos Remedios (Ed.): Molecular Interactions of Actin

ATP is hydrolyzed and inorganic phosphate (Pi) is released, leaving ADP attached.

When the rate of polymerization is greater than that of ATP hydrolysis, actin molecules with ATP should cap that end of the filaments. Depending on whether each end of the actin filaments is capped by either ATP-bound actin (ATP-cap) or ADP-bound actin (ADP-cap), dynamic instability of the filaments may occur (Korn et al. 1987; Carlier 1989). However, in contrast to microtubules, the dynamic instability has not yet been experimentally proved in actin filaments. Thus, the examination of whether this dynamic process occurs is a challenging problem.

About a decade ago, it became possible to visualize single actin filaments under a fluorescence microscope by labeling the filaments with rhodamine-phalloidin (Rh-Ph; Yanagida et al. 1984) or with fluorescein 5-isothiocyanate (FITC; Honda et al. 1986). In both studies, phallotoxins (Wieland et al. 1975) were added in order to suppress the depolymerization of actin filaments due to extremely low concentration (an order of nM) of actin, lower than the critical concentration for polymerization. Because the filament structure is stabilized, it became possible to visualize single filaments for a sufficiently long time to examine quantitatively not only the polymerization process but also the fragmentation process. Thus, the use of fluorescent-dye conjugated phallotoxins was very useful for stably and clearly visualizing the filament under a conventional fluorescence microscope without disturbance of background fluorescence (cf. Ishiwata 1998). The advantage of this technique is that Rh-Ph does not bind to G-actin and the fluorescence intensity of Rh-Ph increases several-fold upon binding to actin filaments (Harada et al. 1991; Huang et al. 1992).

In this chapter, we describe the properties of the polymerization and fragmentation processes of single actin filaments examined by direct observation through the fluorescence image of actin filaments in the presence of phallotoxins under a conventional fluorescence microscope (Tadashige et al. 1992; Masui et al. 1995).

We ask the reader to bear in mind that although the stabilization by phallotoxins is convenient for visualizing single actin filaments, there are several disadvantages to this method: (1) The greatest disadvantage is that spontaneous depolymerization is suppressed (Estes et al. 1981; Coluccio and Tilney 1984; Sampath and Pollard 1991), (2) The structure of actin filaments may be modified by the binding of phallotoxins (Drubin et al. 1993; Lorenz et al. 1993), so that the results may not represent polymerization properties of pure actin filaments. In this respect, however, this method can, conversely, be considered unique in studying the interaction of phallotoxins with actin filaments.

We have recently succeeded in visualizing polymerization and depolymerization of single actin filaments by using fluorescent dye(rhodamine)-labeled actin without using rhodamine-phallotoxins (phalloidin or phallacidin) under evanescent field illumination (Takahashi and Ishiwata 1998; Fujiwara et al. 1998). Thus it is now possible to visualize at a video rate both polymerization and depolymerization processes for every filament. The results will be published in more detail elsewhere.

How to Image the Polymerization (and Fragmentation) Process of Actin Filaments

To analyze polymerization and fragmentation of individual actin filaments under a fluorescence microscope, it is necessary to observe the same filaments at least for 30 min. Although single filaments are visualized in solution under a conventional fluorescence microscope, it is difficult to trace the polymerization process for each filament floating in solution because of its violent Brownian motion (Yanagida et al. 1984; Isambert et al. 1995).

To overcome this difficulty, we fixed short actin filaments to a glass surface through the cross-linked HMM molecules, as schematically illustrated in Fig. 1 [myosin easily adheres to a collodion(nitrocellulose)-coated glass surface], so that we can keep observing the same filaments. Thus, a short filament adhering to the glass surface was used as a nucleus for observing the polymerization process and as a tool to fix the long filaments so as to observe the fragmentation (severing) process.

To visualize the polymerization process at a constant concentration of G-actin, the actin solution was infused into a flow cell just after the addition

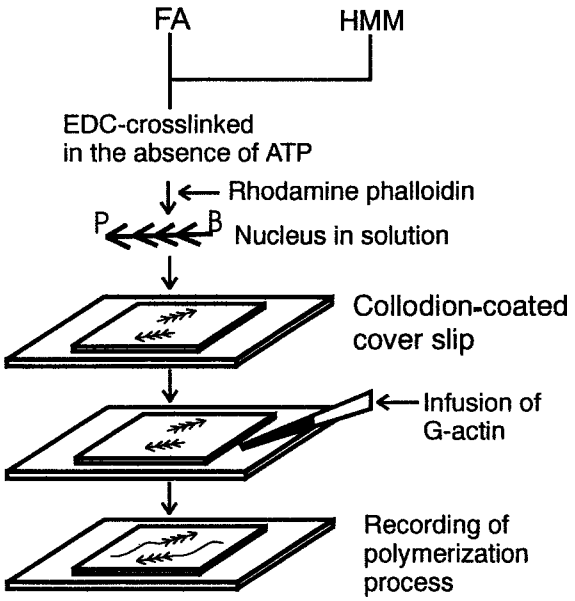

Fig. 1. Scheme showing how to measure the polymerization rate of actin on single actin filaments under a fluorescence microscope. Actin filaments decorated with HMM in the absence of ATP were cross-linked with 1-ethyl-3-(3-dimethyl-aminopropyl)-carbodiimide (EDC) and labeled with Rh-Ph to clearly identify the nuclei (Nishizaka et al. 1993). The EDC cross-linked acto-HMM complexes were mildly sonicated to make filaments short and used as nuclei for polymerization of actin. Immediately after the addition of salt, G-actin solution was infused into the flow cell sandwiched between a pair of coverslips, one of which was coated with nitrocellulose (collodion). The polymerization process was observed under an inverted fluorescence microscope and recorded on a videotape through a SIT camera (C1000; Hamamatsu Photonics). The length of the actin filaments was analyzed using a digital image processor (DIPS-C2000; Hamamatsu Photonics) (Nishizaka et al. 1995)

of salt to the G-actin solution, and the initial process of polymerization was recorded on a videotape at a rate of 30 frames s^{-1}. The length of actin filaments was determined by accumulating and averaging the images for 1 s every 5 (and 6, 7 or 10) min. Thus, the accuracy of the estimation of length change was less than 0.2 μm.

Visualization of the Polymerization Process of Actin Filaments

Figure 2 illustrates a series of fluorescence micrographs showing the polymerization process of individual actin filaments. The concentration of Rh-Ph was reduced to 15 nM, 1/7 that of phalloidin (or phallacidin), which was sufficiently high to image actin filaments. Under this condition, polymerization occurred only at one end of the actin nuclei, corresponding to the B-end.

Judging from the polymerization rate of actin (about 100 nm min^{-1} = 0.6 molecules s^{-1} assuming that the pitch of an actin monomer along the

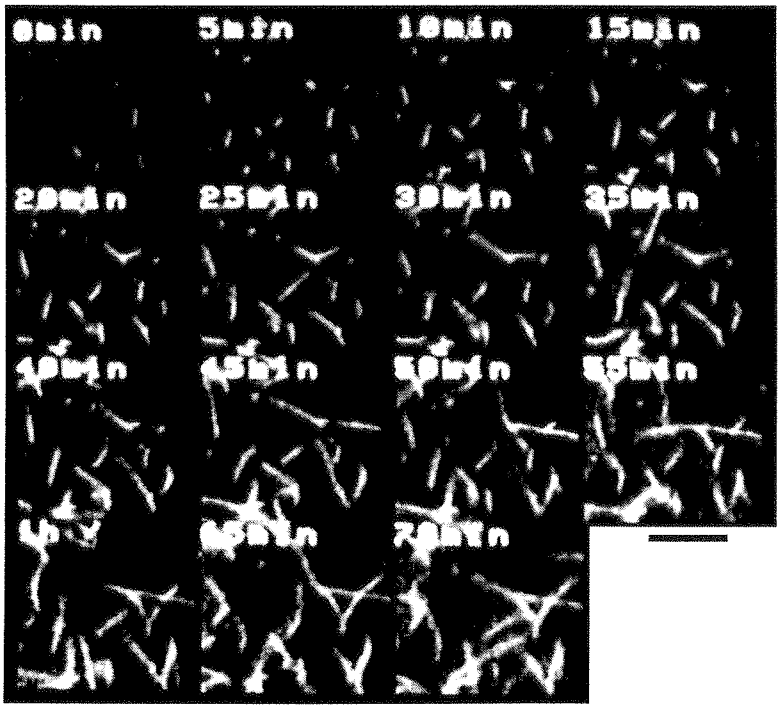

Fig. 2. Fluorescence images showing the time course of the polymerization on single actin filaments. Fluorescence images were recorded for several seconds every 5 min to minimize the photobleaching after the addition of the following actin solution. Condition: 5 μg ml^{-1} G-actin, 30 mM KCl, 1 mM $MgCl_2$, 4 mM ATP, 2 mM MOPS (pH 7), 105 nM phalloidin (Molecular Probes, Inc.), 15 nM Rh-Ph (Molecular Probes, Inc.) and oxygen scavenger system (Harada et al. 1991). The solvent was mixed with G-actin solution containing only ATP and MOPS immediately before the experiments, to minimize the spontaneous polymerization in solution. Temperature 25 °C. Bar, 5 μm

long-pitch helical strand of F-actin to be 5.5 nm) and the concentrations of nuclei and G-actin, the decrease in the concentration of G-actin can be neglected during initial observation (10 min) period. The polymerization rate (shown in Figs. 4 and 5 below) was estimated from the initial phase of elongation for 10 min (cf Fig. 3). We noticed that about one third of the nuclei among those attached to the glass surface did not elongate (see the upper left in each micrograph of Fig. 2). This is probably because G-actin was not accessible to the ends of the nuclei due to an obstacle such as nitrocellulose. Some filaments, which showed bending Brownian motion out of focus, were omitted from the length measurements.

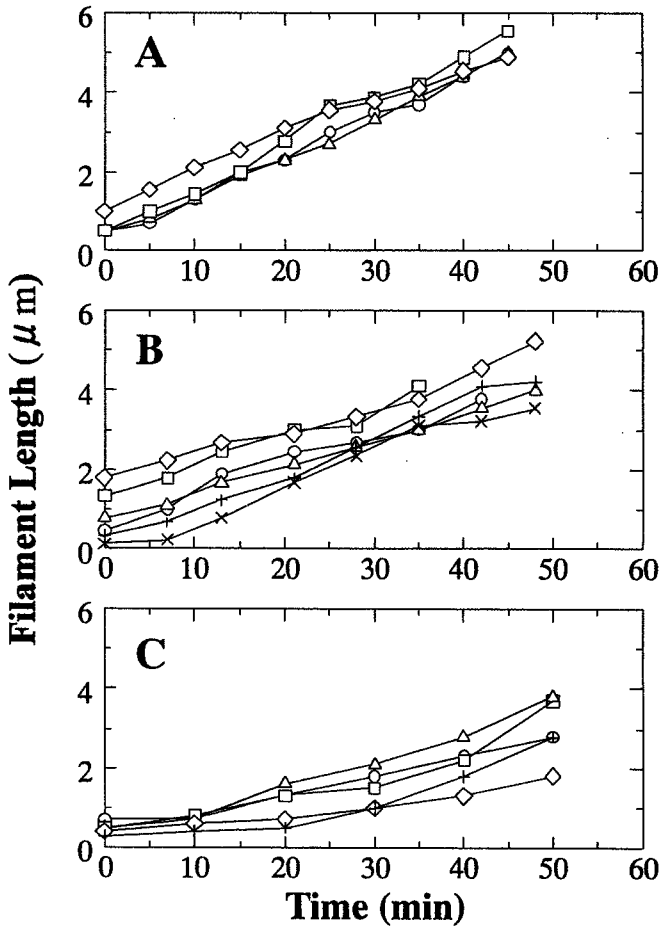

Fig. 3A–C. Time course of polymerization at the B-end of F-actin obtained under a fluorescence microscope at different actin concentrations. Conditions: G-actin, 5 μg ml^{-1} (A, images are shown in Fig. 2), 4 μg ml^{-1} (B) and 3 μg ml^{-1} (C); other solvent conditions, the same as in Fig. 2 (the concentrations of phalloidin and Rh-Ph were maintained at 105 nM and 15 nM, respectively, irrespective of the concentrations of G-actin. Although the total concentration of phalloidin was less than the highest actin concentration examined, we estimated that it was high enough for the binding at the initial stage of polymerization). The filament length at time zero corresponds to the length of nucleus. Temperature 25 °C

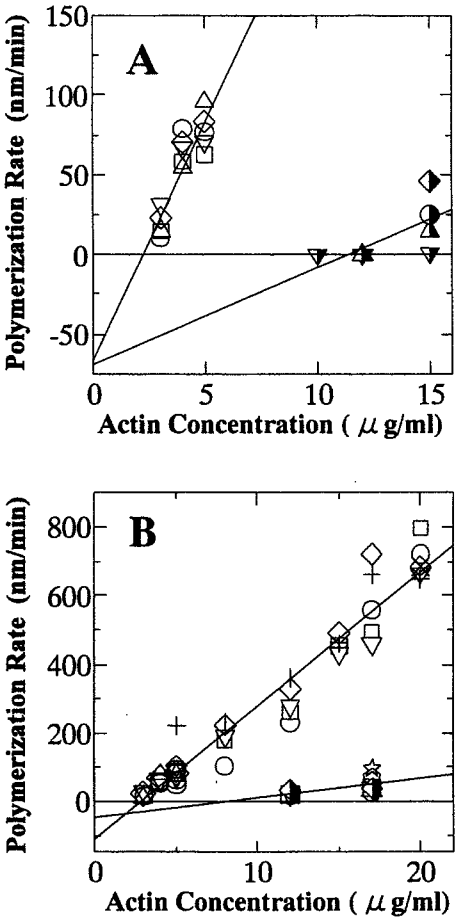

Fig. 4A,B. Initial rate of polymerization vs G-actin concentration in the presence of phalloidin. The polymerization rates at the B- and P-ends of F-actin were examined. When polymerization occurred at both ends of the filament, we decided the end elongated longer to be a B-end and that shorter to be a P-end. (A): polymerization at the B-end in the presence of 1 mM Mg^{2+} (open symbols) or 1 mM Ca^{2+} (half-filled symbols). Conditions as in Fig. 3, except that 1 mM $CaCl_2$ was added in half-filled symbols instead of 1 mM $MgCl_2$. (B) Polymerization at the B-end (open symbols and crosses) or the P-end (half-filled symbols, open star and pentagon) in the presence of Mg^{2+}. The data in A are also included. Different symbols show different preparations of actin. Temperature, 2 °C

Measurement of the Polymerization Process of Actin Filaments

Figure 3 shows an example of the time course of polymerization of individual actin filaments at three different concentrations of G-actin in the presence of phalloidin. The density of nuclei attached to the glass surface was common to all the experiments. On increasing the concentration of infused G-actin, the average rate of polymerization increased.

The polymerization rate varied from filament to filament (Fig. 3). Even in the same filament, the polymerization rate was not constant over 40–50 min but changed with time beyond the resolution of length determination. The accessibility of G-actin to the ends of the filaments may have fluctuated with time due to the adhesion to the nitrocellulose. Also, these results may be attributable to the nonhomogeneity of the local concentration of G-actin and/or the stochastic and cooperative properties of the polymerization process in the presence of phalloidin.

Depolymerization was suppressed by the presence of phalloidin, but there is a possibility that spontaneous fragmentation occurred. This could be one of the causes of length fluctuations during the polymerization process. In practice, however, we did not notice distinct fragmentation, at least in the middle of the filaments.

The rate of fragmentation in the absence of phalloidin was previously estimated in solution experiments to be $7 \times 10^{-7} s^{-1}$ (Kinosian et al. 1993), suggesting that in practice, fragmentation in the presence of phallotoxins does not occur within the period of measurements.

At low concentrations of G-actin, there was a tendency for the polymerization rate to increase with time (Fig. 3). The polymerization curve at $3 \mu g ml^{-1}$ G-actin was convex downward, whereas the curve at $5 \mu g ml^{-1}$ G-actin was nearly straight. This suggests that the polymerization kinetics change with the elongation of the filaments. The shorter the filament, the more the binding of G-actin may be disturbed.

Relation Between Polymerization Rate and Actin Concentration

The average rate of polymerization vs G-actin concentration relation is summarized in Fig. 4. In Fig. 4A, the relation observed at the B-end of F-actin in the presence of Mg^{2+} or Ca^{2+} is compared, while in Fig. 4B, the relation at the B- and P-ends is shown over a comparatively broader range of G-actin concentration.

These experiments were done in the presence of a constant concentration of phalloidin. Contrary to our expectation and differing from previous results obtained in solution (Estes et al. 1981; Coluccio and Tilney 1984; Sampath and Pollard 1991), the critical concentration of polymerization was not zero under all the conditions. This result was not changed even if the polymerization rates were estimated between 40 and 50 min in Fig. 3, where the polymerization rates were larger than the initial ones. However, when the same concentration of phallacidin was used instead of phalloidin, the result was as expected (Fig. 5). In both cases, the same concentration of Rh-Ph, one seventh that of phalloidin (or phallacidin), coexisted in order to visualize single actin filaments.

The relation between the polymerization rate (r) and G-actin concentration (c) can be expressed by:

$$r = k^+c - k^-,$$

where k^+ and k^- are the rate constants for polymerization and depolymerization, respectively. Thus, under the conditions examined in the presence of phalloidin, k^+ was estimated to be $29.6 (nm\,min^{-1})/(\mu g\,ml^{-1})$ $(= 7.5 \times 10^6 M^{-1} s^{-1})$ and $6.2 (nm\,min^{-1})/(\mu g\,ml^{-1})$ $(= 1.6 \times 10^6 M^{-1} s^{-1})$ for the B-end in the presence of Mg^{2+} and Ca^{2+}, respectively (Fig. 4A), and $39.3 (nm\,min^{-1})/(\mu g\,ml^{-1})$ $(= 1.0 \times 10^7 M^{-1} s^{-1})$ and $5.9 (nm\,min^{-1})/(\mu g\,ml^{-1})$ $(= 1.5 \times 10^6 M^{-1} s^{-1})$ for the B-end and the P-end in the presence of Mg^{2+}, respectively (Fig. 4B). In calculating the values in the parentheses, we assumed that the molecular weight of actin is 42 kDa, and the number density of actin molecules along the filament is 2 molecules/5.5 nm.

On the other hand, in the presence of phallacidin, k^+ at the B-end was estimated to be 34.9 $(nm\,min^{-1})/(\mu g\,ml^{-1})$ $(= 8.9 \times 10^6 M^{-1} s^{-1})$ and 5.8 $(nm\,min^{-1})/(\mu g\,ml^{-1})$ $(= 1.5 \times 10^6 M^{-1} s^{-1})$ in the presence of Mg^{2+} and Ca^{2+}, respectively (Fig. 5).

The values of k^+ obtained above in the presence of Mg^{2+} (Figs. 4B, 5) were a little larger than, but consistent with, those obtained in solution under the same solvent conditions except for the absence of phallotoxins (the values of k^+ at the B- and P-ends were, respectively, $6.3 \times 10^6 M^{-1} s^{-1}$ and $1.1 \times 10^6 M^{-1} s^{-1}$; Suzuki and Mihashi 1989). This differs, however, from the results that the addition of phallotoxins reduced the value of k^+ by 20 to 50% (Coluccio and Tilney 1984; Wendel and Dancker 1987; Sampath and Pollard 1991). Such an apparent discrepancy may be attributable to the difference in experimental conditions. Note that the value of k^- was almost zero in the presence of phallacidin, consistent with the previous solution experiments (Estes et al. 1981; Coluccio and Tilney 1984; Sampath and Pollard 1991).

We found that the addition of 10 mM Pi in the presence of phallacidin slightly increased the value of k^+ to 39.0 $(nm\,min^{-1})/(\mu g\,ml^{-1})$ $(= 9.9 \times 10^6 M^{-1} s^{-1})$ and 6.9 $(nm\,min^{-1})/(\mu g\,ml^{-1})$ $(= 1.8 \times 10^6 M^{-1} s^{-1})$ in the presence of Mg^{2+} and Ca^{2+}, respectively, that is, by about 1.1 to 1.2 times (Fig. 5). This demonstrates that Pi does not significantly affect the polymerization rate but stabilizes the filament structure (Nonomura et al. 1975) through the decrease

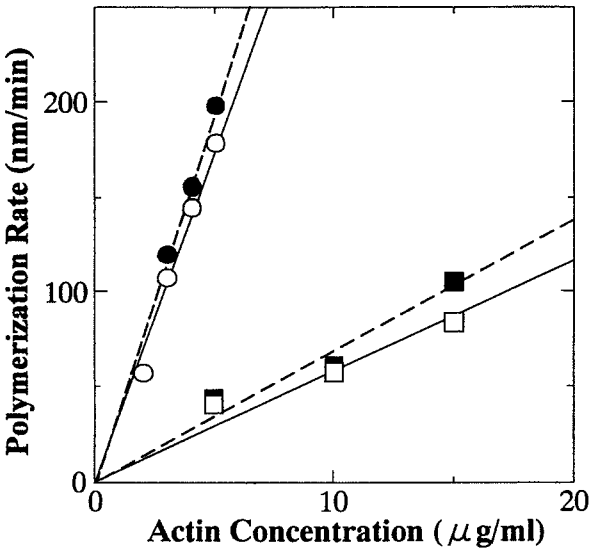

Fig. 5. Initial rate of polymerization at the B-end vs G-actin concentration in the presence of phallacidin. Effects of Pi and divalent cations (Mg^{2+} or Ca^{2+}) were examined. Conditions: various concentrations of G-actin, 30 mM KCl, 2 mM $MgCl_2$ (circles) or $CaCl_2$ (squares), 4 mM ATP, 2 mM MOPS (pH 7), 2 mg ml^{-1} BSA, 1.5 mM NaN_3, with (closed symbols) or without (open symbols) 1.5 mM Pi, 105 nM phallacidin, 15 nM Rh-Ph, 10 mM DTT, 0.3% (w/v) methylcellulose and oxygen scavenger system (Harada et al. 1991). The time course of polymerization of actin filaments was indistinguishable from that in the presence of phalloidin shown in Fig. 3, except that the polymerization curve was slightly convex upward at every G-actin concentration we examined

in the rates of both depolymerization (Rickard and Sheterline 1986, 1988; Funatsu 1986) and fragmentation as described below (Fig. 6).

It is also to be noted that, irrespective of the species of phallotoxins, in other words, independent of whether the critical concentration was zero (Fig. 5 for phallacidin) or not (Fig. 4 for phalloidin), the polymerization rate, k^+, was nearly the same under the same solvent conditions. On the other hand, the value of k^+ for Mg-actin was five-to-six times larger than that for Ca-actin (Figs. 4A, 5). This is in contrast to previous results obtained in solution that k^+ for Mg-actin was, at most, only two times larger than that for Ca-actin (see Estes et al. 1992). This apparent discrepancy may be attributable to the structural changes induced by the binding of phallotoxins and the difference in experimental conditions. Another possibility is that the HMM-cross linked nucleus may have amplified a small difference between the polymerization properties of Mg-actin and Ca-actin.

What is most notable in the above experiments is that the critical concentration for polymerization was practically zero in the presence of 105 nM phallacidin with 15 nM Rh-Ph (Fig. 5) but not zero in the presence of 105 nM phalloidin with 15 nM Rh-Ph (Fig. 4). At first sight, the reason for this difference appears to be attributable to the larger dissociation constant of phalloidin than that of phallacidin with F-actin. In practice, however, the dissociation constants of phalloidin and Rh-Ph with F-actin are, respectively, reported to be 67 and 40 nM (Molecular Probes Data Book; Huang et al. 1992), and those of fluorescent dye-conjugated phallotoxins such as coumarin-, NBD- and bodipy-phallacidin are, respectively, reported to be 24, 18 and 38 nM (Huang et al. 1992). Thus, although the dissociation constant of phallacidin has not yet been reported, there seems to be no large difference between phalloidin and phallacidin. If the dissociation constant itself is practically indistinguishable, the reason for the above difference may be attributable to the different rate constants.

The apparent association rate constant of Rh-Ph for F-actin is reported to be two-to-three orders of magnitude smaller than the rates of polymerization and depolymerization (De la Cruz and Pollard 1994, 1996; $6 \times 10^3 M^{-1} s^{-1}$ at 20 °C; and $5 \times 10^4 M^{-1} s^{-1}$ at 40 °C, Hotta and Ishiwata 1997). If this is also the case for the newly polymerized ends of the filaments, there would be an appreciable probability that the actin molecules once attached to the filament ends are detached, so that the apparent polymerization rate becomes reduced, resulting in the nonzero critical concentration.

This was not the case at least for phallacidin (as observed in Fig. 5), suggesting that the association rate constant of phallotoxins for the ends of the filaments is much larger than that for the bulk of the filaments. In fact, there is a report suggesting that phalloidin binds to the filament ends more rapidly than to the bulk of the filament (Cano et al. 1992). We infer that the rate constant of attachment to the filament ends of phalloidin may be still much slower than that of phallacidin.

Such a subtle difference may be produced by the structural change of actin molecules incorporated into the filament ends. The result shown in Fig. 4A,

that the apparent critical concentration for polymerization was larger in the presence of Ca^{2+} than of Mg^{2+}, can be ascribable to this mechanism, and may be related to the difficulty of nucleus formation for Ca-actin. That is, the association rate of phalloidin to the polymerized filament end may be slower for Ca-actin than for Mg-actin. This difference may be overcome in the presence of phallacidin, because the association rate constant of phallacidin at the polymerized ends is large enough to overcome the smaller association rate constant to Ca-actin. These mechanisms should be quantitatively examined in future.

Fragmentation of Actin Filaments: Effect of Anions at High Ionic Strength

Finally, the fragmentation of individual actin filaments was visualized using the same technique as described above. In this case, however, the long actin filaments polymerized beforehand in the presence of Rh-Ph were attached to the glass surface through the short fragments decorated with cross-linked HMM as shown in Fig. 6 (a similar technique has been used before: Bearer 1991; Maciver et al. 1991; Nishizaka et al. 1993). Various salt solutions were then infused into the cell and their effects on the fragmentation were examined under a continuous flow of the solutions.

As observed in a series of micrographs summarized in Fig. 6, shortening of the filaments in the presence of 3 M KSCN occurred mainly by severing with a lifetime of about 2 min (upper micrographs, –Pi) and 10 min (lower micrographs, +Pi), and finally all the filaments disappeared. Gradual depolymerization from the ends of the filaments was not detected. We examined various kinds of salts composed of K^+ as the cation, and Cl^-, I^-, SCN^-, etc as anions.

We found that the severing abilities were in the order of the Hofmeister series (lyotropic number) for anions, ie, the order according to which the hydrophobic interaction is destroyed: SCN^-, I^-, Cl^-, CH_3COO^-, SO_4^{2-}, etc (for the Hofmeister series, see Melander et al. 1984; Cacace et al. 1997). This is in spite of the fact that severing was largely retarded by phalloidin (for the effect of KI in the presence of phalloidin, see Dancker et al. 1975).

The present results are consistent with the previous results obtained by the phase-contrast image analysis of the dissociation process from the P-end of thin filaments in the I-Z-I brush of myofibrils (Funatsu and Ishiwata 1985; Funatsu et al. 1988), which was prepared by mildly etching the P-end of thin filaments with 0.5 M KCl treatment (Ishiwata and Funatsu 1985). The dissociation rate in the presence of 0.5 M salts in the absence of phallotoxins was in the order of SCN^-, I^-, NO_3^-, Cl^- and SO_4^{2-}, being consistent with the Hofmeister series (Funatsu 1986).

These results suggest that a hydrophobic interaction between actin molecules is important for the stabilization of the filament, even after the polymer structure is stabilized by the binding of phalloidin. However, we cannot completely eliminate the possibility that the interaction between phalloidin and

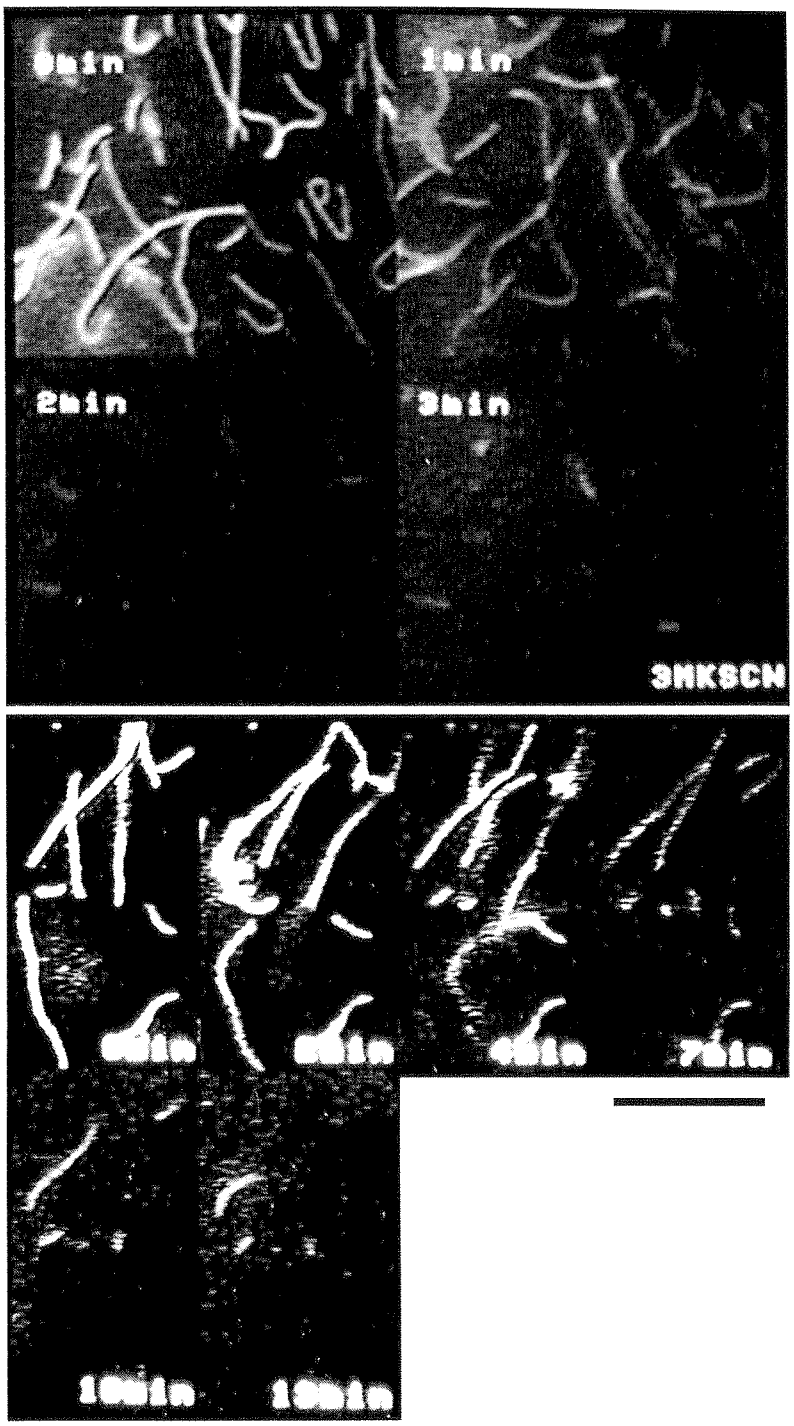

Fig. 6. Fluorescence images showing the time course of fragmentation of actin filaments in the presence of high concentrations of chaotropic anions. To record the time course of fragmentation of actin filaments, the filaments polymerized onto the nuclei of EDC-cross-linked acto-HMM complex in solution were infused into the cell, so that the filaments were attached to the glass surface through the short nuclei portion of the filaments and the polymerized portion of the filaments showed Brownian motion. The assay solvent was then infused. The time (min) after the infusion of the solvent is shown in each micrograph. Conditions as in Fig. 3, except that 3 M KSCN was added instead of 30 mM KCl and in the absence (upper micrographs) or presence (lower micrographs) of 10 mM Pi. Temperature 25 °C. Bars 5 μm

actin is weakened by the anions in the order of the Hofmeister series. It is to be noted that PO_4^{2-} was exceptional because it did not obey the Hofmeister series, ie, in practice, the shortening of the filaments did not occur in the presence of 0.5 M Pi.

The importance of hydrophobic interaction in the polymerization of actin has been recognized for many years (Oosawa and Asakura 1975). Nowadays, this discussion is based on the 3D atomic structure of G-actin (Kabsch et al. 1990) and the molecular model of F-actin (Holmes et al. 1990). These authors suggested that the hydrophobic loop located between subdomains 3 and 4 plays a role in stabilization of F-actin and this suggestion was supported by data from actin mutants or isoforms (Holmes et al. 1990; Allen et al. 1996b; Kuang and Rubenstein 1997).

Although we cannot add any information on the interaction between actin monomers on the atomic level, the results obtained here not only confirmed that the hydrophobic interaction is essential for maintaining the polymer structure but also demonstrated that other kinds of interactions exist between actin monomers, which are stabilized by phalloidin and Pi.

The manner in which phalloidin binds in the 3D structure of F-actin (Drubin et al. 1993; Lorenz et al. 1993; Steinmetz et al. 1998) suggests that phalloidin functions as a glue making connections among actin monomers in the filament. In practice, phalloidin can restore the polymerizability and also the ability of actin to activate myosin ATPase in monomers which have been impaired by chemical modifications of Lys 61 residue with FITC (Miki 1987), with several lysine residues with (m-maleimidobenzoyl)-N-hydroxysuccinimide ester (MBS) (Miki and Hozumi 1991), and by large hydrophobic probes at Cys-374 (Moens et al. 1994). Thus, actin filaments are stabilized by the cooperative nature of several kinds of molecular forces acting between actin and the regulators, ie, phallotoxins and Pi.

It is interesting that the addition of 10 mM Pi substantially lengthened the lifetime of F-actin in the presence of 3 M KSCN (Fig. 6), implying that Pi stabilized the structure of F-actin against the chaotropic effects of anions (for KI, see Dancker and Fischer 1989). For many years, the stabilizing effect of Pi has been well known. For example, with the addition of mM Pi: (1) the fragility of F-actin observed by negative staining in the electron microscope appeared to become stiffer (Nonomura et al. 1975); (2) the depolymerization rate observed in cuvette was slowed down (Rickard and Sheterline 1986, 1988; Carlier 1989); (3) subdomain 2 of the actin monomer in F-actin became oriented so as to interact strongly with the adjacent actin monomers (Orlova and Egelman 1992); and (4) severing activity of gelsolin (Allen et al. 1996a) and actophorin (Maciver et al. 1991) was reduced.

Pi does not greatly accelerate the polymerization rate, as seen in Fig. 5, and suppresses not only the depolymerization but also the fragmentation as observed in Fig. 6, such that Pi shifts the polymerization-depolymerization equilibrium to the polymerization side. The present results strongly suggest that Pi is a stabilizer of the hydrophobic interaction between actin monomers

which is essential for the polymerization of actin. On the other hand, phalloidin stabilizes the F-actin-ADP-Pi complex (Dancker and Hess 1990). Thus, phallotoxins and Pi function as allosteric effectors that synergistically stabilize the structure of actin filaments.

Conclusions

The polymerization and fragmentation processes of individual actin filaments can be visualized by imaging the polymerized filaments through binding of the fluorescent dye, Rh-Ph, under a conventional fluorescence microscope. Thus, the polymerization process at the B- and P-ends of actin filaments can be analyzed in the presence of Mg^{2+} or Ca^{2+}. By measuring the rate of polymerization at various G-actin concentrations, we confirmed that the depolymerization process was inhibited by the attachment of phallotoxins to the filaments (phallacidin was more effective than phalloidin), but the polymerization rate itself was not significantly affected, such that the critical concentration of polymerization was essentially zero. Also, the fragmentation process of filaments due to the addition of high concentrations of chaotropic salts such as KSCN and KI (except Pi) can be observed and stabilization of the hydrophobic interactions by Pi was confirmed. The present study demonstrates that the polymerization and fragmentation dynamics on single actin filaments can be examined quantitatively by fluorescence microscopy.

Acknowledgments. The authors would like to thank Dr JMQ Davies of Waseda University for his critical reading of the manuscript. The authors also thank Miss Ikuko Fujiwara for her assistance in preparing figures. This research was supported in part by Grants-in-Aid for Scientific Research, for Scientific Research on Priority Areas and for the HighTech Research Center Project from the Ministry of Education, Science, Sports and Culture of Japan, and Core Research for Evolutional Science and Technology (CREST) from the Japan Science and Technology Corporation (JST), and a Waseda University Special Grant-in-Aid.

References

Allen PG, Laham LE, Way M, Janmey PA (1996a) Binding of phosphate, aluminum fluoride, or beryllium fluoride to F-actin inhibits severing by gelsolin. J Biol Chem 271:4665–4670

Allen PG, Shuster CB, Kas J, Chaponnier C, Janmey PA, Herman IM (1996b) Phalloidin binding and rheological differences among actin isoforms. Biochemistry 35:14062–14069

Bearer EL (1991) Direct observation of actin filament severing by gelsolin and binding by gCap39 and CapZ. J Cell Biol 115:1629–1638

Cacace MG, Landau EM, Ramsden JJ (1997) The Hofmeister series: salt and solvent effects on interfacial phenomena. Q Rev Biophys 30:241–277

Cano ML, Cassimeris L, Joyce M, Zigmond SH (1992) Characterization of tetramethylrhodaminylphalloidin binding to cellular F-actin. Cell Motil Cytoskel 21:147–158

Carlier M-F (1989) Role of nucleotide hydrolysis in the dynamics of actin filaments and microtubules. Int Rev Cytol 115:139–170

Coluccio LM, Tilney LG (1984) Phalloidin enhances actin assembly by preventing monomer dissociation. J Cell Biol 99:529–535

Dancker P, Fischer S (1989) Stabilization of actin filaments by ATP and inorganic phosphate. Z Naturforsch C44:698–704

Dancker P, Hess L (1990) Phalloidin reduces the release of inorganic phosphate during actin polymerization. Biochim Biophys Acta 1035:197–200

Dancker P, Löw I, Hasselbach W, Wieland Th (1975) Interaction of actin with phalloidin: Polymerization and stabilization of F-actin. Biochim Biophys Acta 400:407–414

De la Cruz EM, Pollard TD (1994) Transient kinetic analysis of rhodamine phalloidin binding to actin filaments. Biochemistry 33:14387–14392

De la Cruz EM, Pollard TD (1996) Kinetics and thermodynamics of phalloidin binding to actin filaments from three divergent species. Biochemistry 35:14054–14061

Drubin DG, Jones HD, Wertman KF (1993) Actin structure and function: Roles in mitochondrial organization and morphogenesis in budding yeast and identification of the phalloidin-binding site. Mol Biol Cell 4:1277–1294

Estes JE, Selden LA, Gershman LC (1981) Mechanism of action of phalloidin on the polymerization of muscle actin. Biochemistry 20:708–712

Estes JE, Selden LA, Kinosian HJ, Gershman LC (1992) Tightly-bound divalent cation of actin. J Muscle Res Cell Motil 13:272–284

Fujiwara I, Takahashi S, Tadakuma H, Ishiwata S (1998) Visualization of polymerization process of single actin filaments under total reflection microscope. Biophysics (Japanese) 38:S63 (Abstr)

Funatsu T (1986) Structural stability and capping proteins of actin filaments. Doct Diss Waseda University

Funatsu T, Ishiwata S (1985) Characterization of β-actinin: A suppressor of the elongation at the pointed end of thin filaments in skeletal muscle. J Biochem 98:535–544

Funatsu T, Asami Y, Ishiwata S (1988) β-actinin: A capping protein at the pointed end of thin filaments in skeletal muscle. J Biochem 103:61–71

Harada Y, Sakurada K, Aoki T, Thomas DD, Yanagida T (1991) Mechanochemical coupling in actomyosin energy transduction studied by in vitro movement assay. J Mol Biol 216:49–68

Hayashi T, Ip W (1976) Polymerization polarity of actin. J Mechanochem Cell Motil 3:163–169

Holmes KC, Popp D, Gebhard W, Kabsch W (1990) Atomic model of the actin filament. Nature 347:44–49

Honda H, Nagashima H, Asakura S (1986) Directional movement of F-actin in vitro. J Mol Biol 191:131–133

Hotta M, Ishiwata S (1997) Temperature dependence of association and dissociation rate constants of rhodamine phalloidin with actin filaments. J Muscle Res Cell Motil 18:491 (Abstr)

Huang Z, Haugland RP, You W, Haugland RP (1992) Phalloidin and actin binding assay by fluorescence enhancement. Anal Biochem 200:199–204

Isambert H, Venier P, Maggs AC, Fattoum A, Kassab R, Pantaloni D, Carlier M-F (1995) Flexibility of actin filaments derived from thermal fluctuations. Effect of bound nucleotide, phalloidin, and muscle regulatory proteins. J Biol Chem 270:11437–11444

Ishiwata S (1998) The use of fluorescent probes. In: Current Methods in Muscle Physiology (ed by Sugi H) Oxford University Press, Oxford, UK, pp 199–222

Ishiwata S, Funatsu T (1985) Does actin bind to the ends of thin filaments in skeletal muscle? J Cell Biol 100:282–291

Kabsch W, Mannherz HG, Suck D, Pai EF, Holmes KC (1990) Atomic structure of the actin: DNase I complex. Nature 347:37–44

Kinosian HJ, Selden LA, Estes JE, Gershman LC (1993) Actin filament annealing in the presence of ATP and phalloidin. Biochemistry 32:12353–12357

Kondo H, Ishiwata S (1976) Uni-directional growth of F-actin. J Biochem 79:159–171

Korn ED, Carlier M-F, Pantaroni D (1987) Actin polymerization and ATP hydrolysis. Science 238:638–644

Kuang B, Rubenstein PA (1997) Beryllium fluoride and phalloidin restore polymerizability of a

mutant yeast actin (V266G, L267G) with severely decreased hydrophobicity in a subdomain 3/4 loop. J Biol Chem 272:1237–1247

Lorenz M, Popp D, Holmes KC (1993) Refinement of the F-actin model against X-ray fiber diffraction data by the use of a directed mutation algorithm. J Mol Biol 234:826–836

Maciver SK, Zot HG, Pollard TD (1991) Characterization of actin filament severing by actophorin from *Acanthamoeba castellani.* J Cell Biol 115:1611–1620

Masui I, Tadashige J, Nishizaka T, Ishiwata S (1995) Microscopic analysis of polymerization process on a single actin filament. Proc Annu Meet Phys Soc Jpn 29:pA3 (Abstr)

Melander WR, Corradini D, Horvath C (1984) Salt-mediated retention of proteins in hydrophobic-interaction chromatography. Application of solvophobic theory. J Chromatogr 317:67–85

Miki M (1987) The recovery of the polymerizability of Lys-61-labelled actin by the addition of phalloidin. Fluorescence polarization and resonance-energy-transfer measurements. Eur J Biochem 164:229–235

Miki M, Hozumi T (1991) Interaction of maleimidobenzoyl actin with myosin subfragment 1 and tropomyosin-troponin. Biochemistry 30:5625–5630

Moens PDJ, Yee D, dos Remedios CG (1994) Determination of the radial coordinate of Cys-374 in F-actin using fluorescence resonance energy transfer spectroscopy: Effect of phalloidin on random assembly. Biochemistry 33:13102–13108

Nishizaka T, Yagi T, Tanaka Y, Ishiwata S (1993) Right-handed rotation of an actin filament in an in vitro motile system. Nature 361:269–271

Nishizaka T, Miyata H, Yoshikawa H, Ishiwata S, Kinosita Jr K (1995) Unbinding force of a single motor molecule of muscle measured using optical tweezers. Nature 377:251–254

Nonomura Y, Katayama E, Ebashi S (1975) Effect of phosphates on the structure of the actin filament. J Biochem 78:1101–1104

Oosawa F, Asakura S (1975) Thermodynamics of the polymerization of proteins. Academic Press, New York

Oosawa F, Kasai M (1962) Theory of linear and helical aggregations of macromolecules. J Mol Biol 4:10–21

Orlova A, Egelman EH (1992) Structural basis for the destabilization of F-actin by phosphate release following ATP hydrolysis. J Mol Biol 227:1043–1053

Pollard TD, Cooper JA (1986) Actin and actin-binding proteins. A critical evaluation of mechanisms and functions. Annu Rev Biochem 55:987–1035

Rickard JE, Sheterline P (1986) Cytoplasmic concentrations of inorganic phosphate affect the critical concentration for assembly of actin in the presence of cytochalasin D or ADP. J Mol Biol 191:273–280

Rickard JE, Sheterline P (1988) Effect of ATP removal and inorganic phosphate on length redistribution of sheared actin filament populations. Evidence for a mechanism of end-to-end annealing. J Mol Biol 201:675–681

Sampath P, Pollard TD (1991) Effects of cytochalasin, phalloidin, and pH on the elongation of actin filaments. Biochemistry 30:1973–1980

Steinmetz MO, Stoffler D, Müller SA, Jahn W, Wolpensinger B, Goldie KN, Engel A, Faulstich H, Aebi U (1998) A correlative analysis of actin filament assembly, structure, and dynamics. J Mol Biol 276:1–6

Suzuki N, Mihashi K (1989) Subunit flow in F-actin under steady-state conditions. Application of a novel method to determination of the rate of subunit exchange of F-actin at the terminals. Biophys Chem 33:177–193

Tadashige J, Nishizaka T, Ishiwata S (1992) Direct observation of the dynamic process of polymerization and depolymerization on single actin filaments. Biophysics (Japanese) 32:S194 (Abstr)

Takahashi S, Ishiwata S (1998) Direct observation of polymerization process of single actin filaments under fluorescence microscope. Biophys J 74:A46 (Abstr)

Wegner A (1976) Head to tail polymerization of actin. J Mol Biol 108:139–150

Wendel H, Dancker P (1987) Influence of phalloidin on both the nucleation and the elongation phase of actin polymerization. Biochim Biophys Acta 915:199–204

Wieland T, de Vries JX, Schäfer AJ, Faulstich H (1975) Spectroscopic evidence for the interaction of phalloidin with actin. FEBS Lett 54:73–75

Woodrum DT, Rich SA, Pollard TD (1975) Evidence for biased bidirectional polymerization of actin filaments using heavy meromyosin prepared by an improved method. J Cell Biol 67:231–237

Yanagida T, Nakase M, Nishiyama K, Oosawa F (1984) Direct observation of motion of single F-actin filaments in the presence of myosin. Nature 307:58–60